UNIVERSITÀ DEGLI STUDI DI PALERMO

Energia e Tecnologie dell'Informazione
Dipartimento di Energia, Ingegneria dell'Informazione e modelli Matematici (DEIM)
ING-IND/33

Prysmian Group

WIRELESS DETECTION OF PD PATTERNS: APPLICATIONS IN SMART GRIDS AND MODERN POWER SYSTEMS

IL DOTTORE
Ing. Antonino Madonia

IL COORDINATORE
Prof. Maurizio Cellura

IL TUTOR
Prof. Eleonora Riva Sanseverino

IL CO-TUTOR
Prof. Pietro Romano

CICLO XXX
2018

Contents

List of Figures....6

List of Tables....14

Abstract....16

Acknowledgments....18

1. Partial Discharges: theory and classification....19

1.1. Introduction....19

1.2 Partial discharges physic....21

1.3 Phase Resolved Partial Discharge Pattern....26

1.4 Partial discharges classification....27

1.4.1 Corona discharge....28

1.4.2 Surface discharge....30

1.4.3 Internal discharge....32

1.4.4 Floating mass....34

1.5 Wireless PD instrument: Pry-Cam Portable....35

1.6 Monitoring PD instrument: Pry-Cam Grids....36

1.7 How to perform an analysis of the acquired PD pattern....37

2. The problem of synchronizing partial discharge pulses....47

2.1 Introduction....47

2.2 Synchronization issue in the wireless acquisition of partial discharges....48

2.3 Evaluation of the voltage angle phase-shift in HV lines....52

2.4 Simulation analysis of the voltage angle phase-shift introduced by the HV lines....53

2.5 Experimental measure of the voltage angle phase-shift 60
2.6 Look up tables for the evaluation of the voltage phase-shift 67
2.7 Conclusion 68

3. Partial discharges measurement in non-sinusoidal regime 69

3.1 Introduction 69
3.2 Measurement setup and acquisition system 70
3.3 Measurements and analysis 73
3.3.1 Sinusoidal voltage waveforms 73
3.3.2 Disturbance generated by HV Switch and the DC supply 75
3.3.3 Square wave 50 Hz/350Hz at rise time 10 µs and 250 µs 77
3.4 Conclusion 86

4. Impact of Harmonics on Interpretation of PD Patterns 87

4.1 Introduction 89
4.2 Measurements setup 92
4.2.1 PD measurements with 3rd Harmonic component 95
4.2.2 PD measurements with 5th Harmonic component 98
4.2.3 PD measurements with 9th Harmonic component 101
4.2.4 PD measurements with 11th Harmonic component 104
4.3 Conclusions 107

5. Partial discharges localization on MV and HV cables 109

5.1 Introduction 109
5.2 PD pulse propagation and attenuation 110
5.3 Measurement on 500-m long unipolar MV XLPE cable 113

5.4 Measurement on EHV cable after the installation 122

5.5 Measurement on short MV cables 126

5.6 Conclusion 132

6. Analysis, recognition and classification of PD phenomena on field during HV test via Pry-Cam instruments 133

6.1 Introduction 133

6.2 PD measurements on HV system at 380 kV in Turkey 139

6.3 PD measurements on HV system at 400 kV in United Kingdom 147

6.4 PD measurements on HV system at 220 kV in Germany 159

6.5 PD measurements on HV system at 110 kV in Finland 168

6.6 PD measurements on HV system at 420 and 330 kV in Norway 174

6.7 PD measurements on HV system at 154 kV in Turkey 179

6.8 PD measurements on MV system at 20 kV in Taormina 184

6.8.1 Typical external noise acquired in MV secondary substations 187

6.8.2 Critical PDs activities acquired on MV components 189

6.8.3 Investigation of ozone levels caused by Partial Discharges 198

6.9 Conclusion 208

Bibliography 209

List of Figures

Figure 1-1. Electric field distribution in a dielectric material with cavity 21
Figure 1-2. PD Inception under sinusoidal voltage. 22
Figure 1-3. Typical Streamer discharges waveform 23
Figure 1-4. Typical Townsend discharges waveform 24
Figure 1-5. Typical Pitting discharges waveform 25
Figure 1-6. Phase Resolved PD Pattern 26
Figure 1-7. Defects on cables 27
Figure 1-8. Corona discharges effects 28
Figure 1-9. Corona discharges on 220 kV outdoor termination 29
Figure 1-10. Surface discharges effects 30
Figure 1-11. Low frequency surface discharges on 20 kV cable termination 31
Figure 1-12. High frequency Surface discharges on 20 kV cable termination 31
Figure 1-13. Internal discharges effects 33
Figure 1-14. Internal discharges on 20 kV cable termination 33
Figure 1-15. Metallic protrusion inside 380 kV cable termination 34
Figure 1-16. Floating mass effect on 380 kV cable termination 34
Figure 1-17. Pry-Cam™ instrument, and iPry-Cam acquisition and processing software 35
Figure 1-18. Pry-Cam™ Grids instrument and Wings sensor 36
Figure 1-19. Acquired PD pattern at different levels of gain and trigger setting 37
Figure 1-20. PD measurements analysis and possible results 39
Figure 1-21. Examples of symmetric PD Patterns 40
Figure 1-22. Examples of a-symmetric PD Patterns 40
Figure 1-23. Examples of steep waveforms and high frequency contents 41
Figure 1-24. Examples of slow waveforms and low frequency contents 41
Figure 2-1. PD Pattern compatible with surface discharge 49
Figure 2-2. PD Pattern compatible with corona discharge 49
Figure 2-3. Remote synchronization of PD measurements carried out with a portable device 50
Figure 2-4. Overhead transmission lines at 220 kV 56
Figure 2-5. Overhead transmission lines at 380 kV 56
Figure 2-6. Line equivalent model 57

Figure 2-7. Transmission line with three conductors per phase in delta tower at 380kV 59
Figure 2-8. Double three phase conductors in vertical tower at 220kV. 59
Figure 2-9. Voltage angle phase-shift compensation in PD measurement through Phase check and Look up tables.....60
Figure 2-10.PhaseCheck device 61
Figure 2-11. Simplified block diagram of the device.....61
Figure 2-12.Oscilloscope example of the measurement performed by the PhaseCheck.....61
Figure 2-13. Data Acquired by Two PhaseCheck on Line 3 at 380 kV 62
Figure 3-1. PD Measurement setup layout 70
Figure 3-2. PD Measurement setup at HV laboratory of Chalmers University 71
Figure 3-3. Pry-Cam Portable prototype 71
Figure 3-4. PD Pattern of Corona discharge at 12 kVpp sinusoidal voltage a) Corona PD pulse; b) Frequency spectrum of the PD pulse.....73
Figure 3-5. PD Pattern of Internal discharge at 14 kVpp sinusoidal voltage a) Internal PD pulse; b) Frequency spectrum of the PD pulse.....74
Figure 3-6. PD Pattern of Surface discharge at 2.2 kVpp sinusoidal voltage a) Surface PD pulse; b) Frequency spectrum of the PD pulse.....74
Figure 3-7. PD Pattern on Motor Stator at 4,8 kVpp sinusoidal voltage a) PD pulse; b) Frequency spectrum of the PD pulse.....74
Figure 3-8. Identification pulses generated by the HV switch and DC supply 75
Figure 3-9. Identification in time (a) and frequency (b) pulses generated by HV switch 76
Figure 3-10. Identification in time (a) and frequency (b) pulses generated by the switched control circuit.....76
Figure 3-11. Identification in time (a) and frequency (b) of the PD pulse of twisted pair specimen with square wave 50Hz at rise time 250 µs.....76
Figure 3-12. Corona PD pattern applying a square waveform of 50 Hz with rise time 250 µs. 78
Figure 3-13. Corona Single side PD pulses and frequency spectrum applying a square wave a) 50 Hz with rise time 10µs b) 350 Hz with rise time 10µ; Corona Double side PD pulses and frequency spectrum applying a square wave c) 50 Hz with rise time 250µs; d) 350 Hz with rise time 250µs. 78

Figure 3-14. Internal PD pattern applying a square wave of 50 Hz with rise time 250 µs. Identification in time (a) and frequency (b) Internal PD applying a square wave of 350 Hz with a rise time of 250µs. 79
Figure 3-15. Internal Partial discharge applying a square wave of 50 Hz with a rise time 10µs superimposed on the voltage remnants 80
Figure 3-16. Comparison of cavity PD activity during tests with square waves of rise times 10 µs and 250 µs (50 Hz) and sinusoidal wave of 50Hz. 80
Figure 3-17. Compared twisted pair PD patterns with square wave 350 Hz at rise time 10 µs and 250 µs 81
Figure 3-18. Twisted pair PD pulses and frequency content applying a) a square wave 350 Hz with rise time 10; b) a square wave 350 Hz with rise time 250 µs 82
Figure 3-19. Comparison of twisted paid PD pattern with square wave 350 Hz at rise times 10 µs and 250 µs. 82
Figure 3-20. Comparison of motor stator PD activity during PASPD tests with square waves of rise times 10 µs and 250 µs (50 Hz) and sinusoidal wave of 50Hz. 83
Figure 3-21. Comparison of motor stator PD activity during STOPD tests with square waves of rise times 10 µs and 250 µs (50 Hz) and sinusoidal wave of 50Hz. 83
Figure 3-22. PD pattern on motor stator applying a 350 Hz square wave with a rise time of 10 µs 84
Figure 3-23. Stator Motor PD pulses and Frequency spectrum applying a square wave of a) 50 Hz with rise time 10µs; b) 350 Hz with rise time 10µs; c) 50 Hz with rise time 250µs; d) 350 Hz with rise time 250µ 85
Figure 4-1. Defect in MV cable specimen 92
Figure 4-2. Measurement setup: arbitrary waveform generator, transformer and cable under test 92
Figure 4-3. Pry-Cam Portable placed on cable close to the defect 93
Figure 4-4. PD Pattern acquired at 5.8 kV of sinusoidal voltage - 94
Figure 4-5. Re-synch function: PD pattern not synchronized, Re-synch toolbox and synched PD pattern 94
Figure 4-6. Analysis of the acquired PD pulse at 5% of 3rd harmonic and phase angle 0° 96
Figure 4-7. Analysis of the acquired PD pulse at 10% of 3rd harmonic and phase angle 90° 96
Figure 4-8. Analysis of the acquired PD pulse at 20% of 3rd harmonic and phase angle 180° 96

Figure 4-9. Analysis of the acquired PD pulse at 5% of 5th harmonic and phase angle 0° 99
Figure 4-10. Analysis of the acquired PD pulse at 10% of 5th harmonic and phase angle 90° 99
Figure 4-11. Analysis of the acquired PD pulse at 20% of 5th harmonic and phase angle 180° 99
Figure 4-12. Analysis of the acquired PD pulse at 5% of 9th harmonic and phase angle 0° ..102
Figure 4-13. Analysis of the acquired PD pulse at 10% of 9th harmonic and phase angle 90° 102
Figure 4-14. Analysis of the acquired PD pulse at 20% of 9th harmonic and phase angle 180° 102
Figure 4-15. Analysis of the acquired PD pulse at 5% of 11th harmonic and phase angle 0° 105
Figure 4-16. Analysis of the acquired PD pulse at 10% of 11th harmonic and phase angle 90° 105
Figure 4-17. Analysis of the acquired PD pulse at 20% of 11th harmonic and phase angle 180° 105
Figure 4-18. Influence of harmonic component on PD amplitude 107
Figure 5-1. Reflection phenomenon: incident (i_i), transmitted (i_T) and reflected (i_R) wave. .110
Figure 5-2. PD Pattern from Omicron™ acquisition system 113
Figure 5-3. Defect on the cable sheath in the 70m section 114
Figure 5-4. Diagram of measuring points 114
Figure 5-5. Point C, external defect: PD Pattern, waveform and frequency content of the pulses 116
Figure 5-6. Point B, 1 m to the left of the external defect: PD Pattern, waveform and frequency content of the pulses 116
Figure 5-7. Point D, 0.5 m to the right of the external defect: PD Pattern, waveform and frequency content of the pulses 117
Figure 5-8. Point E, 1.5 m to the right of the external defect: PD measurement via Pry-Cam™ at 25 kV (maximum amplitude 34 mV).....117
Figure 5-9. Point D - Pulse Waveform 118
Figure 5-10. Point E - Pulse Waveform 118
Figure 5-11. PDs source located in 70 meter of cable section 118
Figure 5-12. Defect propagation on cable layers 120
Figure 5-13. Conductor Shield Defect in a Hot Oil Test 121

Figure 5-14. Photographic analysis of inner semicon defects 121
Figure 5-15. Visual analysis of inner semicon defects 121
Figure 5-16. Diagram of measuring points along the EHV 122
Figure 5-17. PDs source located in joint SXJ 124
Figure 5-18. Circuit under test 127
Figure 5-19. Pry-Cam portable placed on left side of the joint 129
Figure 5-20. Pulse Waveform - Left Side Joint 130
Figure 5-21. Pulse Waveform - Right Side Joint 130
Figure 6-1. New submarine cables route by Prysmian Group 133
Figure 6-2. Submarine cables for offshore wind farm 134
Figure 6-3. AC resonant test system for on-site testing of extruded HV cables 135
Figure 6-4. Block diagram of AC resonant test system for on-site testing of extruded cables 135
Figure 6-5. Electrical diagram of the resonant test system 137
Figure 6-6. Layout of the 380 kV cable line 139
Figure 6-7. Pry-Cam Portable placed on cable and Pry-Cam Grids connected on the joint bay 140
Figure 6-8. RSKF - Variable resonant test system 141
Figure 6-9. Resonant test system with reactors in series during the commissioning 142
Figure 6-10. External noise produced by the frequency converter 143
Figure 6-11. Outdoor termination EU side: PD pattern, waveform and frequency content of the pulses 145
Figure 6-12. Joint bay European side: PD pattern, waveform and frequency content of the pulses 145
Figure 6-13. Joint bay Asian side: PD pattern, waveform and frequency content of the pulses 146
Figure 6-14. Outdoor termination Asian side: PD pattern, waveform and frequency content of the pulses 146
Figure 6-15. AC resonant system connected to the GIS switchgear system 147
Figure 6-16. Underground cables at 400 kV and GIS Termination 147
Figure 6-17. Wing Sensor placed on Cable before starting test HV test 148

Figure 6-18. External Noise – PD Pattern, waveform and Frequency content of the acquired pulse 148
Figure 6-19. Pry-Cam Wings installed on the earth connection of the GIS cable sealing end. 150
Figure 6-20. Acquired External Noise on the ground connection of the GIS cable sealing end 150
Figure 6-21. Representative pattern acquired during the first day of HVAC test 151
Figure 6-22. Acquire PD Pattern at 0° of phase offset 152
Figure 6-23. Acquired PD Pattern at 90° of phase offset 152
Figure 6-24. PD Pattern, pulses waveform and frequency content during the trip 155
Figure 6-25. The effect of the surface discharge on the GIS Test bushing 155
Figure 6-26. Layout of the measurements performed on GIS Switchgear 156
Figure 6-27. Pry-Cam Portable placed on the earth connection of the GIS switchgear. 156
Figure 6-28. Layout of the 220 kV cable line 159
Figure 6-29. Sensitivity check of the Wing Sensor on the outdoor termination 160
Figure 6-30. Sensitivity check performed on outdoor termination at sub-station 160
Figure 6-31. Propagation of the Corona effect 163
Figure 6-32. Acquired PD Pattern on the outdoor termination 163
Figure 6-33. Acquired PD Pattern on Joint Bay 1 164
Figure 6-34. Acquired PD Pattern on Joint Bay 2 164
Figure 6-35. Acquired PD Pattern on Joint Bay 3 164
Figure 6-36. Pry-Cam portable placed on cables near the GIS terminations. 168
Figure 6-37. Pry-Cam portable placed on cross bonding leads inside pillar 168
Figure 6-38. Layout of the measurement points 169
Figure 6-39. Cross-bonding and ground connection of the sectionalized joint 170
Figure 6-40. Un-synced PD Pattern and Resynch function box 170
Figure 6-41. Resynced PD Pattern at 50 Hz 171
Figure 6-42. First PD phenomena: PD pattern, waveform and frequency content of the pulses 171
Figure 6-43. Analysis of the acquired PD Pattern on Phase S and Phase T 172
Figure 6-44. External synch Unit 173
Figure 6-45. Pry-Cam portable placed on outdoor terminations 174

Figure 6-46. Analysis of the acquired PD Pattern on Phase R 175
Figure 6-47. Analysis of the Acquired PD Pattern on Phase S 176
Figure 6-48. Analysis of the acquired PD Pattern on Phase T 176
Figure 6-49. Analysis of the acquired PD Pattern on Phase R 177
Figure 6-50. Analysis of the acquired PD Pattern on Phase S 177
Figure 6-51. Analysis of the acquired PD Pattern on Phase T 178
Figure 6-52. Layout of the 154 kV cable line 179
Figure 6-53. Pry-Cam Portable placed on cable close to the GIS and outdoor termination .. 179
Figure 6-54. Acquired PD Pattern on GIS termination by Omicron System 180
Figure 6-55. Acquired PD Pattern on GIS termination by Pry-Cam Portable 181
Figure 6-56. Measurements performed on GIS Termination with Synch on Phase A 182
Figure 6-57. Acquired PD Pattern on Outdoor termination by Pry-Cam Portable 183
Figure 6-58. Pry-Cam Portable placed on the cables and MV transformer terminations 184
Figure 6-59. Pry-Cam Portable placed on MV close to the switchgear 184
Figure 6-60. Pry-Cam Portable placed on the magazine inspection window 185
Figure 6-61. Measurement Points and acquired PD Pattern 189
Figure 6-62. Substation A - Acquired PD Pattern through inspection window 190
Figure 6-63. Substation B - Measurement acquired on cable 190
Figure 6-64. Measurements performed on Transformer Termination 192
Figure 6-65. Analysis of the acquired PD pattern on transformer terminations 192
Figure 6-66. Analysis of the acquired PD pattern after replacing of the transformer terminations 193
Figure 6-67. Measurement performed on cables close to the switchgear box 194
Figure 6-68. Analysis of the acquired PD pattern on cables 194
Figure 6-69. Analysis of the acquired PD pattern after replacing of the switchgears box 195
Figure 6-70. Comparison of the acquired PD pulses before and after 195
Figure 6-71. Pry-Cam Portable placed on cables 196
Figure 6-72. Analysis of the acquired PD pattern before the cleaning of cable terminations 196
Figure 6-73. Analysis of the acquired PD pattern after the cleaning of cable terminations ... 197
Figure 6-74. Ozone molecular (O_3) 198
Figure 6-75. Ozone formation due to Corona discharge 199
Figure 6-76. Case study 1 - Acquired PD Pattern 203

Figure 6-77. Case study 2 - Acquired PD Pattern 203
Figure 6-78. Case study 3 - Acquired PD Pattern 204
Figure 6-79. Case study 4 - Acquired PD Pattern 204
Figure 6-80. Case study 5 - Acquired PD Pattern 205
Figure 6-81. Case study 6 - Acquired PD Pattern 206
Figure 6-82. Case study 7 - Acquired PD Pattern 206

List of Tables

Table 2-1. ACSR transmission line data 54
Table 2-2. Cable material properties 54
Table 2-3. Cable line data 54
Table 2-4. Overhead transmission line simulation results 55
Table 2-5. Cable line simulation results 55
Table 2-6. Characteristics of overhead transmission lines 57
Table 2-7. Line parameters 57
Table 2-8. Simulation results: line parameters manual data entry 58
Table 2-9. Simulation results: line parameters geometric layout 59
Table 2-10. Comparison of the results between PhaseCheck and simulations (line parameters manual data entry) 64
Table 2-11. Comparison of the results between PhaseCheck and simulations (line parameters geometric layout) 65
Table 2-12. Comparison of the results between simulations and experimental measures 66
Table 2-13. Look up tables for the evaluation of the voltage phase-shift 67
Table 4-1. Influence of the 3rd harmonic on PD measurements 95
Table 4-2. Acquired PD Patterns and Voltage waveform with 3rd harmonic 97
Table 4-3. Influence of the 5th harmonic on PD measurements 98
Table 4-4. Acquired PD Patterns and Voltage waveform with 5th harmonic 100
Table 4-5.Influence of the 9th harmonic on PD measurements 101
Table 4-6. Acquired PD Patterns and Voltage waveform with 9th harmonic 103
Table 4-7. Influence of the 11th harmonic on PD measurements 104
Table 4-8. Acquired PD Patterns and Voltage waveform with 11th harmonic 106
Table 5-1. Measurements on MV cable: pd patterns, waveform and frequency content of the acquired pulses 119
Table 5-2. Reversal PD pattern phenomenon 123
Table 5-3. Measurements on EHV cable: PD Patterns, waveform and frequency content of the acquired pulses 125
Table 5-4. Circuit 1 - PD Patterns, the waveform and FFT analysis of the pulses. 128

Table 5-5. Measurements on Joint: PD Patterns, the waveform and FFT analysis of the pulses 129
Table 5-6. Circuit 2 - PD Patterns, the waveform and FFT analysis of the pulses 131
Table 6-1. PD measurements on Circuit North 144
Table 6-2. Acquired External Noise at different time length levels 149
Table 6-3. Analysis of the acquired PD Patterns during the HV Test 153
Table 6-4. Analysis of the acquired PD Patterns during the HV Test 154
Table 6-5. Analysis of the acquired PD Patterns on different sections of the GIS switchgear 157
Table 6-6. Acquired pulses by Pry-Cam Grids during the sensitivity check on the outdoor terminations 161
Table 6-7. Acquired Pd Pattern on platform sub-station 165
Table 6-8. Analysis of the Corona discharge during the Soak test on Phase Red of the Outdoor Termination 166
Table 6-9. Acquired PD Pattern on HV line at 110 kV 169
Table 6-10. Typical external noise due to the transformer saturation effect 187
Table 6-11. Typical Corona discharges in MV distribution network 188

Abstract

In this thesis, different challenges for various applications of a wireless PD detection instrument are discussed and relevant solutions are proposed. The main purpose is to assess the applicability of such technology both in current HV and MV power systems as well as in future applications for smart grids. The main challenges for these types of diagnostic systems are the following:

- voltage synchronization of Phase Resolved PD pattern;
- PD recognition under non-sinusoidal voltage waveforms;
- PD recognition under sinusoidal voltage superimposed harmonics;
- PD recognition in laboratory and in real world situations under noise and other source of disturbance.

Thanks to the collaboration with Terna, it was possible to carry out several analysis and experimental measurements on HV transmission lines to assess the problems that may be arise when PD measurements is carried out without access to the local voltage signal. In this case, the voltage signal can be taken from a remote location where access to voltage measurement is possible and the voltage phase-shift caused by the operating transmission line must be assessed.

In the second part of the study, the problems arising from PD measurements performed in non-sinusoidal regime to recreate the stresses that may be present in future networks following the presence of AC/DC conversion systems. This topic was addressed thanks to the collaboration with Chalmers University of technology in Gothenburg, SE.

A Further investigation on superimposed harmonic voltage effects on PD measurements has been discussed. The aim of this research was to understand and evaluate the impact of harmonics on partial discharge behaviour, in particular on the PD measurements by means the Pry-Cam portable instrument, and on the PD Pattern acquisition process. The results showed that various harmonic, 3^{rd}, 5^{th}, 9^{th} and 11^{th} superimposed on the fundamental sinusoidal waveform have a significant impact on PD amplitude and PD pattern shapes. The presence of harmonics components can significantly influence the acquisition of the PD pattern and also may arise synchronism problems during the measurements.
In order to assess the capability of the portable instruments of detecting the precise location of the PDs, different comparative tests have been carried out performing measures both with

standard fixed PD measurement system as well as with the portable one. Depth investigation of peculiar experimental cases carried out at the High Voltage Laboratory of Prysmian S.p.a. in Milan (Italy) on a MV and an HV cable are described. To complete this part, a wide description of several exemplary measurements carried out with a portable instrument (Pry-Cam) in several sites is here given. Measures were carried out in Medium and High voltage networks. In detail, it was possible to analyze various noise phenomena and the methodologies, used for correctly assessing the phenomenon under study, are described.

Thanks to Prysmian Electronics, it was possible to perform PD measurements in several European and Extra-European countries during HV testing for commissioning of new cable interconnections at different voltage levels. In addition, the study was also extended to the analysis of PD phenomena in MV distribution networks present in the Sicilian territory. The study gave the opportunity to investigate the main problems encountered in cable lines and MV accessories. In this case, it was also possible to conduct a study on the correlation of ozone levels and the PD sources in MV cabins.

Acknowledgments

I would like to express my sincere appreciation to my tutor Prof. Eleonora Riva Sanseverino, for your constant guidance and encouragement, without which this work would not have been possible. For your endless support and precious advices, I am truly grateful. I am also grateful to my co-tutor Prof. Pietro Romano for his valuable advice and support during tests carried out at the LEPRE lab.

A Special thanks goes to Roberto Candela for believing in me and given the opportunity to become part of the Prysmian Electronics group. In this regard, I can not help but to thank Vincenzo Li Vigni for his valuable advice, teaching and support on field during partial discharge measurements and commissioning. Also regarding the commissioning, I can not forget to thank Giuseppe Fiscelli. In any case, I would like to thank all the guys of Prysmian Electronics for welcoming me like a big family. Thank you guys.

I cannot forget Stefano Franchi, Prof. Giovanni Mazzanti, Ivan Troia and Simone Giannini for the established collaboration and the great work done.

I would like to thank all my friends and life companions Giuseppe Schettino, Michele Fricano, and Marcello Santoro, who have supported and strengthened me during these three years. Thanksgiving particular goes to Prof. Fabio Viola and Prof. Rosario Miceli for their valuable advice and our endless chats.

I thank my family that has always been close to me, supported and encouraged during my studies and achievements. Thanks papà, mamma e Roberta.

Last but not least, I thank my wonderful wife Maria Grazia for her tireless patience, unconditional love and for supporting me in this challenging period of my life. Thank you for everything you are and that you are giving to me.

1. Partial Discharges: theory and classification

1.1. Introduction

The partial discharge (PD) is an electrical discharge that only affects a part of the dielectric existing between two conductors at different voltage. The phenomenon is introduced at microscopic level and affects only a part of the dielectric existing between live parts. Such discharges injure the dielectric material and are responsible for the aging of the material. Partial discharges are in general a consequence of local electrical stress concentrations in the insulation or on the surface of the insulation. Generally, such discharges appear as pulses having a duration of much less than 1 μs [1].

PDs are a consequence of local breakdown either as a result of:

- an electric field increase within or on the surface of the insulation;
- a region of low breakdown electric field.

PDs appear as individual events of very short duration and are always accompanied by emissions of light, sound and heat, as well as electromagnetic pulses and often result in chemical reactions [2].

Defects typically consist of pointed ends of live parts, sharp metal tips or edges, various types of micro-cavity that are generated during the production process (vacuoles in a solid insulation or in gas bubbles in the insulating liquids); such defects may be the cause of local concentrations of electric field resulting in exceeding the limit field value and consequently creating PDs. Generally, partial discharge develops with a mechanism such that it does not adversely affect the component in a normal high voltage test procedure. Although it only involves small amounts of energy, it results in a slow and progressive deterioration of the dielectric, which can lead to the final breakdown of the component at rated operating voltage. Therefore, the degradation phenomena that occur in dielectrics due to the presence of partial discharges cause a lifetime reduction of any component. This lifetime reduction is dependent on:

- the nature of the insulating materials;
- the procedures of workmanship;
- the type of electrical stress;
- the environmental condition;
- other operating conditions.

The partial discharge measurement provides a valid means of checking the health status of the electrical components and detects defects that would otherwise lead to a dielectric breakdown in the future time. Partial discharge measures are common practice for type and acceptance tests and the operating measures are normally provided for determining weaknesses of the components before irreversible damage can occur. Usually the partial discharges measurements are performed both on operating systems as well as during the production process of electric appliances and components: on MV and HV operating systems, on finished products such as cables, terminals and cable joints, insulators, insulating materials in the form of specimens as well as on electrical machine like transformers and generators.

1.2 Partial discharges physic

In order to understand the process of partial discharges formation, reference will be made to the most significant case of discharges into a cavity. The gaseous inclusions in dielectric materials are the main venue of the partial discharge phenomenon and therefore constitute the main cause of deterioration of high voltage electrical components.
A partial discharge can occur if two conditions are satisfied:

- The presence of free electrons inside the cavity;
- The electric field within the cavity must exceed the inception field (the minimum breakdown value)

A simple description of the phenomenon can be made by considering a dielectric specimen containing one cavity to which voltage Eext is applied through two electrodes (Figure 1-1).

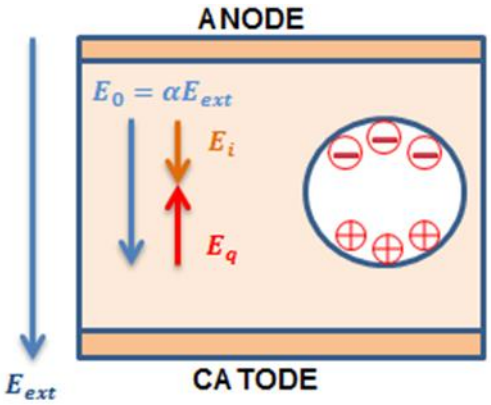

Figure 1-1. Electric field distribution in a dielectric material with cavity

Due to the difference between the dielectric constants ε and ε_0, respectively of the insulating material and of the gas contained in the cavity, the average electric field E_0 in the vacuum is greater than the electric field Eext in the surrounding dielectric and proportional to a factor α dependent on the geometry of the system ($E_0=\alpha \cdot Eext$). The presence of the field E_0 causes the separation between opposite charges inside the cavity. The resulting internal field E_i is equal to the sum between the field applied to the cavity E_0 and the local field due to charges separation E_q. Increasing the applied voltage, Ei can overcome the dielectric strength of the gas and it can give rise to a partial discharge.
Referring to the first half-period, in correspondence of each discharge, E_q increases very quickly, E_i decreases below the value of extinction field and the discharge extinguishes. After

a discharge, the local field decreases because of the recombination phenomenon of positive and negative accumulated charges, or due to drifting on the cavity surface. If E_i increases over the inception field and a free electron is available, another partial discharge can occur (Figure 1-2).

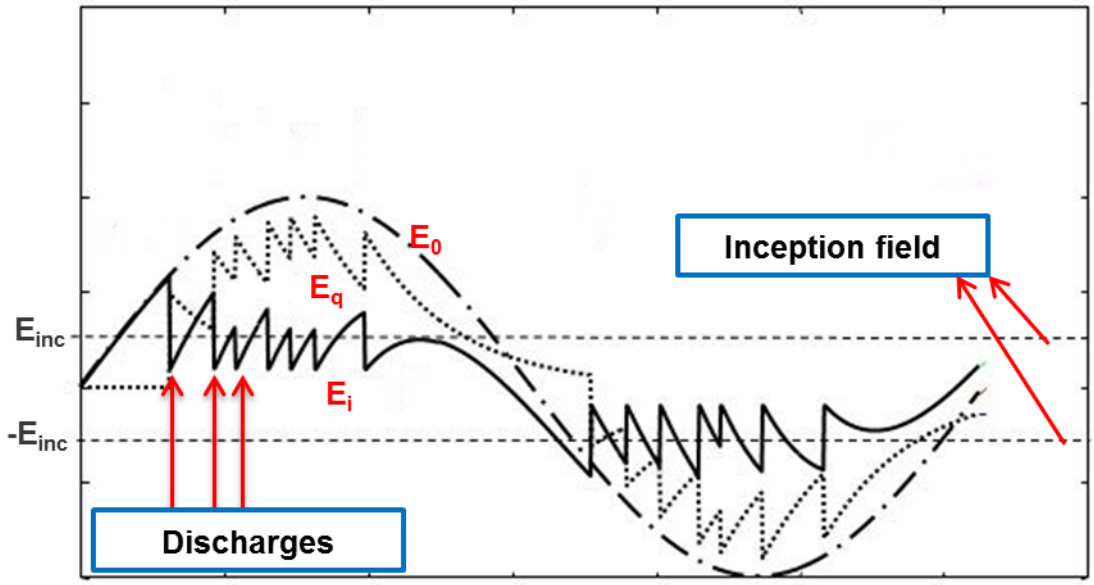

Figure 1-2. PD Inception under sinusoidal voltage.

The minimum breakdown voltage value (or ignition voltage) depends on the size of the cavity, gas trapped, temperature and pressure inside the cavity.

The phenomenon implies the transfer of charge between the cavity walls along the direction of the applied field, their redistribution inside and the emergence of an opposite field to the external one, Eq.

If the characteristics of the cavity are such that they can give rise to a PD, when an electron is accelerated by the electric field, due to collisions within the cavity, an exponential growth of the electronic population may appear. In a few nanoseconds, a discharge channel is formed within the cavity and at the same time there is a reduction of the electric field.

The phenomenon stops when the internal field Ei = E0+Eq reaches a value under which no electronic avalanche can be generated, so the discharge extinguishes.

When the electric field goes below a limit value, the channel disappears, leaving a large amount of positive and negative charge moving into the cavity and towards the internal surface of the cavity for drift motion induced by the field still present.

The partial discharge phenomenon in cavities evolves according to the duration of the discharge activity; in particular, three successive stages can be identified [3]:

- Streamer discharge: this is the stage at the beginning of the discharge activity and is characterized by discharge with a steep front and short duration. The Streamer-like discharge is very fast and its duration is hundreds of picoseconds up to a few nanoseconds (Figure 1-3). The discharges ignite in groups with a very short time period between consecutive discharges (nanoseconds or even a fraction of a nanosecond). The magnitude of a single discharge is approximately constant for a given void height.
  In the cavity, the discharges are distributed spatially on the surface and ignite in rapid succession. Each single discharge consists of a narrow channel namely streamer.

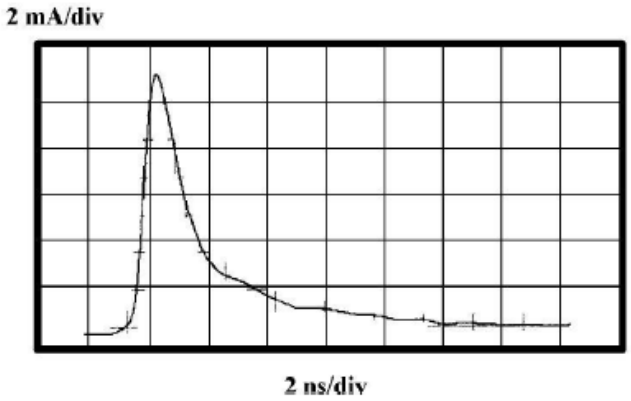

Figure 1-3. Typical Streamer discharges waveform

Streamer discharge features:

- Low rise time and decay time (fast discharge)
- Most energetic and fast events (easily detectable on field)
- High frequency content
- High amplitude

- Townsend discharge: is the stage of aging that is already advanced (after 10 to 60 minutes from streamer discharge process) in which the current pulses are characterized by a longer time duration and proportional to the thickness of the cavity. The discharge mechanism changes. The formation of the discharge is now a slow process and the discharges are called “Townsend-like”. The pulses have a long rise time as several tens of nanoseconds and may have a "landing" on the falling edge with a duration that can reach the order of ten microseconds (Figure 1-4). Contrary to the streamer-like discharges, the magnitude of the single Townsend-like discharges is widely scattered. During this stage, due to the oxidation processes crystals of oxalic acid are formed. These crystals tend to grow with the ongoing discharge activity and they lead to the pitting discharge.

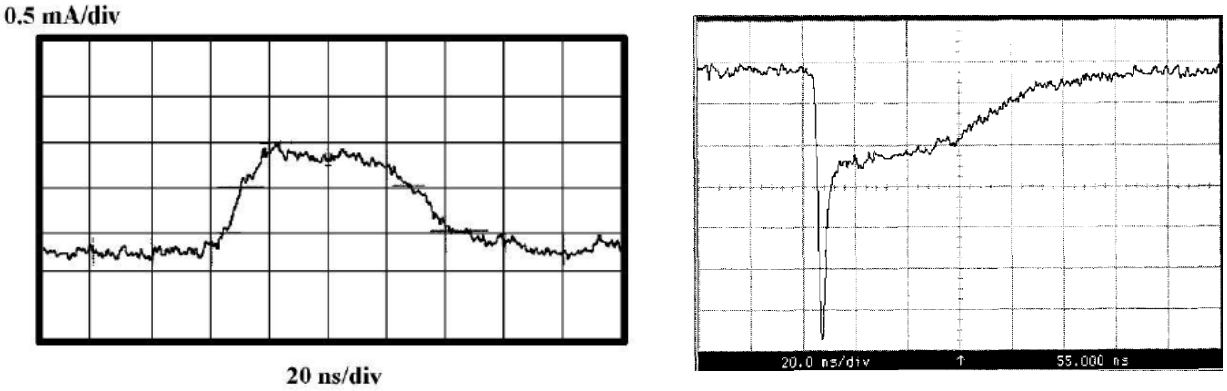

Figure 1-4. Typical Townsend discharges waveform

Townsend discharge features:

- High rise time and decay time (slow discharge);
- Less energetic and detectable;
- Sometimes it can have pronounced peaks;
- Low frequency content;
- Low amplitude.

- Pitting discharges: is the final stage of partial discharge activity, which is initially established at the same time as the Townsend discharges. This stage is characterized by intense degradation of the dielectric leading to the formation of craters (pits). Pitting discharges are characterized by a small pulse amplitude and a high repetition rate, up to several discharges per microsecond (Figure 1-5). The rise time of this discharges is comparable with the streamer pulses, but the decay time is considerably longer, typically 10 to 15 ns.

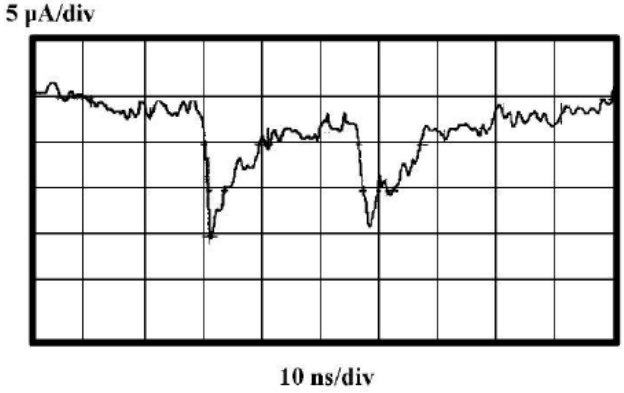

Figure 1-5. Typical Pitting discharges waveform

Pitting discharge features:

- Multiple Streamer types;
- Rise time comparable with the Streamer pulses and high decay time;
- The amplitude is relatively small;
- Low frequency content;
- High repetition rate: in order of several tens per microsecond;
- Less energetic and detectable, probably occurring in the final stage of degradation.

Since this type of discharge phenomenon occurs downstream of a process of early aging and degradation of the dielectric material, the amplitude of the PD pulse is so small that it is not uncommon for a system to appear PD free before the breakdown.

1.3 Phase Resolved Partial Discharge Pattern

To evaluate the presence and critically of partial discharge activity in MV and HV components, the analysis of the Phase Resolved PD Pattern (PRPD) is the first step in what follows, the PRPD will be referred to as 'PD pattern'. In the PD pattern, the amplitude of the acquired pulses is graphed in the vertical axis of the plot, while on the horizontal axis, the phase angle at which the PD pulse occurs is represented. As reported in Figure 1-6, each dot in a PD pattern thus represents a PD pulse and its occurrence phase angle. To obtain a correct PD pattern, it is necessary that the measurement system is correctly synchronized with the frequency of the electric system (50 or 60 Hz).

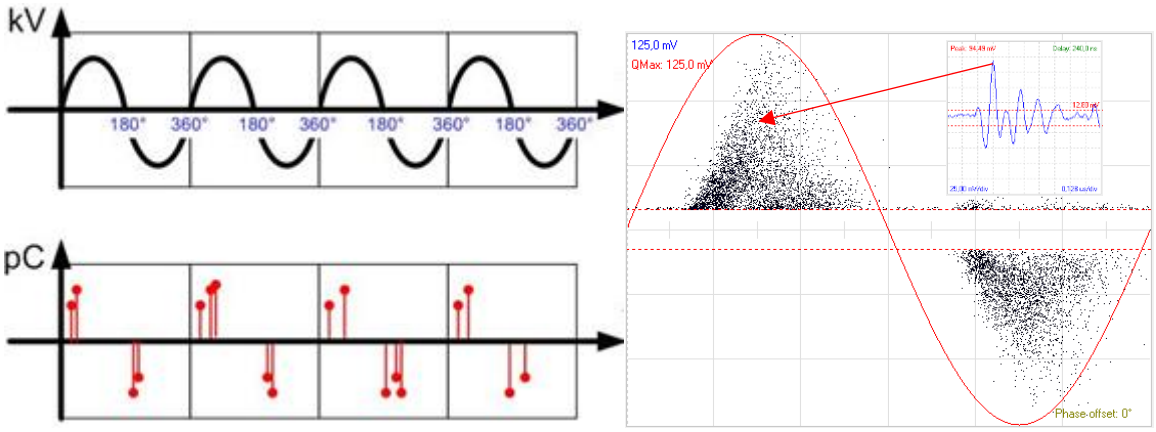

Figure 1-6. Phase Resolved PD Pattern

Based on the type of partial discharges, different types of PD patterns can be generated. Basically, the analysis of the shape of PD pattern, through the PD amplitude and phase angle, allows distinguishing the different types of defects that can be present in the components under test. However, to understand the complete PD phenomenon it is necessary to analyse different parameters such as the waveform and frequency content of the PD pulses as well as the repetition rate.

1.4 Partial discharges classification

Depending on the type of the insulation and the trigger mode partial discharge can be divided in four classes:

- Corona discharges in gases surrounding metallic parts;
- Surface discharge on the insulation surface;
- Internal discharges in the voids or cavities;
- Floating mass discharges;

The main defects that favour the presence of partial discharges are:

- Voids within solid insulation;
- Contamination by particles;
- Irregularities (e.g. sharp points);
- Gas bubbles in liquid insulation;
- Floating particles in gas insulation;
- Mechanical defect or damage in insulation materials.

Figure 1-7. Defects on cables

The presence of cavities in solid dielectric materials is the main cause of partial discharges and constitutes the main cause of deterioration of HV and MV electrical components.

1.4.1 Corona discharge

The Corona effect is a partial electric discharge near conductors, insulating elements, due to an air ionization process caused by a high electric field.
This process is the cause of:

- Materials corrosion generation (ozone production);
- Light emitted mainly in the UV spectrum (not visible to the human eye);
- Radio interference;
- Audio Noise;
- It produces only small amounts of heat.

Corona effect can be a problem because:

- Degradation of Polymer Insulators;
- Creates corrugated surfaces in metal or concrete shells of ceramic insulators;
- Indicates a possible break;
- Indicates an incorrect installation;
- Indicates the need for washing;
- Indicates the possibility of training electrical arches.

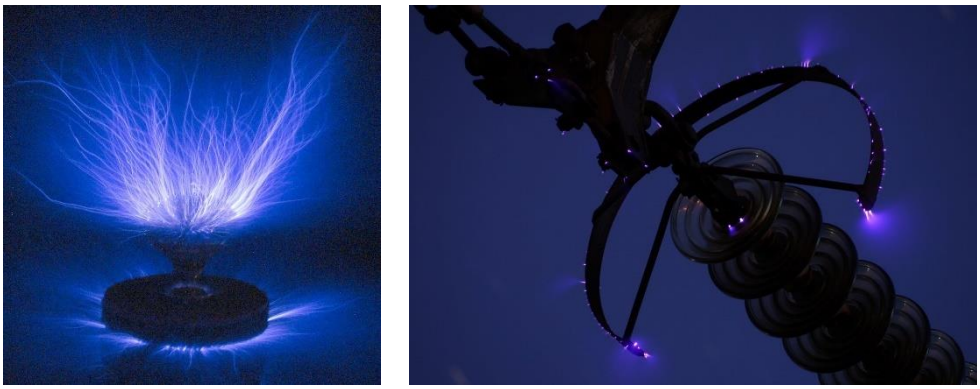

Figure 1-8. Corona discharges effects

The corona discharges occur at points and generally in strongly divergent fields. The Corona in air generates ozone which interacting with the polymeric insulation produces nitrogen, which in turn combined with the water vapour can corrode the metal surfaces of the conductors, thus forming a conductive deposit that leads to full discharge. Particularly critical is the presence of Corona discharges in SF6 insulation in which the products of decomposition of SF6 after a

discharge can corrode the dielectric surfaces of the system, while in oil the same phenomenon of Corona discharges leads to a decrease of the dielectric strength.

Corona discharges are also the most important source of disturbances during partial discharge tests, so it is always advisable to avoid the presence of sharp elements in the measuring area and it is always advisable to always overcome every possible edge or protrusion.

Features of the Corona discharges:

- PDs occur in correspondence of the maximum value of the applied voltage;
- Discharges generally cluster in an amplitude range over the trigger level;
- Frequency spectrum lower than 40 MHz;
- Middle-fast discharges.

In Figure 1-9 the PD Pattern, pulse waveform and frequency content of the Corona discharge on 220 kV outdoor termination is reported.

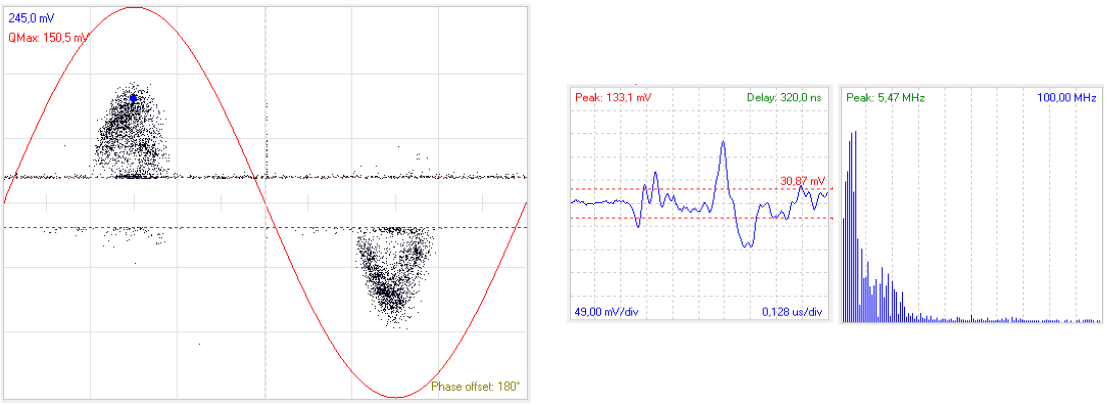

Figure 1-9. Corona discharges on 220 kV outdoor termination

1.4.2 Surface discharge

Surface discharges can occur along the interfaces between different dielectric materials, if there is a high component of the field parallel to the surface. Once the discharge is produced, the variation in the electric field distribution leads to the extension of the discharge to areas other than the initial one. The phenomenon of surface discharges can thus cause deterioration and electrical trees of the dielectric surface and lead to full discharge.

Figure 1-10. Surface discharges effects

This phenomenon damages the surface of the dielectric by thermal effect and the formation of chemical compounds such as nitric acid and ozone which can lead to erosion of the dielectric surface. Depending on the trigger mode the surface discharge can be classified in low frequency (LF) and high frequency (HF) discharges.

The *low frequency Surface discharge* generally occur on the external surface of the electrical components. This type of discharge is characterized by slow pulses and low frequency content. Mainly, this type of PD phenomenon is caused by the presence of humidity or by the accumulation of dust or dirt on outdoor components.

Features of low frequency surface discharges:

- PDs mainly occur in correspondence of zero-crossings of the applied voltage;
- Frequency spectrum lower than 20-30 MHz
- Slow pulses and high decay time.

In Figure 1-11 the PD Pattern, pulse waveform and frequency content of the low frequency Surface discharges on 20 kV cable termination is reported.

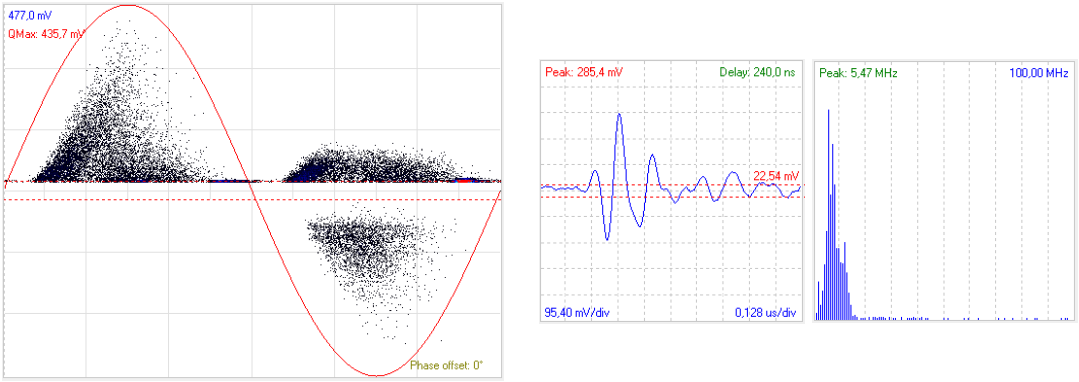

Figure 1-11. Low frequency surface discharges on 20 kV cable termination

The *high frequency Surface discharge* can occur on the inner surface of the components between a conductor material and the adjacent dielectric or semi-conductive layer. This type of discharge, often similar to an internal discharge, is characterized by fast pulse and high frequency content. This type of discharge generally is caused by mechanical defects due to installation errors or defects in production of the electrical components.

Features of high frequency surface discharges:

- PDs mainly occur in correspondence of zero-crossings of the applied voltage;
- Frequency spectrum lower than 40-50 MHz;
- Fast pulses and low decay time.

In Figure 1-12 the PD Pattern, pulse waveform and frequency content of the high frequency Surface discharges on 20 kV cable termination is reported.

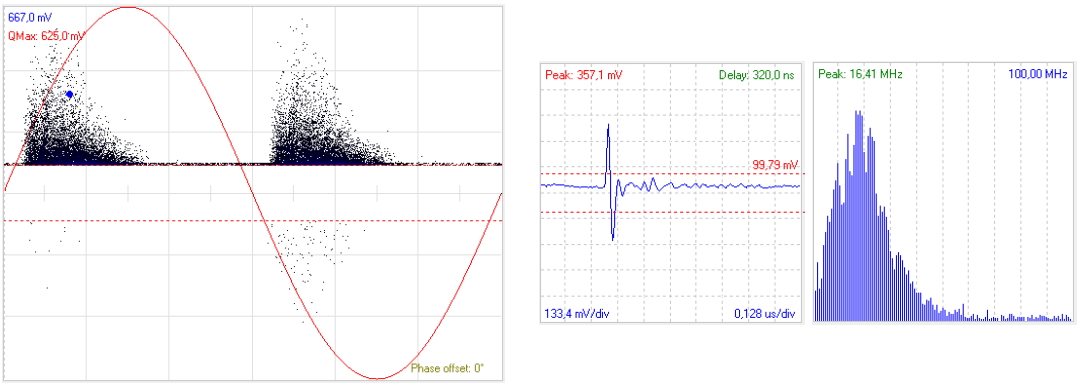

Figure 1-12. High frequency Surface discharges on 20 kV cable termination

1.4.3 Internal discharge

Internal discharges constitute in most cases the main cause of life reduction of a component. Their origin is to be found in the presence of small cavities in the insulation material (void). Such gaseous inclusion may be formed during the manufacturing processes or develop as a result of mechanical stress, electrical stress or thermal cycles.

Inside the vacuoles, air or gases are characterized by a dielectric constant ε that is lower than the dielectric constant of the solid insulation: the electric field Ei in the cavity is thus greater than E_0 in the surrounding dielectric; it can overcome the dielectric strength of the gas and give rise to a discharge that neutralizes some of the surface charges on the opposite surfaces of the vacuum.

Once the discharge is ended, the field in the cavity is the result of the applied outer field and the field oriented in the opposite direction due to the surface charge, so the field distortion due to the presence of the remaining surface charge can cause the subsequent discharge to occur in a different position and for a different value of the supply voltage.

For example, when the supply voltage is reversed, the associated external gets the same direction and, when summing up to the Ei field due to the presence of the remaining surface charge, the resulting field may cause a discharge at a voltage that is lower than the initial one.

The treeing phenomenon (very important in cable technology with extruded polyethylene insulation) is also an internal discharge phenomenon and develops due to the local elevation of the electric field at metal protrusions. In most cases, the process is destructive and leads to full a discharge over a much shorter period than the one before its occurrence.

'Treeing' are ramifications that develop from conducting particles or cavities into a solid insulator; the phenomenon leads to the formation of a main cable trunk and numerous ramifications.

The time needed to generate a branched discharge channel depends on the value of the applied voltage and may take hours, weeks or even years. The property of gases and liquids to penetrate solid insulating materials indicates that they are equipped with a "canal" microstructure. Normally, these channels and cavities contain gases with a dielectric strength that is lower than that of the material; when the discharge begins, the channels and vacuums internal surface become conductive causing a reduction in the voltage drop along the channel.

During the discharge process, a certain amount of residual charge is deposited on the micro-cavity walls.

With low values of the applied voltage there is a discharge resulting in the formation of a spatial charge with a perpendicular direction to the electric field. As the applied voltage increases, also the spatial charge increases and the latter that tends to spread into the channels branching into the material. When the crater has reached a certain depth, it is possible to have a partial discharge phenomenon even near its extreme tip that in a short time leads to material breakdown.

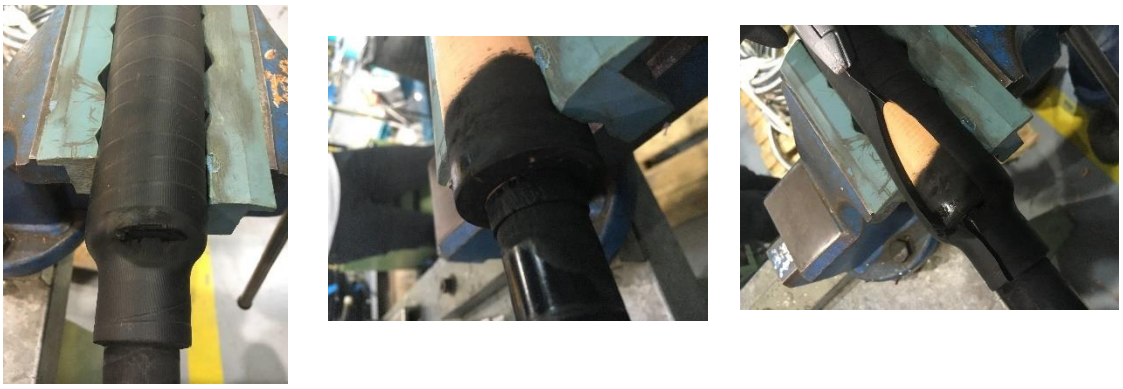

Figure 1-13. Internal discharges effects

Features of the internal discharge:

- Symmetric PD pattern - typical “rabbit ears” shape;
- PDs mainly occur before zero-crossings of the applied voltage;
- Very fast pulses and the pulse has a very low decay time;
- Frequency spectrum lower than 80 MHz.

In Figure 1-14 the PD Pattern, pulse waveform and frequency content of the Internal discharges on 20 kV cable termination is reported.

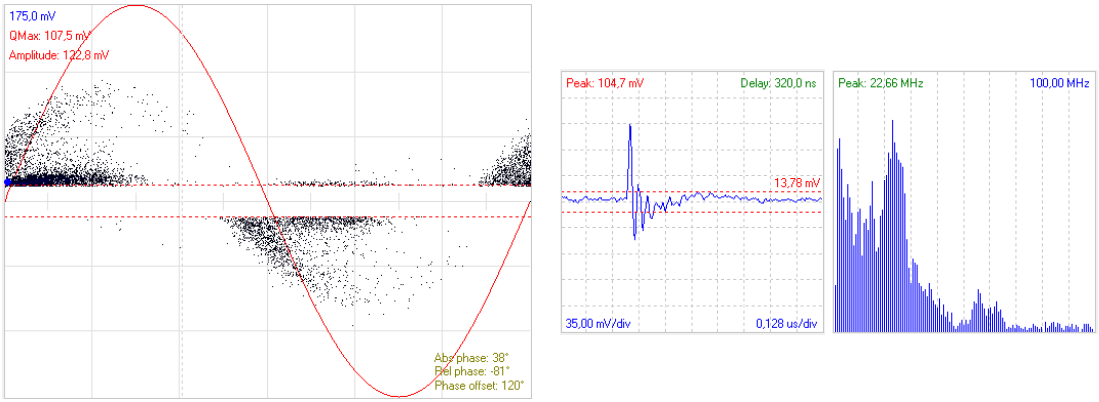

Figure 1-14. Internal discharges on 20 kV cable termination

1.4.4 Floating mass

This kind of discharges take place in correspondence of metallic protrusions or objects not connected to a voltage source and isolated from ground. The electrical potential of a floating mass depends on electric field distribution in space. Under the action of this field a charge distribution may appear on the object surface; inception is favoured when voltage gradient *dv/dt* is maximum and discharges occurs in correspondence of zero crossings, when applied voltage changes her polarity. This phenomenon occurs similarly to corona discharges and is not critical but can disturb measurement activities.

Features of the floating mass effect:

- Middle-fast discharges;
- Harmonic spectrum like corona discharges;
- PDs are clustered, similarly to corona discharges, in a brick-like pattern, but occur in a phase range around the zero crossings.

Figure 1-15. Metallic protrusion inside 380 kV cable termination

In Figure 1-16 the PD Pattern, pulse waveform and frequency content of the Floating mass effect on 380 kV cable termination is reported.

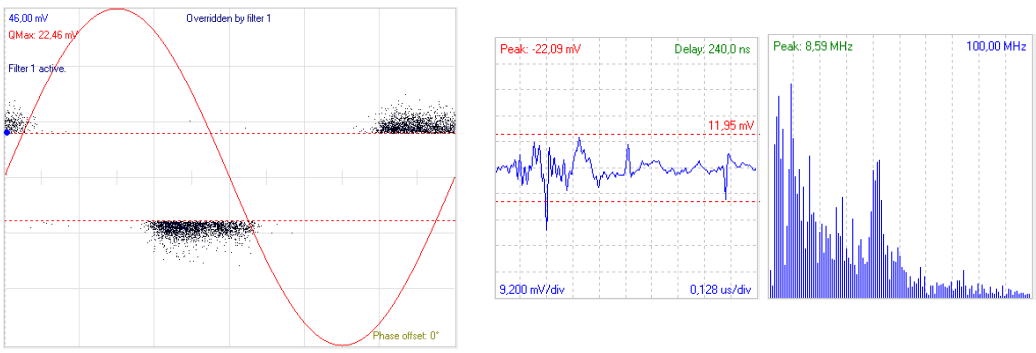

Figure 1-16. Floating mass effect on 380 kV cable termination

1.5 Wireless PD instrument: Pry-Cam Portable

Pry-Cam™ Portable is a wireless device for detection of PDs in HV/MV electric components such as cables. This portable instrument allows performing on-line measurements on powered components, without the need of a galvanic connection, and can be conveniently adopted to locate the PD sources efficiently at a distance from the source. The sensor has a directional behaviour, so during PD measurements the instrument should be directed towards the test object. The maximum directivity of the instrument is towards the sensor principal axis. The antenna probe detects the electromagnetic field produced by each pulse of partial discharge with a bandwidth of 0.1-100 MHz. All pulse signals are acquired, stored, processed and sent to the computer by a Field Programmable Gate Array (FPGA). Samples are acquired with a resolution of 8 bit and a rate of 200 MS/s. In such a way, the PD sensor falls in the Ultra-wide band (UWB) systems [4], [5]. The PD acquisition allows to obtain a set of pulses each characterized by a specific waveform, a phase angle and other additional parameters. The processing operation consists in the separation and classification of the pulses according to their common features. The acquisition and processing software running on iPad™ tablet - called "iPry-Cam" - allows to:

- separate pulses featuring similar waveforms that are generated by the same PD source;
- rejecting incoherent pulses or non-impulsive signals that can be considered as noise.

Figure 1-17 shows the Pry-Cam Portable and iPry-Cam acquisition and processing software displayed on iPad™ tablet.

Figure 1-17. Pry-Cam™ instrument, and iPry-Cam acquisition and processing software

1.6 Monitoring PD instrument: Pry-Cam Grids

The Prysmian Pry-Cam Grids is a measuring system which allows performing online constant PD monitoring by means of Pry-Cam Wings sensors (Figure 1-18) for electric components such as cables, joints, terminations, GIS and transformers. The instrument autonomously performs periodic measures on all the three channels and securely uploads the measurements to the dedicate server by means of the 3G mobile network. The PD monitoring system has the purpose of continuously monitoring the PD activity along the entire route of the underground HV circuit. The continuous monitoring of PD activity will provide information of the state of the line and related accessories and alarms on its wear, aging and potential damages. Pry-Cam Wings sensors are active electromagnetic sensors capable of sensing the PD pulses without the need of a direct connection to the component under test. The Pry-Cam Wings sensor are pre-installed on the HV cables close to the accessories under test. The sensors are not integrated in or galvanic connected to the HV cable system. In this way, the wings sensors are closest to the objects under test (accessories) and will have the best sensitivity for any PDs originating from the accessories.

Figure 1-18. Pry-Cam™ Grids instrument and Wings sensor

1.7 How to perform an analysis of the acquired PD pattern

In order to perform the analysis of the acquired PD pattern it is necessary to carry out a series of fundamental steps to understand if PD phenomena can be considered critical or not, especially when measurements are carried out on high voltage components. To perform a correct analysis of the discharge phenomena, first it is necessary to acquire a good PD pattern. Indeed, the presence of external disturbance or high corona discharge can cover smaller PD phenomena that could be critical. Depending on the type of noise present on site, it is advisable to carry out several measurements with various levels of gain and trigger settings. In Figure 1-19 two examples of acquired PD patterns at different levels of gain and trigger are reported. In the detail, in the PD pattern with high gain level it can be noted how the main PD phenomenon characterized by low amplitude, highlighted in red square, can be clearly visualized and the corona discharge due to the high pulse amplitude is located on the full scale of the PD pattern. Conversely, the PD pattern with low gain level shows how the Corona discharge, characterized by high amplitude covers the main PD phenomenon.

High Gain Level

Full scale 90 mV

Trigger 11.34 mV

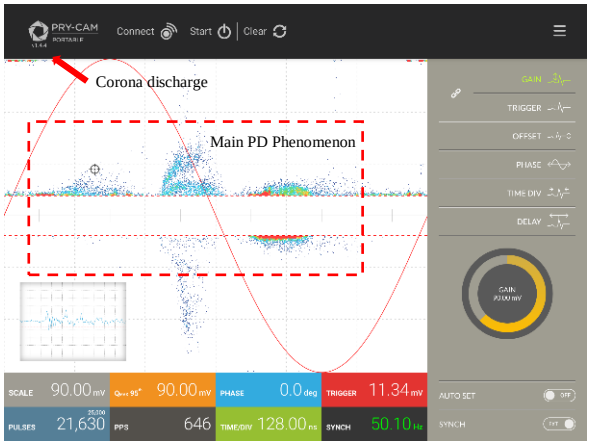

Low Gain Level

Full scale 667 mV

Trigger 36.76 mV

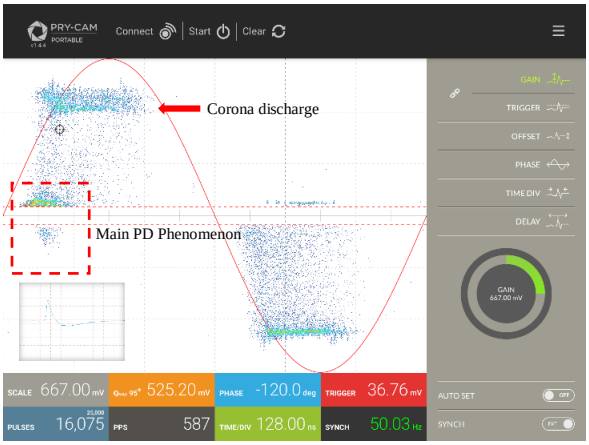

Figure 1-19. Acquired PD pattern at different levels of gain and trigger setting

In order to investigate an insulation degradation process and eventually recognize the presence of a defect on an electric component, is very important to distinguish between different discharge phenomena. This investigation can be carried out through the analysis of:

- PD pattern shape;
- PD pulses shape and Frequency spectrum (FFT);
- PD amplitude;
- Repetition Rate.
- Component type
- System configuration;
- Environmental condition.

PD signals waveform and patterns shape can be different for the same phenomenon type, depending on defect type, and could change during time due to aging processes induced by the discharges, i.e., physical/chemical/geometrical modifications of the discharge site.
Figure 1-20 shows what should be considered during the PD measurements analysis using a wireless portable device and possible results.

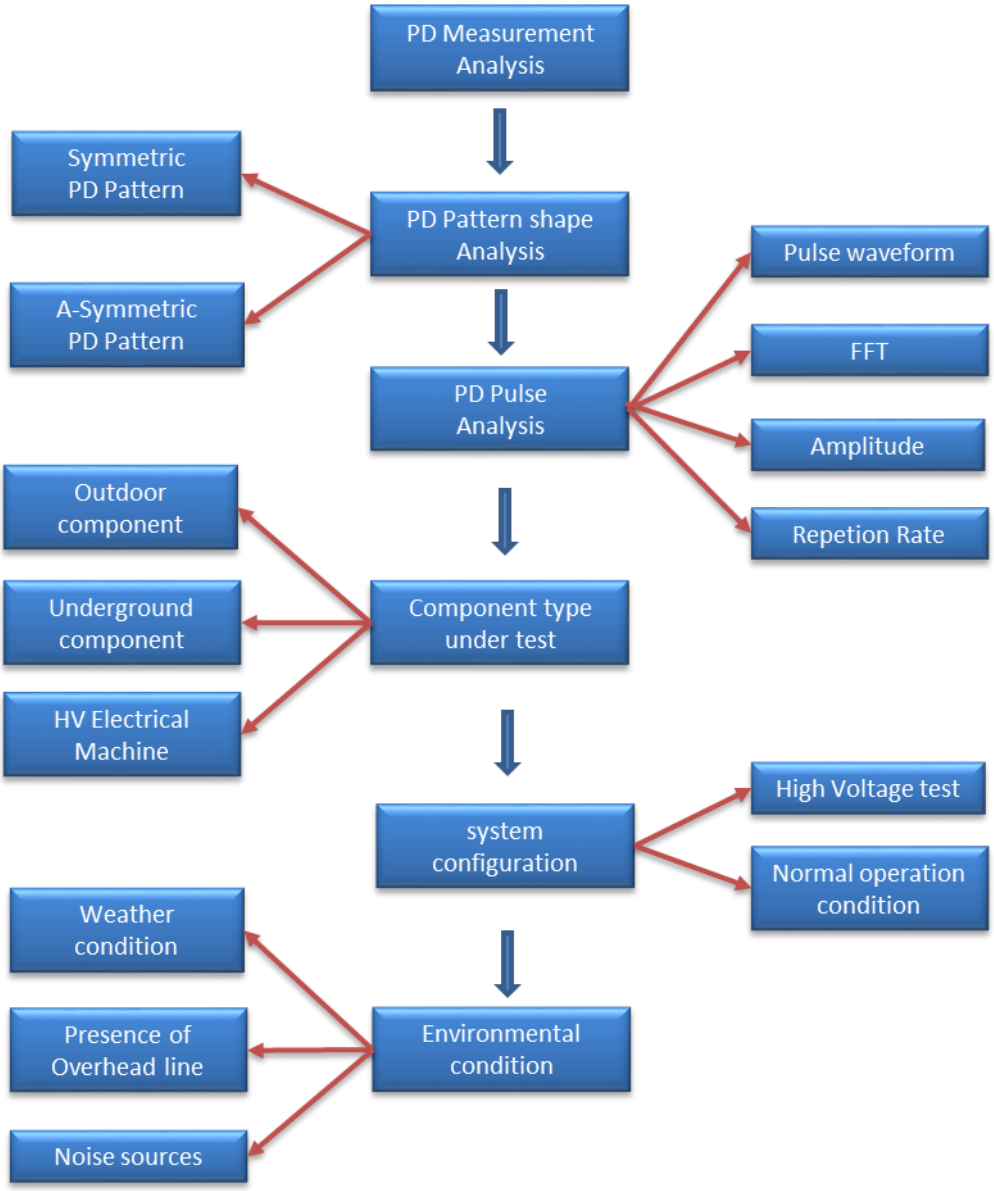

Figure 1-20. PD measurements analysis and possible results

PD pattern shape analysis

The analysis of PD pattern shape is the first step to understand which kind of PD phenomena has been acquired. In particular, it can be acquired the following main PD Pattern shape:

- Symmetric PD Pattern

  The symmetrical shape of the PD pattern is an indication of the presence of a well-defined discharge phenomenon. Typically, the presence of the symmetry could indicate the presence of a potentially critical discharge phenomenon such as high frequency internal or surface discharge. In other cases, it is possible to obtain a symmetric PD pattern in presence of corona discharge or of external disturbances.

  However, it is always necessary to perform the PD pulse analysis to classify the phenomenon as critical or not.

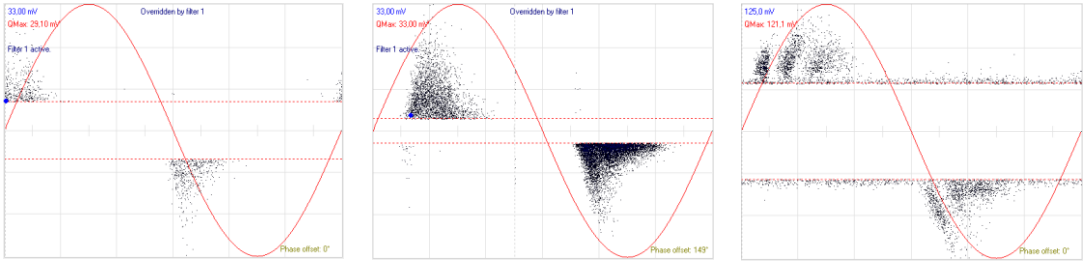

Figure 1-21. Examples of symmetric PD Patterns

- A-symmetric PD Pattern

  Typically, the presence of an asymmetrical PD pattern indicates the presence of a corona discharge or an external disturbance such that it can be classified as non-critical PD phenomenon. In some cases, it is possible to obtain an asymmetric PD pattern in the presence of a phenomenon of critical discharge located in a faraway point, in this case the phenomenon is acquired partially giving origin to an asymmetrical pattern.

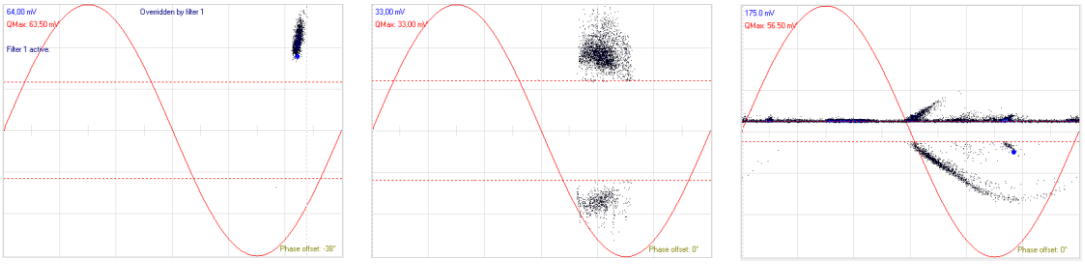

Figure 1-22. Examples of a-symmetric PD Patterns

PD pulses analysis

- Pulse waveform and frequency spectrum (FFT)

The analysis of the waveform and frequency content of the acquired PD pulses allow to understand the critical nature of the PD phenomenon.

- Steep waveform and high frequency content

  The presence of steep pulses with a high frequency content shows the presence of critical PD phenomena like internal or high frequency surface discharges. Typically, the presence of high frequency components above 30 MHz is to be considered critical. however, sometimes it is possible to acquire fast pulses due to the presence of external disturbances, in these cases the analysis of the shape of the pattern can indicate the presence of a fixed disturbance that does not present symmetries or critical positions.

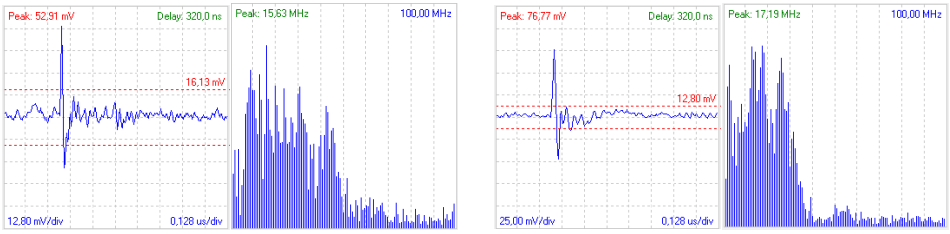

Figure 1-23. Examples of steep waveforms and high frequency contents

- Low waveform and low frequency content

  The presence of slow pulses with low frequency content generally shows the presence of external noises or disturbances. However, it may indicate the presence of low-frequency surface discharges typical of high-voltage terminations or a PD activity far from the measurement point.

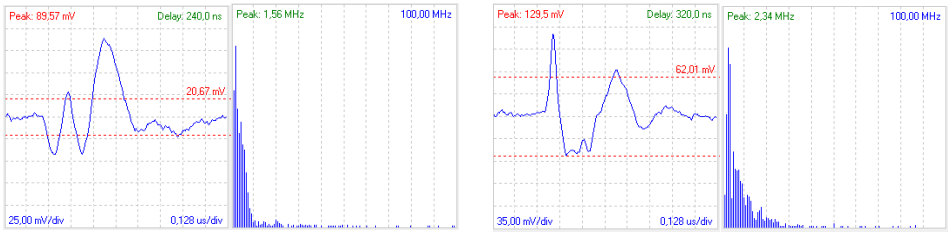

Figure 1-24. Examples of slow waveforms and low frequency contents

- PD amplitude

The PD amplitude makes it possible to understand the magnitude of the acquired PD phenomenon. However, it must be emphasized that non-critical PDs phenomena with high PD amplitude such as corona discharge or external noise can be acquired such as to cover any smaller PDs activities. In these cases, it is necessary to carry out a series of measurements with different gain and trigger settings to acquire even the smallest PDs activities. By itself, the analysis of the PD amplitude does not provide sufficient information to classify a PD phenomenon; it is always necessary to perform the analysis of the pulses to obtain a correct analysis of the PD phenomenon. However, the analysis of the PD amplitude is essential when several measurements have been performed on a circuit in which there are many components. Through the analysis of the PD amplitude at different points of the system under examination it is possible to understand where the PD activity is localized.

- Repetition Rate

Another parameter that helps to understand the magnitude of PDs phenomena is the repetition rate, i.e. the number of acquired pulses per second. This parameter is important when two PDs phenomena must be compared with similar characteristics (in terms of amplitude, waveform and frequency content of the acquired pulses) that may be present on components close to each other. In this case, the analysis of the repetition rate allows to understand which PD phenomenon has the highest number of discharges and to avoid diagnosing the presence of a PD phenomenon on an integral component affected only by an inductive or capacitive coupling phenomenon (crosstalk effect).

<u>Component type</u>

The analysis of the PD measurement can be conditioned by the type of components under test. Indeed, depending on the type of component, different types of PDs phenomena or disturbance can occur, such as:

- Low frequency surface discharge on Outdoor termination;
- Corona effect on GIS (Gas Insulated System);
- External noise on ground connection of the HV machine;
- External noise on ground connection of the Joint.

System configuration

It is necessary to consider if the PD measurement was carried out during a high voltage test for commissioning of a new line or if the measurement was carried out during the normal operation condition of a line. During a high voltage test, PD patterns could show a low frequency surface discharge and several corona effects due to the connection of the AC resonant system.

Environmental condition

The weather conditions must be taken into consideration especially when measurements are carried out on HV outdoor components, as outdoor termination or transformer termination. The presence of humidity or dirt could cause the presence of several PDs phenomena on the external surface of the component under test. Furthermore, when measurements are performed in substations, the presence of overhead line or other HV component in air (insulator and bus bar) close to the measuring point generates high corona phenomena which can influence the PD measurement on the component under test. Moreover, the presence of disturbed phenomena conducted or irradiated by noise sources such as communication devices, antennas or power electronic components can not be excluded. In this case it is necessary to analyze the waveform and frequency content of the acquired pulse and classify these external noises before making the measurement on the component under test.

To perform a correct analysis of the PDs phenomena it is necessary to take into consideration all the issues that have been above listed. It is not indeed possible to carry out the analysis based on a single characteristic. Moreover, since every PD phenomenon has different characteristics and takes place in a different condition, it is not possible to analyze a phenomenon from another similar one. The experience and the execution of large number of measurements are the basis for a correct analysis of the PDs phenomena.

The next chapters will discuss the applications of the wireless measuring technique in current MV/HV power systems and future smart grids.
Indeed, thanks to the ability to carry out PD measurements quickly and easily, without needing cable connections and bulky devices, the portable instrument can be used in all power systems without any limitation. In order to improve the performance of the instrument, various interest issues on the wireless acquisition PD system have been thus analyzed.

Initially, the problem of voltage phase angle synchronization was analyzed for the analysis of acquired PD phenomena at remote points. In fact, when measurements carried out on accessories such as termination or joints in places where it is not known with precision the phase angle of the voltage, the pulses are acquired without considering the phase-shift of the voltage present at the measuring point. In this case, the acquired pulses are placed in the PD pattern with a phase error that could indicate a condition of incorrect criticality. To evaluate the voltage angle phase-shift introduced by a transmission line, several simulations were performed considering different configurations and lengths. Moreover, thanks to the support and development of an electronic device by Prysmian Electronics staff, various phase-shift measurements have been performed on three main HV lines in Sicily.

Subsequently, an investigation was carried out on non-sinusoidal partial discharge measurements. The purpose of this research was to evaluate the PD behaviour with unconventional waveforms such as square wave at 50/350 Hz at different rise times. Various measurements have been carried out on a series of specimens to recreate the types of PD, such as Corona, surface and internal discharge. This work investigates the influence of repetitive steep pulses on different types of test objects exposed to square wave voltages applying two measurement systems each based on different detection principles, the first one based on a resonant PD decoupler and the second one on an antenna sensor with a flat frequency response and the challenges involved. Results reveal an influence of the rise time was observed with both systems however different information were available dependent on the principle used and the PD characteristic versus noise and remnants of the applied voltage.

After, the analysis of superimposed harmonic voltage effects on PD measurements has been discussed. The aim of this research was to understand and evaluate the impact of harmonics on partial discharge behaviour, in particular on the PD measurements by means the Pry-Cam portable instrument, and on the PD Pattern acquisition process. To visualize the influence of harmonic on PD, several measurements were carried out for a sinusoidal voltage waveform with magnitude 5,8 kV, containing harmonics components at 5%, 10% and 20%. Moreover, to visualize the influence of harmonic phase angle on PD, the measurements were performed considering for each harmonic component a phase angle of 0°, 90° and 180°.
The results showed that various harmonic, 3^{rd}, 5^{th}, 9^{th} and 11^{th} superimposed on the fundamental sinusoidal waveform have a significant impact on PD amplitude and PD pattern shapes. The presence of harmonics components can significantly influence the acquisition of the PD pattern and may arise synchronism problems during the measurements.

An accurate PD location method relying on a novel portable PD detection system based on wireless technology has been discussed. the problem of PDs localization on MV and HV cables via Pry-Cam Portable was performed on three different cases: for the MV cable, conventional PD measurements were performed in the laboratory by means of a standard acquisition system; PD activity was detected, but the system allowed the operator to localize the PDs only on a length of 70 m. Aiming at a more accurate pin-pointing of the defect, more measurements were carried out using the novel wireless PD detection system, whereby the source of PD activity was located and identified as a batch of internal defects on the inner semicon. For the EHV cable, PD measurements were performed after the installation on site by means of the novel wireless PD detection system at different points along the HV cable. As a result, PD activity was located on cable accessories. In the last case, the measurements were performed on two short MV cables in HV lab to testing the PD localization method by means Pry-Cam Portable. In this case, the measurements have been performed on two cable circuits in which and each one is composed by a short MV cable with two cable termination and one joint in the middle. This proves how PD detection portable instruments are able, in cases like this, to locate the PD source and provide indications for its correct classification.

Finally, several issues during the HV test on field performed by means Pry-Cam portable are discussed. The aim of this study is to understand and classified different PD phenomena and external noise/disturbance that occurred during the HV test, at different voltage levels, on new submarine and underground cables.

Moreover, further investigation has been performed on MV distribution network through several PD measurements performed on the MV line and their accessories. In this case, the survey highlights how PD monitoring within distribution networks increases the degree of reliability and safety of the power grid. The use of technologies capable of performing partial discharge measurements combined with ozone measurements in MV secondary cabins is one of the possible applications on future smart grids.

2. The problem of synchronizing partial discharge pulses

2.1 Introduction

The asset management evaluation for transmission and distribution systems is a complex and non-standardized exercise in various parts of the world [6]. In addition, based on the available age statistics of the power system components, it appears that the pace of their replacement is essentially linked to their useful life (often several decades). This makes it particularly important to have corrective or programmed maintenance using non-invasive survey tools. One of these is certainly the wireless measurement of partial discharges [7][8]. The use of portable devices for the partial discharge also appears indispensable where the relief with traditional instruments is impossible. This often happens in hardly accessible sites and on cable lines and power components that are not feasible to disarm. Diagnosis through partial relief is an essential procedure for assessing the health status of electrical components and is one of the critical parameters that can be evaluated during components (cables, terminations, joints), but also during their installation and operation. Traditional testing for partial discharge tests requires disconnection of the electrical system, requiring the installation of special sensors on the equipment and then the execution of measurements. Therefore, tested circuits must necessarily remain discharged during partial discharge measurements (usually several hours). Additionally, as the length of the cable in the cable or mix increases, the signal deterioration increases and therefore the acquisition of partial discharge from one or both ends become even less accurate. In fact, a signal traveling along a cable or line attenuates in the path that connects the source of the pulse and the sensor, until it is confused with the noise. The wireless partial-mode measurement devices, available on the market for some years [9], outweigh the already stated limitations of traditional sensors, thus also allowing a more accurate localization of the partial discharge phenomenon, exploiting the directional capacity of the sensors. One of the most relevant parameters for diagnostics is based on the Phase Resolved Partial Discharge (PRPD) pattern analysis, in which the partial discharge pulse amplitude is schematized along with the 50 Hz voltage wave as a function of phase [10]. The partial discharges generated by different sources generate several PRPDs, for which the discharge trigger phase angle is a discriminating element to locate the source of the partial discharge impulse.

2.2 Synchronization issue in the wireless acquisition of partial discharges

The measurement system portability enables performing measurements in different test sites of the MV or HV circuit, allowing the localization of the PD source by exploiting the sensitivity and directionality of the sensor. One of the most peculiar parameters for identifying the different PD activities relies on the analysis of the phase resolved PD (PRPD) pattern, where the amplitude of the PD pulses is plotted versus the phase angle of the supplying line voltage [4]. PDs generated by different sources generate different PD patterns, where the phase angle is crucial for discriminating the source of the PD phenomenon. The analysis of PD measurements relies on parameters such as [11]:

- amplitude of the partial discharge qi - peak value of the single partial discharge pulse;
- trigger voltage Vi - instantaneous voltage value applied when partial discharge occurs;
- Phase angle φ - Phase in degrees on a supply voltage cycle at the location where the PRPD is acquired

The presence of PDs is characterized by groups of pulses having similar shape and amplitude; therefore, the phase angle φ is the first discrimination parameter. This parameter allows identifying the presence of internal, surface or corona discharges. For instance, PD patterns of corona effects are usually featured as a group of dots across the maximum of the positive and negative voltage curve. An error of 30° in the PD acquisition could lead to an erroneous interpretation of critical surface PDs (Figure 2-1) – indicating a serious defect on the MV/HV accessory - as corona effect (Figure 2-2) which can be usually classified as a not dangerous phenomenon.

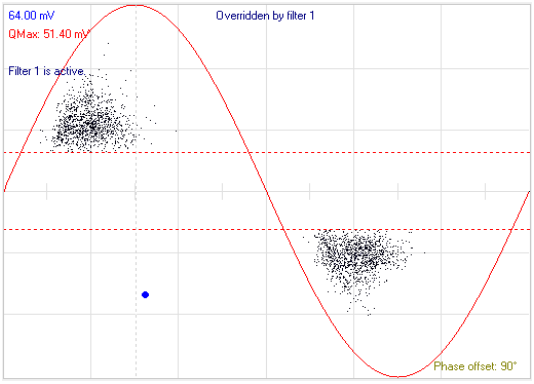

Figure 2-1. PD Pattern compatible with surface discharge

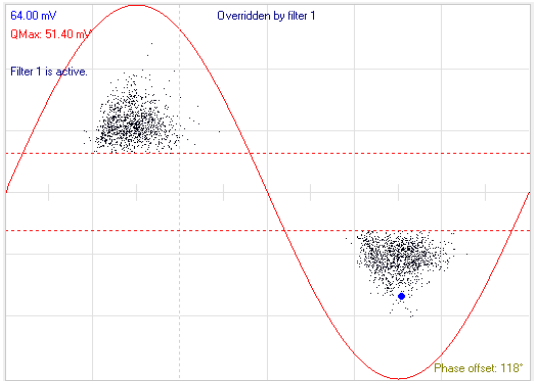

Figure 2-2. PD Pattern compatible with corona discharge

An accurate phase angle measurement is thus extremely important for PD detection and classification. The use of wireless PD diagnosis tools requires reliable ways for synchronizing the instrument with the AC power supply voltage of the equipment under test. The use of portable systems for the PD identification have led to a breakthrough in the field of diagnostics [12]. The system on which the measurement is performed should not be disconnected and the measurement can be carried out in rapidly and safely. However, to obtain a precise measurement of the PD activity, it is necessary to know the phase angle of the partial discharge phenomenon to correctly identify the type of discharge affecting the system or the line under examination. The frequency/phase reference is usually acquired by means of sensors integrated in the wireless PD instrument or by using external sources, such as current clamp, rogowski coil, Current Transformer or even light source.

A quite significant problem is avoiding any phase-shift between the PD measuring system and the voltage supplying the test point where the measurement is taken. For instance, when PD measurements are performed on a termination without any load on the line, the capacitive current flowing on the line leads to a 90 degrees' phase-shift if a current clamp is used as synchronization source. Another common example is when the artificial light is used as frequency source, especially inside substations; in this case the phase-shift depends by many factors and it is not always easy to calculate the proper phase offset.

Therefore, to be able to evaluate for each impulse the phase value with respect to the sinusoidal voltage must be correctly synchronized with the measuring instrument. Based on the above-mentioned problem, the activity carried out under this study aims to evaluate and quantify the actual phase-out of voltage, introduced by a transmission and / or distribution line, in order to improve accuracy and the performance of a portable device for the relief of partial discharges.

In this work, reference is made to the Pry-CamTM [13] instrument, which allows the detection of partial discharges (PD) on HV and MV electrical components such as cables, joints, terminals, transformers, GIS and rotating machines. The instrument allows PD measurements on powered components using an electromagnetic sensor [4] without the need for a galvanic connection, and to transfer them in real time to a tablet using Wi-Fi protocol. The measurements are then loaded onto a remote server to be stored and further analyzed later (Figure 2-3).

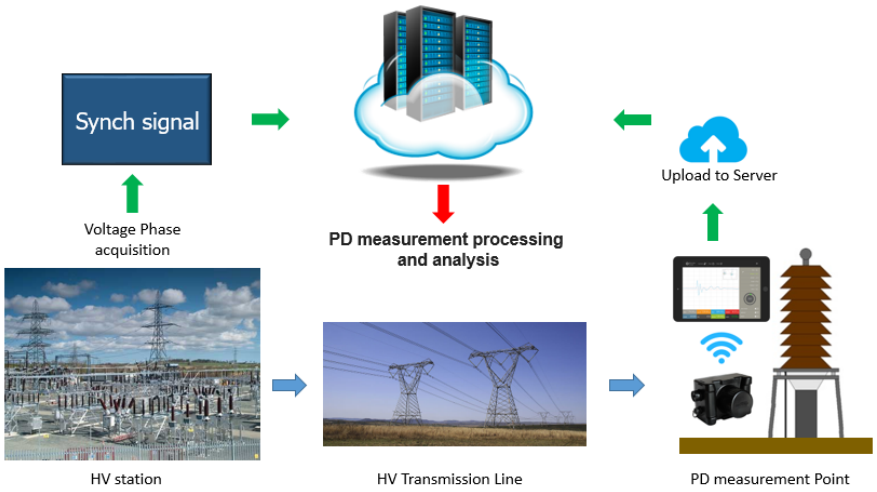

Figure 2-3. Remote synchronization of PD measurements carried out with a portable device

In the proposed method, a dedicated unit can be installed in few substations of the grid, acquiring the phase angle together with a precise time reference (i.e. derived from Global Position System). Where a Phasor Measurement Unit (PMU) [14][15] is already available at the substation, its GPS time reference can be used, instead of using a separate GPS receiver and antenna. Phase angle and the precise timestamp can be made accessible on a centralized synchronization server; in this way, PD measurements performed without proper synchronization can be corrected by correlating the timestamp of the PD pulses with the synchronization server. The phase-shift angle should be calculated and may be compensated by the knowledge of the line length and load current.

The aim of this work is:

- to describe the problem of synchronization phase voltage for wireless PD diagnosis;
- to describe a possible solution to the problem through a customized low cost electronic device.

At first, different simulations in modelled real-world test cases, showing various loading conditions and distances, are compared to actual measurements taken on the transmission network. To understand how the transmission line determines a voltage angle phase-shift, various simulations in PSCAD with different overhead transmission lines operating in Sicily, Italy, have been carried out. In fact, it can be easily proved that the phase-shift produced by a transmission or distribution line may cause mis-interpretation of the PD diagnostic results. If instead such displacement can be estimated, it is possible to obtain a correct PD measurement without phase-shift offset introduced by the transmission line.

Later, thanks to a custom electronic device, henceforth Phase Check, the voltage angle phase-shift has been measured, at the two ends of the considered HV overhead transmission lines. The measures on HV networks have been conducted with the support of the “Plants division” of Terna Rete Italia Spa (Italian Transmission System Operator) that has made available its facilities for validating the results obtained from the PSCAD simulations and the “Phase Check” acquisitions.

It is expected that the voltage angle phase-shift in cable lines is greater than on overhead transmission lines. However, for this work, measurements have been performed on overhead lines only, due to the simpler authorization request process for accessing the substations.

2.3 Evaluation of the voltage angle phase-shift in HV lines

In order to evaluate, first theoretically and then empirically, the voltage angle phase-shift between two ends of a line, simulations were carried out, by means of an equivalent line model and relative line constants, and subsequently measurements were carried out on three main HV transmission lines present in the Sicilian territory. The first objective is to assess whether the voltage angle phase-shift introduced under standard operating conditions can be significant for the diagnosis and acquisition of partial discharges. The second goal is to provide, after validation with other measurement systems, a look up table to correct the available measures.
The analysis of the synchronization problem was therefore first simulated by modelling an HV overhead transmission system at 150 kV, 220 kV and 380 kV, and an HV cable at 245 kV. The simulations aim to quantify the voltage angle phase-shift introduced by each transmission system, considering different configurations of the power transmitted according to the maximum carrying capacity. Subsequently, thanks to the collaboration established with Terna Rete Italia, measurements were made on three of the main HV power lines (two 220 kV electrodes and 380 kV electrodes) in Sicily to validate some of the data obtained from the simulations. During the measurements, thanks to the OMICRON CMC 356/256 measuring instrument, the real active and reactive power transits were acquired on the lines under examination. The acquired data allowed a further simulation study to verify the reliability of the line model employed in the first phase of the study and validate the measurements detected by the PhaseCheck device. In this second study, the simulations were conducted by considering, initially, the equivalent line model and relative positive and zero constants and then using the configurations and characteristics of the tower and conductors of the lines in question.

2.4 Simulation analysis of the voltage angle phase-shift introduced by the HV lines

To evaluate the phase-out of the voltage introduced by a transmission line, the simulations were conducted considering the electrical and dimensional parameters of three aerial lines with a nominal voltage of 150 kV, 220 kV and 380 kV, and a cable line with rated voltage of 245 kV. The simulations were carried out using PSCAD software, considering at first different load configurations, depending on the maximum carrying capacity of the individual lines. To evaluate the propagation of the voltage wave, the simulations were carried out considering the following conditions:

1. line length of 100 km;
2. power transmitted dependent on line capacity:
   - 380 kV → 250 MW - 500 MW - 1000 MW
   - 220 kV → 50 MW - 100 MW - 200 MW
   - 150 kV → 50 MW - 75 MW - 100 MW
   - 245 kV → 50 MW - 100 MW - 200 MW (cable line)
3. evaluation of the voltage waves propagation every 10 km and at the end of the line.

Subsequently, in paragraph 2.5, the simulations were reworked based on the current active and reactive power transitions, in line with the results obtained in experimental measurements.

The simulated overhead line consists of an ACSR conductor with diameter 31.5 mm (sections of aluminium 519.5 mm^2 and steel 65.80 mm^2) [16], whose characteristics are shown in Table 2-1.

Table 2-1. ACSR transmission line data

Primary Parameters	
Positive sequence	**Zero sequence**
r = 0.05487 [Ω/km]	r0 = 0.3089 [Ω/km]
$l = 1.274 \cdot 10^{-3}$ [H/km]	$l0 = 0.9833 \cdot 10^{-3}$ [H/km]
$c = 9.162 \cdot 10^{-9}$ [F/km]	$c0 = 5.845 \cdot 10^{-9}$ [F/km]
Secondary Parameters	
Surge Impendence	Zc = 374.637 [Ω]
Wavelength	λ = 5840.6 [km]
Velocity of Propagation	v = 292030 [km/s]
Complex propagation constant	γ = 0.0001+ j 0.0011 [rad/km]

The cable used in the simulation is three single phase aluminium conductors with Cross Linked Polyethylene (XLPE), cross section of 1000 mm2 and designed to operate at a rated voltage of 245 kV. The main features and data of the cable line are shown in Table 2-2 and Table 2-3.

Table 2-2. Cable material properties

Cross section of Conductor	Al - 1000 [mm^2]
Insulation	XLPE - 19.1 [mm]
Relative Permittivity XLPE	2.3
Metallic sheath	Al - 1.2 [mm]
Plastic sheath	HDPE - 4 [mm]
Maximum working voltage	245 [kV]
DC resistance of conductor	0.0291 [Ω/km]
AC resistance of conductor	0.0405 [Ω/km]
Inductance	0.382 [mH/km]
Capacitance	0.204 [μF/km]
Positive sequence resistance	0.04053 [Ω/km]
Positive sequence reactance	0.119 [Ω/km]

Table 2-3. Cable line data

Inductance	323.2 [μH/km]
Capacitance	154.4 [nF/km]
Surge Impendence	Z_C = 47.525 [Ω]
Wavelength	λ = 2781.6 [km]
Velocity of Propagation	v = 139080 [km/s]
Complex propagation constant	γ = 0.0004 + 0.0023 [rad/km]

The simulation results are show in Table 2-4 and Table 2-5, for the overhead and the cable line. They show, as it can be expected, the increase of the voltage angle phase-shift for increasing supplied power values, with different voltage rating for equal line length.

Table 2-4. Overhead transmission line simulation results

Overhead line	250 MW		500 MW		1000 MW	
	δ [°] 100km	δ [°] 10km	δ [°] 100km	δ [°] 10km	δ [°] 100km	δ [°] 10km
380 kV	2.72	0.27	5.35	0.53	10.47	1.06

Overhead line	50 MW		100 MW		200 MW	
	δ [°] 100km	δ [°] 10km	δ [°] 100km	δ [°] 10km	δ [°] 100km	δ [°] 10km
220 kV	2.42	0.23	4.74	0.47	9.25	0.94

Overhead line	50 MW		75 MW		100 MW	
	δ [°] 100km	δ [°] 10km	δ [°] 100km	δ [°] 10km	δ [°] 100km	δ [°] 10km
150 kV	5.09	0.51	7.53	0.76	9.91	1.01

Table 2-5. Cable line simulation results

Cable line	50 MW		100 MW		200 MW	
	δ [°] 100km	δ [°] 10km	δ [°] 100km	δ [°] 10km	δ [°] 100km	δ [°] 10km
220 kV	3.66	0.27	6.08	0.49	10.73	0.94

A comparison between the 220 kV overhead and cable lines simulation shows that, per equal length and power supplied, the voltage angle phase-shift is comparable with a deviation about 1.5°. In fact, the higher reactive power engaged in cable line allows to partly compensate the voltage angle phase-shift.

From the simulation results it can be noted that the maximum voltage angle phase-shift on a HV line is around 10°. If PD measurements are acquired and phase sync corrected with such phase reference, an error up to 15° does not usually lead to misleading interpretation in the analysis of the PD pattern. Even if it is possible to correct this phase-shift by the knowledge of the line length and the load current, in most of the cases this will not be necessary.

Based on the simulation results reported above, three main HV overhead lines have been identified in the Sicilian territory on which to measure phase voltage measurements and to evaluate the actual voltage angle phase-shift introduced by the overhead lines.
The HV overhead lines in the study are:

- Line 1 – Bellolampo-Caracoli at 220 kV in double 3-phase - length: 50 km;
- Line 2 – Bellolampo-Partinico at 220 kV in double 3-phase - length: 26 Km;
- Line 3 – Chiaramonte Gulfi-Priolo at 380 kV in single 3-phase - length: 60 Km.

The first aim of the simulations is to see whether the phase-shift introduced by standard operating conditions can be meaningful for PD diagnosis. The second aim is to provide, after validation with other measurement systems, a look up table to assess the phase-shift or correct other available measures. To evaluate the voltage angle phase-shift introduced by a transmission line, the simulations were conducted on three overhead transmission lines with a rating voltage of 220 kV and 380 kV. The overhead transmission lines considered for the simulations consist in an ACSR conductor with diameter 31.5 mm (aluminium section 519,5 mm^2 / steel section 65,80 mm^2) [16].
Figure 2-4 shows the overhead transmission lines at 220 kV, in particular the lines from Bellolampo to Caracoli stations (BLL-CAR) and from Bellolampo to Partinico stations (BLL-PRT). The overhead transmission line at 380 (red line) kV from Chiaramonte Gulfi to Priolo stations (CHI-PRI) is shown in Figure 2-5.

Figure 2-4. Overhead transmission lines at 220 kV

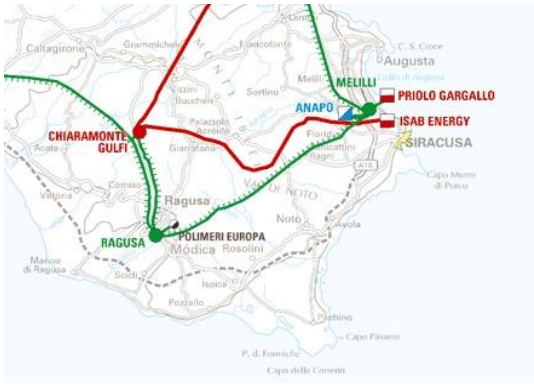

Figure 2-5. Overhead transmission lines at 380 kV

The lines mentioned above have been first studied through extensive simulations. Then the results of the latter have been compared with the experimental measurements. The simulations were performed considering the actual line length and the power level transmitted detected on site during measurements.

Therefore, simulations are performed considering the line parameters, calculated since the data provided by Terna Rete Italia. The overhead transmission lines characteristics are shown in Table 2-6. Lines specifications were provided by the Italian TSO (Table 2-7).

Table 2-6. Characteristics of overhead transmission lines

Line	Characteristics of overhead transmission lines	
	Voltage rating [kV]	Length [km]
BLL - CAR	220	50.9
BLL - PRT	220	26
CHI - PRI	380	60.9

Table 2-7. Line parameters

Constants / Line	Overhead transmission lines		
	BLL - CAR	BLL - PRT	CHI - PRI
r [Ω/km]	0.549e-4	0.549e-4	0.182e-4
XL [Ω/km]	0.400e-3	0.401e-3	0.270e-3
XC [MΩ·km]	347.961	347.876	233.843
r_o [Ω/km]	0.191e-3	0.3170e-3	0.251e-3
XL_0 [Ω/km]	0.100e-2	0.132e-2	0.110e-2
XC_0 [MΩ·km]	452.859	540.443	440.414

In Table 2-7, the symbols r, XL and XC represent the service constants, while the symbols r_0, XL_0 and XC_0 are indicative of the zero constants of the overhead lines.

The simulations were conducted using the Bergeron Model that is based on a distributed LC-parameter travelling wave line model, with lumped resistance (Figure 2-6). It represents the L and C elements of a PI Section in a distributed manner (i.e. it does not use lumped parameters). It is roughly equivalent to using an infinite number of PI Sections, except that the resistance is lumped (1/2 in the middle of the line, 1/4 at each end).

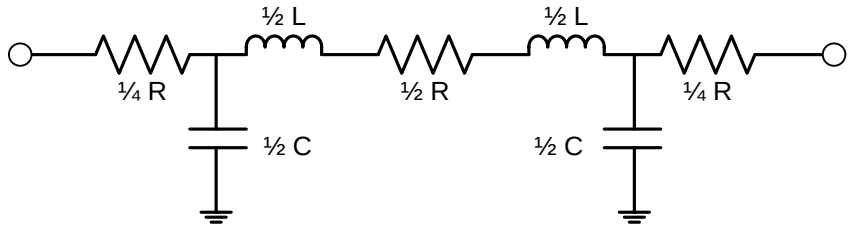

Figure 2-6. Line equivalent model

At this stage, simulations were carried out immediately after gaining real power transits on the lines in question (Table 2-8), taken on site during the measurements.

Table 2-8. Simulation results: line parameters manual data entry

Line	Simulation Results				
	Rating Voltage [kV]	***Length [km]***	***Power Transmitted [MW]***	***Reactive Power [MVAR]***	***Phase-shift [°]***
BLL - CAR	220	50.9	48	- 7,07	1.17°
BLL - PRT	220	26	45	- 45	0.70°
CHI - PRI	380	60.9	690	- 10,84	4.48°

As it is shown in Table 2-8 the line CHI-PRI with a higher transmitted power determines a greater voltage phase-shift.

In a transmission system with greater lines lengths and significant amounts of transported power, the phase error may become quite significant. For example, the simulations show that a transmission line with the same characteristics and the same transmitted power of CHI-PRI but with a length of 200 km, the voltage angle phase-shift introduced by the line is approximately 13.72°. This phase error magnitude could lead to a wrong assessment of the PD patterns. The PDs are characterized by groups of pulses having similar shape and amplitude; therefore, the phase angle φ is a very important parameter which allows to identify the presence of internal, surface or corona discharges.

A further simulation has been performed with the real geometric layout of the conductors in order to obtain more accurate results. In this way, the simulator computes using the Bergeron Model the constant values from the geometric layout. The transmission line geometric layout, at voltage rating of 380 kV, is composed of three conductors per phase in delta tower (Figure 2-7). In this configuration, each phase can carry 1500 A with a three-phase nominal power of 1000 MVA. The configuration layout for transmission lines at the rating voltage of 220 kV is double three phase conductors in a vertical tower as shown in Figure 2-8. In this configuration, each phase can carry 500 A with a three-phase nominal power of 200 MVA.

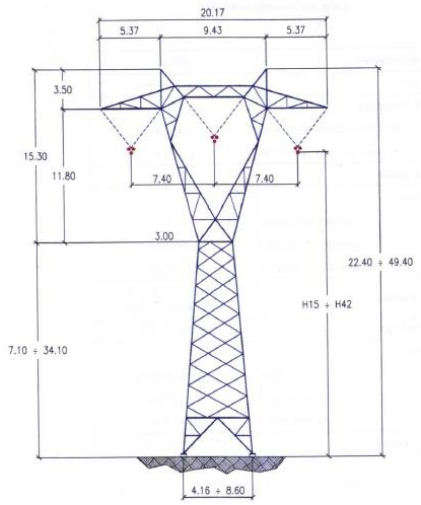

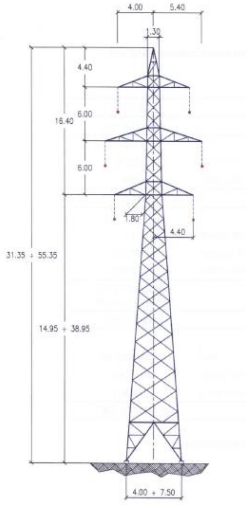

Figure 2-7. Transmission line with three conductors per phase in delta tower at 380kV

Figure 2-8. Double three phase conductors in vertical tower at 220kV.

A greater power transport determines a high current flow which results in a greater voltage angle phase-shift. Table 2-9 shows transmitted power and relevant phase-shift for comparable line lengths. The simulations were performed considering the actual active and reactive power transits measured on site. The large reactive power transit in the case of the line BLL-PRT was due to a particular operating condition of the electrical system.

Table 2-9. Simulation results: line parameters geometric layout

Line	**Simulation Results**				
	Rating Voltage [kV]	***Length [km]***	***Power Transmitted [MW]***	***Reactive Power [MVAR]***	***phase-shift [°]***
BLL - CAR	220	50.9	48	- 7,07	1.05°
BLL - PRT	220	26	45	- 45	0.68°
CHI - PRI	380	60.9	690	- 10,84	4.11°

In the next section, the data obtained from PhaseCheck measurements will be presented.

2.5 Experimental measure of the voltage angle phase-shift

In Figure 2-9 the overall architecture of the wireless PD diagnosis system using the “Phase Check” and the look up table is shown. The “Phase Check” system acquires the voltage phase angle at the ends of the line and an absolute time reference by GPS; this data is then sent to the Look Up Table Server.

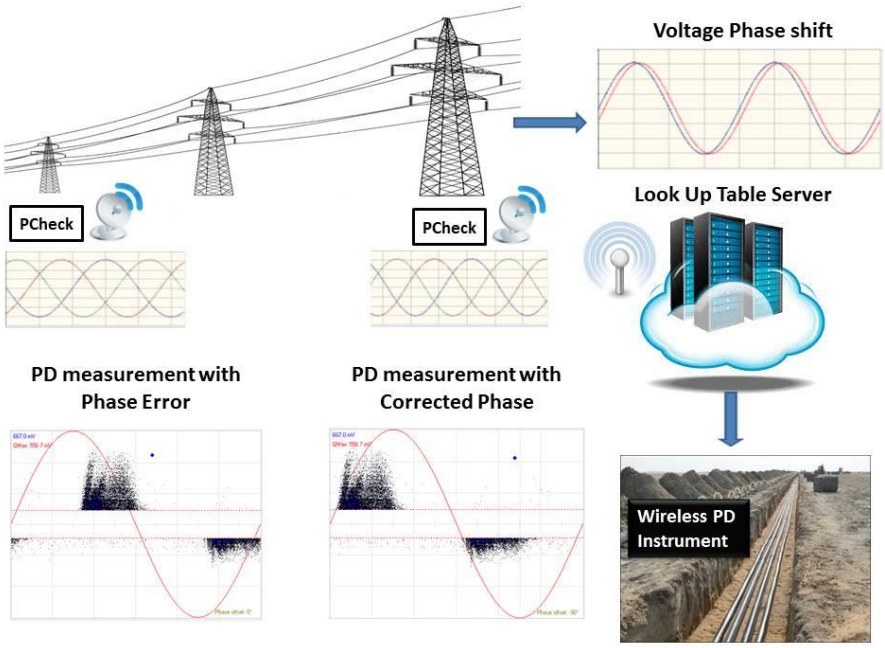

Figure 2-9. Voltage angle phase-shift compensation in PD measurement through Phase check and Look up tables.

On the server, the detailed information of the line length is loaded, the phase-shift is calculated and then the worst condition corrected voltage angle phase-shift is deduced. If the operating conditions are available, the server could also perform a simulation of the line and output the precise phase-shift. In this way, the PD measurement in different sites can be corrected to obtain a PD pattern with an accurate phase angle.

The experimental activity described above was preceded by a system for evaluating the voltage angle phase-shift detected at the two ends of the line. The system, called 'PhaseCheck', consists of a pair of identical instruments, one of which is depicted in Figure 2-10, and useful for assessing the phase-out angle of power in power networks. The voltage offset angle produced by the line was then measured by installing the two devices, designed and developed by Prysmian Electronics [17], in their respective start and end stations.

Figure 2-10.PhaseCheck device

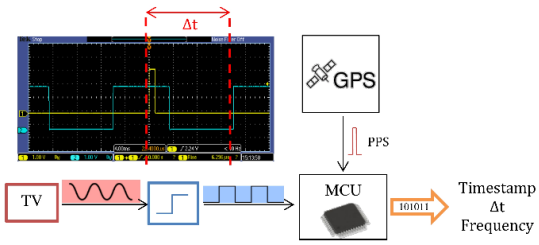

Figure 2-11. Simplified block diagram of the device

The circuit design is made by an analog frontend that is connected to the voltage transformer (TV) output in the substation (Figure 2-11); this signal (in the range of 100 V) is converted to a square wave. Voltage transformers (TV) have a precision class of 0.2 or 0.5 in relation to the type of measuring assembly. The limits of the voltage (or ratio) and angle error must comply with the requirements of the reference standard for voltage transformers EN 60044-2 [18]. In relation to the precision class 0.2 and 0.5, the phase angle error introduced by a TV is equal to ± 0.3 and ± 0.6 centiradians, which in degrees is ± 0.171 ° in the first case and ± 0.343 ° in the second case. In order to obtain a perfectly synchronized measurement, and considering that there are two devices, one for each substation, it is necessary to provide a GPS antenna with the corresponding receiver to obtain the exact reference time-reference between the two instruments. A GPS receiver and its amplified antenna make the time-reference circuit; when the GPS receiver acquires the minimum number of satellites, a 1-second pulse (PPS) is generated and acquired as interrupt by an 8-bit microcontroller (MCU). In the interrupt routine, the MCU calculates by means of an internal counter (1μs of resolution) the time difference between the received PPS and the next rising-edge of the square wave generated from the AC voltage. For the sake of clarity, the same principle can be performed by using a 2-channel oscilloscope like in Figure 2-12.

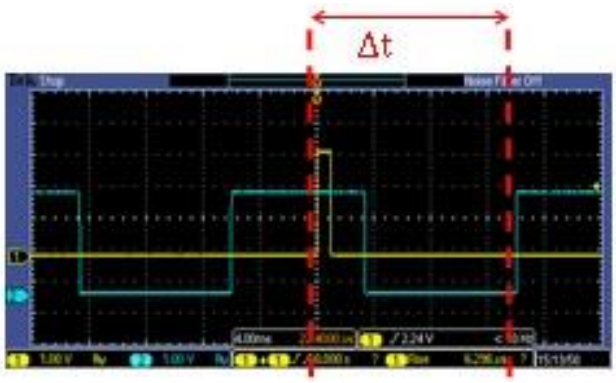

Figure 2-12.Oscilloscope example of the measurement performed by the PhaseCheck.

It can be noted in blue the square wave obtained from the TV output, while the PPS generated by the GPS receiver of the PhaseCheck is depicted in yellow. The time difference Δt between the rising-edge of the PPS and the next rising-edge of the square wave can be easily obtained. The time-stamp and the value of the counter, representing the Δt, are locally stored and sent by a serial link to the PC. The frequency of the square wave is also calculated and transmitted to the PC. In order to calculate the phase-shift between two points in a transmission line, two twin PhaseCheck units were used, each placed at one end of the line and connected to the respective TV on the same HV phase. The resulting files were saved on the two laptop computers connected to the PhaseCheck units at the two sites and then compared at the end of the measurement session. For the same time-stamp value, the difference of the counters in the two files was obtained, hence the resulting phase-shift. The voltage angle phase-shift introduced by the overhead line, was calculated starting from the same the time-stamp value, which was acquired by the two devices, by performing the relative difference of the measured time values. For better understanding, an example of the voltage angle phase-shift computation has been reported in Figure 2-13.

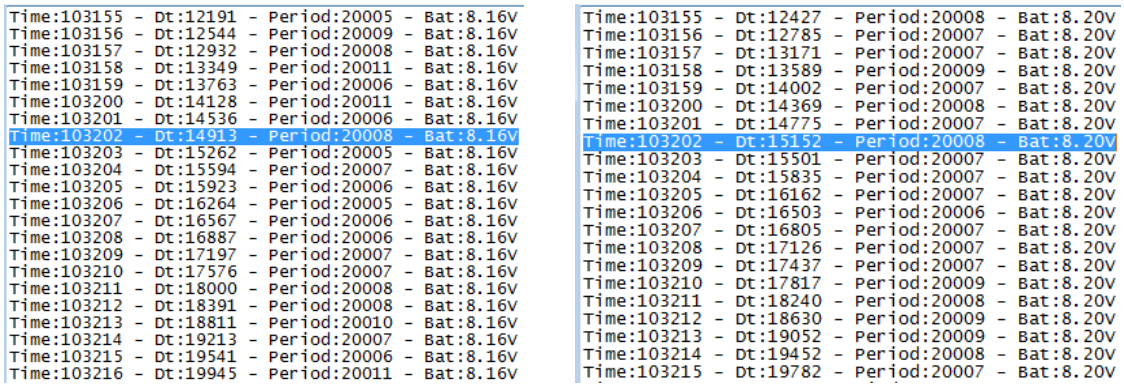

Starting Substation - PhaseCheck 1 Arrival Substation - PhaseCheck 2

Figure 2-13. Data Acquired by Two PhaseCheck on Line 3 at 380 kV

Considering the time-stamp value of 103202, highlighted in blue in Figure 2-13, the phase-shift value is obtained by performing the difference between the time of the arrival station and the time of the starting station by returning the time-shift value in degrees:

$$\Delta(\Delta t) = 15152 - 14913 = 239 * 360/20000 = 4.30°$$

Where 20000 represents the period of square wave voltage expressed in μs (20 ms = 20000 μs). In this example, the voltage angle phase-shift introduced by the overhead line is 4.30 °.

The voltage angle phase-shift measurements were conducted simultaneously with the help of the Omicron CMC356 / 256 measurement system and Siemens Sigra analysis and processing software, made available by Terna Rete Italia, for a further comparison term with the data recorded. The measurements carried out, thanks to the support of Terna Rete Italia, allowed to validate the results obtained from the simulations and to test the accuracy and reliability of the device.

The first measurement was performed on the Line 1 - Bellolampo-Caracoli at 220 kV in double 3-phase. Both measuring systems were connected to the central phase of the overhead line, so the voltage and current values for a phase were acquired. At the time of measurement, the power transmitted was about 16 MW per phase, for a total transmitted power of about 48 MW. Several measurements were taken with different acquisition times, at the end of the measurement was found a phase-shift of 1.03 °. During the simulation, a deviation of phase angle of about 1.17 ° was found. The simulated data has an error respect to the measured data of 11.97%. Considering the precision of the TV, installed in both substation, and imagining that phase errors are suppressed by the phase-shift due to the voltage propagation, both measures can be corrected. In the worst case, considering that the TV precision class is 0.5, the angle error introduced by the two TV is ± 0.686 °. In this case, the error introduced by the TV is comparable with the result of the simulation (1.17 °). Therefore, in the case of short lines with modest active power transmitted, the phase angle is very small (order of 1 °) and therefore the correctness of the simulations cannot be verified using the measurements made. For re-synchronizing the instrument, however, remembering that only a phase error greater than 15 ° could lead to incorrect interpretation of the PD pattern, a phase-shift of the order of 1 ° is not significant and does not lead to an erroneous interpretation of the PD pattern.

The second measurement was carried out on the Line 2 – Bellolampo-Partinico at 220 kV in double 3-phase. During the measurement, the power transmitted was about 15 MW per phase, for a total transmitted power of about 45 MW. Compared to the previous case, the layout of the power grid was such as to record a high level of reactive power. Due to the reduced length of the line, 26 km, and the operating conditions, a phase offset of 0.74 ° average was measured. The simulation confirms the measured data, since the calculated phase-shift was 0.70 °, with a negative error of -5.71%.

The third measurement was done on Line 3 – Chiaramonte Gulfi-Priolo at 380 kV in single 3-phase. In this case, the overhead line has a configuration with three conductors per phase and a significantly higher transfer power. The choice of this type of overhead line has been made to ensure better quality of the detected data. A higher transmitted power causes, in fact, a higher voltage phase-shift.

During the acquisition, the transmitted power was about 230 MW per phase, with a total of about 690 MW of the three-phase transmission power. Under these operating conditions, the phase-shift angle was on average 4.24 °. During the simulation, the phase-shift was 4.48 °. In this case, the committed error is 5.35%. Unlike previous cases, the phase error introduced by the two TVs of ± 0.686, in the case of precision class 0.5, allows to correct the measurements made in the two substations and provide a much more accurate and reliable indication of the actual phase-shift introduced by the transmission line. In the specific case, the measured phase-shift will be 4.24 ° ± 0.686. The simulated value, in this case, deviates from the value measured by a positive error of 9.95% to a negative error of -20.66%.
Table 2-10 shows the results of the simulations carried out in PSCAD, considering the line constants of the three HV overhead lines, and the experimental results obtained from the measurements made with the PhaseCheck device on the three overhead lines under test.

Table 2-10. Comparison of the results between PhaseCheck and simulations (line parameters manual data entry)

Line	Rating Voltage [kV]	Length [km]	Power Transmitted [MW]	Reactive Power [MVAR]	PhaseCheck phase-shift [°]	PSCAD phase-shift [°]	Error %
BLL - CAR	220	50	48	-7,07	1.03	1.17	11.96%
BLL - PRT	220	26	45	-45	0.74	0.70	-5.87%
CHI - PRI	380	60	690	-10,84	4.24	4.48	5.35%

A further simulation with the configurations and characteristics of the Tower and conductors has allowed to obtain even more accurate results. Unlike the previous case, in which the simulations were conducted by inserting the fundamental constants of the lines, in this case, the actual distances and arrangement of the conductors were introduced for each tower configuration (see Figure 2-7 and Figure 2-8).

From the results obtained, an error reduction was occurred. In detail: the error for the Line 1 – BLL-CAR is equal to 2.83% compared with 11.96% of the previous case; for the Line 2 BLL-PRT the error, already negative in the previous case, is further reduced at -8.82%; for the Line 3 – CHI-PRI the error undergoes a reversal of the sign at -3.92%. As summarized in Table 2-11.

Table 2-11. Comparison of the results between PhaseCheck and simulations (line parameters geometric layout)

Line	Rating Voltage [kV]	Length [km]	Power Transmitted [MW]	Reactive Power [MVAR]	PhaseCheck phase-shift [°]	PSCAD phase-shift [°]	Error %
BLL - CAR	220	50	48	-7,07	1.03	1.06	2.83%
BLL - PRT	220	26	45	-45	0.74	0.68	-8.82%
CHI - PRI	380	60	690	-10,84	4.24	4.08	3.92%

Even in this case, the phase error introduced by the TV should always be considered, which in the case of small phase-shift do not allow to fully appreciate the result obtained in simulation. However, considering the appreciable voltage angle phase-shift, as in the case of the Line 3 – CHI-PRI with a phase-shift of 4.24 ± 0.686, the simulations performed with the geometric layout of the conductors have determined a positive error of 17.17% and a negative error of -14.8%.

Therefore, the measures taken have allowed validation of the results obtained by the simulations and the accuracy and reliability of the PhaseCheck system. Table 2-12 shows the results of the simulations and the results of the measurements made with PhaseCheck.

Table 2-12. Comparison of the results between simulations and experimental measures

Line	**Simulation Vs PhaseCheck**				
	Simulation Manual Data Entry		***Simulation Geometric Layout***		***Measured PhaseCheck***
	phase-shift [°]	***Error%***	***phase-shift [°]***	***Error%***	***phase-shift [°]***
BLL - CAR	1.17°	11.97%	1.05°	1.90%	1.03°
BLL - PRT	0.70°	-5.71%	0.68°	-8.82%	0.74°
CHI - PRI	4.47°	5.36%	4.11°	-3.92%	4.24°

2.6 Look up tables for the evaluation of the voltage phase-shift

In many cases do not know the power transmitted on the line, but only the zero crossing of the voltage wave through the PhaseCheck experimental system, it is useful to identify the phase-shift values in the worst case that can correct the PD pattern and to proceed to an identification of the PD phenomena.

In a transmission system with considerably long lines (over 200km) and with considerable amounts of energy transported, phase error can become quite significant. For example, the simulations show that a transmission line with the same characteristics and the same transmitted power of the line CHI-PRI but with a length of 200 km, the voltage angle phase-shift introduced by the line is about 13.72 °. This phase error, therefore, could lead to an erroneous evaluation of the PD pattern, so it is necessary to compensate the phase-shift by proper instrument recalibration. As shown in Table 2-13, the look up table for the evaluation of the Phase-shift error determines the voltage level, line length, and the relative phase-shift introduced by the line. Given the degree of misalignment measured, the system should provide an indication of the actions to be taken in order to acquire correctly the PD pattern. In the case below, the Resynch action in green does not need any correction given the degree of phase-shift, the orange indication indicates that a correction may be made at the discretion of the operator, instead the indication in red requires the operator to perform adequate re-synchronization so as not to get false positives during the analysis.

Table 2-13. Look up tables for the evaluation of the voltage phase-shift

Line	Type	Vn [kV]	Length [Km]	Phase-shift [°]	Action suggested
BLL - CAR	Overhead line	220	50	1.03°	NO Resynch
BLL - PRT	Overhead line	220	26	0.74°	NO Resynch
CHI - PRI	Overhead line	380	60	4.24°	NO Resynch
CHI - PRI*	Overhead line	380	200	13.72°	Resynch
Linea 5	Cable	245	100	10.73°	Resynch

2.7 Conclusion

In this chapter, the problem of the voltage angle phase-shift due to overhead transmission line was discussed and explored by using a custom electronic equipment. The objective of the study was the assessment of the accuracy of the simulations results, in order to deduce look up tables as support tool for the identification of the actual phase displacement and suitably correct the data collected by the PhaseCheck device in a remote location.

Although the phase-shift measured in the considered experimental conditions are small, longer transmission lines and higher levels of active power transits can cause a greater phase error between the two ends of the line. An excessive phase error, up to 15°, may result in a wrong interpretation of the PD patterns, giving rise to the possibility of obtaining false positives or negatives in the diagnosis for the HV/MV devices. For this reason, it was proposed the possibility to use as reliable synchronization reference the remotely measured AC voltage of the same phase by which the component under PD test is supplied, at the nearest accessible substation.

The experimental measures have proved the correctness of simulated values and that it is possible to create a Look Up Table to deduce the phase-shift determined by the voltage wave propagation along a transmission line, based on line length and electrical features. The next step is to evaluate the voltage phase-shift in cable line, since the phase-shift is greater than overhead transmission line due to cable parameters.

3. Partial discharges measurement in non-sinusoidal regime

3.1 Introduction

In modern power transmissions systems power electronics devices are used for rapid switching and can generate High Voltage High Frequency (HVHF) oscillations which may be as a consequence of resonance, overvoltage due to fast switching operations (power inverters perform fast switching operations thanks to IGBT) [22], leading to undesirable degradation of cable insulation. Because of several technical and economic advantages, cross linked polyethylene (XLPE) high voltage cables have been widely used in power transmission and distribution systems. However, ageing deterioration of XLPE insulating material cannot be avoided because it is made of polymeric material. The use of fast switching components, such as Insulated-Gate Bipolar Transistors (IGBTs), Thyristors (SCRs) and Mosfets (FETs), puts components and cables under a greater stress due to the presence of waveforms different from the classical 50 Hz sinusoidal shape. The presence of the square [24] and PWM [25] waveforms can stress the insulating system, due to the fast voltage switching polarity and short rise times [26]. Partial discharge (PD) will thus occur with higher probability leading to insulation degradation or indeed a complete component failure. Mainly, the PDs are dependent of the voltage rise time as when varying the rise time, the number and the amplitude of the discharges changes [27].

In order to understand PD phenomena under non-sinusoidal voltage a deep investigation thank to the collaboration to the Chalmers University of Goteborg has been conducted. This chapter describes measurements performed by means of the PD measurement system present on the High Voltage laboratory of the Chalmers University and the Pry-Cam Portable prototype.

3.2 Measurement setup and acquisition system

The main aim of this work is to evaluate the PD activity with applying square waves at different voltage frequencies with different rising/falling times using two different detection methods. Both analysis of individual PD pulses in time and frequency domains were performed and used as complements.

The objects tested were chosen to replicate the defects typically appearing in real applications: corona (point to plane, and needle-needle configurations), internal (three layers with the cavity hole of 4 mm of diameter in the center disc), surface discharges (twisted pair) and a three-phase motor stator to compare the responses of the acquisition systems on a complex insulation system. The tests on different PD sources were performed with sinusoidal wave at 50 Hz, square wave frequency of 50/350 Hz with short (10 µs) and a longer rise time (250 µs). To carry out tests has been used the measurement setup for generating the voltage waveform at different frequencies with different rising/falling times. The system shown in Figure 3-1 is designed with the main objective to generate square or PWM voltages with different rise times and filtering levels (smoothness) [28]. The setup is based on a high voltage switch (Behlke HTS 501-03-GSM), with the main objective to generate square shaped voltages of different rise times, then a traditional AC PD test circuit, employs a 50/60 Hz HV transformer, a filter resistor of 100 kΩ to limit power system noise and a coupling capacitor of 100 pF connected in parallel with the PD source. More details about both these setups can be found in [29].

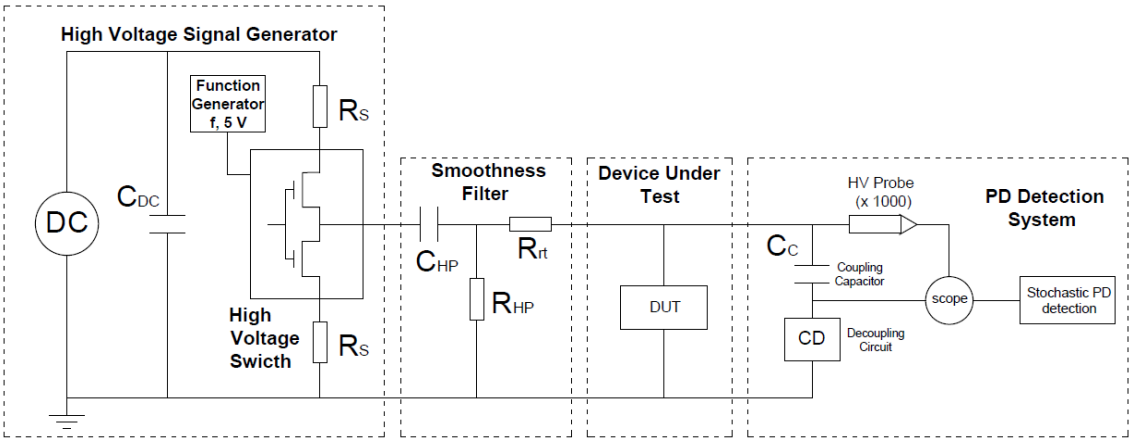

Figure 3-1. PD Measurement setup layout

The PDs are acquired by two acquisition systems each based on different operating and data processing methods. The first, shown in Figure 3-2 , is based on a Resonant PD Decoupler (RPDD) [30] and the second one on an antenna sensor with a flat frequency response [5], a Pry-Cam Portable prototype as shown in Figure 3-3.

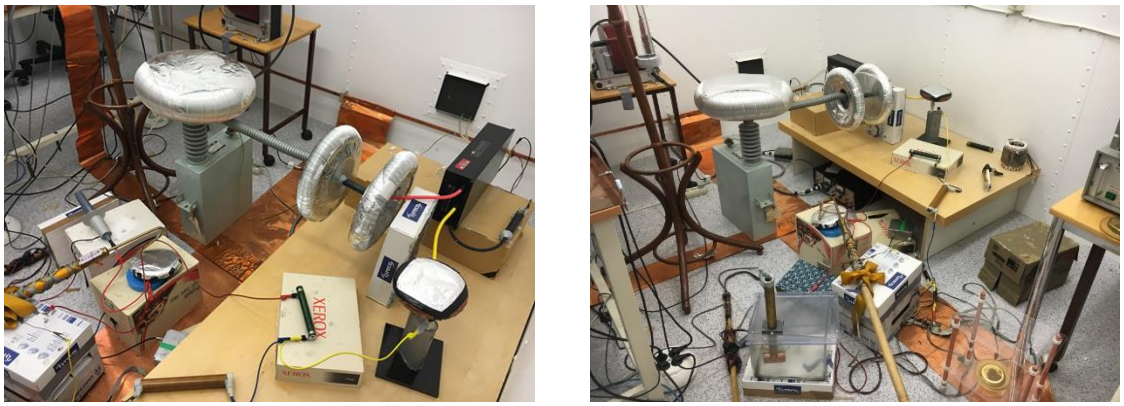

Figure 3-2. PD Measurement setup at HV laboratory of Chalmers University

Figure 3-3. Pry-Cam Portable prototype

The two PD acquisition systems present various differences mainly concentrated in the signal acquisition philosophy. The RPDD system is based on resonant decoupler that get pulses only in the bandwidth of interest filtering the noises due to remnants and commutations. This procedure allows discriminating partial discharge from disturbances with different frequency content as well as phase locked disturbances. All PDs are acquired in terms of shape, amplitude and phase with high resolution. However, at the same time, the filter changes the pulse shape making it unnecessary to attempt to identify any discharge's phenomenon. To present results in terms of patterns and statistical parameters it may be necessary a post processing analysis.

The Pry-Cam Portable Prototype system based on a PD antenna sensor, unlike the first, acquire all the signals with flat response. The instrument allows to apply four different filters both on-line and off-line. Each filter is applied selecting the pulse from the pattern and removing the

discharges on the basis of pulse shape correspondence. Pry-Cam Portable can discriminate the PDs as a function on different type of shape and amplitude. The antenna PD sensor system identifies the various noise sources characterized by shape and frequency content different from partial discharge pulses. Furthermore, it is possible to estimate each pulse shape in real time to identify the presence of the PD or pulses due to noise.

Therefore, the combined use of the two PDs measuring systems has allowed to comprehensively examine the phenomenon of PDs not only with sinusoidal system setup but above all with various applied voltage waveforms.

3.3 Measurements and analysis

3.3.1 Sinusoidal voltage waveforms

The conventional interpretation of different PD sources was made by applying a sinusoidal 50 Hz input. PD pulse shape, rise time, equivalent time length and frequency spectrum are generally used to recognize the time-frequency characteristics of PD signals. As reported in the literature, it is a well-recognized fact that antenna sensors are able to provide additional information on PD phenomena identification by pulse shape analysis in time and frequency domains [31]-[33]. This possibility is strongly related to the bandwidth and gain of the antenna sensor. Analysis of individual PD pulses in time and frequency domains was performed and it may provide additional useful information about PD phenomena.

The acquired PD pattern is shown in Figure 3-4 for Corona discharges, obtained in needle-needle configuration, in which the colormap represents the number of discharges. It must be emphasized that the red sinusoidal waveform in the PD Pattern is only a reference. the Figure 3-4 shows the time and frequency domain analysis of a corona PD pulse, Fast Fourier transform (FFT) was applied to the digital signal in order to obtain the Single-Sided Amplitude Spectrum of PD.

- Corona discharge

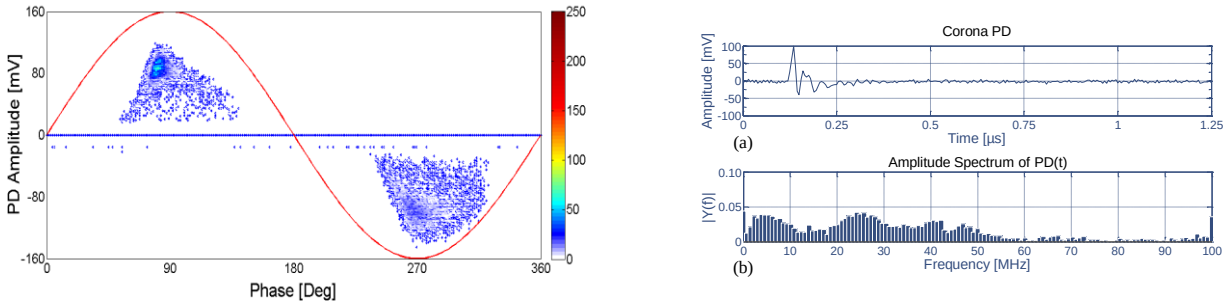

Figure 3-4. PD Pattern of Corona discharge at 12 kVpp sinusoidal voltage
a) Corona PD pulse; b) Frequency spectrum of the PD pulse.

In Figure 3-5 - Figure 3-7 the PD patterns, pulses shape and frequency content of the internal discharge, surface discharge (Twisted Pair) and PD in Motor Stator are reported.

- Internal discharge

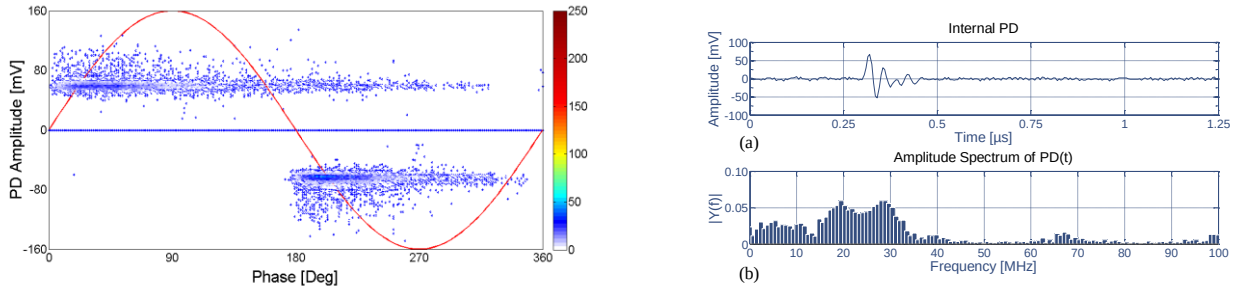

Figure 3-5. PD Pattern of Internal discharge at 14 kVpp sinusoidal voltage
a) Internal PD pulse; b) Frequency spectrum of the PD pulse

- Surface discharge (Twisted pair)

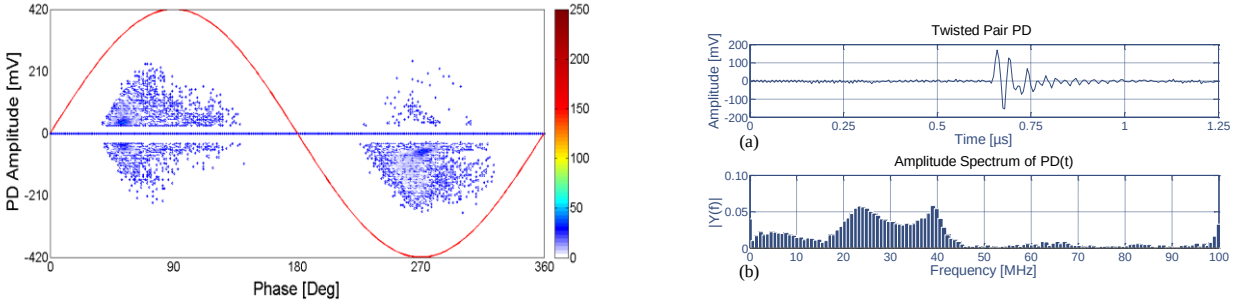

Figure 3-6. PD Pattern of Surface discharge at 2.2 kVpp sinusoidal voltage
a) Surface PD pulse; b) Frequency spectrum of the PD pulse

- PD in Motor Stator

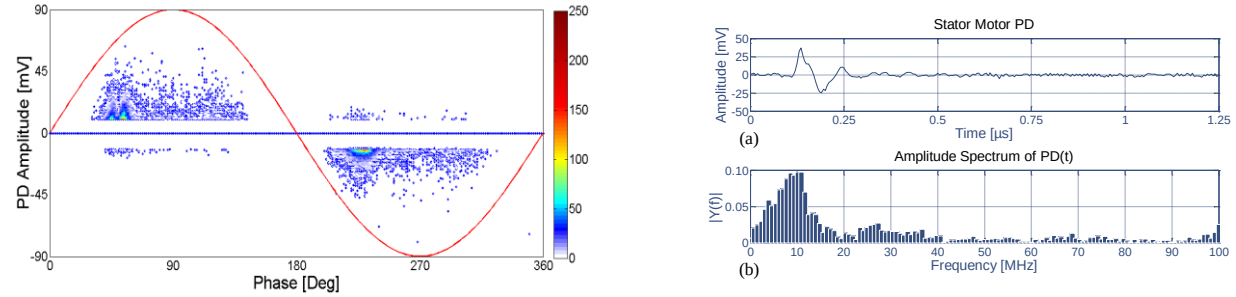

Figure 3-7. PD Pattern on Motor Stator at 4,8 kVpp sinusoidal voltage
a) PD pulse; b) Frequency spectrum of the PD pulse

The pulse analysis is achieved utilizing the portable digitizer to obtain an accurate estimation of the PD shape. This function analyzed each individual pulse in terms of FFT content, to characterize and identify accuracy, PDs, presence of noise. In the previous measurements noise was not present and the frequency content was 20-40 MHz for Corona, internal and surface phenomena. Conversely, it can be noted that the PDs within the motor stator has a lower frequency content, around 10 MHz, and is likely affected by the travelling time through the stator.

3.3.2 Disturbance generated by HV Switch and the DC supply

To generate square waveforms, the HV switch (Behlke HTS 501-03-GSM) with an auxiliary DC supply voltage have been used. Both systems generated high frequency pulses which were detected during the PD acquisition. The High Voltage (HV) switch generated an impulse every rising and falling time of the square wave. The control circuit (DC supply), in turn, generated some high frequency pulses with a repetition rate that depended on the chosen signal frequency. However, both phenomena have a deterministic and not stochastic behaviour, while spurious signals were identified and removed. Both signals have been identified in time and frequency domains and distinguished from partial discharges. In Figure 3-8, a clear example of surface PD pattern with square wave 50 Hz and rise time of 250 µs show the presence of pulses generated by HV switch and DC power supply. In particular, inside the circle HV switch pulses, while inside the frame the noise due to the DC supply control circuit were identified.

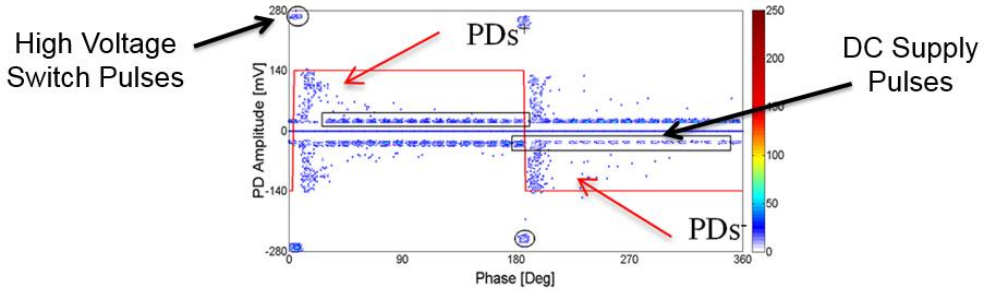

Figure 3-8. Identification pulses generated by the HV switch and DC supply

The time and frequency analysis of pulses generated by the HV switch are shows in Figure 3-9 and Figure 3-10. The big pulse signal remnant from the polarity shift contains higher amplitude spectrum in the frequency range between 30 and 40 MHz while the internal switching noise also shows a lower frequency content.

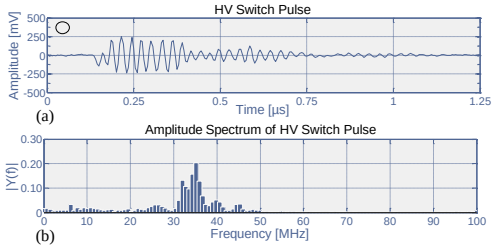

Figure 3-9. Identification in time (a) and frequency (b) pulses generated by HV switch

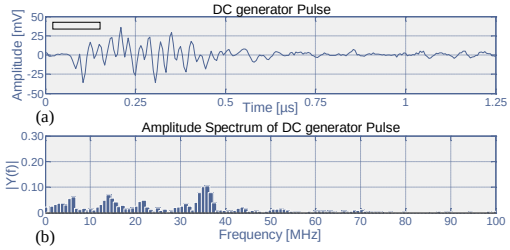

Figure 3-10. Identification in time (a) and frequency (b) pulses generated by the switched control circuit

However, the PD pulse and the frequency content are different compared to the switching pulses frequency and this can be assessed in Figure 3-11.

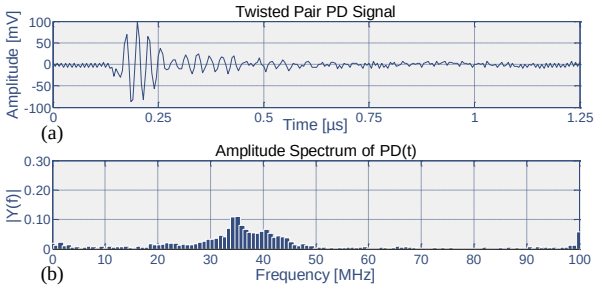

Figure 3-11. Identification in time (a) and frequency (b) of the PD pulse of twisted pair specimen with square wave 50Hz at rise time 250 µs

3.3.3 Square wave 50 Hz/350Hz at rise time 10 µs and 250 µs

In most cases, different PD phenomena can be identified and classified by means of pattern recognition analysis for sinusoidal waveforms [34]. Using square waveforms, the classical methods for partial discharge identification based on the shape of the discharge pattern is no longer usable. Phase angle $\Delta\varphi$, statistical parameters such as Weibull and others standard statistical parameters are not significant with square waves, so the classical statistical analysis cannot be applied [47].

One of the main characteristics observed for square waves is that most PDs are concentrated at the rising and falling edges of the applied voltage waveform. The adoption of different rise times allows evaluating its influence on the partial discharge phenomena. In particular, it was observed in all the measurements made, that the phase angle of discharges was lower in the case of square wave with rise time of 10 µs compared to the case of 250 µs, which is a consequence of PDs occurring only on the edges.

As expected the voltage remnant was higher and more oscillatory in the captured data with the shorter rise time than in the case of 250 µs rise time. Furthermore, from the tests it was generally observed that the frequency content of the PDs did not change for 50 Hz or 350 Hz square waves, as expected.

- Corona discharge

Initially the analysis was conducted on Corona PD with point to plane (single side) and needle-needle (double side) configurations. In Figure 3-12 a needle-needle corona PD pattern with square waveform 50 Hz at rise time 250 µs is shown. The pattern illustrates the presence of discharge phenomena close to the waveform rising/falling times and the PDs amplitude is found slightly larger than that achieved in the sinusoidal case due to the rapid voltage variation at the polarity shift.

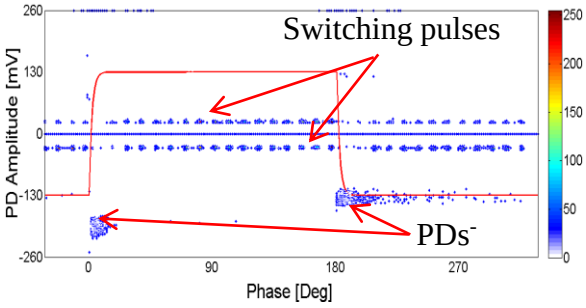

Figure 3-12. Corona PD pattern applying a square waveform of 50 Hz with rise time 250 µs.

For a better understanding of Corona PD phenomena, different Corona PD pulses with square wave 50 Hz at rise time 10 µs for single side configuration and corona PD pulse with square wave 50 Hz at rise time 250 µs for double side configuration are shown in Figure 3-13, where the pulse waveform and their frequency spectrum are reported. It can be observed a continuity of the frequency content for each configuration. Regardless the square wave frequency, in both configurations, the PD amplitude is comparable. In this way, the FFT analysis allows to identify two corona discharges having different origin.

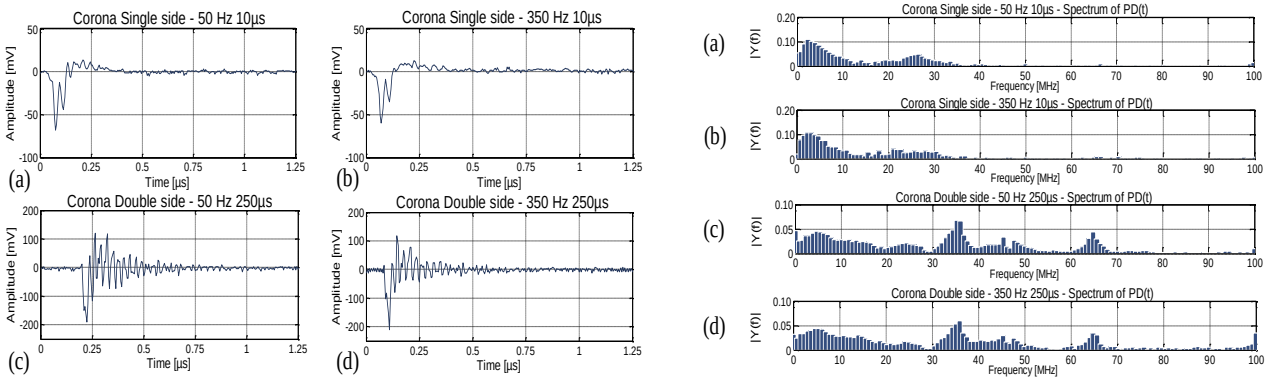

Figure 3-13. Corona Single side PD pulses and frequency spectrum applying a square wave a) 50 Hz with rise time 10µs b) 350 Hz with rise time 10µ; Corona Double side PD pulses and frequency spectrum applying a square wave c) 50 Hz with rise time 250µs; d) 350 Hz with rise time 250µs.

- Internal discharge

The acquisition of cavity discharges with Pry-Cam Portable prototype has presented more difficulties than for other defects, especially with the shorter rise time. Internal PDs with a 50 Hz square wave with 250 µs rise time are presented for a measured amplitude comparable to the switch noise. Therefore, the system acquires both types of pulses. Figure 3-14 shows the PD pattern with the cavity discharges near the polarity shifts and the switch internal noise spread out over the complete period. It is however still possible to visually distinguish the PD pulses from the noises.

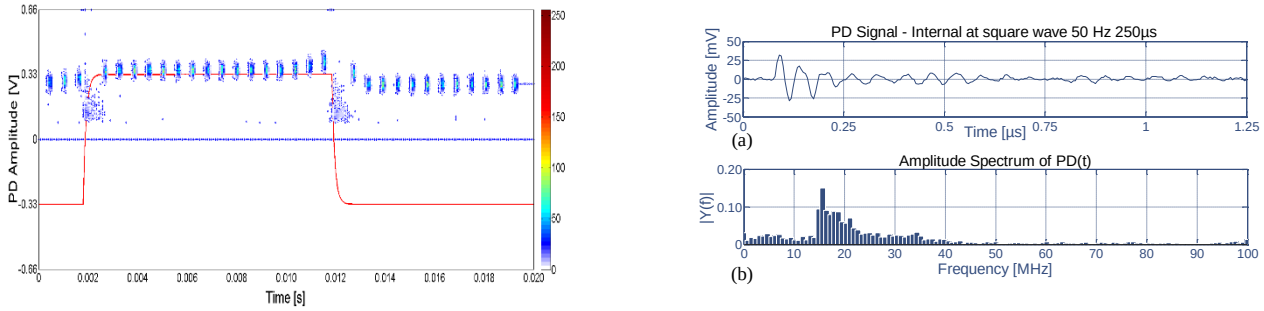

Figure 3-14. Internal PD pattern applying a square wave of 50 Hz with rise time 250 µs. Identification in time (a) and frequency (b) Internal PD applying a square wave of 350 Hz with a rise time of 250µs.

Most PDs were located at the square wave polarity change, while a few were evenly distributed across the period. Here the PD amplitude was comparable or even smaller than the magnitude of the switch noise. Similar result was obtained at 350 Hz, where only two switch noise pulses appear. In both cases a typical pulse shape was acquired and the amplitude spectrum analysis can be performed. The frequency content, even if comprised between 15 and 40 MHz like in the sinusoidal case, presented a quite different shape distribution.

An even more demanding condition for the Pry-Cam portable instrument was a measurement when applying a square wave with a rise time of 10 µs. In such conditions, the instrument was only able to identify the pulses generated by HTS HV switch. The reduced rise time implies a lower phase angle and the PDs appear often superimposed to the voltage remnants. This difficulty was due to acquisition dead time between one pulse and the subsequent, which in this case hides all PDs on the vertical sides of the waveform and for this reason it is necessary to change the single pulse time acquisition window from 1 to 10 µs. In this way, the shift of the recording time up to 10 µs, allows assessing some of the PDs superimposed to the voltage remnants. In Figure 3-15, it is possible to observe the 10 µs voltage rise time (blue line) and the voltage remnant in which PDs are present after the first microsecond (red line). In this case, the

PDs appear only in the first few microseconds after the remnants while with longer rise times the influence of the voltage remnant is less prominent.

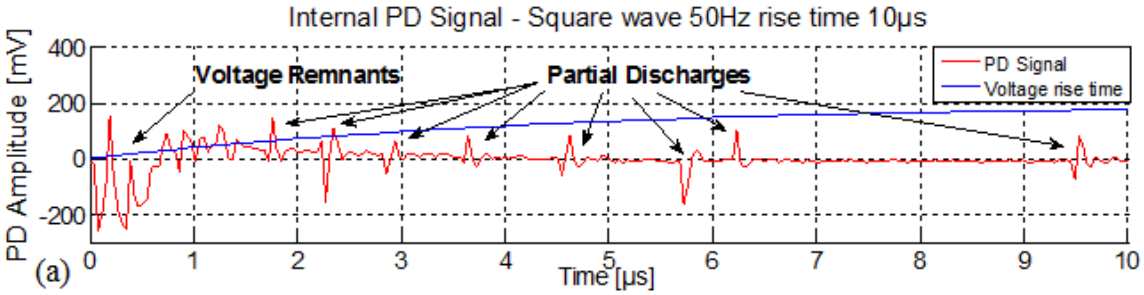

Figure 3-15. Internal Partial discharge applying a square wave of 50 Hz with a rise time 10µs superimposed on the voltage remnants

It is thus observed that the acquisition of PDs become more difficult with the antenna sensor for rise times less than a few tens of microseconds. With the Resonant PD system, the effect of the voltage's rise time is illustrated in Figure 3-16, where a comparison among square waves of 10 µs and 250 µs rise times (50 Hz) and the 50 Hz sinusoidal waveform are shown. A progressive concentration of PDs to the voltage flank and a high PD magnitude can be observed. In [30] it is however shown that in relation to the rise time, the time delay is increased when the rise time decreases.

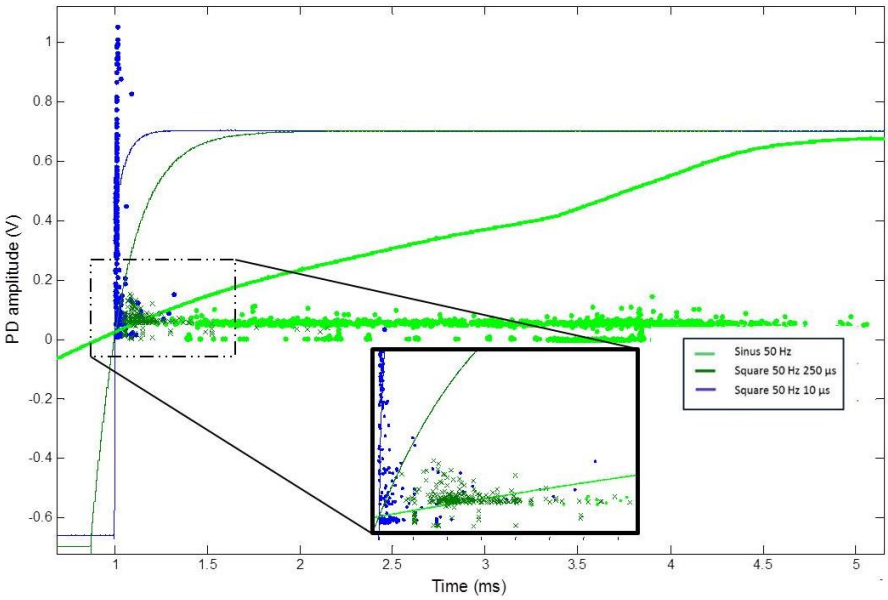

Figure 3-16. Comparison of cavity PD activity during tests with square waves of rise times 10 µs and 250 µs (50 Hz) and sinusoidal wave of 50Hz.

- Surface discharge (twisted pair)

The third defect analysed is surface discharges in twisted pair specimens. Figure 3-17 illustrates the PD pattern obtained by means of Pry-Cam Portable when applying 350 Hz square wave for both 10 and 250 µs rise times. As it can be seen, also in this case there is a strong dependency on the rise time. For the rise time of 10 µs (red pattern), PDs are predominantly localized on the vertical sides of the waveform and their amplitudes are higher. In the second case, with a rise time of 250 µs (blue pattern), the PDs amplitude is lower and conversely PD pulses were arranged on a greater phase range.

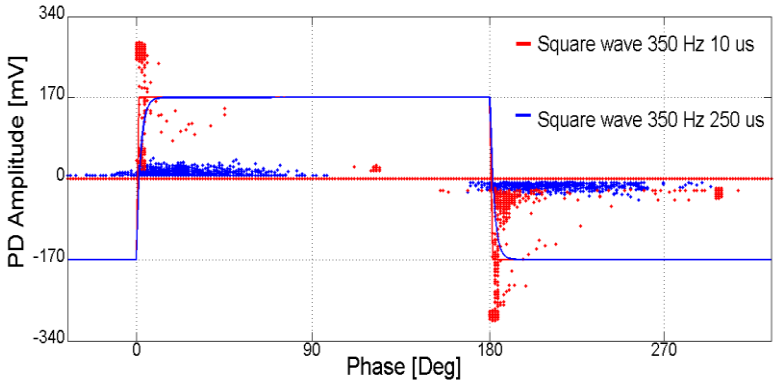

Figure 3-17. Compared twisted pair PD patterns with square wave 350 Hz at rise time 10 µs and 250 µs.

Figure 3-18 shows the analysis of a PD pulse with square wave 350 Hz at 10 µs and at 250 µs rise time respectively. From the comparison, it can be noted that the two pulses have substantially different amplitudes, due to the different rise times. The first PD pulse has an amplitude equal to 180 mV while the second has an amplitude of about 40 mV. The dashed red line, inserted in the first PD pulse picture, indicates the order of magnitude of the second PD pulse.

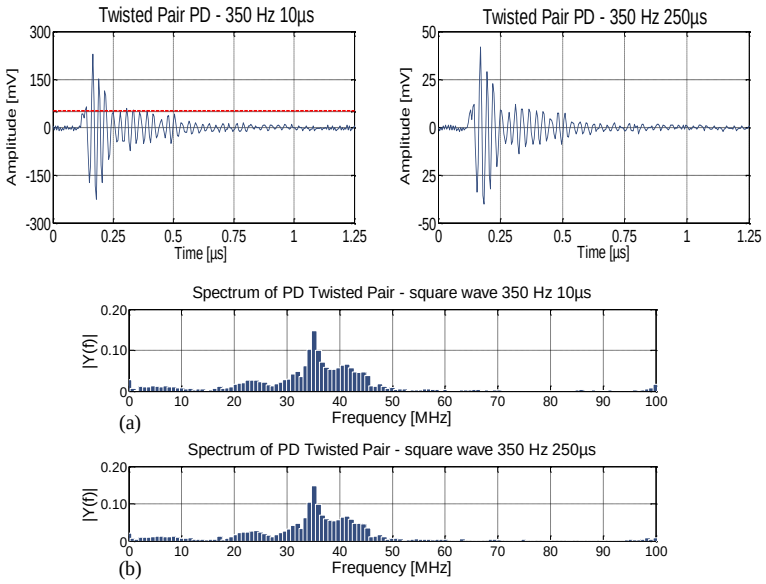

Figure 3-18. Twisted pair PD pulses and frequency content applying a) a square wave 350 Hz with rise time 10; b) a square wave 350 Hz with rise time 250 µs.

By the frequency analysis it can be noted that for different rise times the Frequency Spectrum was concentrated in the frequency range between 30 and 50 MHz.

Similar results were obtained with Resonant PD system, as shown in Figure 3-19. Twisted pair acquisition with square wave 350 Hz at rise time 10 µs and 250 µs respectively have shown the same trend of the patterns. The number of PDs detected follows the number of polarity shifts and the PD amplitudes are larger for a shorter rise time. The longer rise time also reveals more PDs per cycle but with smaller magnitude. The PDs that appear in twisted pair test object have overall larger magnitude than the noise, which facilitates the detection process.

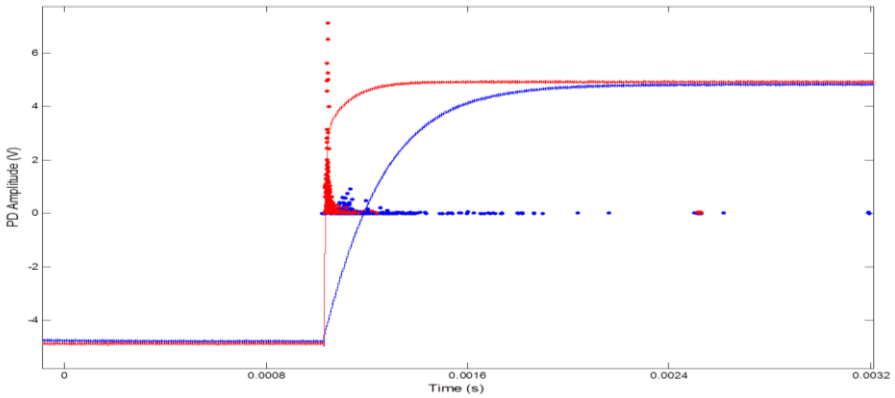

Figure 3-19. Comparison of twisted paid PD pattern with square wave 350 Hz at rise times 10 µs and 250 µs.

- PD in Motor Stator

The comparisons of PD activity in the motor stator setup, for the 10 µs and 250 µs waves as well as for the sinusoidal waveform of 50 Hz are respectively illustrated for PASPD and STOPD systems in Figure 3-20 and Figure 3-21. Here again a progressive increase in PD amplitudes can be observed for shorter rise times, whereas their magnitudes for a longer rise time and the sinusoidal waveform are about the same. The dynamic range used in the STOPD system is however larger. The PD magnitudes close to the polarity shift are here larger than the switching noise, which better facilitates the data analyses that are done on-line. For PASPD system the triggering level is set below the switching noise and thus more challenging to resolve the PDs, which requires an additional post processing to quantify the actual exposure.

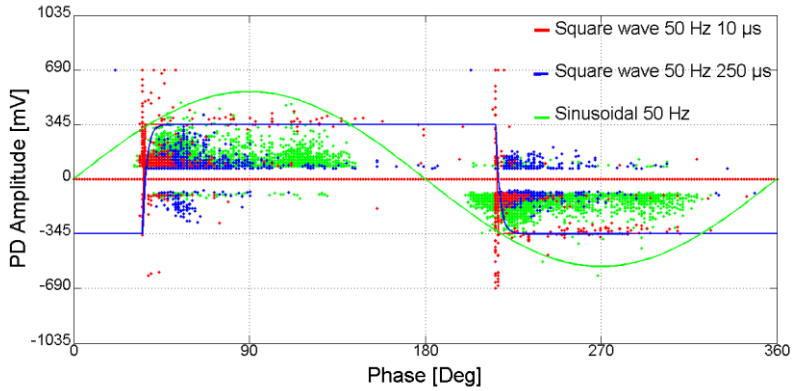

Figure 3-20. Comparison of motor stator PD activity during PASPD tests with square waves of rise times 10 µs and 250 µs (50 Hz) and sinusoidal wave of 50Hz.

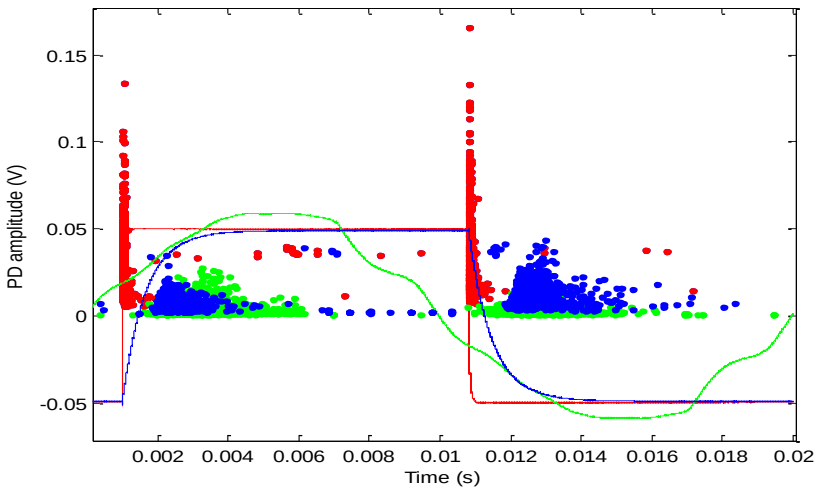

Figure 3-21. Comparison of motor stator PD activity during STOPD tests with square waves of rise times 10 µs and 250 µs (50 Hz) and sinusoidal wave of 50Hz.

In Figure 3-22 it is shown the motor stator PD pattern resulting from a 350 Hz square wave with a rise time of 10 µs. In this case the phase shifted switching pulses are made by the DC supply while the PDs are distributed mainly near the rising/falling times. In this case, these PD pulses have an amplitude less than the switching pulse made by High Voltage Switch, while compared to the DC supply switching pulse are about the same magnitude.

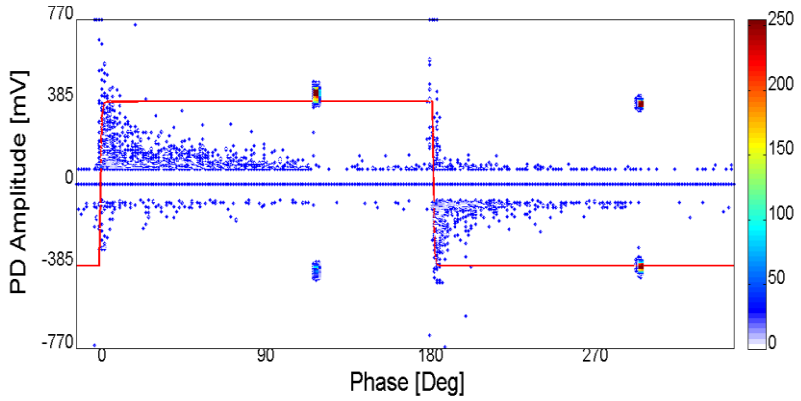

Figure 3-22. PD pattern on motor stator applying a 350 Hz square wave with a rise time of 10 µs

A further comparison on stator motor test with square wave 50Hz/350Hz at rise time 10 µs/250 µs are shown below. In Figure 3-23 different stator motor PD pulses, for each case, are compared. As can be seen, the pulses at rise time 10 µs and 250 µs, about 60 mV and 20 mV respectively, have similar shape and amplitude.

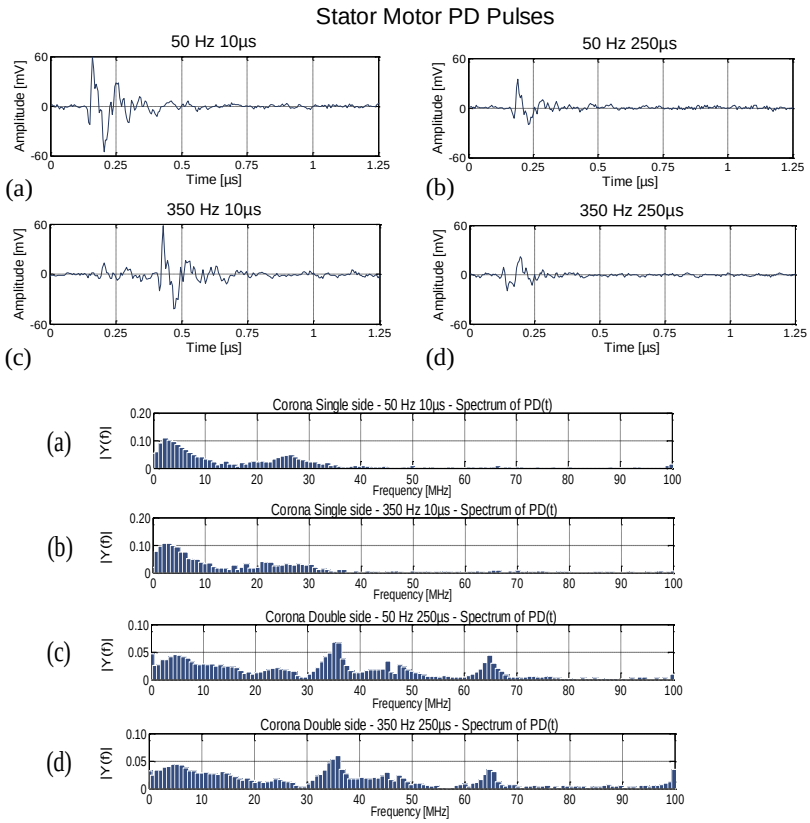

Figure 3-23. Stator Motor PD pulses and Frequency spectrum applying a square wave of a) 50 Hz with rise time 10µs; b) 350 Hz with rise time 10µs; c) 50 Hz with rise time 250µs; d) 350 Hz with rise time 250µ

Of particular importance is the fact that for square-wave with different rise times and frequency, even if the partial discharges have different amplitudes as a function of the inception voltage (rise time), the frequency content of the individual discharges is the same. Therefore, it is possible to identify the phenomena of partial discharge and characterize the pulses as a function of the frequency content.

3.4 Conclusion

It is demonstrated that there are several features, important for effective detection of PD signals appearing at rapidly changing test voltages from power electronic devices. The main requirement is the ability to synchronize to substantially higher frequencies than the normal power frequency. It was shown that the rise times of the square wave voltage has significant influence on the PD characteristics as detected by both systems. The shape of discharges and the frequency spectrum might allow to obtain additional data to identify the different discharge phenomena even when the visual study of the PD patterns is not able to help in the defect identifications process.

This work has also demonstrated that PDs can be detected by various sensing methods with comparable sensitivity. It is thus more the design features that may enable a PD measurements system to be used for power electronic waveforms than the sensing principle itself as in all insulation systems tested it was possible to detect the presence of PDs and observe changes in amplitude for square shaped voltages.

4. Impact of Harmonics on Interpretation of PD Patterns

In this chapter, the analysis of superimposed harmonic voltage effects on PD measurements is reported. Partial discharge measurements are extremely important for assessment of high voltage electrical insulation integrity. Generally, the influence of harmonics is not considered, however it might have significant influence on results interpretation. The problem of harmonic influence on the test voltage is crucial not only for the partial-discharge measurements, but also for the proper interpretation and assessment of PD defects in insulating systems. Harmonic modulation of the test voltage, for certain combinations of harmonics, may result in the acceleration of PD activity, thus having direct impact on the endurance and lifetime of the electrical insulation. The aim of this research is to understand and evaluate the impact of harmonics on partial discharge behaviour, in particular on the PD diagnosis by means the Pry-Cam portable instrument, and on the PD Pattern acquisition process. Typically, in laboratory and diagnostics tests focused on measuring partial discharges, a pure sinusoidal voltage waveform is assumed. However, in practice the frequency content of the applied voltage is rarely so ideal and the presence of higher order harmonic frequency components has a significant impact on the PD phenomenon in electrical insulation systems.

The measurements were conducted on a MV cable specimen in which a defect was made in the semiconductive layer in order to generate a high frequency surface discharge. The MV cable specimen, initially, was subjected to sinusoidal voltage waveform with magnitude of 5.8 kV, and the PD Pattern was acquired as a reference for the execution of the subsequent tests in the presence of harmonics. To visualize the influence of harmonic on PD, several measurements were carried out for a sinusoidal voltage waveform with magnitude 5.8 kV, containing harmonics components at 5%, 10% and 20%. Moreover, to visualize the influence of harmonic phase angle on PD, the measurements were performed considering for each harmonic component a phase angle of 0°, 90° and 180°.

The results showed that various harmonic, 3^{rd}, 5^{th}, 9^{th} and 11^{th} superimposed on the fundamental sinusoidal waveform have a significant impact on PD amplitude and PD pattern shapes. On each case, the phase angle 180° exhibits the sharpening of the voltage waveform and results in an increased PD magnitude and intensity relative to phase 0°.

The presence of harmonics components can significantly influence the acquisition of the PD pattern and also may arise synchronism problems during the measurements. In this case, in

order to acquire a correct PD pattern shape, the re-synch function described in section 4.2 had to be performed. The cited function allows resynchronize the PD pattern at 50Hz and to obtain a precise shape of the PD phenomenon.

4.1 Introduction

The evolution of power systems continues to increase nonlinear loads, leading to locations of high harmonic content and reduction of power quality not experienced previously. The influence of harmonics on insulation systems causes losses, lifetime and dielectric material degradation. Higher harmonic content in voltage waveforms is usually associated with dielectric heating in insulating materials which has accelerated the aging process of the material. Electrical, thermal and mechanical stresses are usually combined to form life time models of insulation systems. In general, the effect of voltage distortion on insulation degradation is associated to thermal aging, but that the effect of voltage peak and waveform can be predominant. Indeed, the voltage peak is the dominating factor for accelerating the degradation of insulation systems fed by both low frequency and high frequency harmonic components. The additional factors are voltage RMS, shape and thermal stress for low frequency harmonics [35]-[37]. An awareness of the impact of harmonics is especially important in modern diagnostics of powers equipment, which is increasingly based on PD phase-resolved patterns. In AC power grids and networks, sinusoidal voltage usually contains various harmonics caused by loads and resonances in the system. The presence of harmonics in a simplest case may be quantified by means of THD (Total Harmonic Distortion) defined as ratio of accumulated effective harmonics amplitude to fundamental harmonic.

$$THD = \left(\sqrt{\sum_{k=2}^{N} U_k^2} \right) / U_1 \qquad (1)$$

Where U1 is the effective value of the fundamental at 50Hz, U_k is the effective value of successive voltage harmonics and N is the total number of considered harmonics. Harmonic distortion may be measured by looking at the output spectrum and observing the values of the harmonics components with respect to the amplitude of the fundamental signal. The value is usually expressed as a ratio in %. THD can be only treated as a rough estimation of voltage quality in the context of its impact on PD. Harmonics distort voltage waveforms which, in turn, impacts on PD behavior. Thus, in modern diagnostics it is of utmost importance to properly understand and interpret the presence of harmonics when measuring and analyzing PDs.

The problem of harmonic influence is common to all measurements based on acquisition of phase resolved partial discharge images. The effect of-non-sinusoidal voltage on power networks is to produce harmonics. This phenomenon is crucial for proper identification and classification of PD patterns.

Diagnostic phase-resolved partial discharge patterns are greatly influenced by the presence of harmonic content on a purely sinusoidal excitation voltage. Factors, including the phase relationship and the magnitude of the harmonic content relative to the fundamental, may influence the resultant waveform potentially leading to the following effects:

- changes in maximum discharge magnitude;
- changes in the phase location of discharge activity;
- changes in the number density of the discharge activity;
- changes to regions with no discharge activity, known as ‘dead zones’;
- asymmetrical discharge activity for positive and negative cycles.

These changes in the partial discharge patterns are deceptive and can lead to erroneous conclusions about the insulation’s integrity. Varying degrees of harmonics occur in real power networks and they also often exist in laboratory voltage supplies. Hence the influence of harmonics must be acknowledged and accounted for in all partial discharge measurements [38]-[40].

The detection of PD signals in the industrial environment is associated with the following issues:

- disturbances, influencing the effective signal-to-noise ratio;
- the influence of high-voltage waveform, especially important in phase-resolved PD acquisition synchronized with the period of test voltage.

The latter problem results from the presence of harmonics of the supply voltage infiltrating the PD measuring circuits. The experimental results, reported in [41]-[45], show how the various harmonic compositions superimposed on the fundamental sinusoidal waveform have a significant impact on PD intensity and maximum charge. In consequence, PD patterns, phase, and amplitude distributions are distorted and influence the derived statistical parameters as well. A study reported in [46] investigates the effect of voltage affected by the presence of harmonics on intrinsic aging of cable and capacitor insulating materials, shown that the factor predominant

on aging acceleration due to the voltage distortion is voltage-peak increase, but also waveform slope and voltage rms value have statistical significance.

The test-voltage harmonics influencing the waveform are changing discharge inception and extinction conditions, which result from the instantaneous voltage level during the period. The endurance of electrical insulation is dependent on applied voltage; thus, the harmonic modulation also has an effect on insulation lifetime. The influence of harmonics in the PD measurements is of fundamental importance for proper interpretation of the results, and thus for assessment of equipment condition.

The experiments reported in the following sections show the influence of harmonics in the PD measurements on proper interpretation of the PD analysis.

4.2 Measurements setup

In order to investigate the impact of harmonic components on Partial Discharge mechanism and on interpretation on PD Patterns, several tests were carried out on a medium voltage cable specimen in which a defect was made in the semiconductive layer, as shown in Figure 4-1. In particular, the defect was carried out in order to generate a typical high-frequency PD phenomenon.

Figure 4-1. Defect in MV cable specimen

As reported in Figure 4-2, to generate different voltage waveforms, an arbitrary waveform generator was used through a special software able to recreate different types of waveforms. In detail, the waveform was built using a software with the designated characteristics as magnitude of amplitude, phase and THD. After this, through a connection with GPIB port, this signal was sent to the function generator which in turn generated the low voltage waveform. In order to supply the cable specimen, low voltage waveforms were sent to a single-phase voltage transformer which reported the voltage signal constructed at a high voltage supply according to the transformation ratio 380 V / 100 kV.

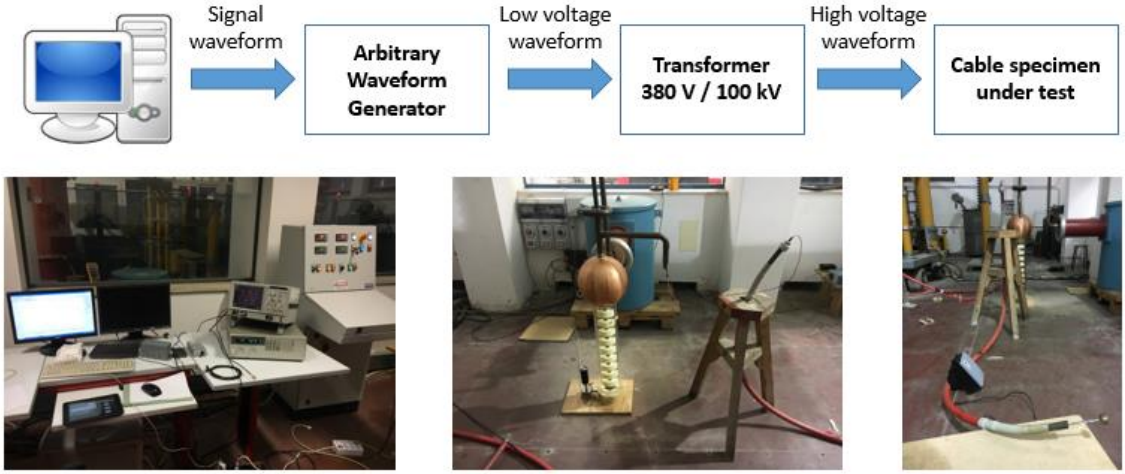

Figure 4-2. Measurement setup: arbitrary waveform generator, transformer and cable under test

In particular, the PD voltage inception of the defect in cable specimen had been tested at sinusoidal voltage, initially, in such a way as not to ruin and to cause sudden perforation of the specimen. The sinusoidal voltage signal was generated at a voltage of 22 Vrms, which corresponds to a value of 5.8 kV at the voltage transformer output.

In order to understand the impact of the harmonic components on the PD mechanisms, the measurements have been performed considering the following configuration of harmonics components:

- 3^{rd} Harmonic component at 5%, 10%, 20% and phase angle 0°, 90°, 180°;
- 5^{th} Harmonic component at 5%, 10%, 20% and phase angle 0°, 90°, 180°;
- 9^{th} Harmonic component at 5%, 10%, 20% and phase angle 0°, 90°, 180°;
- 11^{th} Harmonic component at 5%, 10%, 20% and phase angle 0°, 90°, 180°.

For all PD measurements, with different harmonic component waveforms, it wanted to keep the voltage value of 22 Vrms, that correspond to 5.8 kV, in order to not determine high discharge values that can compromise the execution of the tests.
During all measurements, Pry-Cam Portable was placed on the cable close to the defect as reported in Figure 4-3.

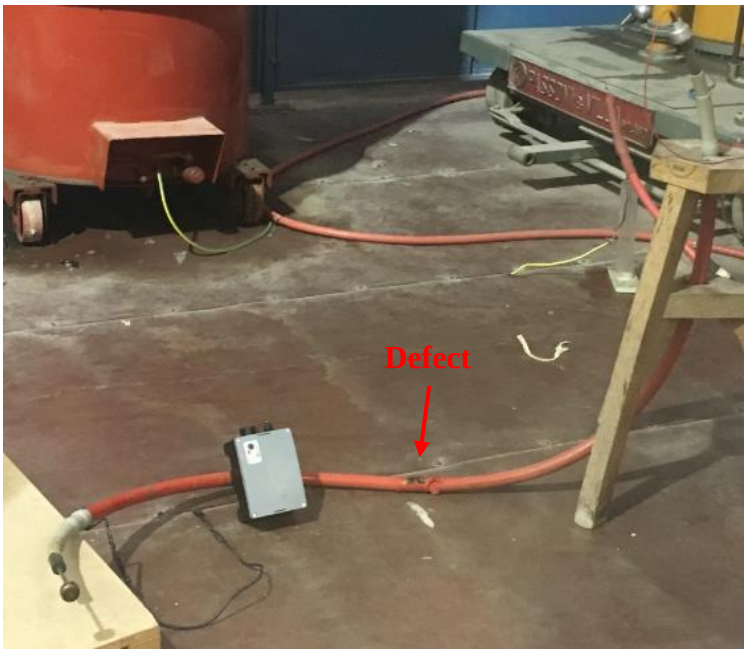

Figure 4-3. Pry-Cam Portable placed on cable close to the defect

At first, the PD measurement has been performed at 6 kV and 50 Hz sinusoidal voltage. The acquired PD pattern show a high frequency surface discharge characterized by fast pulse and frequency content up to 40 MHz as reported in Figure 4-4. The PD maximum amplitude was registered at 22.35 mV.

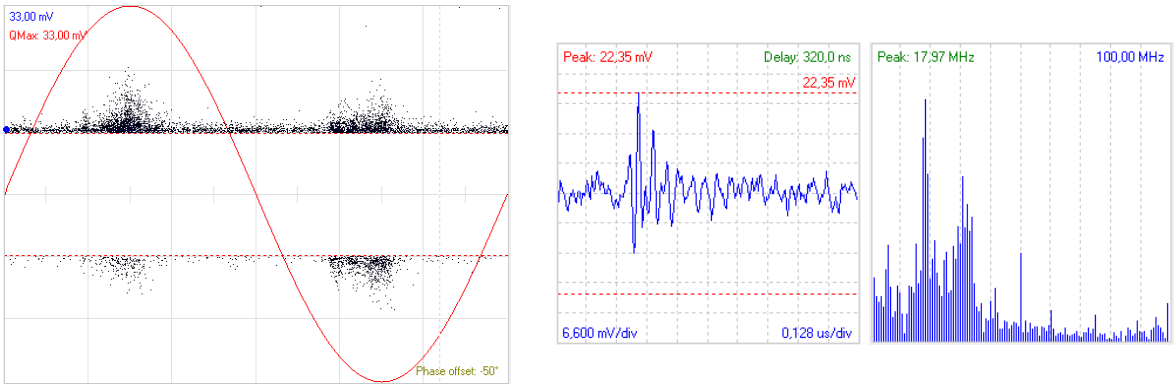

Figure 4-4. PD Pattern acquired at 5.8 kV of sinusoidal voltage -

During the PD measurement at sinusoidal voltage the synchronism was acquired by internal antenna sensor of the Pry-cam Portable. In this case, through the electrical field generated by the supply voltage it can be acquired a correct synch at 50 Hz. However, during the PD measurements carry out in presence of harmonic components, several issues have been arising to acquire a correct synch. Indeed, based on the magnitude of the harmonic component, the instrument can not acquire a correct synch at 50 Hz, because the internal sensor can not catch the frequency of the fundamental waveform. In this case, an external synch device was used to acquire the synch by the artificial light (100 Hz) and acquired the 50 Hz frequency; in this manner, the Pry-cam Portable was able to acquire the correct synch and PD pulses were acquired at 50 Hz, but due to the supply voltage by the transformer, the acquired impulses did not create a correct PD pattern because the power supply frequency and the acquisition frequency it was not perfectly aligned. Therefore, in order to obtain a correct PD pattern performed in presence of harmonics components, re-synch function was used (Figure 4-5).

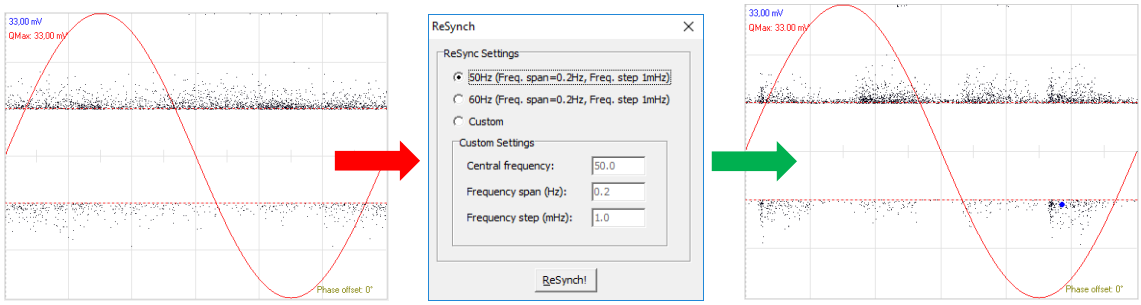

Figure 4-5. Re-synch function: PD pattern not synchronized, Re-synch toolbox and synched PD pattern

4.2.1 PD measurements with 3rd Harmonic component

The measurements were carried out for a sinusoidal voltage waveform with magnitude 5.8 kV, containing 3rd harmonic components (150 Hz) at 5%, 10% and 20%. The evolution of the PD pattern for three phase positions 0°, 90° and 180° and the corresponding voltage waveforms have been reported in Table 4-2. It can be observed that local extrema and variations of local slope changes in the voltage waveform are reflected in the PD pattern. For each case, the PD measurements show a higher increase of the PD amplitude at phase angles of 90° and 180° compared to the pure sinusoidal waveform. As reported in Table 4-1, it is not the THD level but the phase angle of the harmonic component that has a major influence on the PD amplitude. In fact, as the phase angle changes, there is the formation of local extremes such as to increase the slope of the waveform and therefore determine a greater stress. The measurements carry out with a phase angle equal to 0°, has been altered the waveform of the applied voltage and modified the shape of acquired PD patterns. However, there were no appreciable changes in the PD amplitude.

Table 4-1. Influence of the 3rd harmonic on PD measurements

Harmonic Order	% Magnitude per Harmonic	Phase φ	THD %	Max Pd amplitude [mv]	Increased PD amplitude
3rd	**5%**	**0°**	5.04%	22.35	0%
		90°	5.01%	59.46	166%
		180°	4.98%	55.43	148%
	10%	**0°**	10.00%	21.31	-5%
		90°	9.98%	59.97	168%
		180°	9.93%	64.00	186%
	20%	**0°**	19.67%	22.61	1%
		90°	19.66%	64.00	186%
		180°	19.59%	64.00	186%

Further analysis has been performed on the acquired PD pulses. In detail, as reported below in Figure 4-6, Figure 4-7 and Figure 4-8, the analysis of the pulse waveform and relative frequency content did not show any particular changes. For simplicity have been reporter three different cases in order to understand how the harmonic components did not change the PD pulse waveform but only the amplitude of the PD phenomenon.

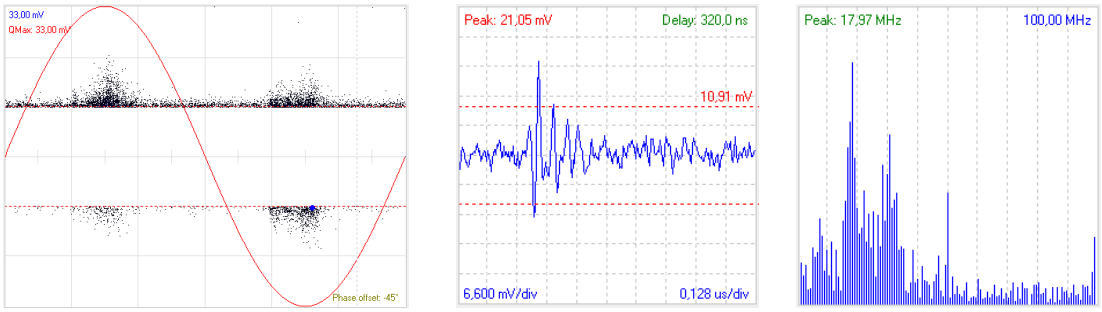

Figure 4-6. Analysis of the acquired PD pulse at 5% of 3rd harmonic and phase angle 0°

The analysis of frequency spectrum reported in Figure 4-6, show the presence of several frequency components due to the low amplitude of the PD pulse localized above the noise level.

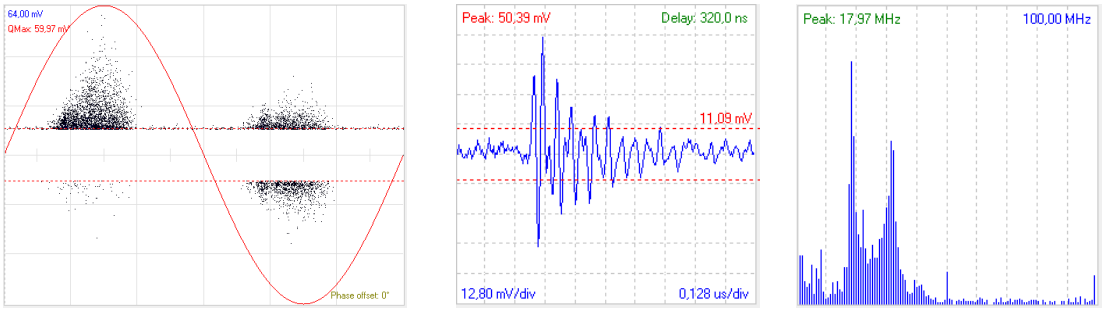

Figure 4-7. Analysis of the acquired PD pulse at 10% of 3rd harmonic and phase angle 90°

By comparing the frequency contents of the acquired PD pulses, it can be noted how the spectrum remains unchanged. The only peculiarity it can be noted that in presence of high magnitude of the harmonic component, the frequency spectrum of the PD pulse was more definite and the noise does not affect the harmonic content of the PD phenomenon.

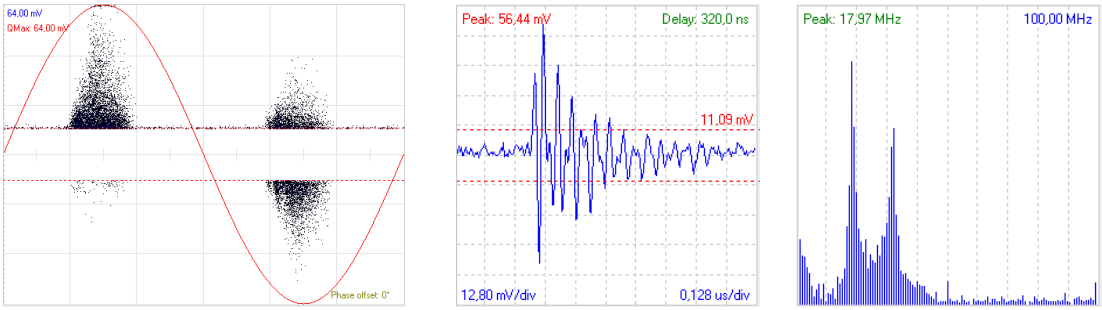

Figure 4-8. Analysis of the acquired PD pulse at 20% of 3rd harmonic and phase angle 180°

Table 4-2. Acquired PD Patterns and Voltage waveform with 3rd harmonic

5% of 3rd Harmonic		
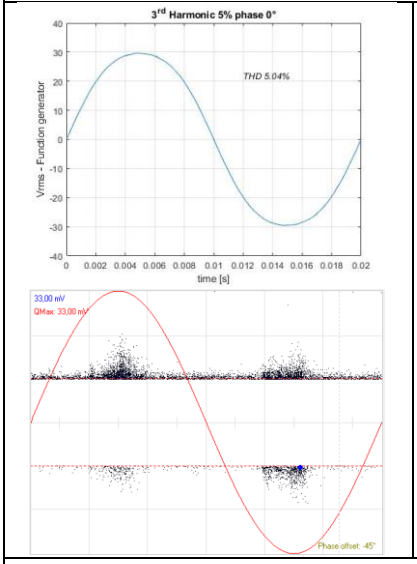	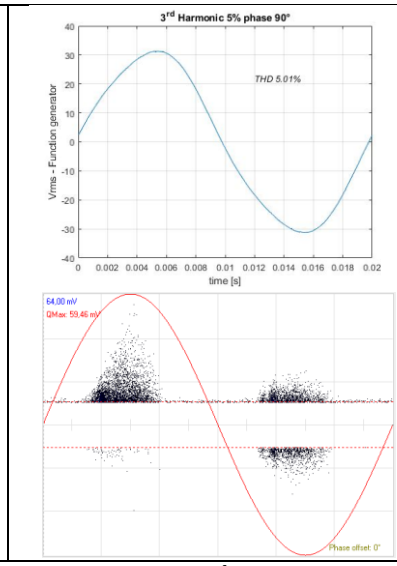	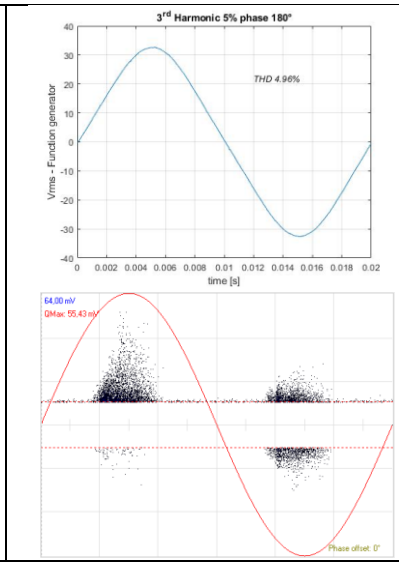
10% of 3rd Harmonic		
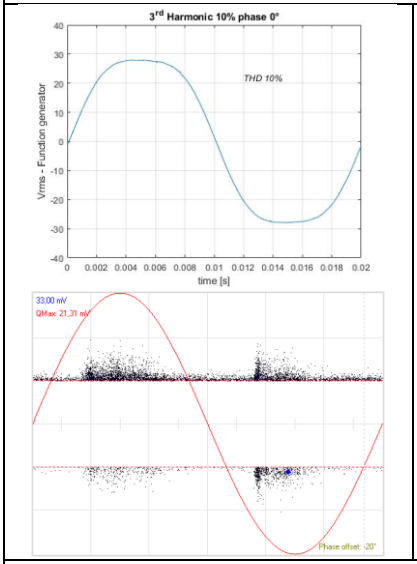	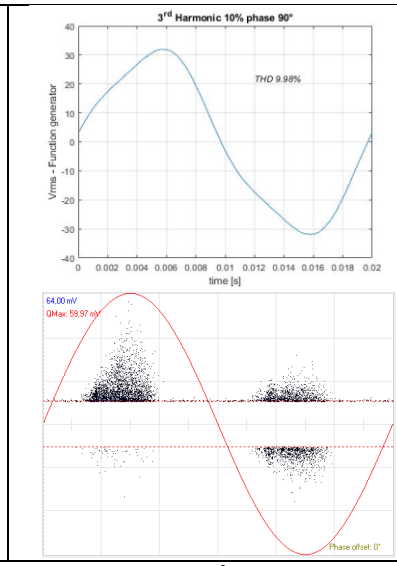	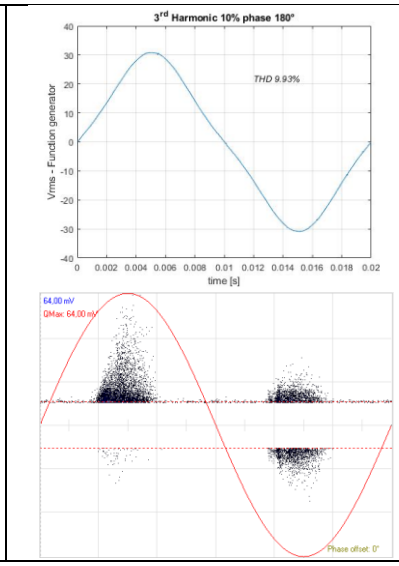
20% of 3rd Harmonic		
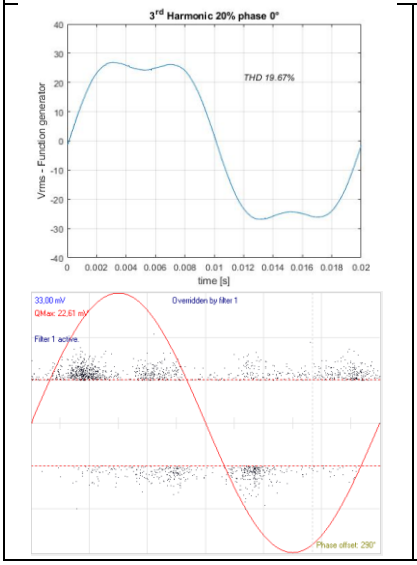	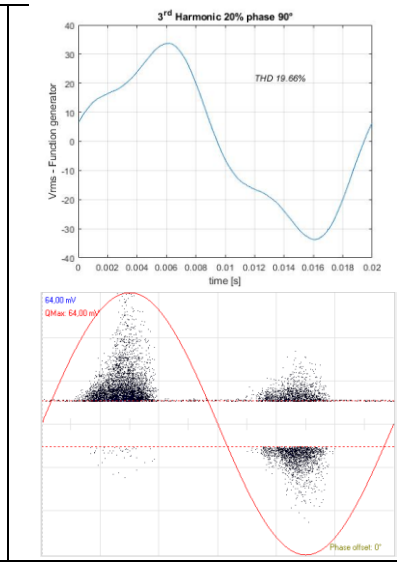	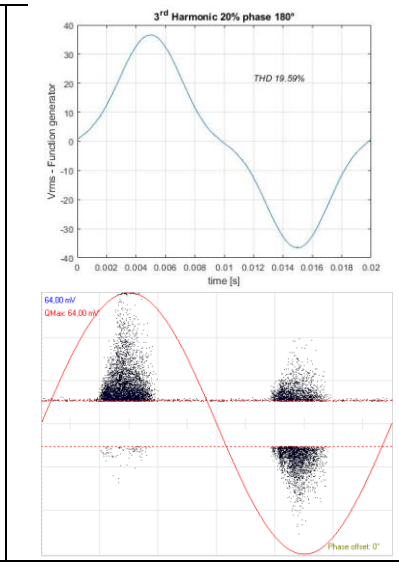

4.2.2 PD measurements with 5th Harmonic component

The measurements were carried out for a sinusoidal voltage waveform with magnitude 5.8 kV, containing 5th harmonic components (250 Hz) at 5%, 10% and 20%. The evolution of the PD pattern for three phase positions 0°, 90° and 180° and the corresponding voltage waveforms have been reported in Table 4-4. In this case, adding 5th harmonics results in a split of main PD group into two sub-clusters. The effect of the PD pattern split increases with the magnitude of the harmonic component. Indeed, applying a waveform with 20% of 5th harmonic it can be noted the same PD Pattern split effect for each phase angles and greatest increasing of the PD amplitude compared to the other case with 5% and 10% (Table 4-3). PD patterns follow the waveform causing a significant alteration of the original acquired PD patter with a sinusoidal waveform. Moreover, it is possible to note that with respect to the case previously analyzed, only in one case (waveform with 5% and phase angle 0°) there was a slight increase of the PD amplitude, while the remaining cases show a substantial increase of the PD amplitude caused mainly by a significant change of the waveform.

Table 4-3. Influence of the 5th harmonic on PD measurements

Harmonic Order	% Magnitude per Harmonic	Phase φ	THD %	Max Pd amplitude [mV]	Increased PD amplitude
5th	**5%**	**0°**	5.05%	23.91	7%
		90°	5.03%	43.83	96%
		180°	5.02%	44.55	99%
	10%	**0°**	10.04%	27.89	25%
		90°	10.03%	37.80	69%
		180°	10.01%	41.65	86%
	20%	**0°**	19.76%	60.24	170%
		90°	19.75%	56.44	153%
		180°	19.73%	60.47	171%

The analysis of the acquired PD pulses, reported below, did not show any changes on the pulse waveform and frequency content. For simplicity have been reporter three different cases in order to understand how the harmonic components did not change the PD pulse waveform but only the amplitude of the PD phenomenon.

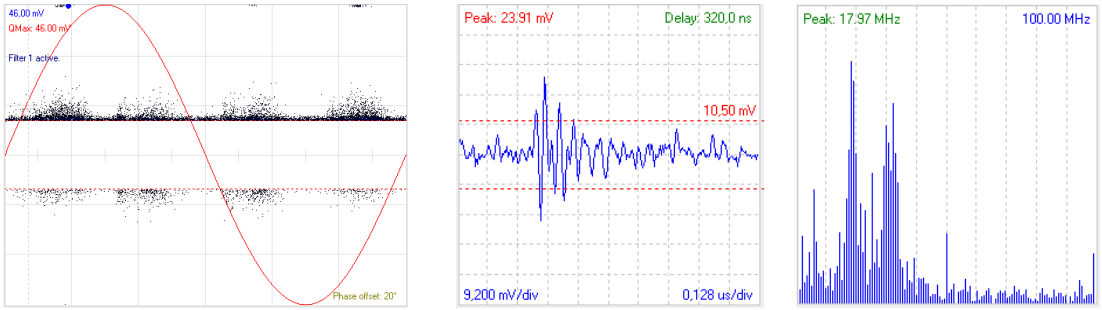

Figure 4-9. Analysis of the acquired PD pulse at 5% of 5th harmonic and phase angle 0°

The presence of 5th harmonic component causes the PD pattern split in two PD phenomena characterized by same pulse waveform and frequency content. Even in this case, the analysis of frequency spectrum reported Figure 4-9 show the presence of several frequency components due to the low amplitude of the PD pulse localized above the noise level.

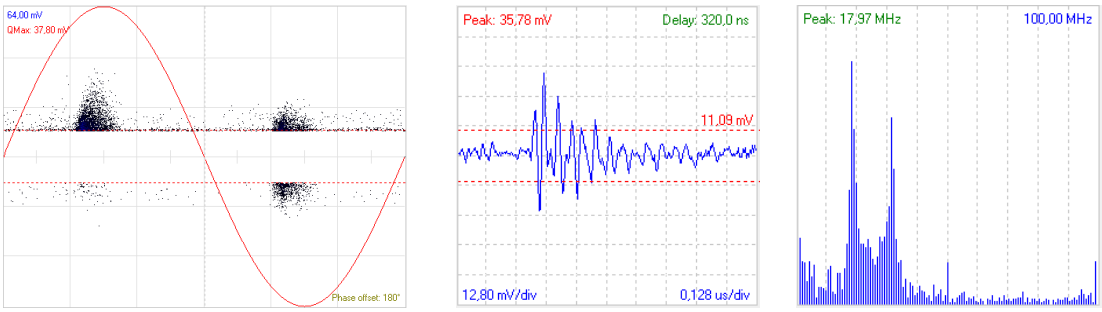

Figure 4-10. Analysis of the acquired PD pulse at 10% of 5th harmonic and phase angle 90°

By comparing the frequency contents of the acquired PD pulses, it can be noted how the spectrum remains unchanged.

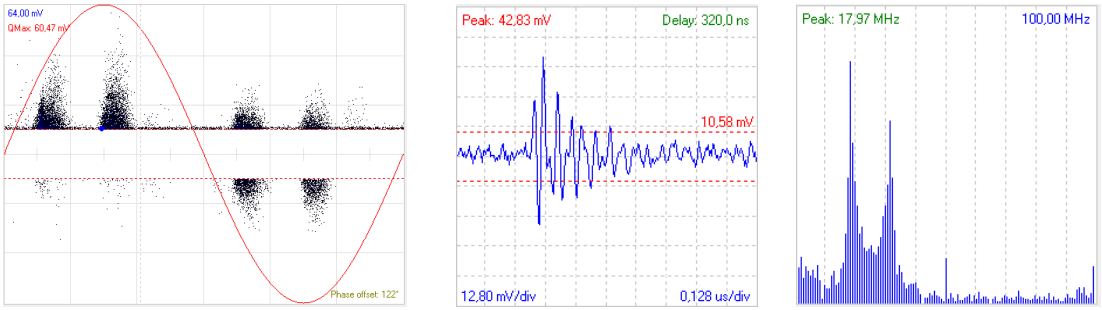

Figure 4-11. Analysis of the acquired PD pulse at 20% of 5th harmonic and phase angle 180°

Table 4-4. Acquired PD Patterns and Voltage waveform with 5th harmonic

5% of 5th Harmonic		
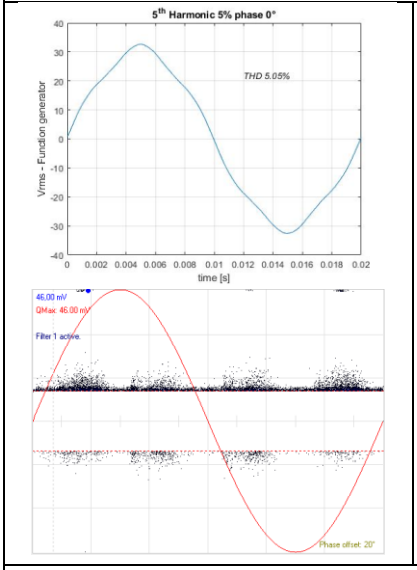	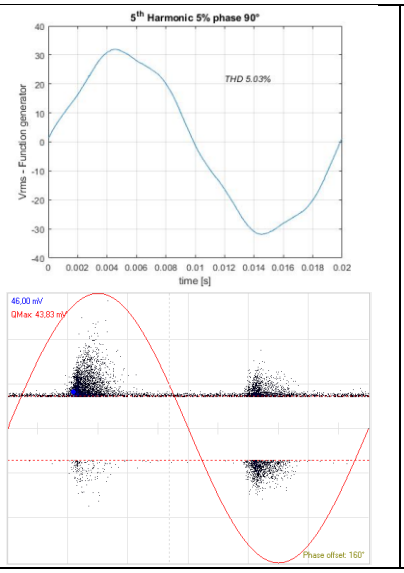	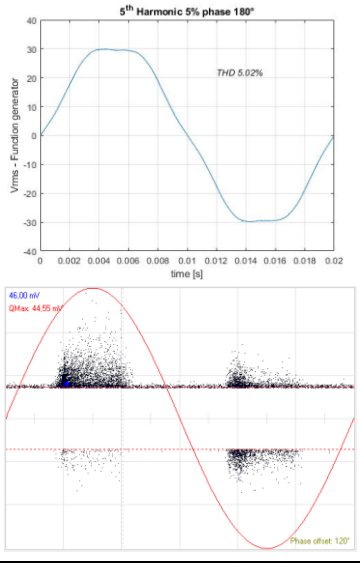
10% of 5th Harmonic		
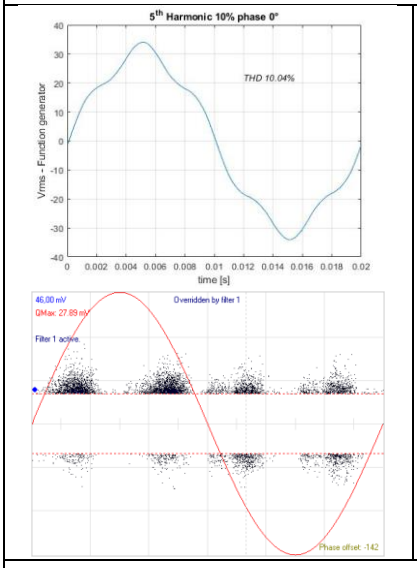	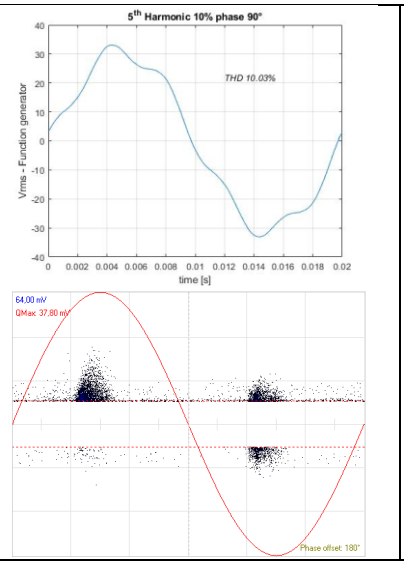	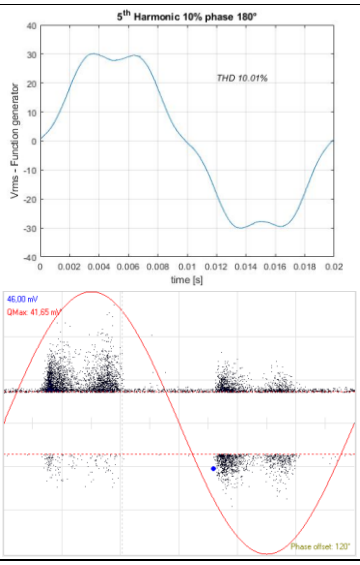
20% of 5th Harmonic		
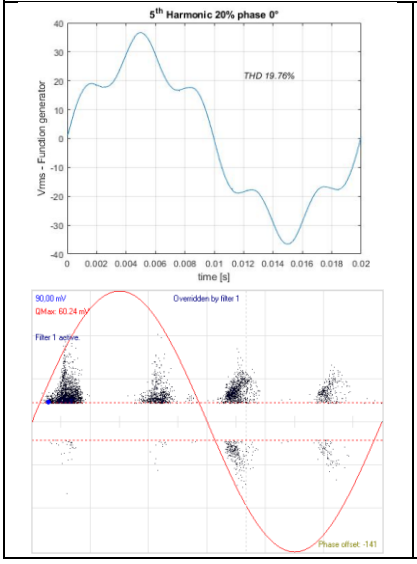	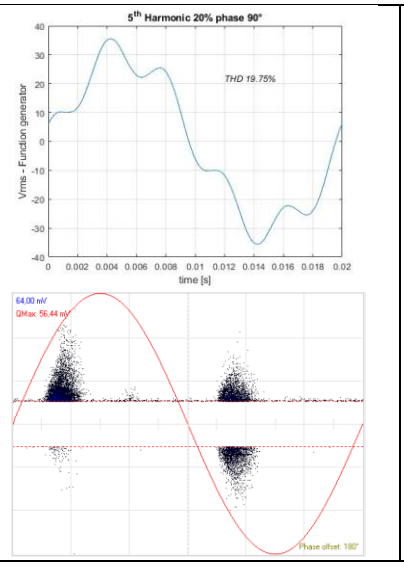	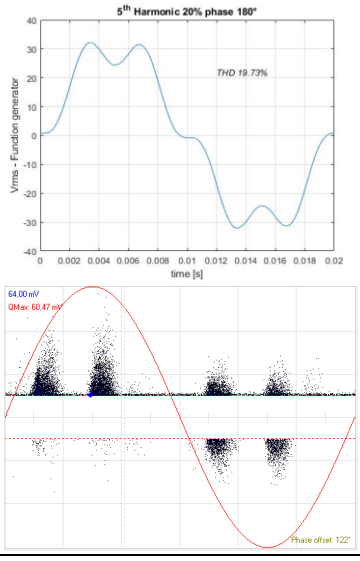

4.2.3 PD measurements with 9th Harmonic component

The measurements were carried out for a sinusoidal voltage waveform with magnitude 5.8 kV, containing 9th harmonic components (450 Hz) at 5%, 10% and 20%. The evolution of the PD pattern for three phase positions 0°, 90° and 180° and the corresponding voltage waveforms have been reported in Table 4-6.

The presence of 9th harmonic components causes a considerable waveform distortion and the formation of several peaks. The presence of these local extremes determines the PD pattern split into several parts, up to create three sub-patterns for each half-period. Moreover, the presence of these local extremes characterized by steep slopes determines a greater stress than the previous waveforms with 3rd and 5th harmonics, such as to considerably increase the PD amplitude. It must be emphasized that the waveforms chosen for this experiment have been taken considering a similar level of the THD factor, in order to emphasize that, in addition to the harmonic amplitude, the phase angle is crucial. In fact, even if a 5% amplitude of the harmonic component is applied, the phase angle causes a considerable increase of the PD amplitude.

Table 4-5.Influence of the 9th harmonic on PD measurements

Harmonic Order	% Magnitude per Harmonic	Phase φ	THD %	Max Pd amplitude [mV]	Increased PD amplitude
9th	**5%**	**0°**	5.16%	39.12	75%
		90°	5.16%	46.06	106%
		180°	5.14%	46.77	109%
	10%	**0°**	10.26%	46.00	106%
		90°	10.26%	80.08	258%
		180°	10.24%	73.70	230%
	20%	**0°**	20.18%	46.00	106%
		90°	20.19%	90.00	303%
		180°	20.02%	90.00	303%

The analysis of the acquired PD pulses, reported in Figure 4-12, show a lower frequency spectrum component due to the slow and oscillating pulse waveform. In this case, the PD amplitude was lower compared to the other case at high magnitude of harmonic component reported in Figure 4-12 and Figure 4-13. The latter cases, conversely did not show any particular changes on the pulse waveform and relative frequency content. For simplicity have been

reporter three different cases in order to understand how the harmonic components did not change the PD pulse waveform but only the amplitude of the PD phenomenon.

By comparing the frequency contents of the acquired PD pulses, it can be noted how the spectrum remains unchanged.

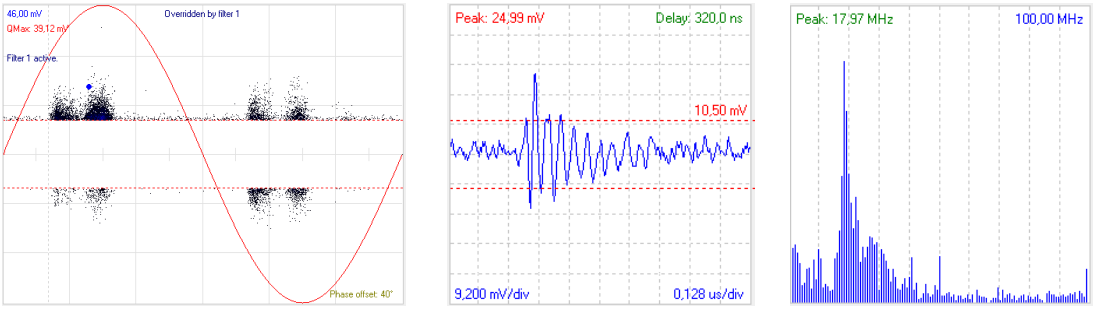

Figure 4-12. Analysis of the acquired PD pulse at 5% of 9th harmonic and phase angle 0°

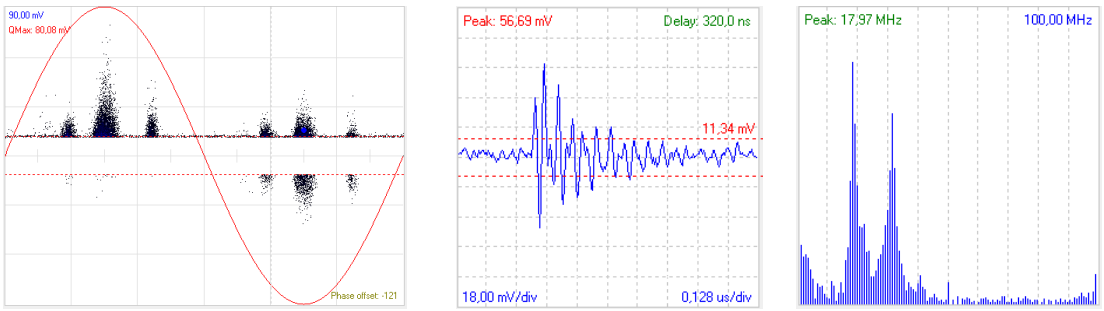

Figure 4-13. Analysis of the acquired PD pulse at 10% of 9th harmonic and phase angle 90°

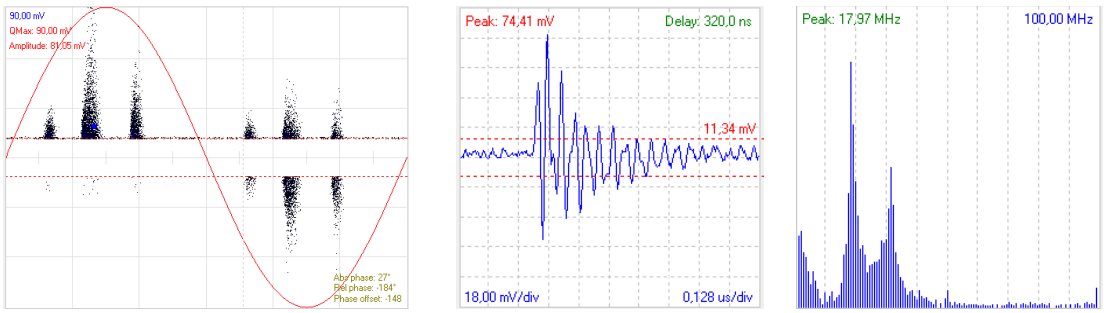

Figure 4-14. Analysis of the acquired PD pulse at 20% of 9th harmonic and phase angle 180°

Table 4-6. Acquired PD Patterns and Voltage waveform with 9th harmonic

5% of 9th Harmonic		
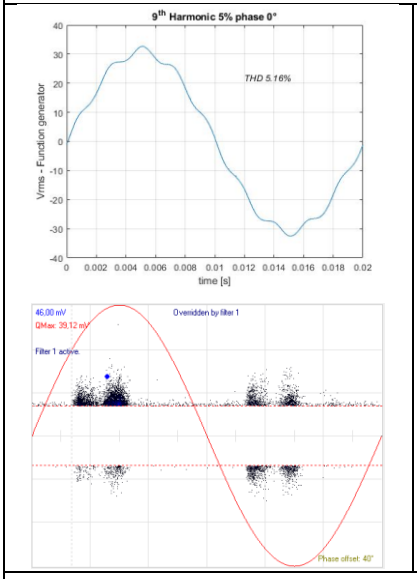	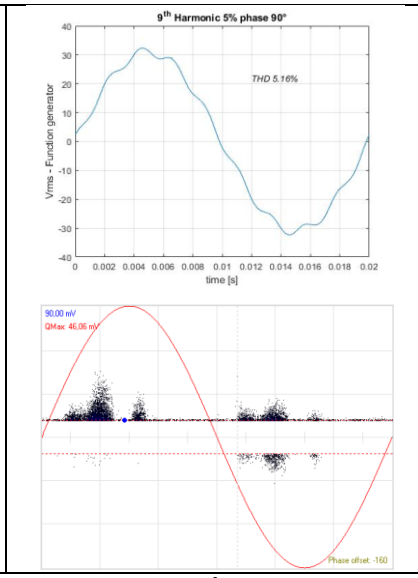	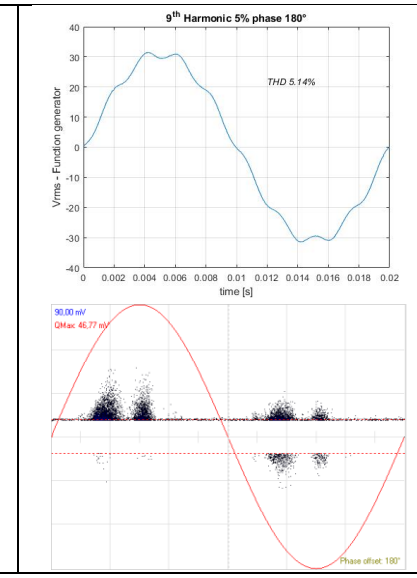
10% of 9th Harmonic		
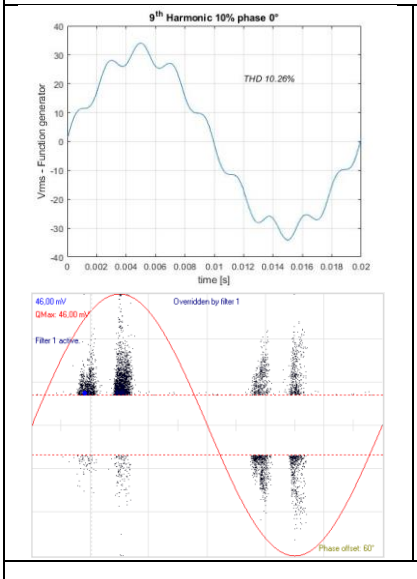	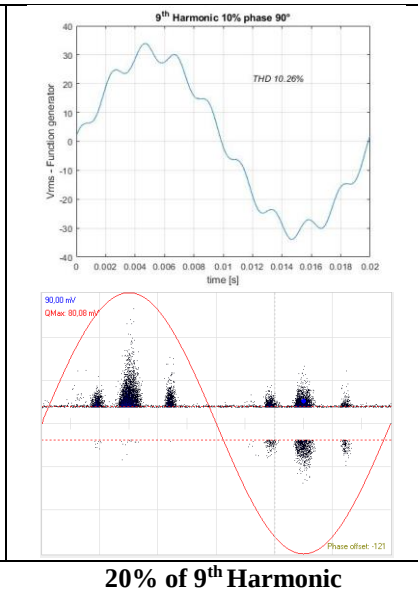	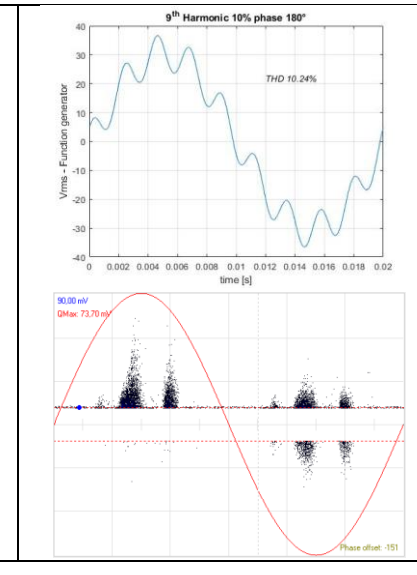
20% of 9th Harmonic		
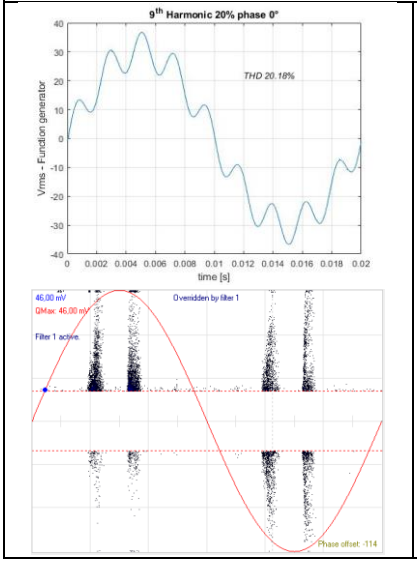	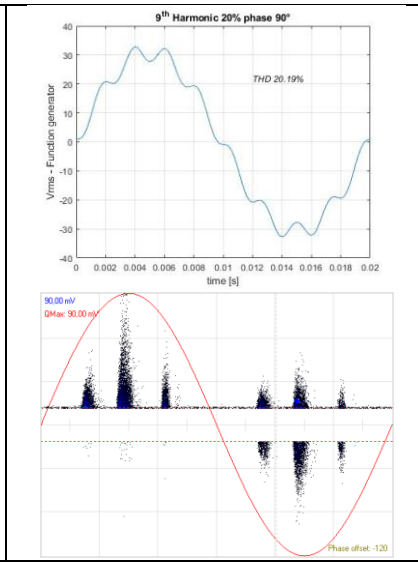	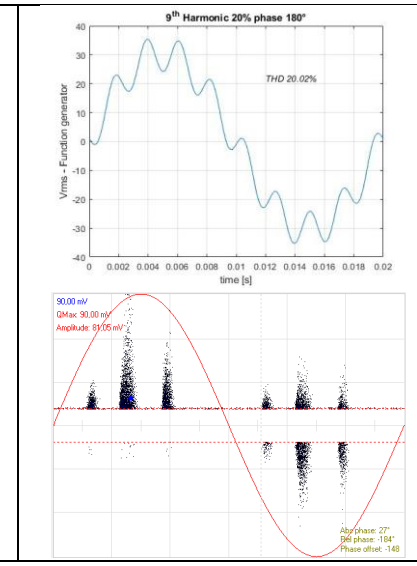

4.2.4 PD measurements with 11th Harmonic component

The measurements were carried out for a sinusoidal voltage waveform with magnitude 5.8 kV, containing 11th harmonic components (550 Hz) at 5%, 10% and 20%. The evolution of the PD pattern for three phase positions 0°, 90° and 180° and the corresponding voltage waveforms have been reported in Table 4-4.

The examined case turns out to be the worst from the point of view of the interpretation of the PD pattern because the initial shape of the discharge phenomenon is completely lost. Even in the presence of 5% amplitude there were the PD pattern split and higher increase of the PD amplitude compared to the previously cases. Indeed, The addition of these harmonics to the main sinusoidal component results in variation of peak voltage and time derivative dv/dt along the phase.

It can be noted how increasing the magnitude of the harmonic component alters the waveform trend, causing the inception of the PD at each peak of the waveform. Therefore, the presence of this type of stress determines the increase of the discharge activity which could compromise the integrity of the component.

As reported in Table 4-7, considering the same magnitude of the harmonic component and THD level, the phase angle is the parameter that most influences the increase of the PD amplitude.

Table 4-7. Influence of the 11th harmonic on PD measurements

Harmonic Order	% Magnitude per Harmonic	Phase φ	THD %	Max Pd amplitude [mV]	Increased PD amplitude
11th	**5%**	**0°**	5.0%	28.98	30%
		90°	5.0%	57.40	157%
		180°	5.0%	59.53	166%
	10%	**0°**	9.94%	64.00	186%
		90°	9.94%	76.54	242%
		180°	9.93%	77.95	249%
	20%	**0°**	19.58%	46.00	106%
		90°	19.60%	90.00	303%
		180°	19.59%	90.00	303%

Even in this case the analysis of the pulse waveform and relative frequency content did not show any changes. For simplicity have been reporter three different cases in order to understand how the harmonic components did not change the PD pulse waveform but only the amplitude of the PD phenomenon. The analysis of the acquired PD pulses, reported in Figure 4-15, show

a lower frequency spectrum component due to the slow and oscillating pulse waveform. As the previously cases, the PD amplitude was lower compared to the other case at high magnitude of harmonic component reported in Figure 4-16 and Figure 4-17.

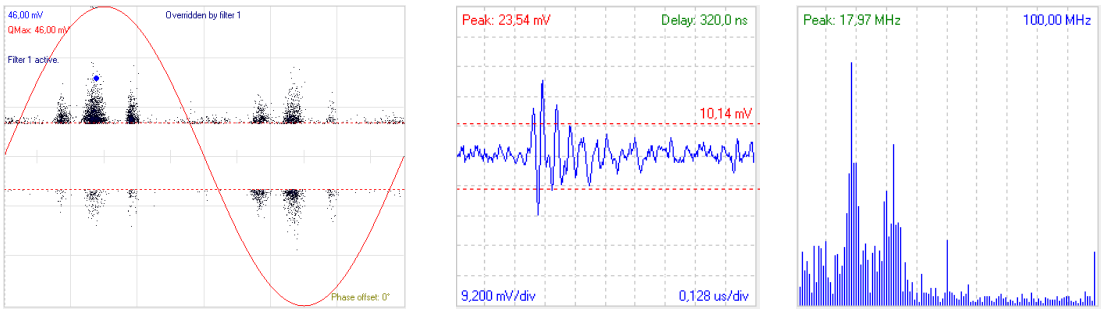

Figure 4-15. Analysis of the acquired PD pulse at 5% of 11th harmonic and phase angle 0°

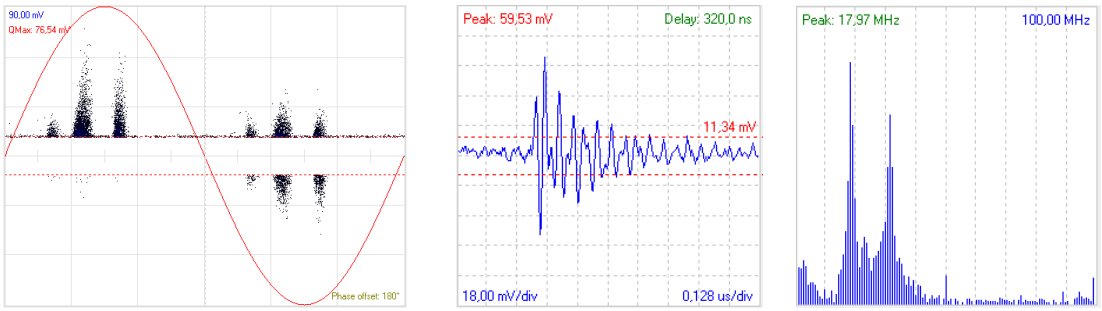

Figure 4-16. Analysis of the acquired PD pulse at 10% of 11th harmonic and phase angle 90°

By comparing the frequency contents of the acquired PD pulses, it can be noted how the spectrum remains unchanged. The only peculiarity it can be noted that in presence of high magnitude of the harmonic component, the frequency spectrum of the PD pulse was more definite and the noise does not affect the harmonic content of the PD phenomenon

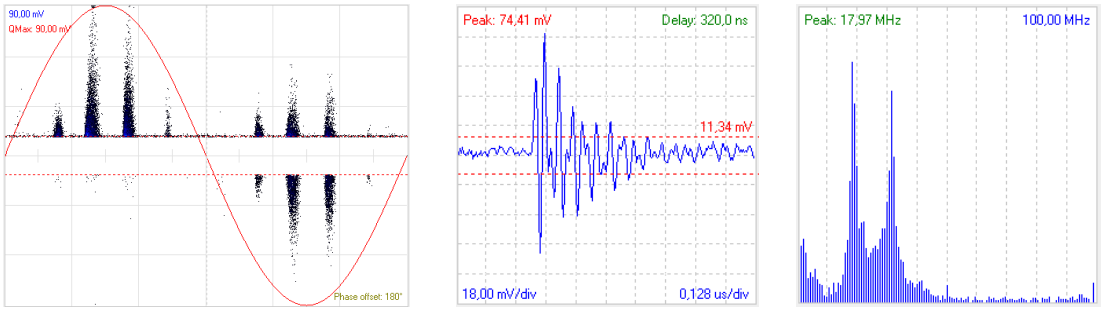

Figure 4-17. Analysis of the acquired PD pulse at 20% of 11th harmonic and phase angle 180°

Table 4-8. Acquired PD Patterns and Voltage waveform with 11th harmonic

5% of 11th Harmonic		
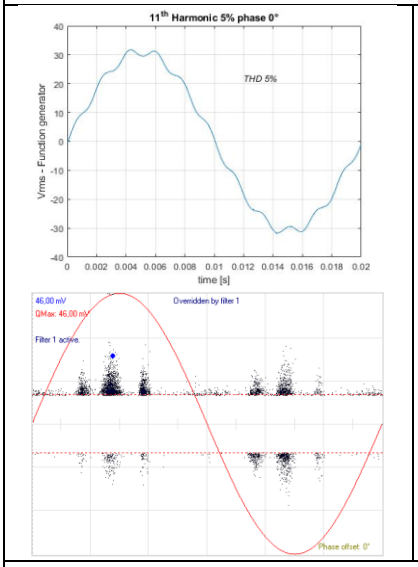	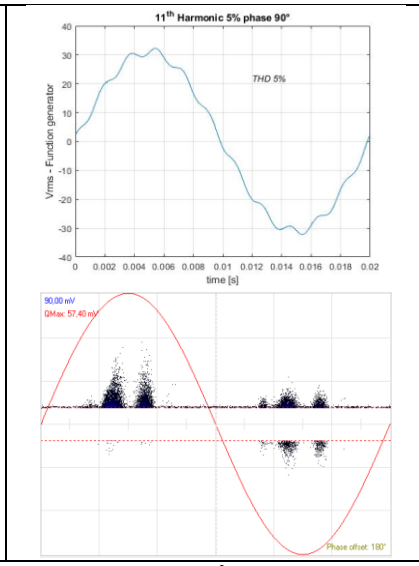	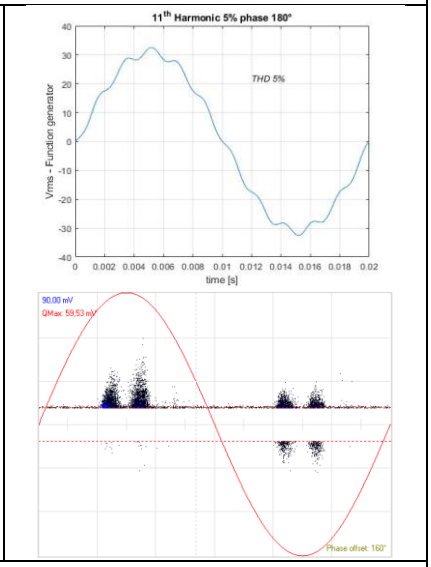
10% of 11th Harmonic		
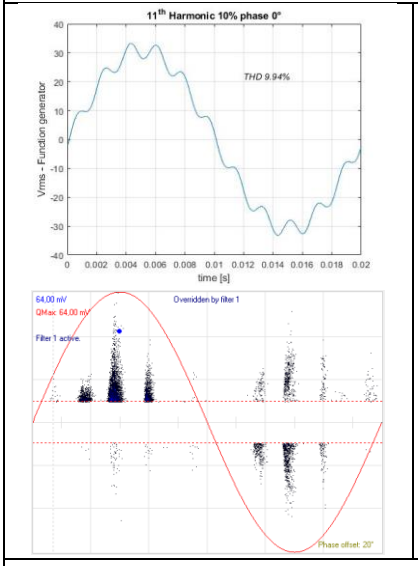	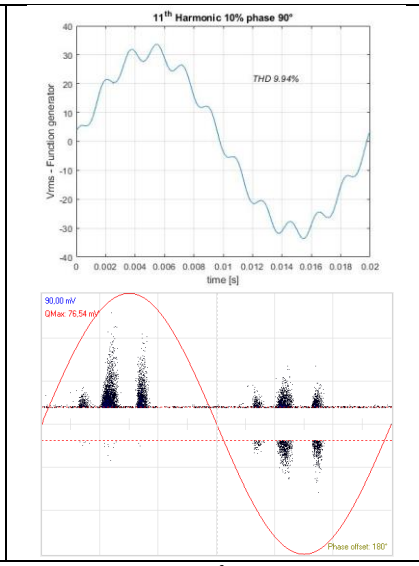	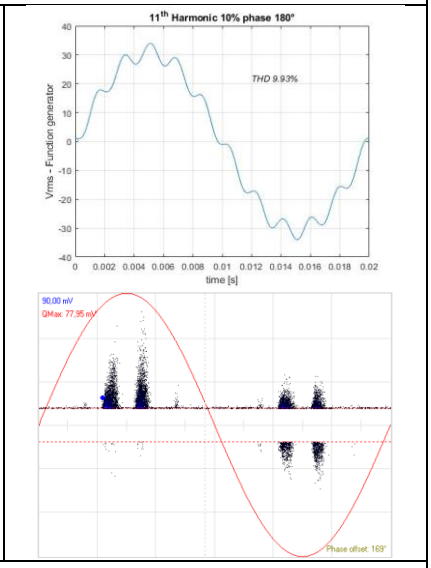
20% of 11th Harmonic		
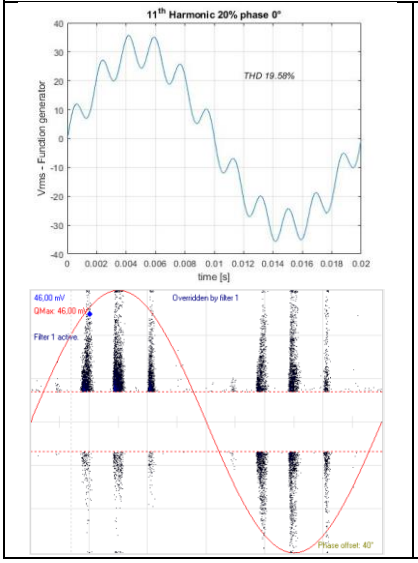	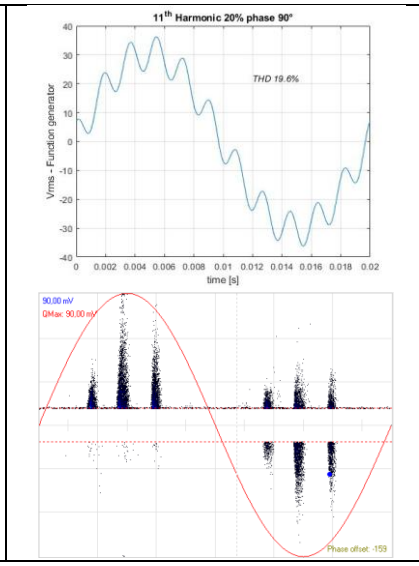	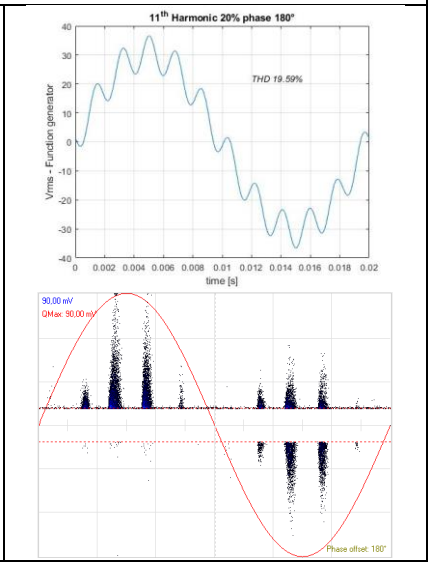

4.3 Conclusions

The presented results show how the underlying influence of harmonics, occurring in the applied voltage during PD measurements, can influence the interpretation of the PD pattern and PD behavior. Experimental results highlighted that various harmonic compositions superimposed on the fundamental sinusoidal waveform have a significant impact on PD amplitude and may increase in reference to sinusoidal measurement. The sinusoidal waveform, modulated by harmonics, may exhibit higher crest value than the fundamental sinusoidal trace and poses several local extrema. The maximum PD pulse is associated with the increased local slope steepness dv/dt and follows the crest value. It can be observed that local extrema in the voltage waveform are reflected in the PD pattern. Thus, the presented results underline the high sensitivity of PD measurements to voltage harmonics. The parameters reflecting the waveform spectral quality like THD, are rather superficial and do not provide unique and reliable signature of the applied voltage especially regarding phase angle variations. Thus, it is recommended for the analysis of the PD measurement, that voltage spectrum including higher harmonics must be considered. In addition, during the PD acquisition, voltage magnitude and phase can be influence the proper interpretation of PD patterns.

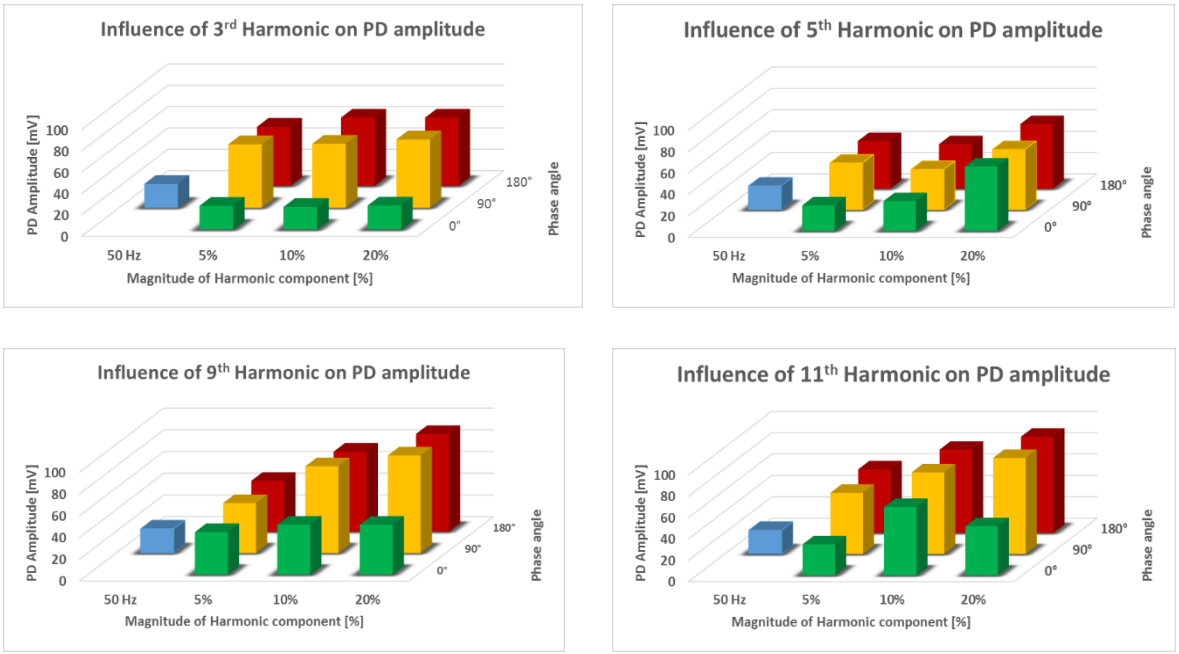

Figure 4-18. Influence of harmonic component on PD amplitude

It must be emphasized that various harmonic compositions superimposed on the fundamental sinusoidal waveform did not undergo any changes on the pulse waveform and their frequency

content but only the PD amplitude increases at different harmonic components. As reported in Table 4-6, the measurement results show the influence of the phase angle of the harmonic component on the PD amplitude compared to the pure sinusoidal amplitude. It can be noted that in all cases, the worst condition occurs in the presence of phase angles of 90 ° and 180 °. The presence of a harmonic component with phase 0 °, alters the shape of the acquired PD pattern but determines an increase a lower PD amplitude compared to cases with 90 ° and 180 °. In according to CEI EN 50160, in the electricity networks it is necessary to maintain a THD level, including all harmonics up to the 40^{th} order, less than 8% to ensure sufficient quality of the supply voltage waveform. However, as was evidenced by the measurement results, a low THD level does not determine the absence of local peaks in the waveform. Therefore, in addition to the evaluation of THD level it is necessary to evaluate the frequency spectrum of the applied waveform. It is concluded that knowledge of harmonic content of applied voltage is essential and critical in proper assessment of PD impact.

5. Partial discharges localization on MV and HV cables

5.1 Introduction

In this chapter, the problem of the PDs localization on MV and HV cables by means Pry-Cam Portable has been analyzed. Three real cases of the PD localization on XLPE AC cables are given:

- 500-m long unipolar MV XLPE cable 18/30 kV, 240 mm^2 Al;
- EHV cable with different accessory like outdoor terminations and joints;
- Short MV cables with different accessories like two cable termination and one joint.

Regarding the first case, initially conventional PD measurements were performed on the whole length by using a standard acquisition system (Omicron^{TM}); PDs activity was detected, but the system did not allow the operator to localize the PDs source. A visual inspection highlighted the presence of an excoriation in the outer sheet. Aiming at a more accurate pin-pointing of the defect, more measurements were carried out in the proximity of the outer defect using a portable PD detection system. These measurements showed PDs activity, whose source was located and identified as consisting in internal defects on the inner semicon in proximity of the external excoriation.

In the second case, PD localization was performed on field on a HV cable, during an after-laying PD test; in this case, the cable line encompasses different accessories like outdoor terminations and joints, which could be affected by PDs. Since the test was performed in the field, detailed information about the actual length and the features of the cable line were not available.

In the last case, the measurements were performed on two short MV cables in HV lab in order to test the PD localization method by means Pry-Cam Portable. In this case, the measurements have been performed on two cable circuits in which each one was composed by a short MV cable with two cable terminations and one joint in the middle. Due to the short cable length several reflection phenomena were found. However, due to the possibility of performing different measurements at different positions it was possible to correctly identify the source of discharge in each circuit. This proves how PD detection portable instruments are able, in cases like this, to locate the PD source and provide indications for its correct classification.

5.2 PD pulse propagation and attenuation

When PD pulses propagate along the cable, they are subjected to several phenomena that determine a signal variation and make the detection and interpretation of the acquired pulse more complicated. These phenomena are:

- **Attenuation:** when a PD signal runs through the cable, it loses frequency content due to an attenuation phenomenon. Consequently, as the distance travelled increases, it is increasingly difficult to correctly measure the PD phenomenon. It depends on the insulation material of the cable, the semiconductor material, the cable geometry, the technology used to measure, especially regarding the ability of the noise eliminator.
- **Distortion:** this phenomenon occurs because different frequency harmonics travel along the cable at different propagation speeds. The dispersion effect for frequencies below 100 MHz can be attributed to the variation of capacity at different frequencies. As the frequency increases, the semiconductor layers evolve from a resistive behaviour to capacitive behaviour and this results in a decrease in capacity between ground and conductor and an increase in propagation speed. Consequently, some harmonics propagate with greater speed than the others and, in the domain of time, the pulse will be distorted depending on the distance travelled.
- **Reflection:** when a PD phenomenon occurs, the PD signal propagates in both directions of the line. When the wave reaches a point on the line where there is an impedance variation, part of the wave is transmitted and the remainder reflected. The amount of reflected and transmitted energy depends on the impedance of the transition point Z_T and the characteristic impedance of the Z_C line in which the wave propagates.

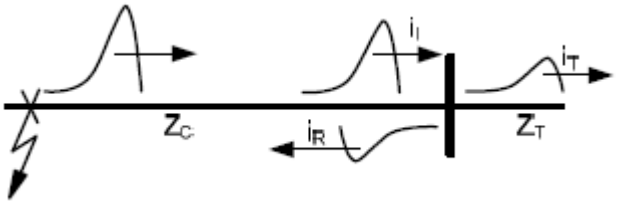

Figure 5-1. Reflection phenomenon: incident (i_I), transmitted (i_T) and reflected (i_R) wave.

PD tracking can be carried out by means of Time Domain Reflectometry (TDR) [48], based on recording and comparing the traveling times of reflected components of pulses propagating in opposite directions from the PD source [49][50]. As PDs must be detected against a noise background, the chance of tracking a pulse in the time domain is more or less directly proportional to the signal-to noise ratio and inversely proportional to the pulse width [50]. Also, to a good approximation the PD pulse amplitude rises with the detection bandwidth (up to a limit associated with the PD signal width) [50][51].

On the other hand, PD pulses in power cables spread while traveling from the PD source due to the combination of two well-known phenomena, namely:

- high frequency attenuation, i.e. attenuation of the high frequency components of a wave as it travels along the cable;
- dispersion, i.e. frequency-dependence of the propagation velocities of the wave components.

High frequency attenuation thus implies a loss of high frequency components from the PD-induced signal, which in turn spreads the signal and narrows the optimum detection bandwidth, thereby reducing the PD pulse amplitude proportionally to the bandwidth. Conversely, the noise drops as the square root of the bandwidth only. Overall, this leads to a decrease of the signal-to noise ratio, hence of the detection sensitivity as the PD pulse propagates along the power cable. High frequency attenuation in shielded power cables stems from: 1) dielectric losses in cable insulation; 2) losses in the semiconducting layers due to the propagation of the radial displacement current through their resistance. These two “non-ideal” phenomena with respect to the shielded power cable regarded as a simple cylindrical coaxial capacitor can be evaluated by modelling the shielded power cable as a network of parallel resistances and capacitances. In this way, high frequency attenuation and spread of the PD pulse can be evaluated accounting for cable dielectric properties as a function of propagation distance.

The conclusion reported in [50]is that “a 5 pC PD source in a typical distribution class cable can be located with good accuracy in a well-shielded environment”. However, these considerations hold in the presence of one single defective point, but PD source location based on TDR is much more troublesome in the presence of more defective points where PD activity might take place. Furthermore, a factory or the site where the power cable is located are likely to behave quite differently from a well-shielded environment. Moreover, accuracy worsens quickly with the increase of cable length and high frequency losses.

All these considerations suggest that in practical situation an accurate location of PD sources with conventional PD detection devices might be not so easy to achieve. Hence an alternative wireless PD detection device, capable of a local screening throughout the whole cable length might offer complementary and alternative information that might result of decisive importance for a more accurate tracking of cable system section(s) including the PD source(s).

5.3 Measurement on 500-m long unipolar MV XLPE cable

The cable under test is a 500-m long delivery length of unipolar MV (18/30 kV) XLPE-insulated cable, with 240 mm^2 aluminium conductor cross-section. Once produced, the cable is subjected to PD testing in factory according to IEC 60270.

Several PD measurements showed PD activity on this cable, but locating the defect was not easy on such 500-m long cable batch. PD measurements using a traditional – i.e. an OmicronTM – acquisition system was carried out at the prescribed voltage of 31 kV and PD activity was recorded with maximum amplitude of 149 pC (Figure 5-2).

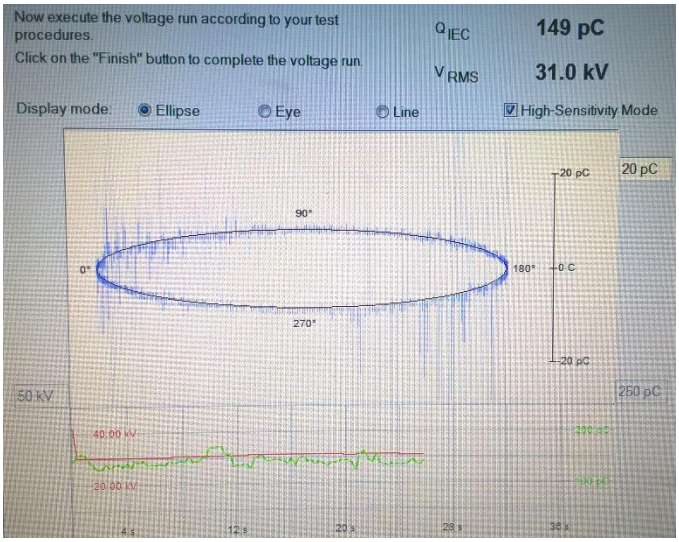

Figure 5-2. PD Pattern from Omicron^{TM} acquisition system

Therefore, the conventional method of PD measurements allowed bounding the location of the PD source within a 70-m section of cable using the travelling wave method. As well known, such method relies on the fact that a PD occurring at a certain point along the cable generates two voltage pulses travelling towards cable ends at a speed that depends on relative permittivity of the insulation [52]-[54].

From a visual inspection on the 70-m cable section, a visible excoriation on the cable sheath suggested the probable location of the PD source (Figure 5-3).

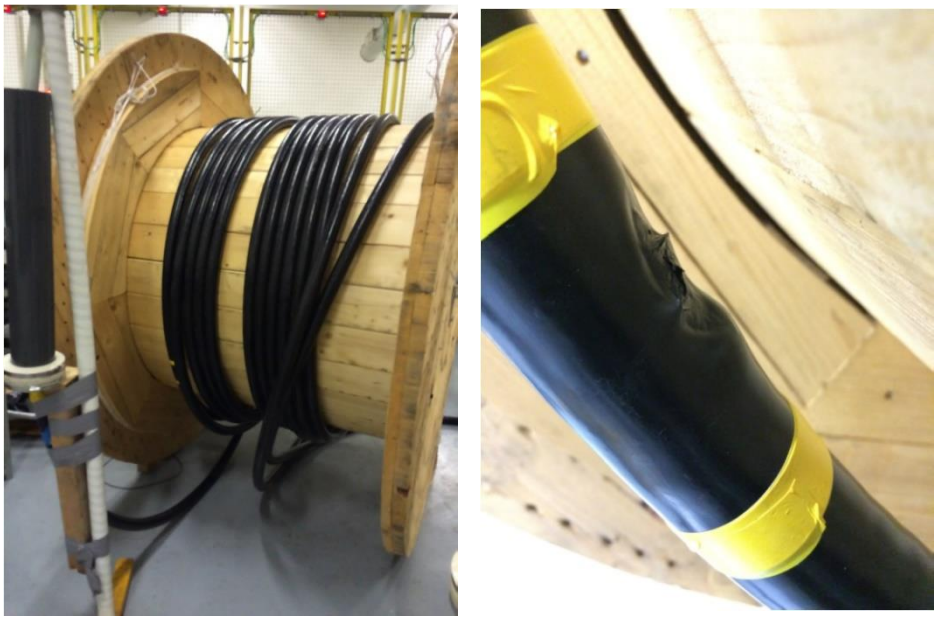

Figure 5-3. Defect on the cable sheath in the 70m section

To identify and locate the PDs source, several PD measurements were performed using the Pry-Cam^{TM} portable at different points of the cable section, as shown in Figure 5-4.

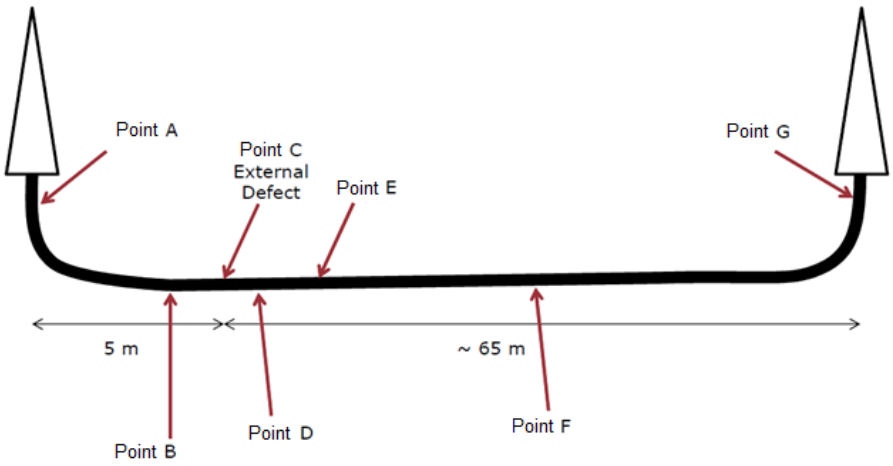

Figure 5-4. Diagram of measuring points

The external defect was taken as a reference for subsequent measurements. In particular, the following measurements were performed:

a) at the termination closer to the external defect;

b) at 1 m to the left of the external defect;

c) at the external defect;

d) at 0.5 m to the right of the external defect;

e) at 1.5 m to the right of the external defect;

f) at 12 m to the right of the external defect

g) at the termination farther from the external defect.

To perform the PD measurements, silicone oil insulated cable terminations were mounted. Then, the cable was powered using a 35-kV rated AC generator. The PD measurements via Pry-Cam™ portable were carried out all at a voltage of 25 kV, the inception voltage of the PD activity previously determined via the traditional acquisition system and verified using Pry-Cam™.

The measurements carried out via Pry-Cam™ at points A and G (cable terminations closer to and farther from the external defect, respectively) and at point F (far from the external defect) show no PD activity, but only background noise as reported in Table 5-1.

At first, the measurement was performed at 25 kV on point C close to the external defect. The acquired pulses show a PD activity with maximum amplitude of 37.67 mV (Figure 5-5).

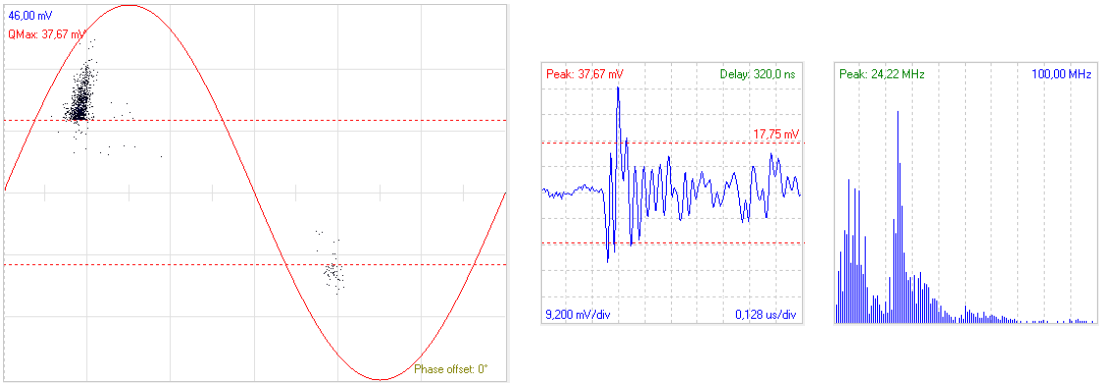

Figure 5-5. Point C, external defect: PD Pattern, waveform and frequency content of the pulses

Then, the measurement was performed at 1 m to the left of the defect (point B) to understand if the defect on outer Sheath was the source of PD. The acquired pulses in this case shows a reduction of the PD activity with slightly-reduced maximum amplitude of 36.14 mV (Figure 5-6). The analysis of the PD pattern and of the PD pulse maximum amplitude show that PD source was not located in correspondence of the external defect on the outer sheath. To find the exact position of the PD source further investigations were performed along the cable.

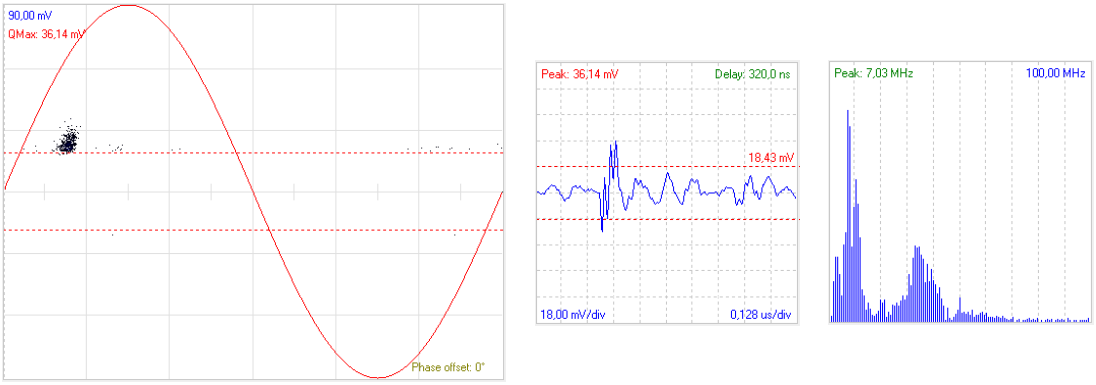

Figure 5-6. Point B, 1 m to the left of the external defect: PD Pattern, waveform and frequency content of the pulses

The measurement performed at 0.5 m to the right of the external defect (point D) shows a rise of the PD activity with a significant increase of the maximum amplitude of 49.61 mV (Figure 5-7). Such increase highlights that the real defect causing PDs is not related to the visible excoriation (Figure 5-3), but is probably an internal defect.

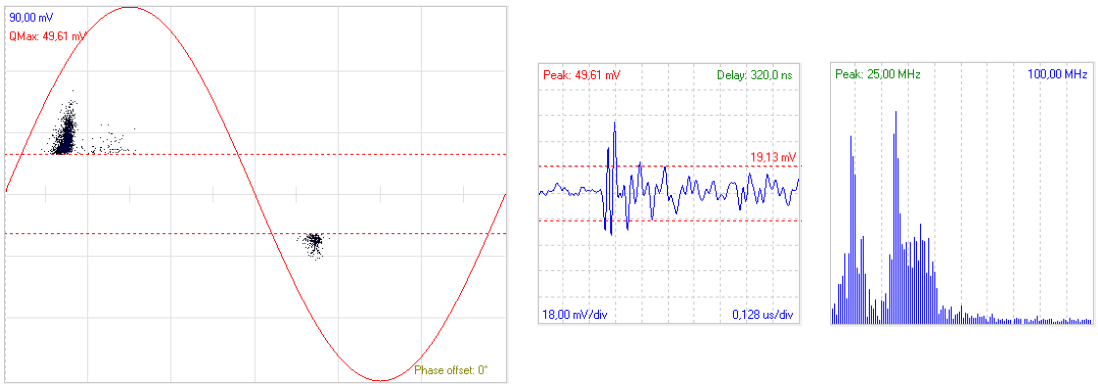

Figure 5-7. Point D, 0.5 m to the right of the external defect: PD Pattern, waveform and frequency content of the pulses

The measurement carried out at 1.5 m to the right of the external excoriation (Point E) shows a reversal shape of the PD pattern, as well as a reduction of the PD maximum amplitude to 35.50 mV (Figure 5-8).

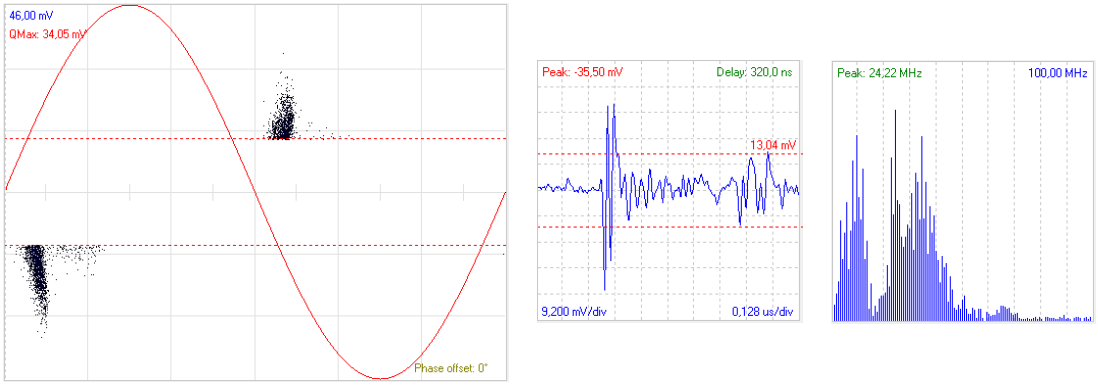

Figure 5-8. Point E, 1.5 m to the right of the external defect: PD measurement via Pry-Cam™ at 25 kV (maximum amplitude 34 mV).

Also, as reported in Figure 5-9 and Figure 5-10, by comparing of the acquired pulses it can be noted how the PD pulses change the polarity. In the detail, the acquired pulse on Point D has a negative polarity. Conversely, the acquired pulse on Point E show a positive polarity even that the PD pulse becomes a negative polarity. In this case, to understand the polarity it is necessary compared the first trend of the PD pulse.

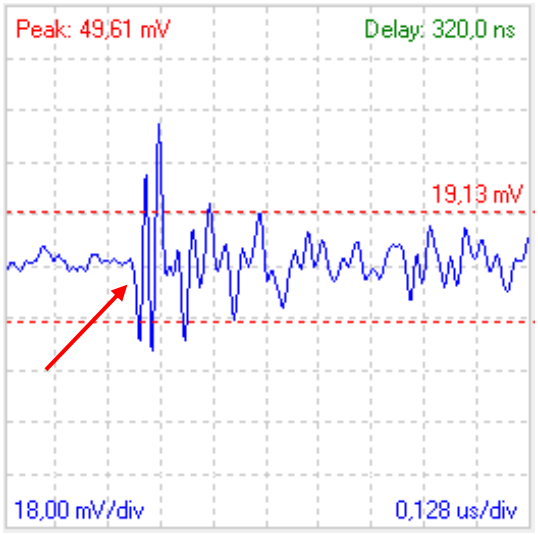

Figure 5-9. Point D - Pulse Waveform

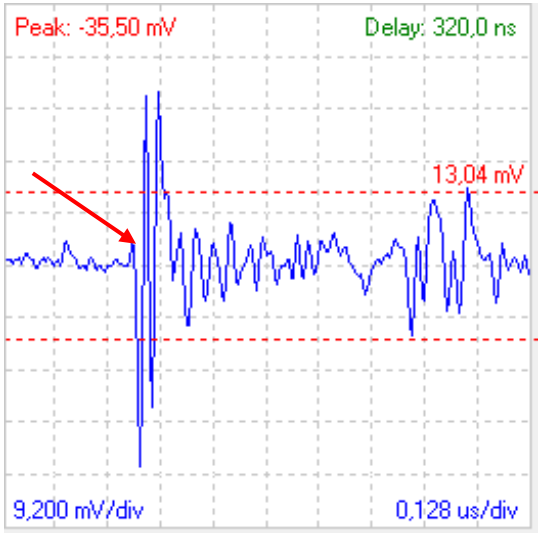

Figure 5-10. Point E - Pulse Waveform

The PD pattern inversion and the PD amplitude reduction denote that the PD source was just passed by the Pry-Cam^{TM} portable, as sketched in Figure 5-11.

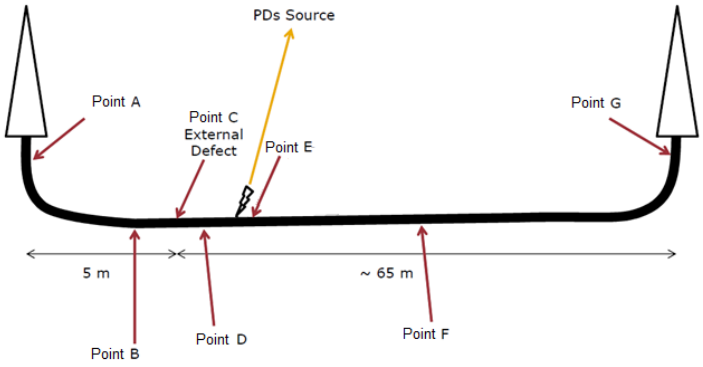

Figure 5-11. PDs source located in 70 meter of cable section

The measurements performed on each point are reported in Table 5-1. For each point, the PD pattern as well as the waveform and the frequency content of the PD pulses are reported in the same table. The critical PD activity was highlighted in orange and red square, in particular, it can be noted how the PD pattern changes getting closer to the defect, located on Point D at 0.5 m to the right of the external defect.

Table 5-1. Measurements on MV cable: pd patterns, waveform and frequency content of the acquired pulses

Point A	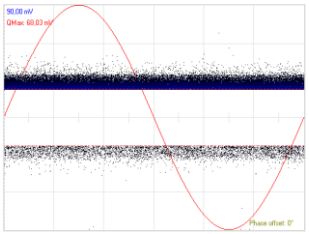	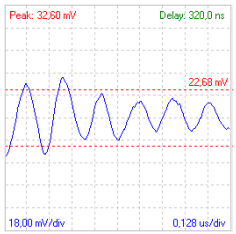	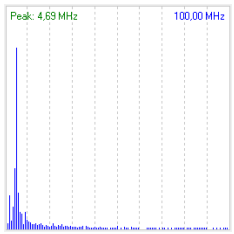	Background Noise
Point B	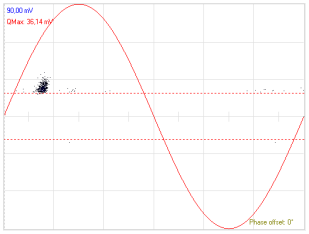	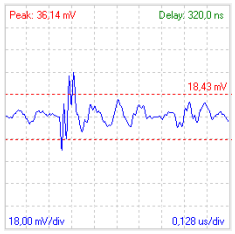	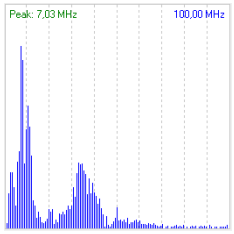	36.14 mV
Point C	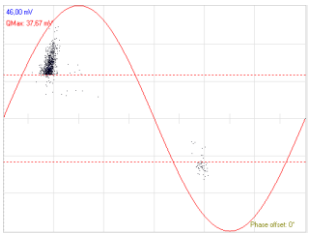	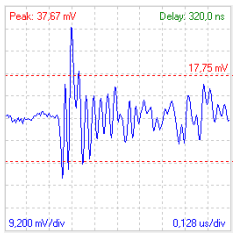	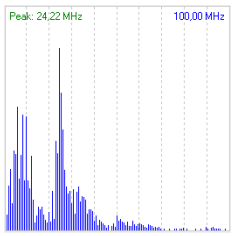	36.67 mV
Point D	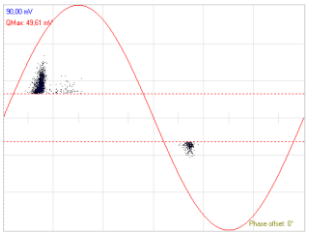	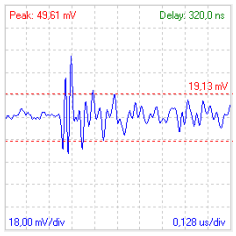	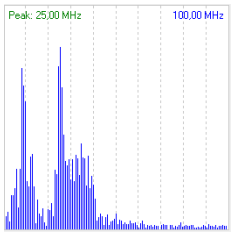	49.61 mV
Point E	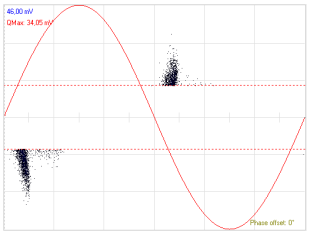	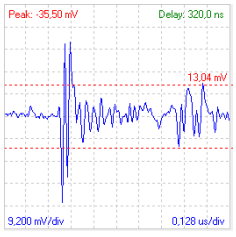	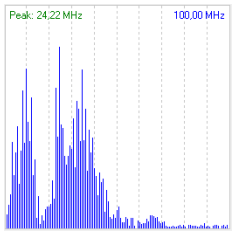	35.50 mV
Point F	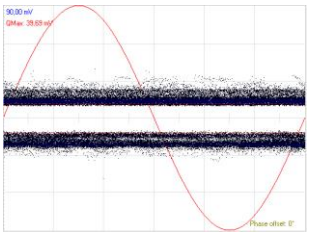	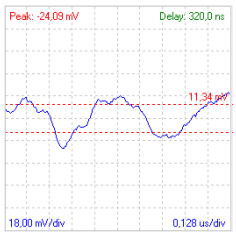	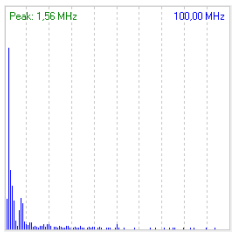	Background Noise
Point G	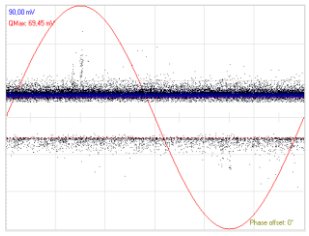	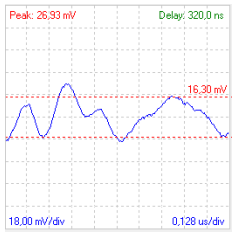	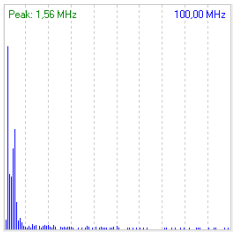	Background Noise

Hence the externally-visible defect on the cable sheath is close to the real PDs source, but is not the cause of the detected PD activity. The point where partial discharge activity was detected with maximum amplitude was indeed about 1 meter away from the external defect as demonstrated not only by the above-measurements, but also by a closer inspection of the damaged cable. The defect found on the outer sheath is due to an improper overlapping of semiconducting swelling tapes laid onto the insulation shield, which generated a bulge of tinned copper strips and consequently a defect in the external PE sheath. Figure 5-12 shows how the manufacturing defect propagates from the inside to the outside of the various cable layers.

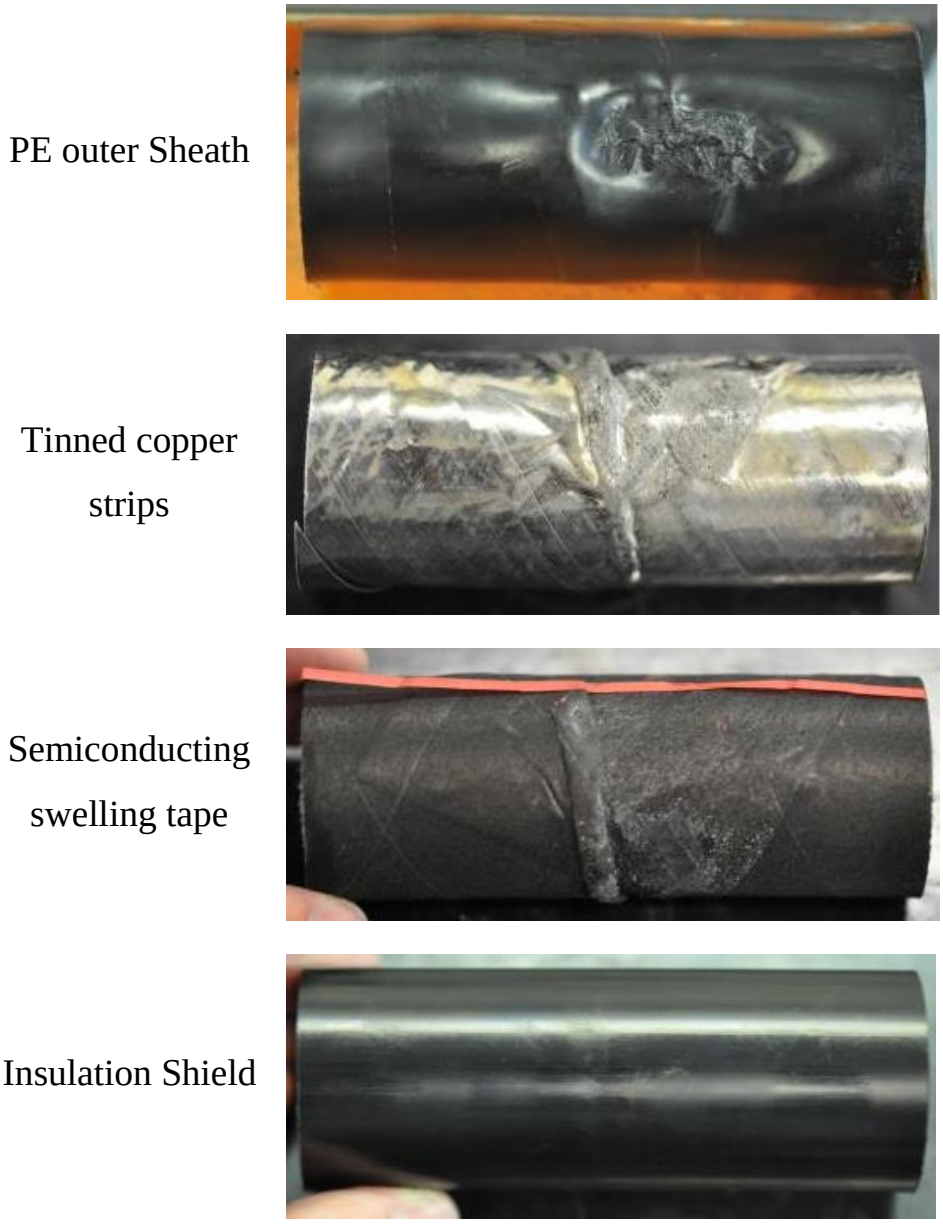

Figure 5-12. Defect propagation on cable layers

A 1 m cable section, adjacent to the defects shown above, was analyzed preparing 10 sections – 10 cm-long each - to check whether the PD activity detected was to some extent associated with problems/bubbles/ imperfections on the various parts of the same cable. Several tears on the inner semicon were found, which were the likely cause of the PD activity. These cracks produced large imperfections in the dielectric, giving rise to voids. The surface of the inner semicon can be made visible by the well-known Hot Oil Test, which consists in sinking the damaged portion of the cable into a hot-silicone oil bath, since XLPE becomes transparent when immersed into hot-silicone oil at a temperature of 150°C and reveals in detail the surface structure of the inner semi-conductive layer. Figure 19 shows the inner semicon defects in a Hot Oil Test, where red arrows highlight the defects between the insulation and the inner semicon.

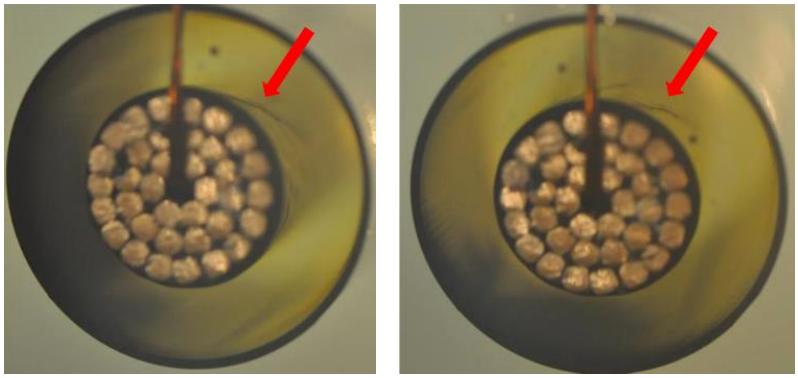

Figure 5-13. Conductor Shield Defect in a Hot Oil Test

The analysis of the cable section shows numerous cracks and tears in the inner semicon. The PD activity probably generated from one of these splits and penetrated into the insulation material. Figure 5-14 and Figure 5-15 show the visual and the photographic analysis of inner semicon defects respectively.

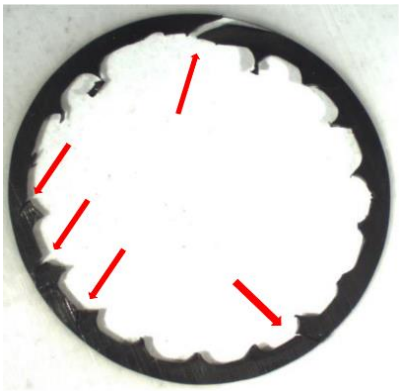

Figure 5-14. Photographic analysis of inner semicon defects

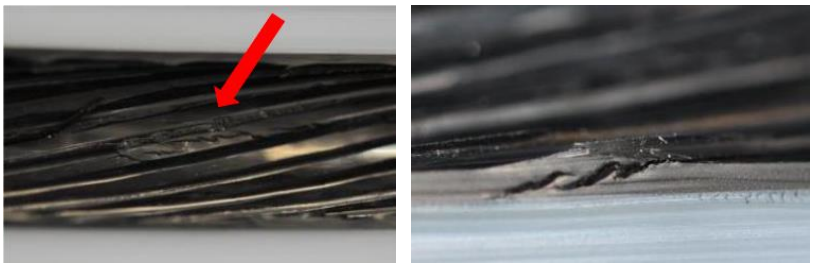

Figure 5-15. Visual analysis of inner semicon defects

5.4 Measurement on EHV cable after the installation

The circuit under test is a 250-meter length of unipolar EHV 220/380 kV XLPE-insulated cable line, with 2500 mm^2 copper conductor installed on site for Pre-Qualification (PQ) test, features different EHV accessories as reported below:

- 1 composite bushing outdoor termination, TES;
- 1 ceramic bushing outdoor termination, TPE;
- 1 Back to Back (B2B) SF_6- insulated metal-clad connection;
- 1 sectionalized joint, SXJ;
- 1 straight joint, SJ.

PD measurements were performed by means of the Pry-Cam™ portable at different points along the EHV cable line, both at proper locations on the cable and close to each accessory, as displayed in Figure 5-16, namely:

1) at the composite bushing outdoor termination TES;
2) after the Back to Back (B2B) SF_6- insulated metal-clad connection;
3) at the left side of the sectionalized joint SXJ;
4) at the right side of the sectionalized joint SXJ;
5) at the straight joint SJ;
6) at the ceramic bushing outdoor termination TPE.

The PD measurements via Pry-Cam™ portable were carried out all at a voltage of 1.7 U_0 = 1.7(380/√3) = 1.7(220) = 374 kV, where U_0 references the rated phase to ground operating voltage, that compared to the rated voltage of 380 kV, phase to phase, suggests the presence of a defect in the cable or in the accessories.

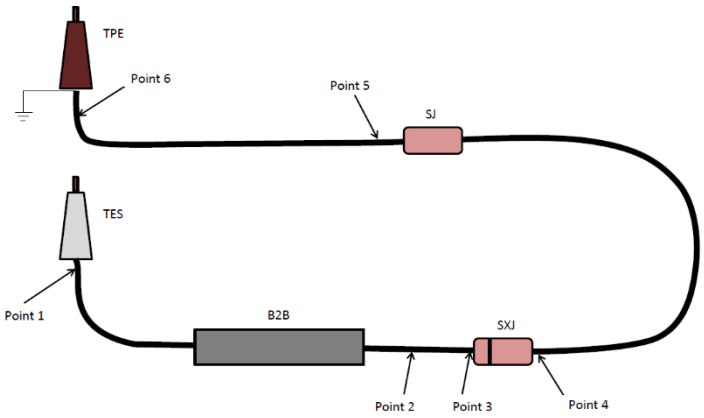

Figure 5-16. Diagram of measuring points along the EHV

The measurements were performed on the EHV cable by means Pry-Cam™ from points 1 to 6, cable terminations TES and TPE respectively. The measurements carried out at points 1, 5 and 6 did not show any critical PD activities, but only low frequency surface on the external side of outdoor terminations TES and TPE. On the contrary, at points 2, 3 and 4, PD activity was found and located between point 3 and 4 as is indicated by the reversal pattern phenomenon in Table 5-2. In the detail, the measurements performed at point 2 between the B2B SF6-insulated metal-clad connection and the sectionalized joint SXJ shows a PD activity with maximum amplitude of 23.69 mV. The measurement performed at Point 3, to the left of the sectionalized joint SXJ, shows a rise of the PD activity with a largely increased maximum amplitude of 47.87 mV. The increase of the maximum amplitude suggests that the PD source is close to the measurement point. The measurement carried out at point 4, to the right of the sectionalized joint (SXJ), shows a reversal in the shape of the PD pattern, as well as a reduction of the PD maximum amplitude to 36.42 mV.

Table 5-2. Reversal PD pattern phenomenon

Point 2	Point 3	Point 4
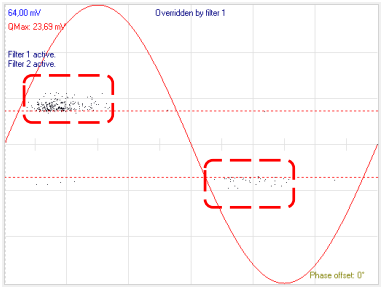	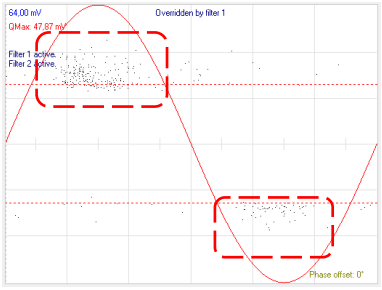	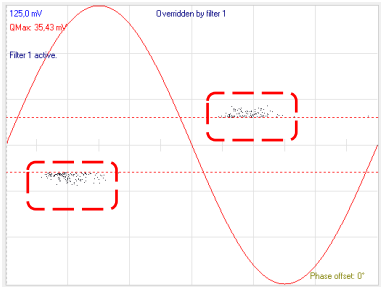
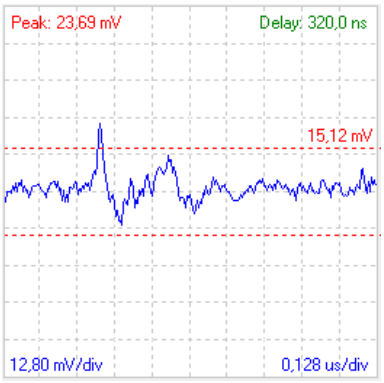	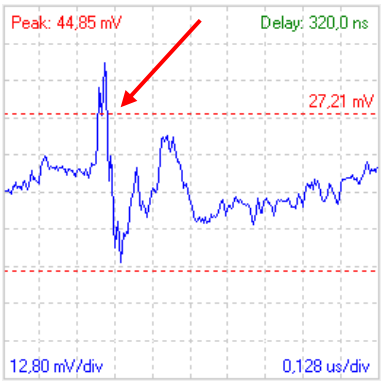	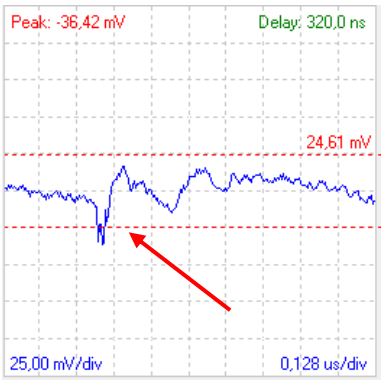
Max PD amplitude 23.69 mV	Max PD amplitude 47.87 mV	Max PD amplitude 36.42 mV

The PD pattern inversion and the PD amplitude reduction denote that the PD source was just passed by the Pry-CamTM portable as reported in Figure 5-17.

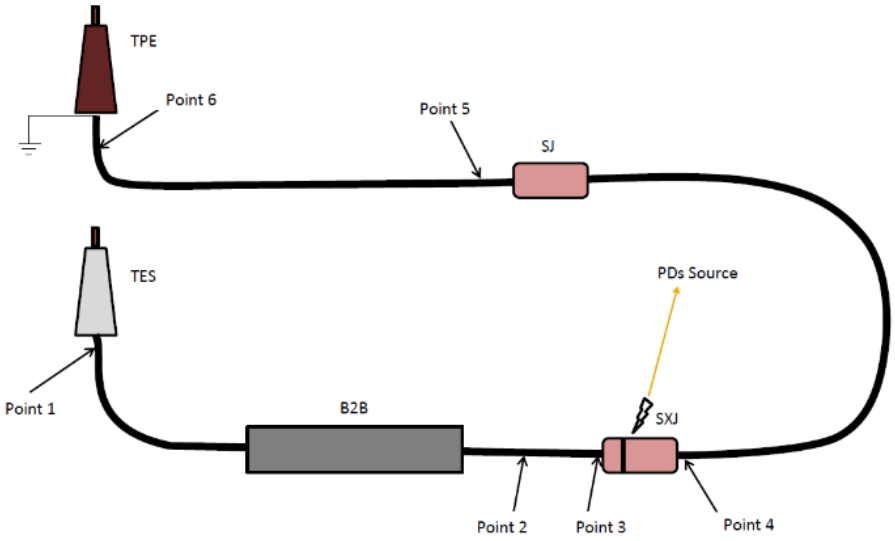

Figure 5-17. PDs source located in joint SXJ

The measurements performed on each point are reported in Table 5-3. For each point has been reported the PD pattern, the waveform and the frequency content of the PD pulses. The critical PD activity was highlighted in orange and red square, in particular it can be noted how the PD pattern changes getting closer to the defect, located on the sectionalized joint SXJ.

Table 5-3. Measurements on EHV cable: PD Patterns, waveform and frequency content of the acquired pulses

Point 1 TES	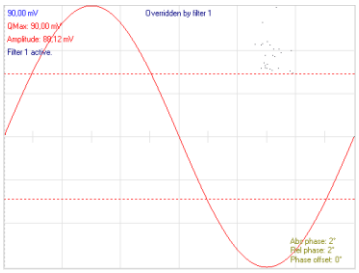	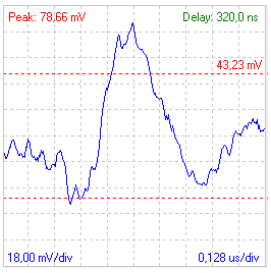	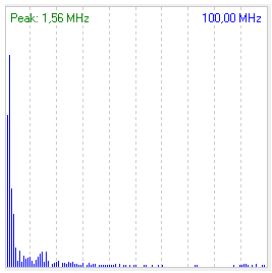	Low Frequency Surface on TES No critical PD
Point 2 After B2B	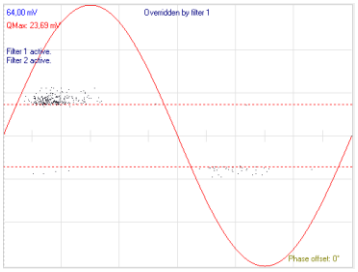	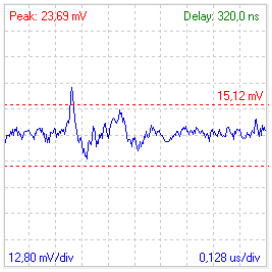	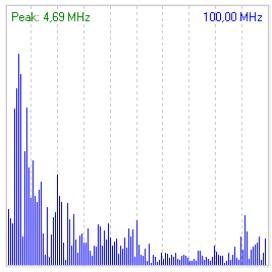	High Frequency Surface on SXJ 23.69 mV
Point 3 Left side SXJ	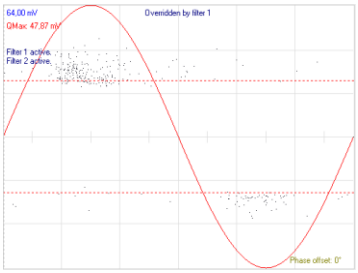	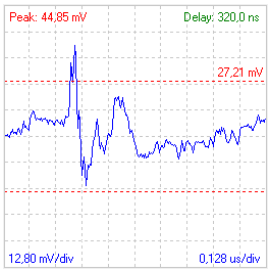	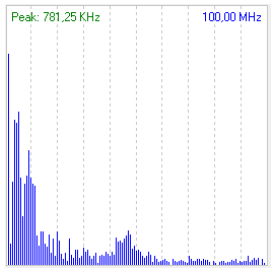	High Frequency Surface on SXJ 47.87 mV
Point 4 Right side SXJ	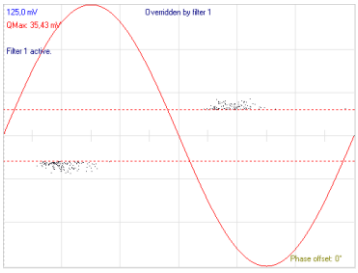	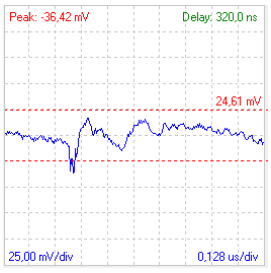	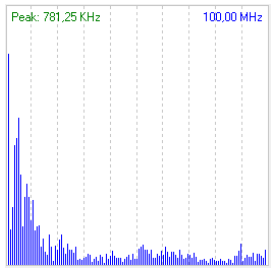	High Frequency Surface on SXJ 36.42 mV
Point 5 SJ	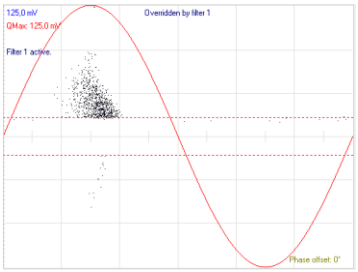	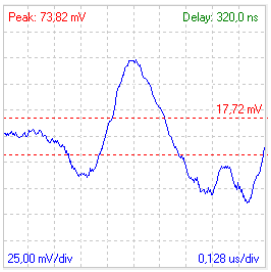	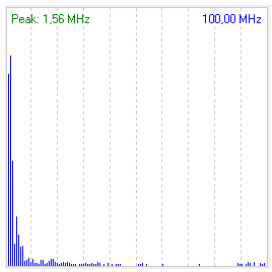	Low frequency Surface on TPE No critical PD
Point 6 TPE	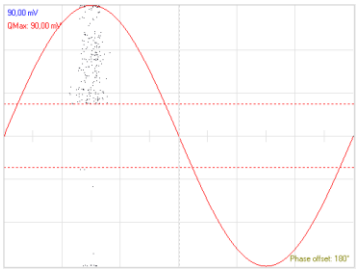	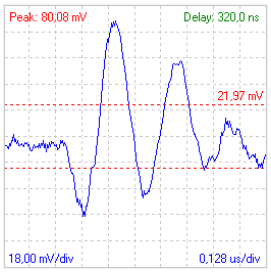	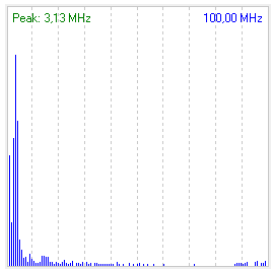	Low frequency Surface on TPE No critical PD

5.5 Measurement on short MV cables

In addition, the study was also extended to the components present in the MV distribution networks. In this case, the investigation was carried out at the high-voltage laboratories of INNOGY, a German Distribution System Operator (DSO), in which several tests and partial discharge measurements were carried out on circuits specially designed to verify the potential of the Pry- Cam Portable for the localization of defects on medium voltage terminations and joints. The measurements were performed on two MV circuits in the HV laboratory by means Pry-Cam Portable. In particular, the purpose of this study was to verify if the Pry-Cam Portable was able to acquire, identify the partial discharges on MV cable and accessories as well as to locate the exact location of the PD sources. Each circuit was composed by two cable terminations and one joint as shown below in Figure 5-18.

The measurements have been performed on both circuits placing the Pry-Cam Portable on different positions in order to identify and locate the PD sources.

In the detail, the measurements were performed on:

- Close to the Cable termination at left side;
- On the right side of the Joint;
- On the joint;
- On the left side of the Joint;
- Close to the Cable termination at right side.

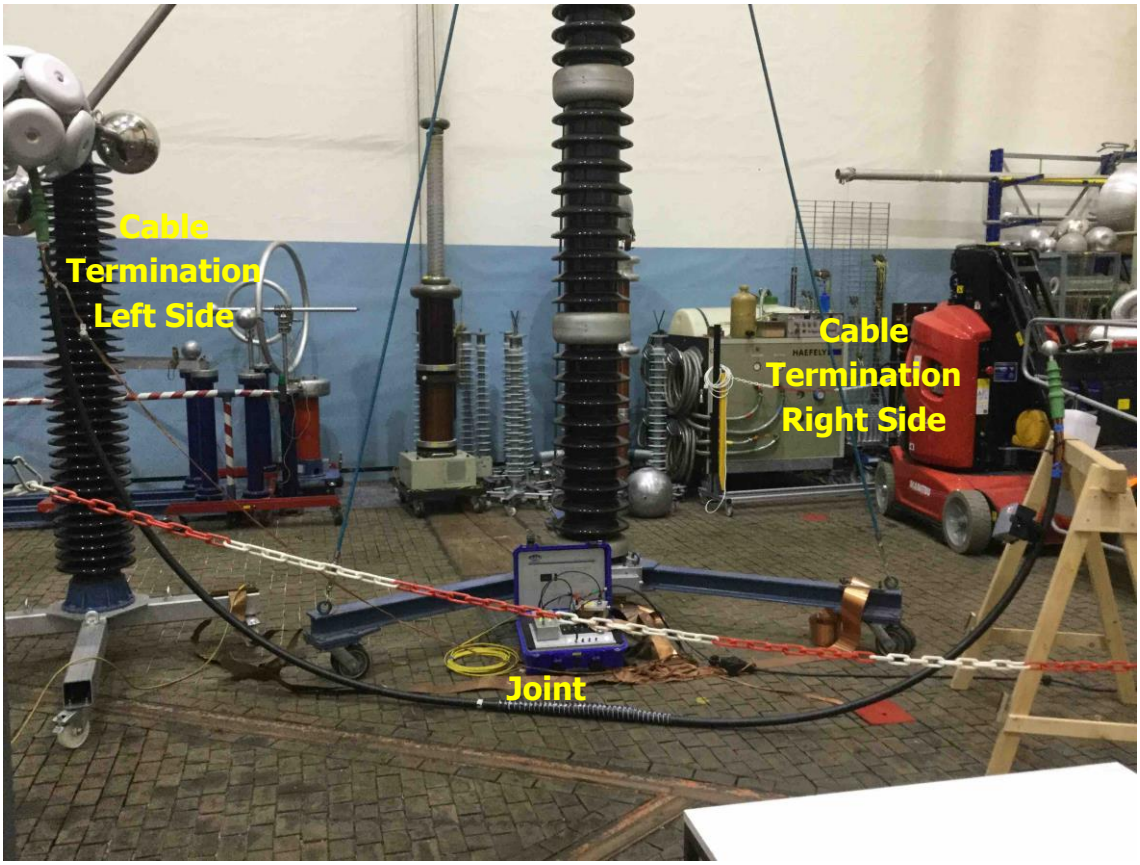

Figure 5-18. Circuit under test

The measurements on circuit 1 were performed at the voltage of 16 kV. By comparing the acquired pulses, it can be noted clearly the presence of critical PDs on the joint. In detail, the acquired pulses on joint show a steep waveform and high frequency content up to 50 MHz. Conversely, the acquired PD pattern on two cable terminations shows oscillating pulses, due to the pulse propagation on the short cable, and the frequency content is up to 30 MHz. Moreover, by comparing the PD amplitude, it can be noted that due to the propagation phenomena, the PD amplitude on the cable termination at the right side was higher. In this case, during the propagation, the pulse overlaps phenomenon results in an increase in amplitude. For each measurement the PD pattern, the waveform and FFT analysis of the pulses are reported in Table 5-4.

Table 5-4. Circuit 1 - PD Patterns, the waveform and FFT analysis of the pulses.

Cable termination Left side	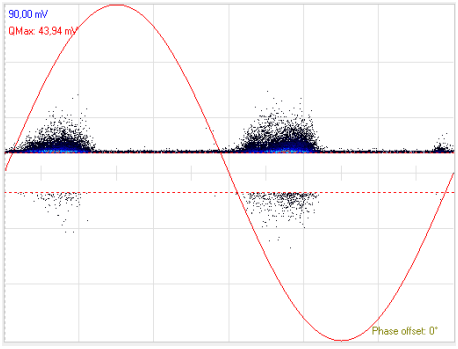	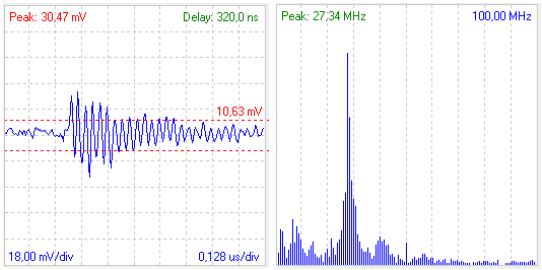
Joint	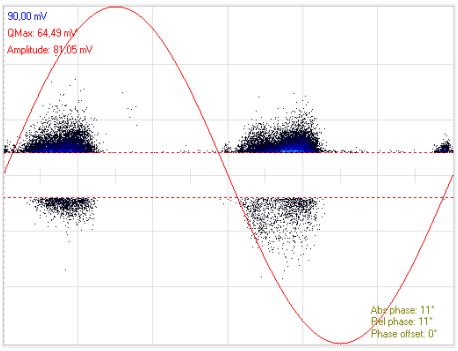	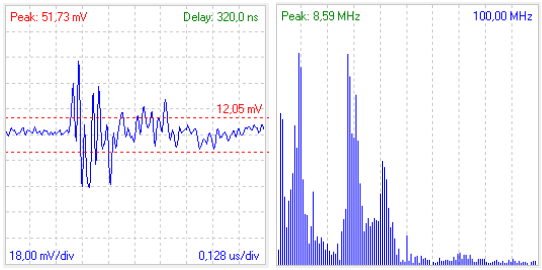
Cable termination Right side	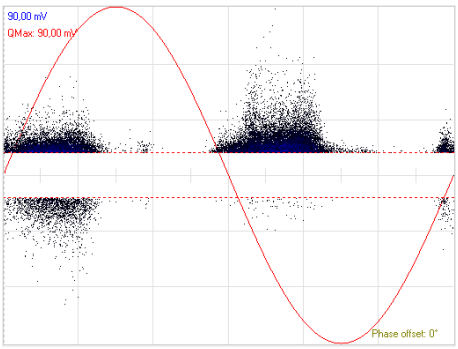	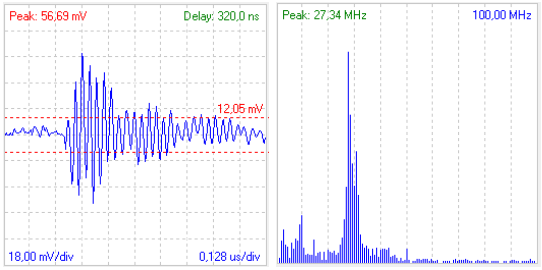

Furthermore, the measurements performed on the right and left sides of the joint show how the PD pulses change the polarity. The Pry-Cam Portable was placed close to the joint as reported in Figure 5-19.

Figure 5-19. Pry-Cam portable placed on left side of the joint

In this case, as reported in Table 5-5, due to the short length of the cable, it is not possible distinguish the inversion of the PD pattern. In a cable, the pulse propagates away from the PD source in both directions and due to the short length of the cable the PD pulses, during the propagation, reflected waves sum up and determine the formation of strongly oscillating pulses which in some cases may have a greater amplitude than the initial discharges.

Table 5-5. Measurements on Joint: PD Patterns, the waveform and FFT analysis of the pulses

Joint Left side	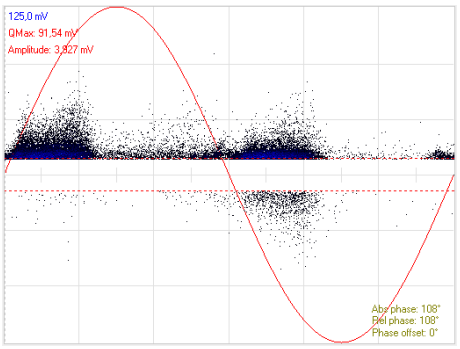	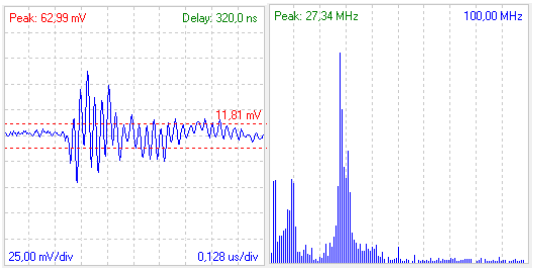
Joint Right side	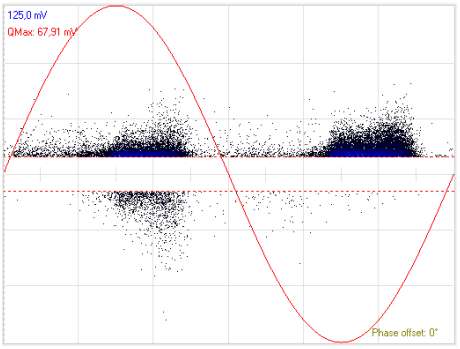	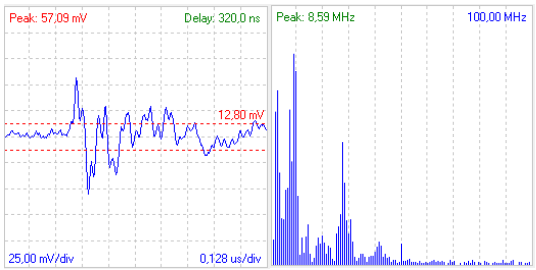

As reported in Figure 5-20 and Figure 5-21, by comparing of the acquired pulses it can be noted how the PD pulses change the polarity. In the detail, the acquired pulse on the left side of the joint (Figure 5-20) has a negative polarity, though the position of the PD pulse was in the

positive half period due to the oscillatory phenomenon. Conversely, the acquired pulse on the right side of the joint (Figure 5-21) shows a positive polarity and a different pulse waveform because in this case the defect is close to the measurement point.

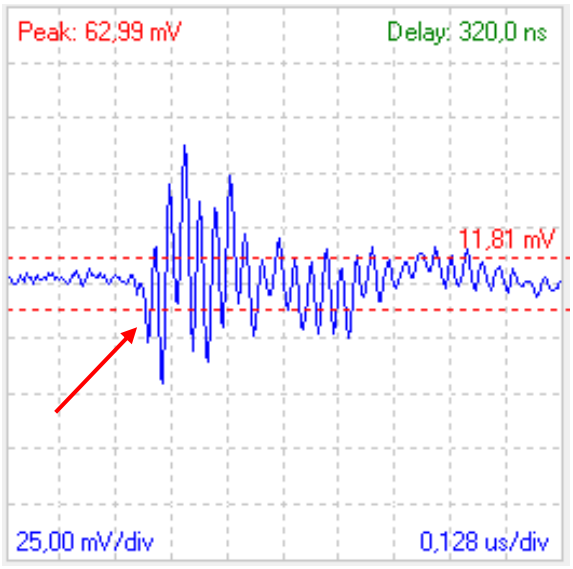

Figure 5-20. Pulse Waveform - Left Side Joint

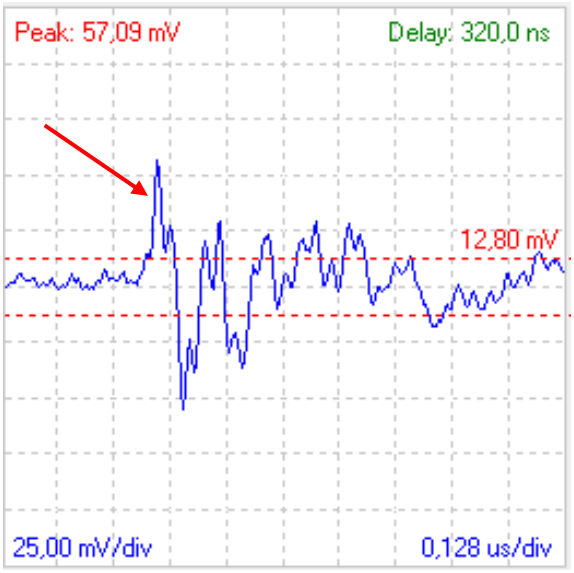

Figure 5-21. Pulse Waveform - Right Side Joint

This particular case study shows how to locate and identify the PD source on a joint. The analysis of the PD pattern allows understanding which component was affect by defect. Moreover, by comparing the pulses waveforms it is possible to locate the exact position of the defect in a cable.

The measurements on circuit 2 have been performed at the voltage of 37 kV. By analysing the PD pattern and by comparing the aquired pulse it was possible understand that the PD activities were located on the cable termination on the right side. s. In the detail, the acquired pulses show middle-fast waveform and the frequency content is up to 30 MHz. In this case, the acquired PD pulses show high amplitude and the waveform of the pulses has a saturated shape due to the nearness of the Pry-cam Portable to the defect on cable termination. Conversely, the acquired PD pattern on the cable termination at left side of the joint show oscillating pulses, due to the pulse propagation on the short cable, and the frequency content is lower than 20 MHz. For each measurement, the PD Pattern, the waveform and FFT analysis of the pulses are reported in Table 5-6.

Table 5-6. Circuit 2 - PD Patterns, the waveform and FFT analysis of the pulses

Cable termination Left side	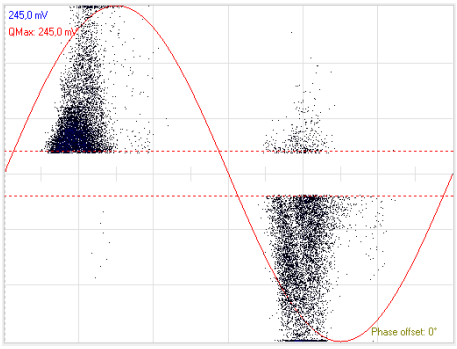	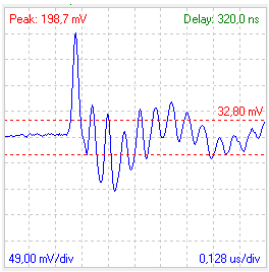	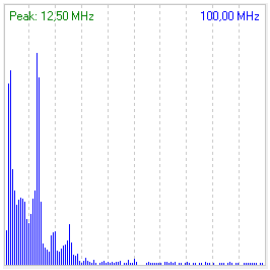
Joint	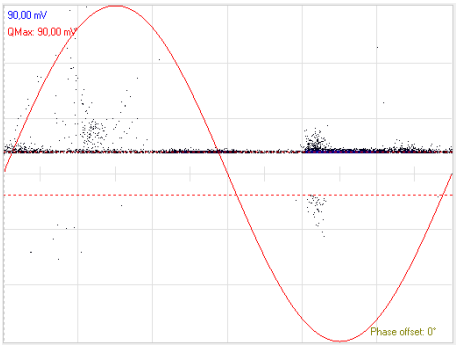	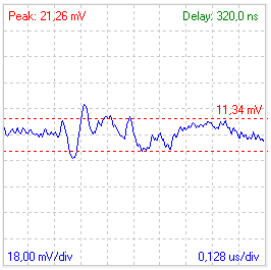	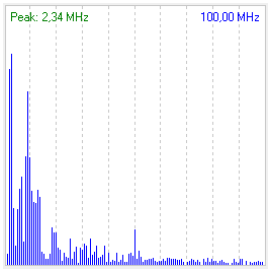
Cable termination Right side	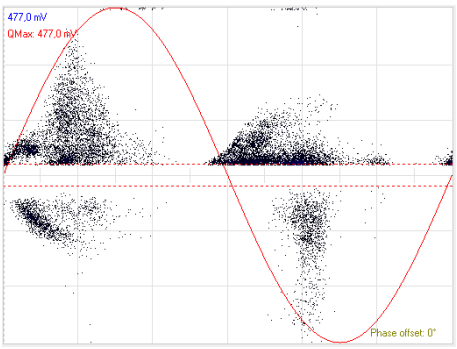	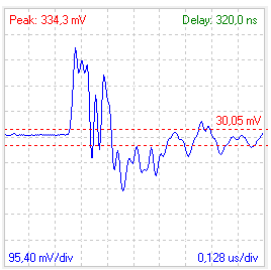	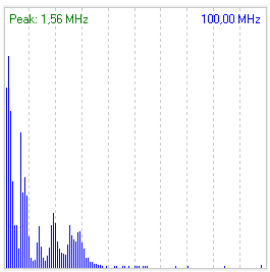

5.6 Conclusion

In this work, the potential of the Pry-Cam instrument has been demonstrated with respect to traditional measuring systems in locating and identifying cable defects.

At first, the study was conducted on two real cases, in particular the measurements and localization of PDs were carried out on a medium voltage cable at the Prysmian High Voltage Laboratory in Milan, after which several measurements were made on high voltage cable during HV type test. In this case, the circuit in question had a more complex structure than the MV cable due to the presence of the various test accessories, such as terminals and different types of joints. In either case, it was possible to correctly identify the source of the discharge and the exact location where it was located. The traditional partial discharge measurements are able to detect the presence of partial discharges throughout the system under examination. However, since these systems are fixed they are not able to locate the exact location of the discharge source.

Subsequently, the measurements and localization of PDs were performed on two MV short circuits at the high-voltage laboratories in German, to verify the potential of the Pry-Cam Portable for the localization of defects on medium voltage terminations and joints. Even in this case, it was possible locating the exactly defect position on both circuit by analysing the waveform and frequency content of the acquired PD pulses.

As results, thanks to the ease of use of the Pry-Cam, it can perform a complete screening of the whole system by positioning the device at different points. After measurements, accurate analysis can be made to identify the source of discharge. In particular, the analysis consists of comparing the different PD patters, with particular attention to the amplitude and frequency content of the acquired pulses. Of particular importance is the inversion of the PD Pattern and therefore the change of pulse polarity. The inversion of the PD pattern allows identifying the point where the discharge source and then the defective component is located.

6. Analysis, recognition and classification of PD phenomena on field during HV test via Pry-Cam instruments

6.1 Introduction

In this chapter, several events appearing during the HV on site test performed by means Pry-Cam portable are discussed. The aim of this study is to understand and classify different PD phenomena and external noise/disturbance that may occur during the HV test, at different voltage levels, on submarine and underground cables.

Most faults that occur in HV cables and accessories (i.e. outdoor terminations and joint) are due to the presence of electrical stress on the weaker points of dielectric materials. In particular, in areas where the local electric field is greater than the dielectric strength of the materials or the dielectric material degrades to the point where it cannot withstand the applied voltage. To avoid sudden failures, these defects must be found before the cable is commissioned, for this reason on-site tests are carried out to assess the quality and integrity of the whole cable system. In recent years, more transmission power cables with lengths up to several tens kilometers are installed. In the detail, these projects concern the connection of different geographic areas around the world by new HVAC and HVDC submarine cables route by Prysmian Group, as reported in Figure 6-1.

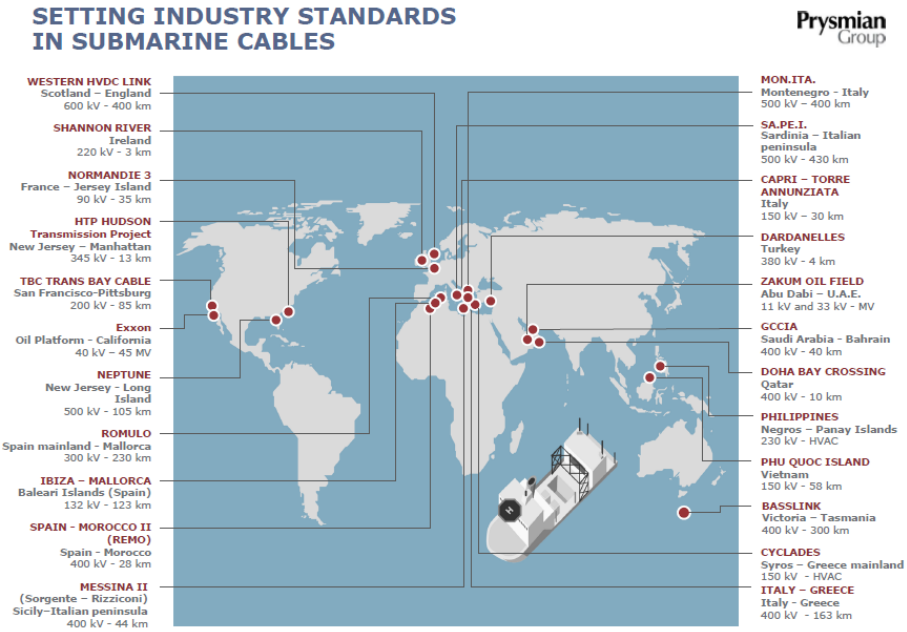

Figure 6-1. New submarine cables route by Prysmian Group

In addition to the possibility to interconnect different geographic areas, submarine cables are also used for the connection of offshore wind farms

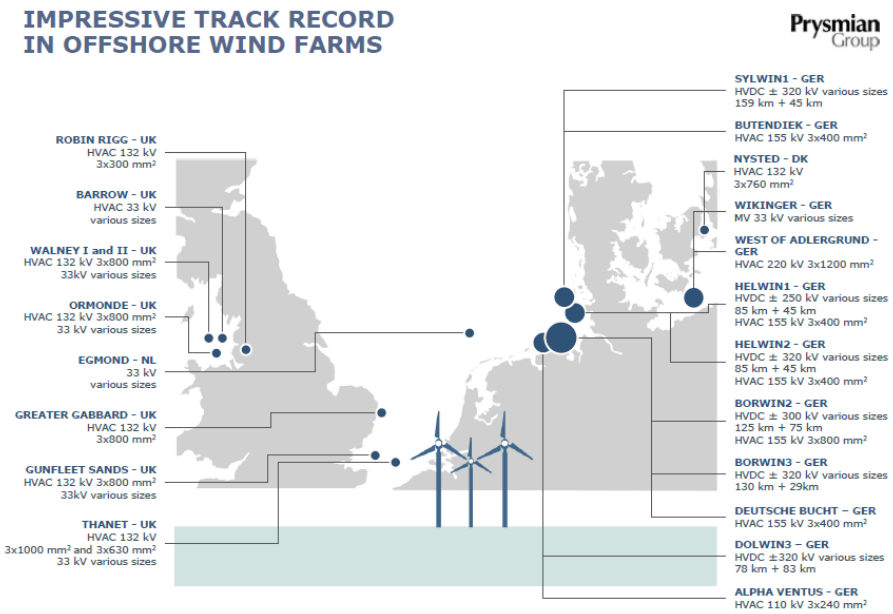

Figure 6-2. Submarine cables for offshore wind farm

Based on high demand on reliability of those connections, requirements about more detailed testing is needed. It must be emphasized that, once produced, cables are subjected to PD testing in factory according to IEC 60270 for quality control purposes. However, the standard IEC 60840 and IEC 62067 are not made for this kind of cable installations, because to build longer distance cables it is necessary to connect together on site more lengths of cable by using several joints. As reported in [55][56], the defect caused by installation are in the range of 3-10% of the installed circuit.

Newly installed or service aged AC transmission power cables with a length of more than 10 kilometers represents a large capacitive load with a large amount of reactive current needed to energize. As an example, for a 13 km long 150 kV XLPE-insulated cable, with test voltage 220 kV, 50 Hz a test power of up to 40 MVA is needed [58]. Generally, for transmission power cables the most common accepted testing method is the AC resonant Test (Figure 6-3).

Figure 6-3. AC resonant test system for on-site testing of extruded HV cables

The AC resonant test system with variable frequency mainly consists of the frequency converter, the exciting transformer, the coupling capacitors and high voltage reactors with fixed inductance or with variable frequency.

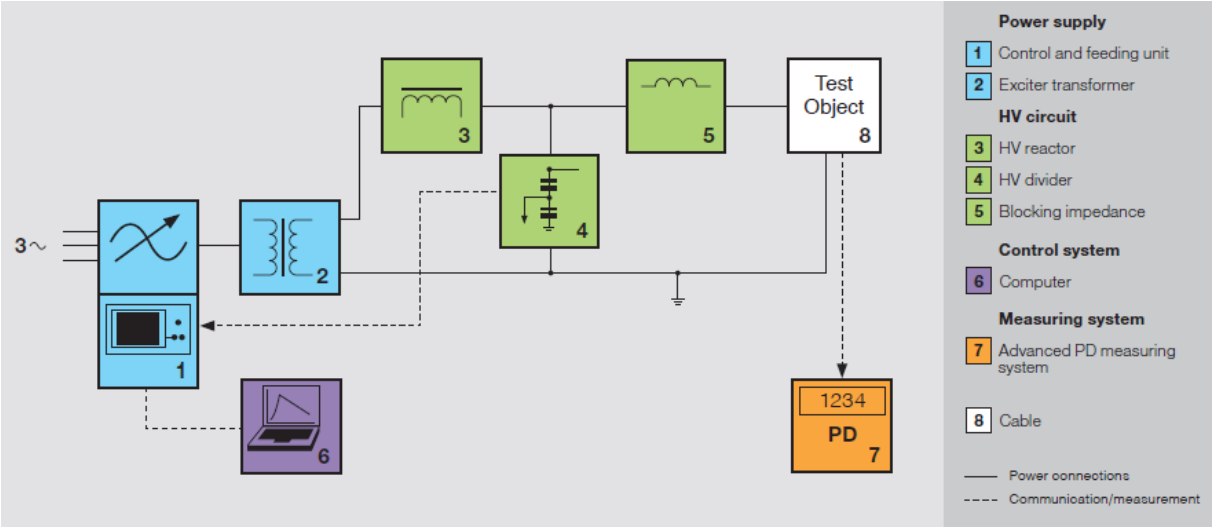

Figure 6-4. Block diagram of AC resonant test system for on-site testing of extruded cables

In detail, as reported in Figure 6-4, the control and feeding unit consists of a static power inverter and a control system. The power inverter converts the three-phase input voltage into a single-phase output voltage with a rectangular waveform.

The frequency is automatically adapted exactly to the resonant frequency of the HV series resonant circuit formed by the resonant reactor and the cable to be tested. The test voltage is regulated by the inverter output voltage and measured by a calibrated measuring system consisting of a peak voltmeter and voltage measuring divider.

The exciter transformer isolates the inverter from the test circuit and increases the inverter output voltage, depending on the required test voltage and losses of the HV series resonant

circuit. In case of a failure in the cable to be tested, high transient voltages can be generated in the HV circuit. The blocking impedance protects the reactor against such transient overvoltage. The test system can be conveniently controlled by a PLC and an operator panel implemented in the control and feeding unit. Sensitive PD measurement on joints and cable terminations can be performed by means of an advanced PD measuring system. [57]

The AC resonant Test system is able to perform tests on extruded cables according to IEC 60840 and 62067 after they have been installed. These standards require testing with AC voltage in the frequency range from 20 Hz to 300 Hz. Test system and test object form a series resonant circuit that due to the physics guarantees a pure sinusoidal waveform of the test voltage. In case of cable failure, only minimal damage may occur due to the limited amount of energy stored in the test circuit. The operating frequency range determines the wide load range for testing very short cables to cable lengths of several kilometers. A standard three-phase diesel generator can be used for the feeding of the test system and the modular design allows several test systems to be connected in series or parallel to enable testing with higher voltages or power requirements. [57]

Generally, the AC resonant Test system can be used to perform:

On-site test: the main application for the AC resonant test system is the AC withstand testing after the cable has been installed. These tests will be repeated during the lifetime of the cable. The tests can be combined with PD diagnosis on cable joints and terminations.

Routine test: the system can also be used for tests on super-long cables, for example, submarine cables in the factory. [57]

In Figure 6-5 an electrical diagram of the resonant test system is reported. To be independent from a stationary power supply a motor generator set is used. The frequency converter generates a variable voltage and frequency output which is applied to the exciter transformer. The exciter transformer excites the series resonant circuit consisting of the reactor's inductance L and the cable capacitance C. Even though the frequency converter creates harmonics the output voltage shows a pure sine wave. The resonance is adjusted by tuning the frequency of the frequency converter according to the formula [58][60]:

$$f = \frac{1}{2\pi \cdot \sqrt{L \cdot C}} \qquad (2)$$

The tuning range of the test system is determined by the converter's frequency range:

$$\frac{C_{max}}{C_{min}} = \left(\frac{f_{max}}{f_{min}}\right)^2 \qquad (3)$$

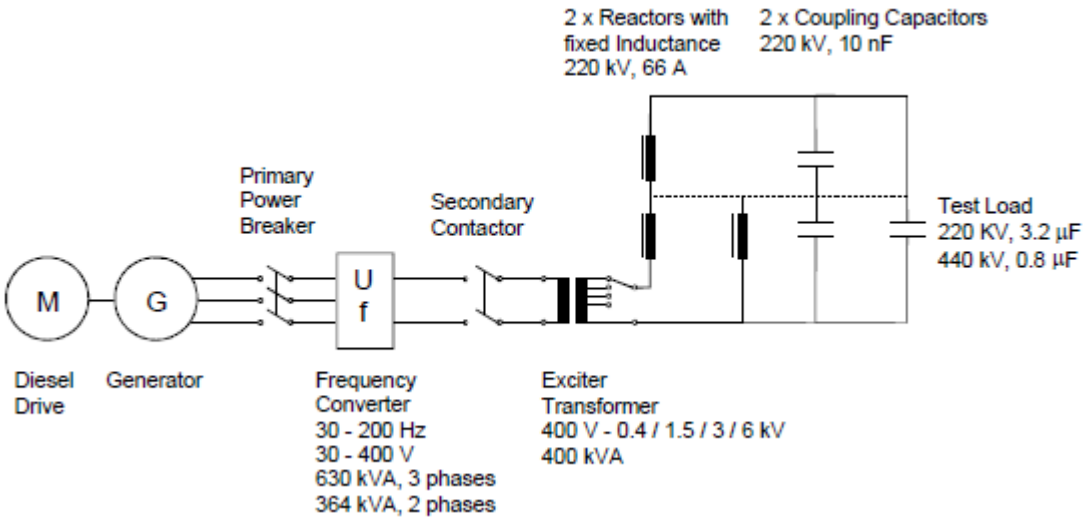

Figure 6-5. Electrical diagram of the resonant test system

Depending on the voltage level and the capacitance of the cable the test system can be extended by a second reactor. For longer power cables up to 150 kV and more than 10 km, the second reactor is connected in parallel. For test voltages up to 440 kV a series connection of the two reactors has to be realized [58].

Thanks to the several PD measurements performed by means Pry-Cam instruments (Pry-cam Portable and Pry-Cam Grids) on different HV systems it was possible to obtain a complete classification of the various disturbance phenomena and typical partial discharge. The survey has been conducted on cables and accessories during the normal operation condition but

especially during the HV test performed on the new installed transmission power cables. The measurements have been performed on several HV installations characterized by different rating voltage, from 110 kV up to 420 kV, type of cables and accessories like GIS Termination, OutDoor Sealing End (ODSE) and joints.
The investigation has been performed during the commissioning of the following HV systems:

- 2 submarine cables line at 380 kV in Turkey;
- underground cable line at 260 kV in United Kingdom;
- submarine cable line at 220 kV in Germany.
- underground cable line at 110 kV in Finland;

As stated above, depending on the type of cable system, high voltage tests (Commissioning) were carried out by using a multiple AC resonant Test. The resonance frequency, depending on the type of cable, is normally around on a frequency range of 30 to 40 Hz. This allows to reach voltage values of 1.5 or 1.7 U0, where U0 references the rated phase-to-ground operating voltage. Otherwise, when the line under test has a very long length, as in the case of the underground cable line in Finland and the submarine cable line in Germany, it was not possible to perform the AC resonant Test due to the high reactive capacitive power of the cable. In this case, the high voltage test was carried out by means of a "Soak Test" energizing the line in no-load condition directly from the HV electrical system. In this specific case, in addition to energizing the line, the compensation systems present on both ends of the line are fed.
Moreover, the investigation was extended to HV system during the normal operating condition. In this case, during all measurements the electric systems were working and the lines were in normal activity, submitted to their rated voltage and were loaded by the current as is in continuous operation. This survey has been performed on the following HV system:

- submarine cable at 420 kV and underground cable at 300 kV in Norway;
- underground cable at 154 kV in Turkey.

In addition, the study was also extended to the MV distribution network. In particular, an investigation was carried out in Taormina (Messina, Italy) on the distribution network through the collaboration with E-Distribuzione, an Italian DSO, during the ordinary service of the network. The measurements were performed on several components such as MV terminations, transformer terminations, joints and cables.

6.2 PD measurements on HV system at 380 kV in Turkey

Partial Discharges (PD) measurements were performed for Turkish TSO in Çannakkale, Turkey, during the commissioning of the line at 380 kV. The HV submarine interconnection is composed by double circuit at 380kV between Europe and Asia and across the Dardanelles strait in Turkey. The link has a double 380 kV AC power transmission circuit with a rating of 1000 MW for each circuit. For the project route spanning approximately 4.1km under the sea, six power cables XLPE, 1x1600mm^2, and two submarine fiber optic cables were laid with maximum sea depth of 90 meters. Circuits were completed by 1.5 km of underground power cables (XLPE, 1x2000mm^2) in total. The submarine power cables and underground power cables used in the project were interconnected at water level landfalls with special sea/land transition joints.

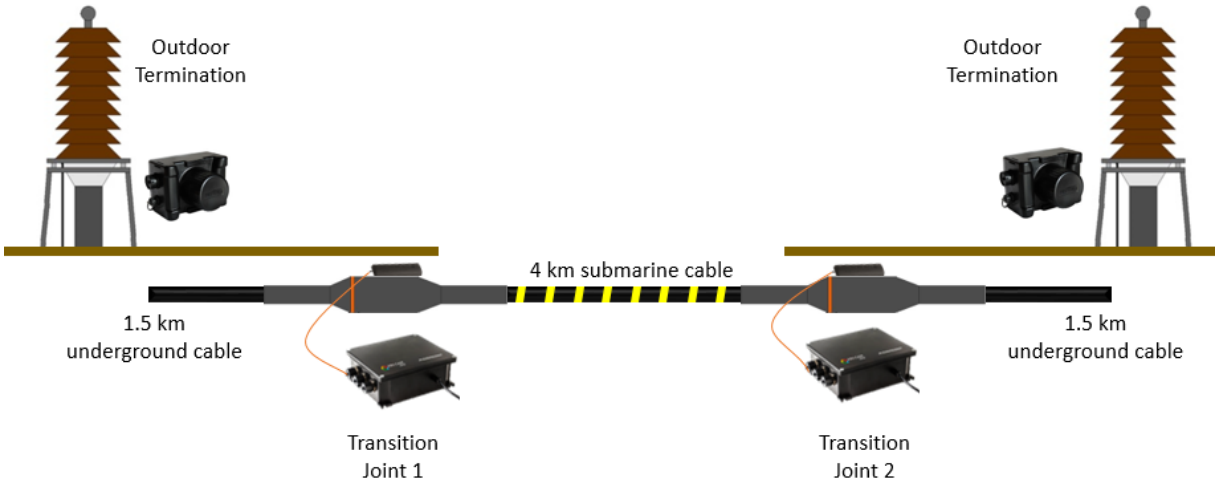

Figure 6-6. Layout of the 380 kV cable line

In order to check the health status of the whole system, during the commissioning, the measurements have been acquired by Pry-Cam Portable on the outdoor terminations and by Pry-Cam Grids on joints (Figure 6-7), through the link box present on the joint bays, on each side of the system under test.

Pry-Cam Portable

Pry-Cam Grids

Figure 6-7. Pry-Cam Portable placed on cable and Pry-Cam Grids connected on the joint bay

The commissioning test was performed one phase at a time at different of voltage levels with a resonant generator. The frequencies used for each phase were:

Circuit South		Circuit North	
Phase Red	35.55 Hz	Phase Red	36.04 Hz
Phase Yellow	35.03 Hz	Phase Yellow	35.93 Hz
Phase Blue	34.86 Hz	Phase Blue	35.71 Hz

At the beginning of the commissioning, the phase under test has been energized at the voltage level of 150 kV, 220 kV and 270 kV (phase to ground), 1 minute for each voltage level. At this time, it is necessary to monitor the condition of the accessories in order to avoid any critical damage due to a wrong installation of the components, in this case when the voltage goes up and critical PD arise it is recommendable to interrupt the test. If the whole system does not show any critical PD activities, it is necessary to increase the voltage and keep monitoring. The commissioning starts when the voltage of 330 kV (phase to ground) is reached and finishes after one hour.

On site withstand voltage testing is an essential part of a cable laying and commissioning project. Cables and accessories are tested separately during routine testing in the factory. Testing on site is a check of proper assembly of cable and accessories together. With longer lengths of cable, the system used to test the cable also has to be of larger rated power. For this reason, to perform the commissioning was employed a Variable Frequency Resonant Test System (RSKF) by HAEFELY HIPOTRONICS for on-site cable test. The RSKF system is based on a modern frequency converter to facilitate such testing with fixed core and variable frequency reactors operable between 20-300 Hz. These reactors are lighter and more powerful as compared to the variable inductance fixed frequency reactors. The RSKF is a modular system (Figure 6-8) and can be combined in parallel and series configuration for higher current or voltage requirements. It allows an easy integration with existing fixed-gap reactors.

Figure 6-8. RSKF - Variable resonant test system

The Figure 6-9 shows the Resonant test system used during the commissioning performed using the AC resonant test system with two reactors connected in series in Turkey.

Figure 6-9. Resonant test system with reactors in series during the commissioning

When the line was energized, and the first voltage step of 150 kV was reached, the Pry-Cam portable placed on the cable acquired the PD pattern reported in Figure 6-10. The acquired PD pattern shows an external noise produced by the frequency converter.

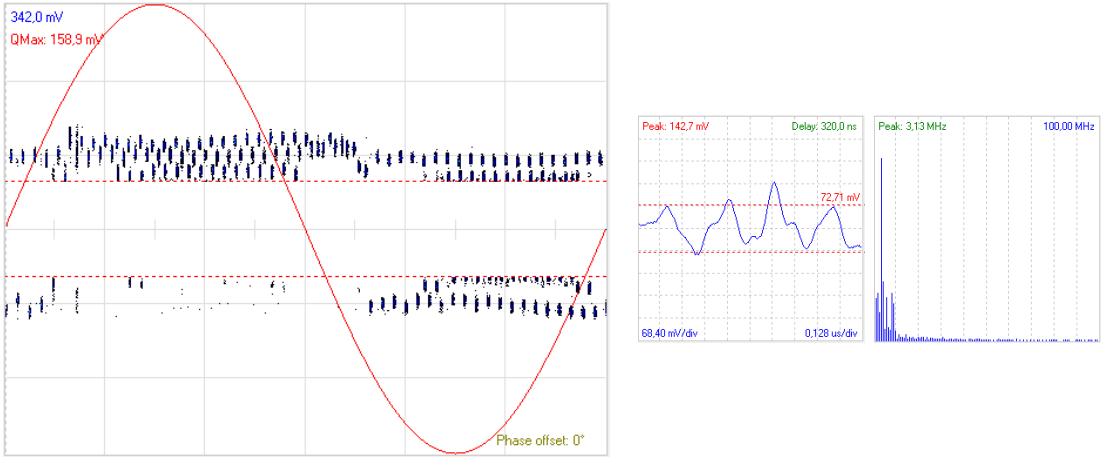

Figure 6-10. External noise produced by the frequency converter

Also, it must be emphasized that during the measurements Pry-Cam portable has acquired PD pulses with the correct frequency of the supply voltage equal to 35 Hz.

Each phase of the two circuits has been powered from the European side by the AC resonant system. The commissioning started when the voltage has reached the value of 330 kV. For test purposes, the voltage was maintained for one hour during which the partial discharge measurements were carried out. At the end of the test, it was necessary to wait 12 hours to allow the reactors to cool down before performing the test on the other phase.

In Table 6-1 have been reported the acquired PD patterns of the Circuit North on each phase of the component. As reported below, it can be noted that several PD activities have been acquired on the component located on the European side because the AC resonant system was located on the same side. Conversely, the acquired PD patterns on the Asian side show a smaller presence of the PD phenomena due to low frequency surface discharge and Corona effect.

Table 6-1. PD measurements on Circuit North

Circuit North			
Test Point	Red Phase	Yellow Phase	Blue Phase
European side Outdoor termination	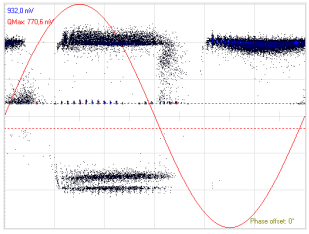	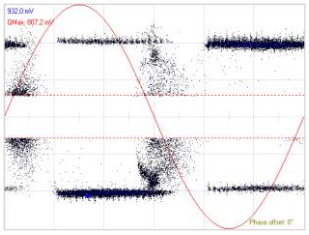	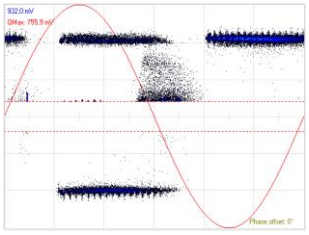
European side Joint bay	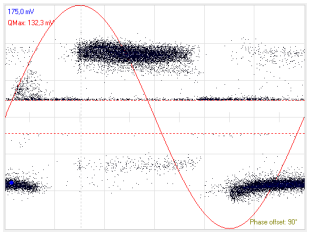	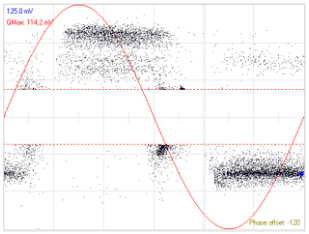	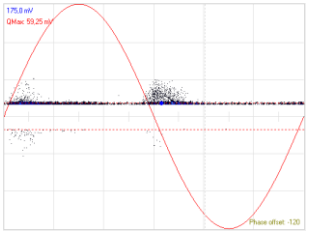
Asian side Joint bay	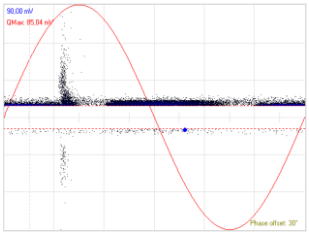	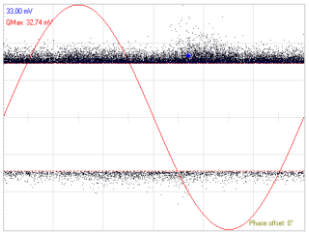	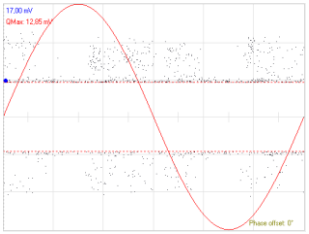
Asian side Outdoor termination	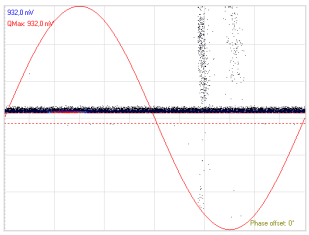	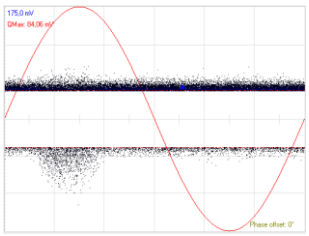	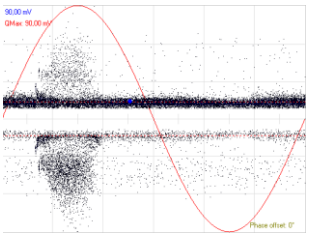

As an example, the analysis is carried out on a red phase of circuit North.

The PD patterns on the outdoor termination at European side show a low frequency surface discharge, highlighted in green, and corona effect, highlighted in blue, due to the connection of the AC resonant system. The PD pattern, the waveform and FFT analysis of the pulses are reported in Figure 6-11.

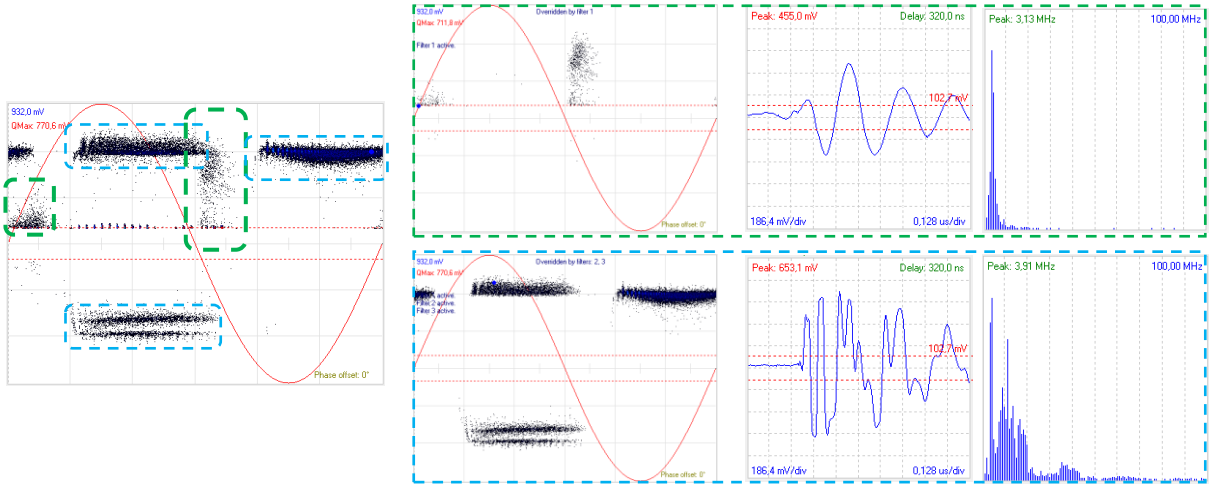

Figure 6-11. Outdoor termination EU side: PD pattern, waveform and frequency content of the pulses

In the same side, the PD pulses acquired on the joint bay shows the same phenomena acquired on the outdoor termination with a lower amplitude due to the propagation and attenuation effects. The PD pattern, the waveform and FFT analysis of the pulses are reported in Figure 6-12.

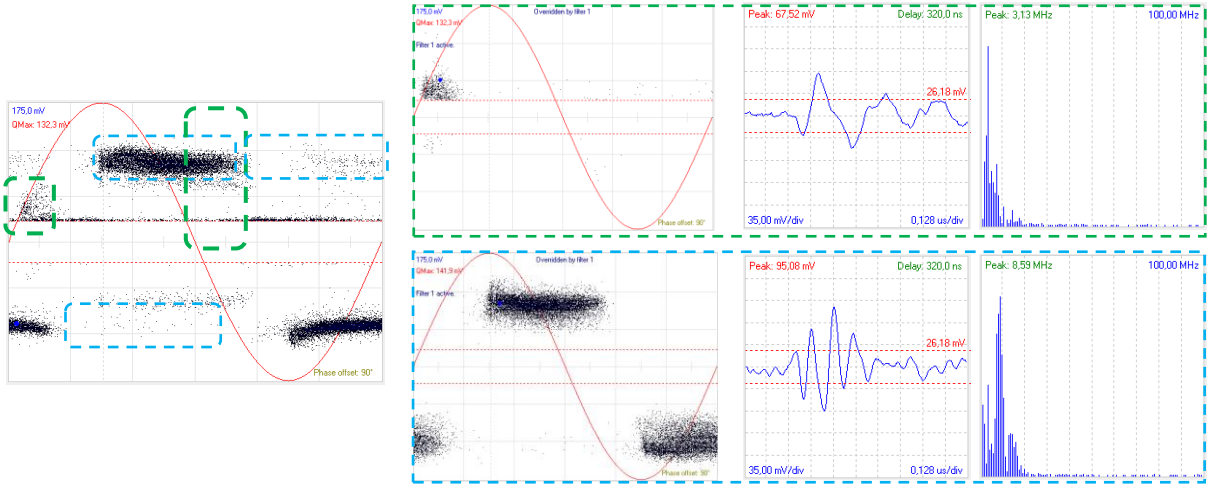

Figure 6-12. Joint bay European side: PD pattern, waveform and frequency content of the pulses

As compared to the previous case, the measurements performed on Asian side on joint bay did not show any low frequency surface discharge due to the presence of the AC resonant system,

but only the corona effect coming from the outdoor termination. The PD pattern, the waveform and FFT analysis of the pulses are reported in Figure 6-13

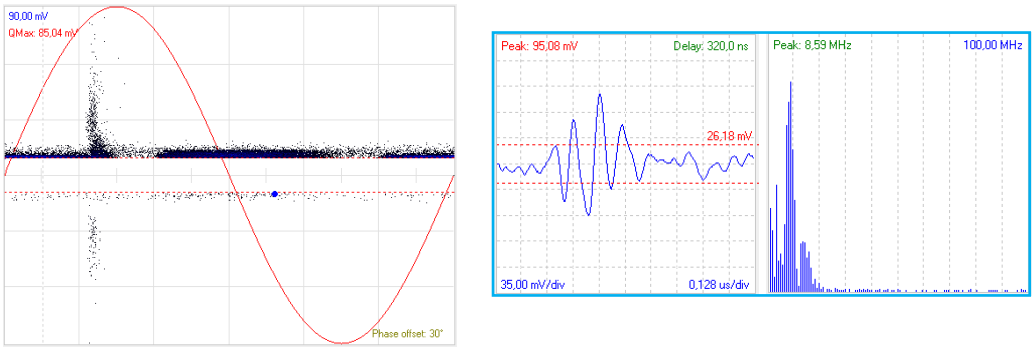

Figure 6-13. Joint bay Asian side: PD pattern, waveform and frequency content of the pulses

As discussed in the previous case, the PD patterns show the same corona effect with a higher amplitude as compared to the PD pulses acquired on joint bay. Even in this case the measurements performed did not show any low frequency surface discharge due to the presence of the resonant generator. The PD pattern, the waveform and FFT analysis of the pulses are reported inFigure 6-14

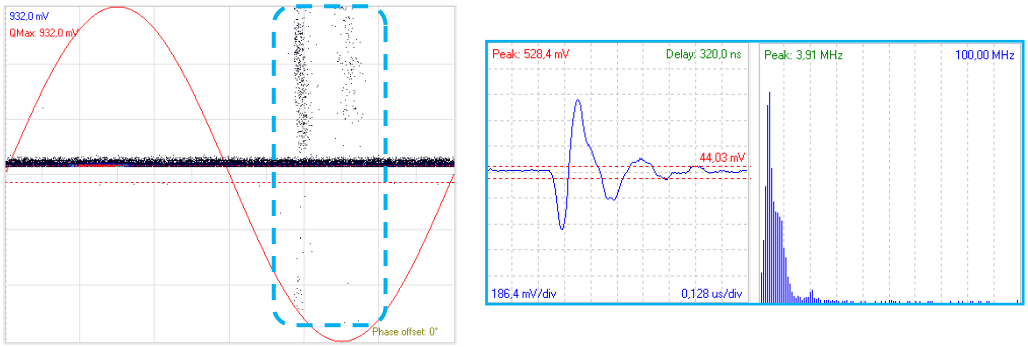

Figure 6-14. Outdoor termination Asian side: PD pattern, waveform and frequency content of the pulses

6.3 PD measurements on HV system at 400 kV in United Kingdom

PD measurements were performed during the commissioning of the underground cable at 400kV, in particular the measurements have been performed on Blue phase of GIS termination. During this survey, electrical signals were acquired and processed by means of the Prysmian Pry-Cam and Pry-Cam Grids, two measuring systems which allow performing online partial discharge measurements without galvanic connection to the system under test and with a very high precision and sensitivity. The test duration was planned in 24 hours and the electric system was energized at 260 kV phase to ground with AC resonant system.

Figure 6-15. AC resonant system connected to the GIS switchgear system

Figure 6-16. Underground cables at 400 kV and GIS Termination

At the beginning the Wing sensor was placed on cable close to the GIS termination as reported in Figure 6-17.

Figure 6-17. Wing Sensor placed on Cable before starting test HV test

However, a particular high noise level (Figure 6-18) was found on site before starting the test and after investigations, the probable source of the noise was located to a medium wave antenna very close to the site.

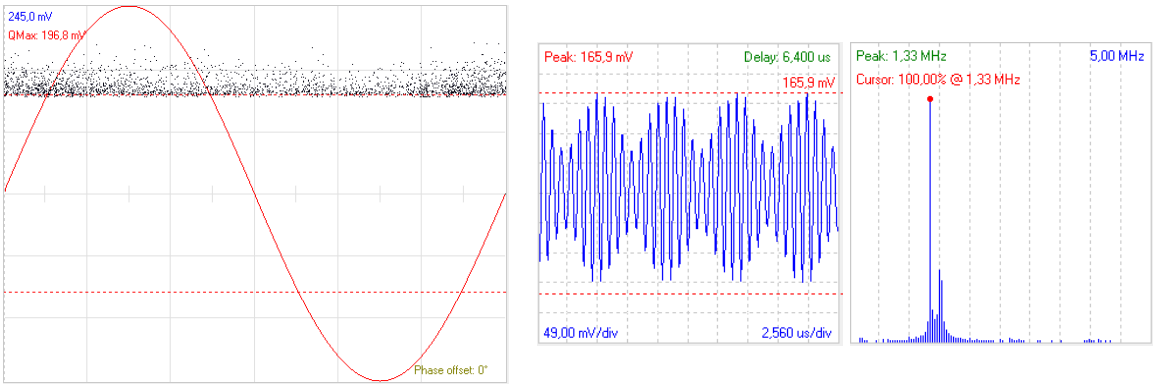

Figure 6-18. External Noise – PD Pattern, waveform and Frequency content of the acquired pulse

In order to better understand the noise phenomenon, several measurements have been performed setting different time length levels of the acquisition system. In Table 6-2 the measurements performed at time length from 1µs to 40µs are reported. It must be emphasized that setting a different time length, in particular by increasing the time scale, leads to a reduction of the frequency spectrum scale. In this case, the frequency spectrum goes from 100 MHz for an acquisition at 1 µs to 2.5 MHz for an acquisition at 40 µs. Clearly the acquired PD pulses at high time length show the real waveform of the external noise with a constant amplitude about of about 165 mV and the peak of frequency spectrum in a range of 1.33 – 1.56 MHz.

Table 6-2. Acquired External Noise at different time length levels

Time Length	PD Pattern	Waveform	FFT	Frequency Spectrum range
1 µs	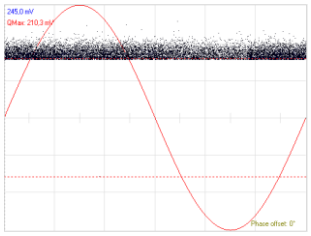	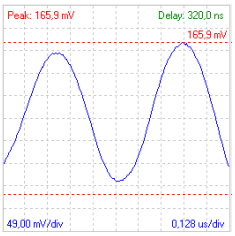	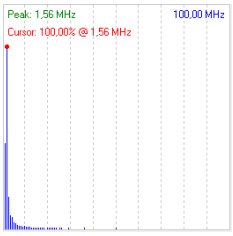	100 MHz
2 µs	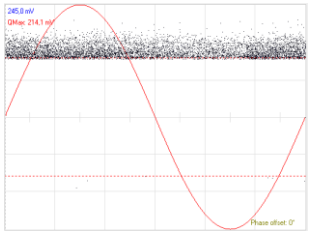	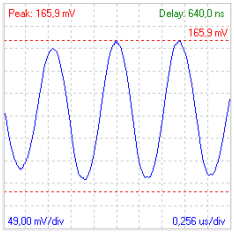	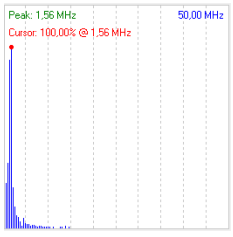	50 MHz
5 µs	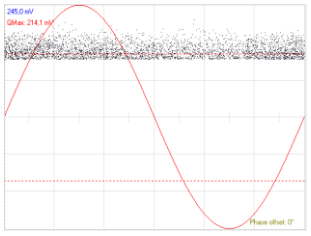	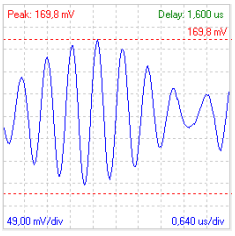	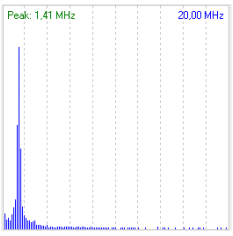	20 MHz
10 µs	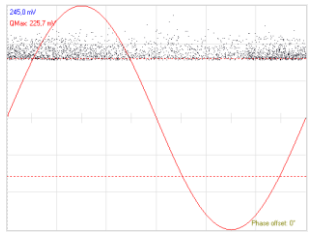	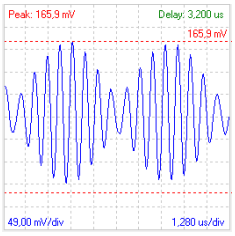	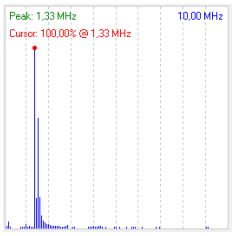	10 MHz
20 µs	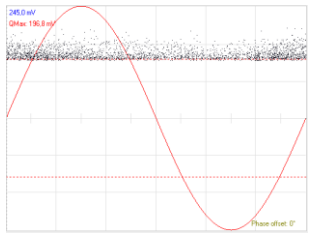	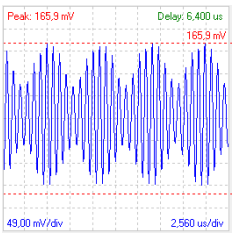	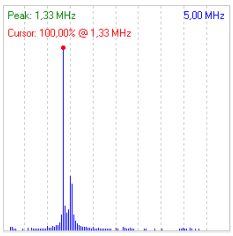	5 MHz
40 µs	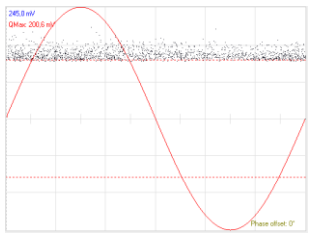	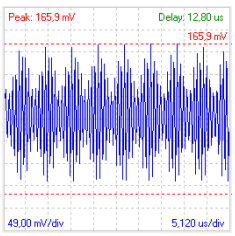	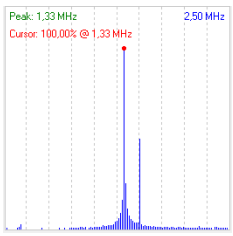	2.5 MHz

This noise was considerably strong at the cable terminations on the GIS system, thus the Wing PD sensor has been installed on the blue phase ground connection of the cable sealing (Wings

sensor – Figure 6-19), where the noise level was lower. This position of the sensor provided good sensitivity for reliable PD measurements.

Figure 6-19. Pry-Cam Wings installed on the earth connection of the GIS cable sealing end.

The acquired external noise on the ground connection of the GIS cable sealing end has a lower amplitude compared to the previous measurements acquired directly on the cable. In particular, in Figure 6-20 are reported the waveform and frequency spectrum of PD pulses. The maximum amplitude in this case was about 67 mV compared to the value of 169 mV, acquired on the previously acquired case.

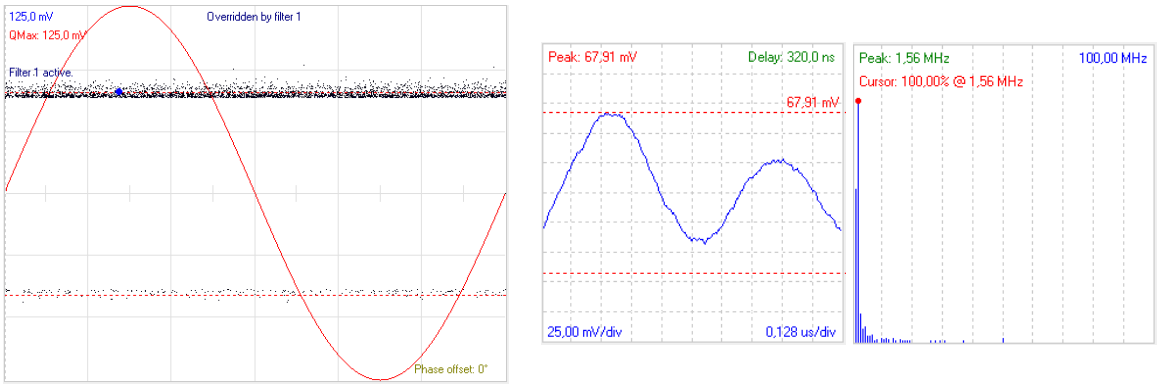

Figure 6-20. Acquired External Noise on the ground connection of the GIS cable sealing end

During the test, many acquisitions have been performed, all showing similar results and the presence of particular surface PDs, highlighted in yellow, likely due to the connection of the resonant system to the test bushing by means of an aluminum pipe or due to the presence of some metallic protrusion within the GIS system. The acquired pulses present steep waveform and high frequency content up to 40 MHz typical of the surface PD activity. Also, the presence of the noise generated by the frequency converter of the resonant system can be noted. This kind of noise is typical during the commissioning performed through the AC resonant system and was classified as an external disturbance and filtered out during the test. A representative PD acquisition is shown in Figure 6-21.

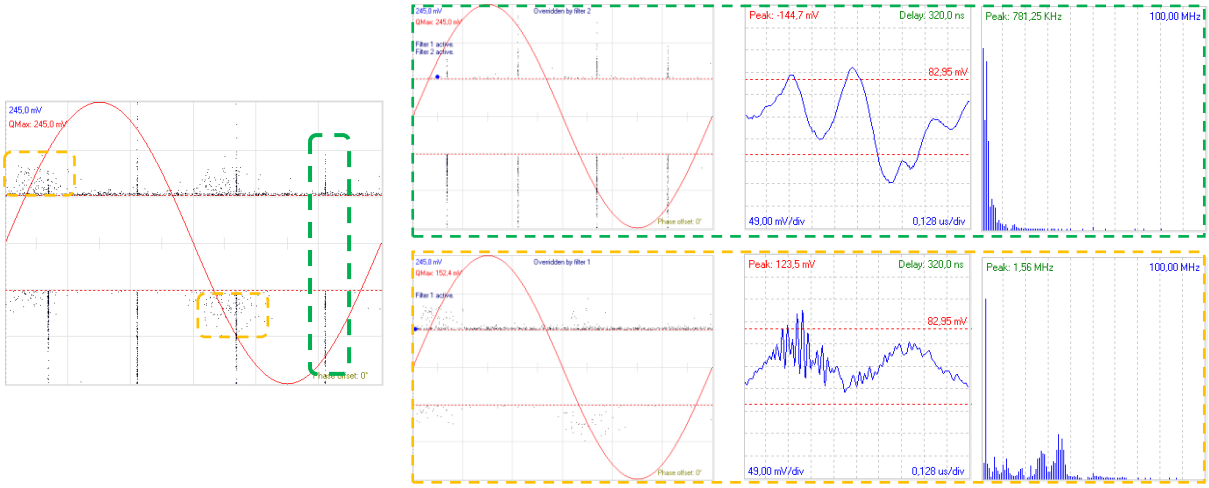

Figure 6-21. Representative pattern acquired during the first day of HVAC test

After approximately 10 hours, the power system tripped down. As reported below, the analysis of the PD measurements, hour by hour, before and during the trip (Table 6-3 and

Table 6-4), shows surface PD activities characterized by different amplitude. In particular, two phenomena can be observed, the first highlighted in yellow square, classified as high frequency surface discharge characterized by fasted pulses and frequency content up to 40 MHz due to the likely presence of the metallic protrusion within the GIS system. The latter, highlighted in blue square, classified as low frequency surface discharge with slower pulses and frequency content up to 20 MHz, due to connection (aluminum tube) to the resonant system.

It should be noted that the HV test has been performed through the AC resonant system in no-load condition. In this case the cable under test was subject to the transit of a capacitive current dependent on the characteristics of the cable itself. Considering that the cable was in no-load condition, in order to perform the analysis of acquired PD patterns, it was necessary to shift the acquired PD patterns of 90° in accordance with the internal synchronism provided by the power supply of the Pry-cam Grid, to obtain the correct position of PD phenomena. An example of PD Pattern with phase shifting is reported below. In the detail, as reported in Figure 6-22 the acquired PD pulses were in wrong position such as an internal discharge position before the zero crossing. As reported in Figure 6-23, a phase angle correction of 90° of the PD Pattern shows the right position of the PD phenomenon. The corrected PD pattern allow to classify these PD phenomena as surface discharges.

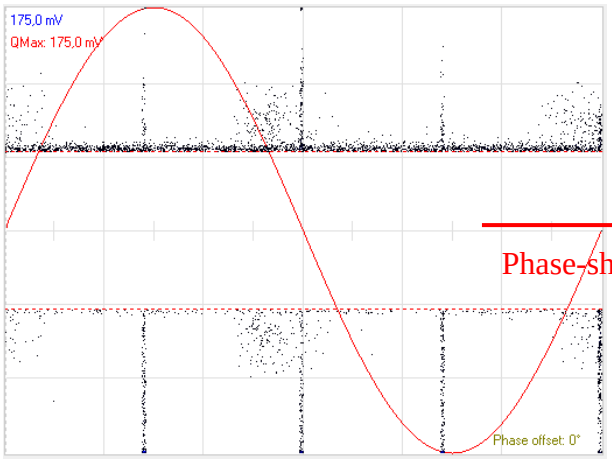

Figure 6-22. Acquire PD Pattern at 0° of phase offset

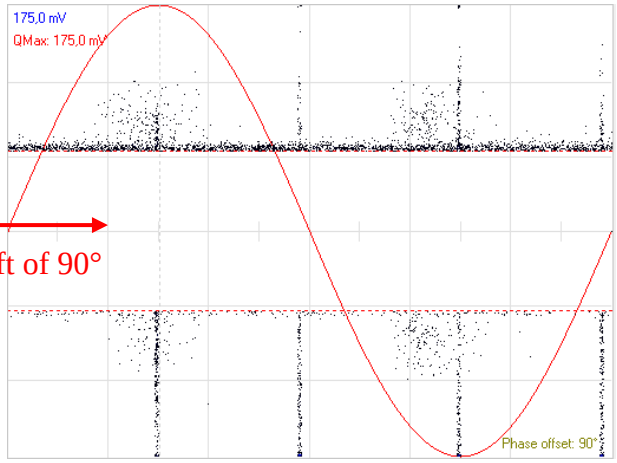

Figure 6-23. Acquired PD Pattern at 90° of phase offset

In Table 6-3and

Table 6-4 the analysis of the acquired PD Pattern in each hour is reported.

Table 6-3. Analysis of the acquired PD Patterns during the HV Test

1st hour	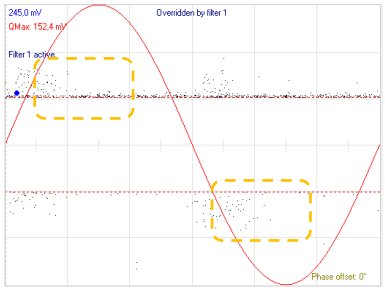		HF surface discharge PD amplitude 160 mV FFT 40 MHz
2nd hour	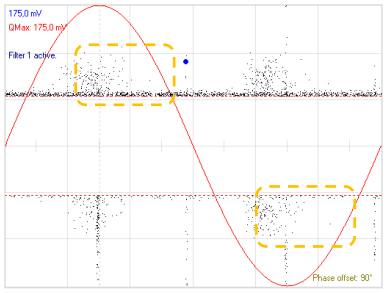		HF surface discharge PD amplitude 114 mV FFT 50 MHz
3rd hour	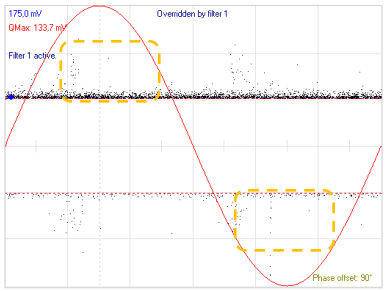	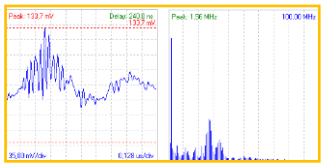	HF surface discharge PD amplitude 133 mV FFT 40 MHz
4th hour	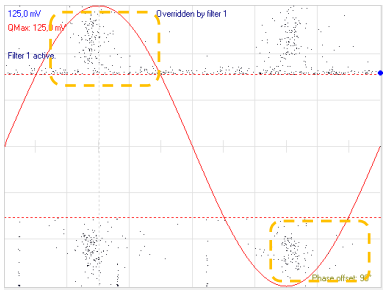	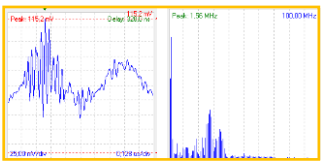	HF surface discharge PD amplitude 115 mV FFT 40 MHz
5th hour	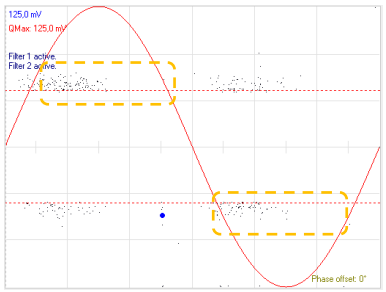	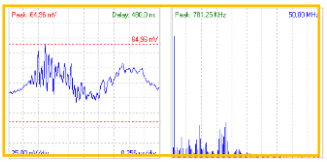	HF surface discharge PD amplitude 64 mV FFT 50 MHz

Table 6-4. Analysis of the acquired PD Patterns during the HV Test

6th hour	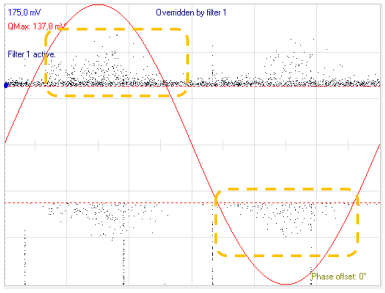		HF surface discharge PD amplitude 130 mV FFT 50 MHz
7th hour	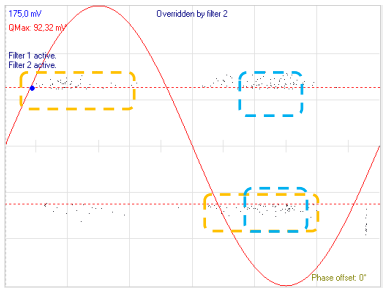	 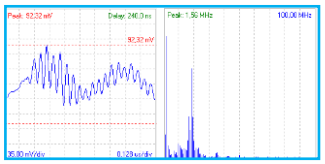	HF surface discharge PD amplitude 86 mV FFT 40 MHz LF surface discharge PD amplitude 92 mV FFT 20 MHz
8th hour	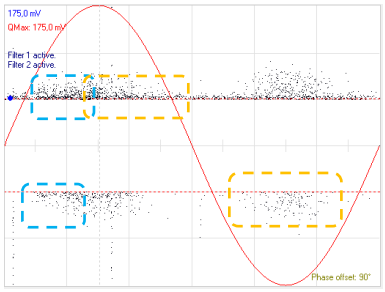	 	HF surface discharge PD amplitude 106 mV FFT 50 MHz LF surface discharge PD amplitude 84 mV FFT 20 MHz
9th hour	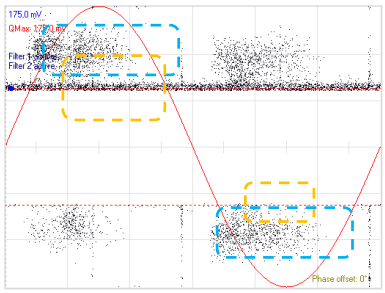	 	HF surface discharge PD amplitude 121 mV FFT 50 MHz LF surface discharge PD amplitude 168 mV FFT 30 MHz
10th hour	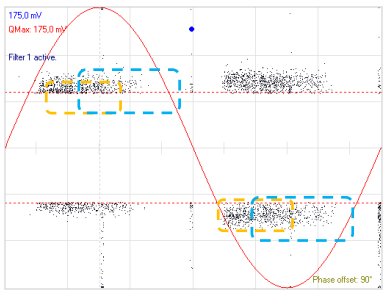	 	HF surface discharge PD amplitude 95mV FFT 50MHz LF surface discharge PD amplitude 110 mV FFT 30 MHz

After 10 hours the system tripped down, but the acquired PD pattern still shows the same PD phenomena as reported in Figure 6-24. Two attempts to restart the HVAC test have been performed, resulting in two new trips at 240kV and while ramping up to 130kV (approximately 60kV).

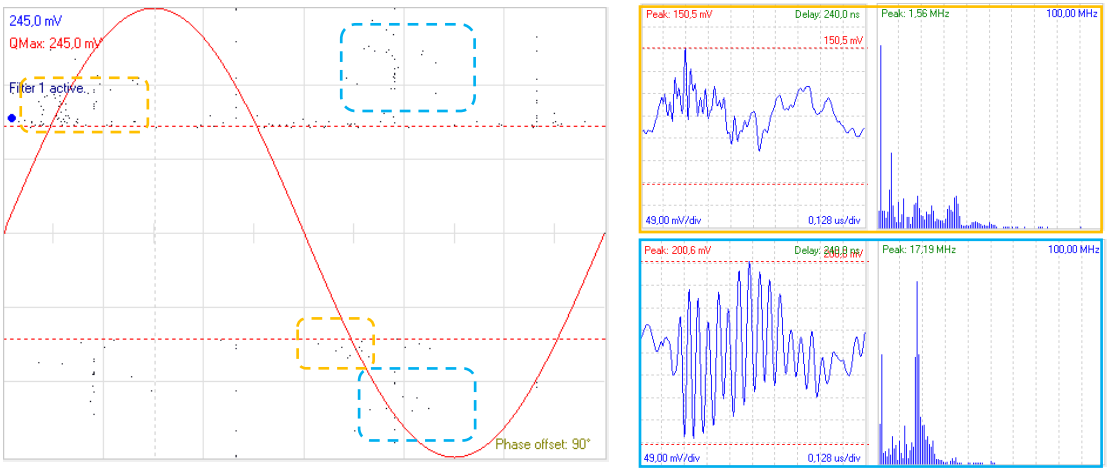

Figure 6-24. PD Pattern, pulses waveform and frequency content during the trip

Once the test was stopped it was necessary to understand the causes that led to the system trip down. The system shutdown may be due to a cable failure at a distant point of the line so as not to be acquired during the PD monitoring system or due to the presence of critical discharges inside the GIS system to cause a discharge to its indoor. As reported in Figure 6-25, after a visual inspection of the whole system, a burning trace was found on the GIS test bushing due to the presence of the surface discharge during the HV test.

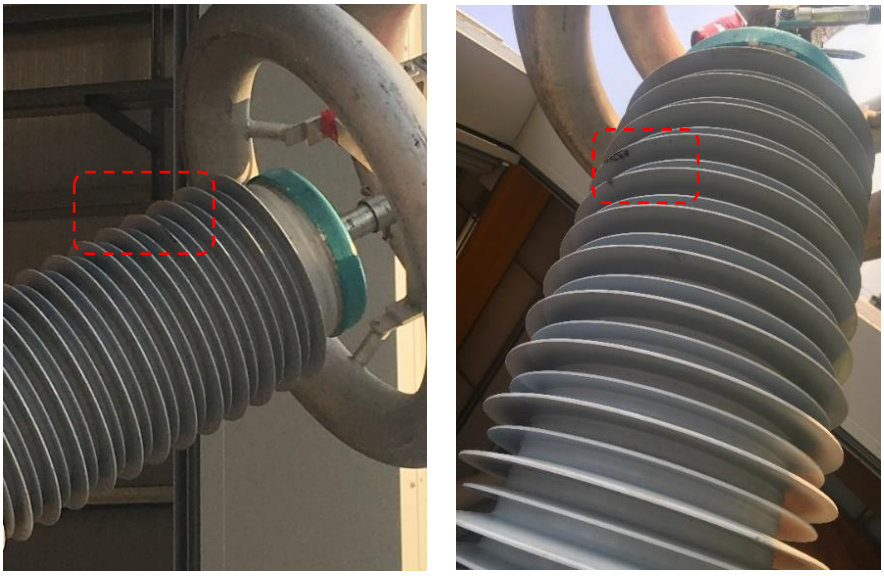

Figure 6-25. The effect of the surface discharge on the GIS Test bushing

In this case, the presence of dust or humidity on external side of GIS test bushing has caused the formation of heavy surface discharge activities causing the deterioration of the insulation material.

Further tests were performed in order to locate the section of the circuit which might have caused the fault during the HV test. In particular, the cable sealing end was grounded and sectionalized; different short 260kV HVAC test were performed on the switchgear by adding subsequent sections of the GIS system, with cable sealing end disconnected from the circuit.

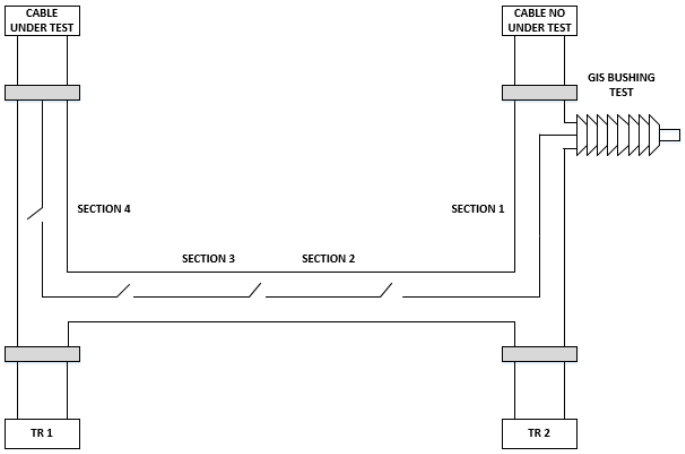

Figure 6-26. Layout of the measurements performed on GIS Switchgear

To perform this survey, PD measurements were performed by placing the Pry-Cam instrument on the ground connection of the GIS switchgear (Pry-Cam Portable - Figure 6-27). The analysis of the measurements has shown the presence of the same high frequency surface discharge acquisitions during the HV test.

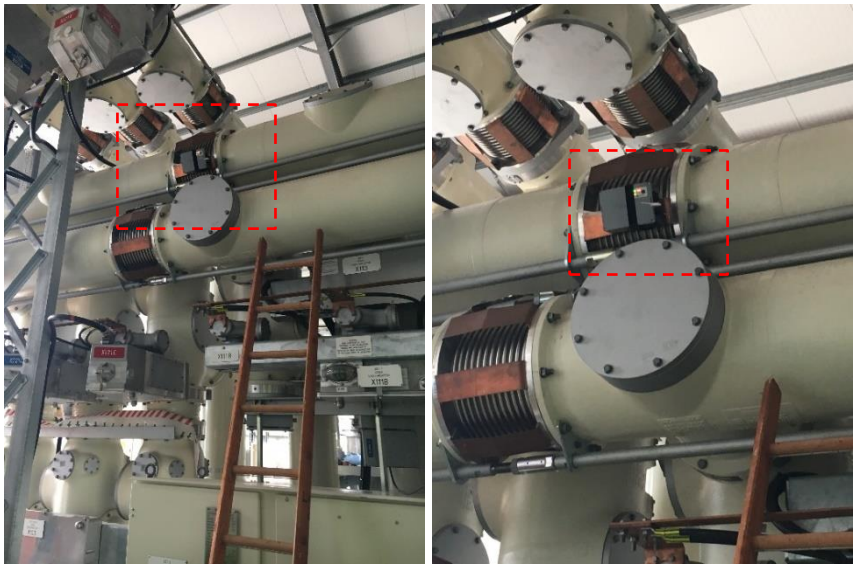

Figure 6-27. Pry-Cam Portable placed on the earth connection of the GIS switchgear.

Table 6-5. Analysis of the acquired PD Patterns on different sections of the GIS switchgear

Section 1	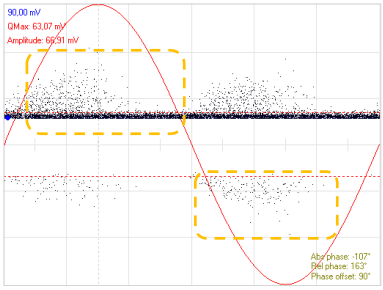	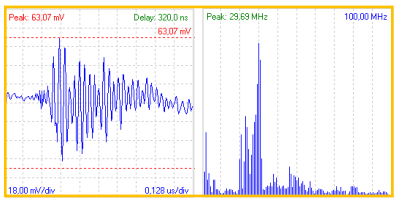	HF surface discharge PD amplitude 63 mV FFT 50 MHz
Section 2	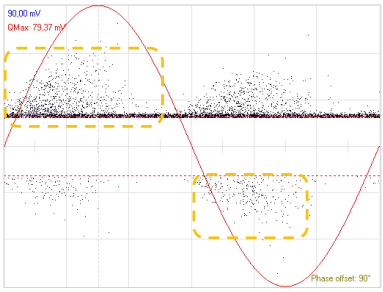	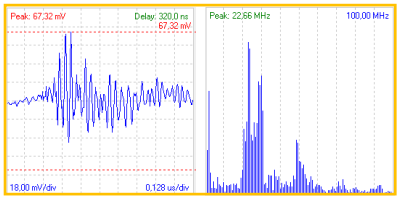	HF surface discharge PD amplitude 67 mV FFT 60 MHz
Section 3	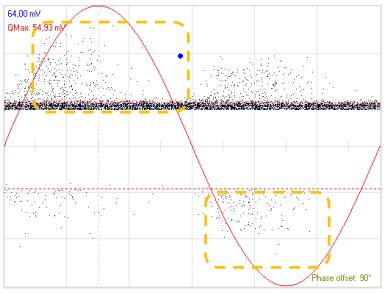	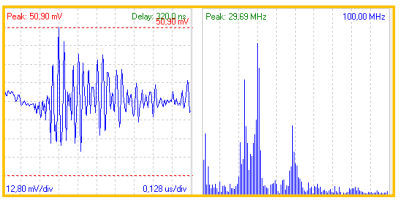	HF surface discharge PD amplitude 50 mV FFT 60 MHz
Section 4	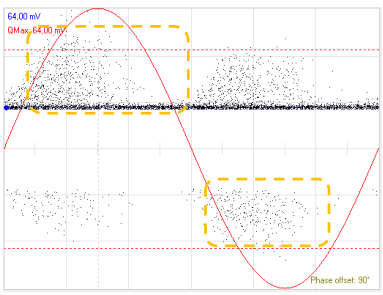	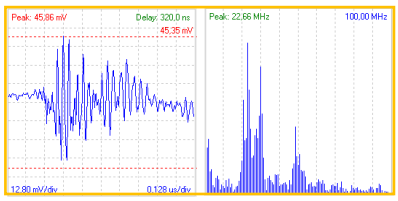	HF surface discharge PD amplitude 45 mV FFT 60 MHz
Entire system	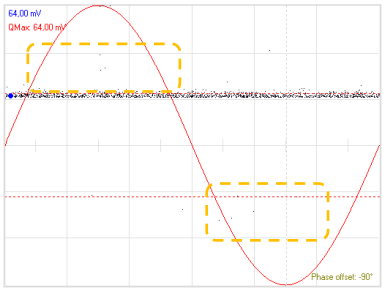	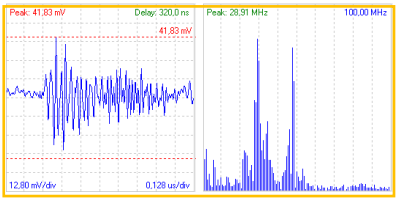	HF surface discharge PD amplitude 41mV FFT 60MHz FAULT

The measurements performed on different sections of the GIS switchgear show the presence of the same high frequency surface discharge. In this case, it can be noted how the pulse waveform has a more oscillating trend and the acquired pulses have a lower amplitude as compared to the measurements performed during the HV test, conversely the analysis of the pulses show a higher frequency content up to 60 MHz. As a result, the analysis of the acquired PD Patterns shows the presence of the high frequency surface discharge within GIS system. Therefore, during the HV test, these PD pulses propagated on the cable and due to the resonance effects of the GIS system have been acquired with higher amplitude on the ground connection of the GIS termination located outside the substation.

However, it is much more important to note that after the reintroduction of the last section of the switchgear (cable sealing end), during the ramping up, the system tripped down approximately at about 130kV due to the presence of the fault in the cable under test. Even in this case, the measurements did not show any different PD activities because the fault was located at a vary far point, about 3 km.

6.4 PD measurements on HV system at 220 kV in Germany

During the Soak test on the line at 220 kV, PD measurements have been performed by means of Prysmian Pry-Cam Grid, a measuring system which allows performing online constant PD monitoring by means of Pry-Cam Wings sensors (Figure 6-28). The test duration was planned in 24h at the operating voltage of 220 kV. In particular, the monitoring was performed on 7 test points, 4 on-shore on the land side and 3 off-shore on the platform side. In particular, the measurements were acquired on the following components:

On-shore side (sub-station and Joint bays):

- Outdoor terminations;
- Joint bay 1;
- Joint bay 2;
- Joint bay 3;

Off-shore side (Off-Shore Station):

- GIS submarine cable terminations;
- Shunt reactor 1;
- Shunt reactor 2.

All accessories have been simultaneously monitored from one computer with dedicated software. The electric system was energized at 220 kV under no-load condition.

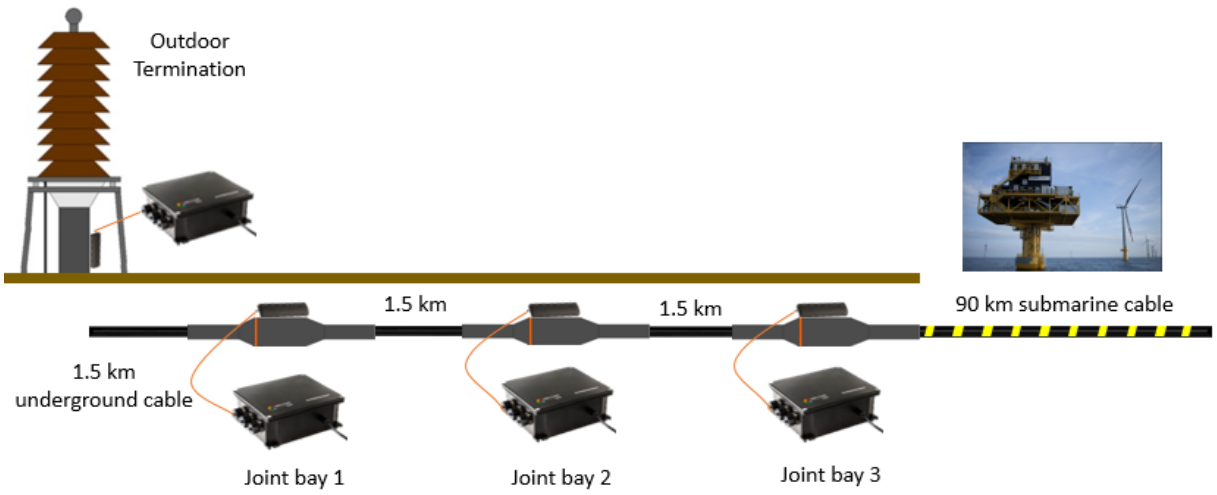

Figure 6-28. Layout of the 220 kV cable line

Sensitivity Check of the Wings sensors (Figure 6-29) has been performed before starting the 24h Uo soak test. A calibrator has been connected in order to inject the pulses on the outdoor terminations at the sub-station and on the GIS submarine cable terminations at the platform, in two different moments, between the conductor and ground (ground connection of the termination temporary disconnected from earth). It has been checked that the closest sensors to the injection point were able to detect those pulses. This test has been performed for all the three phases on both landside and platform side.

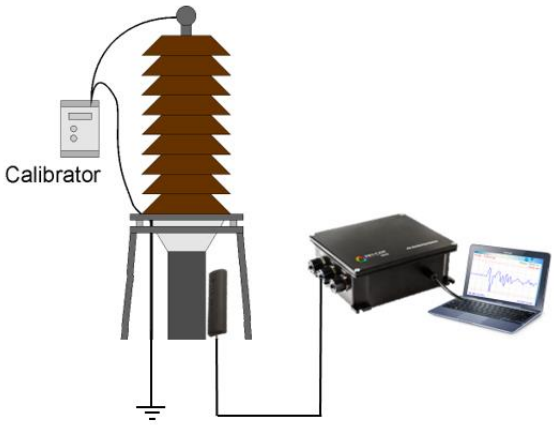

Figure 6-29. Sensitivity check of the Wing Sensor on the outdoor termination

At first the conductors and metallic screens have been grounded on both sides of the circuit. Then, the positive lead of the calibrator was connected via a connection wire to the conductor of the cable and the negative lead of the calibrator has been connected to ground and to the metallic screen. The calibrator has been switched at the amplitude level of 100 pC. Then, the grounding of the connected conductor was removed from the side where the calibrator was installed (Figure 6-30).

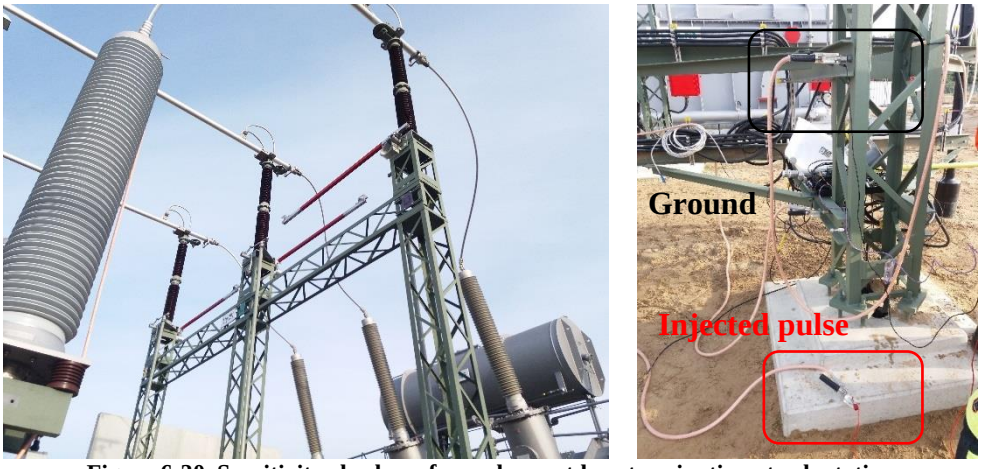

Figure 6-30. Sensitivity check performed on outdoor termination at sub-station

The computer connected to the Pry-Cam Grids performed the acquisition of the injected pulses sensed by the wings sensors. After this, grounding was connected again and the calibrator was removed. The procedure was repeated on the other two phases.

In Table 6-6 are reported the acquired pulses by Pry-Cam Grids during the sensitivity check procedure performed on the outdoor termination at sub-station. In particular, it can be noted that the injected pulse of 100 pc it was approximately equivalent of 100 mV. The same sensitivity check procedure was performed on the GIS on the platform side, however due to the low pulse amplitude injected from the calibrator, 10 pC, it was not possible to acquire the PD patterns as in the previous case.

Table 6-6. Acquired pulses by Pry-Cam Grids during the sensitivity check on the outdoor terminations

Red Phase	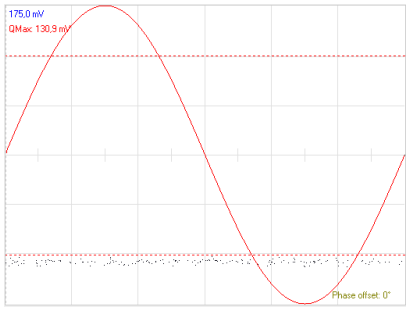	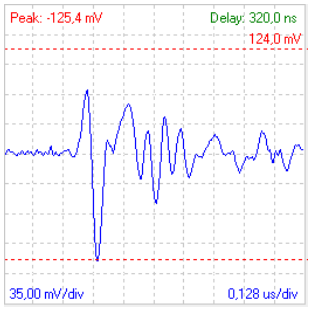
Yellow Phase	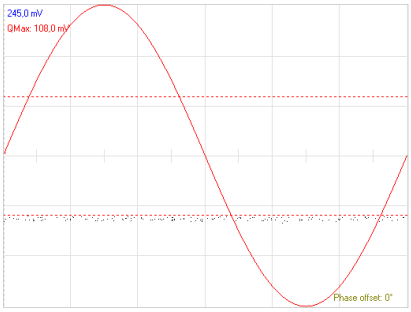	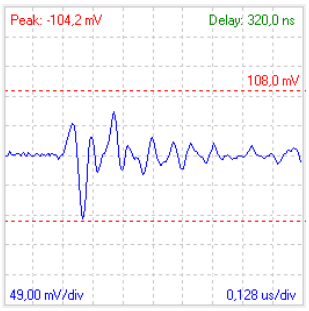
Blue Phase	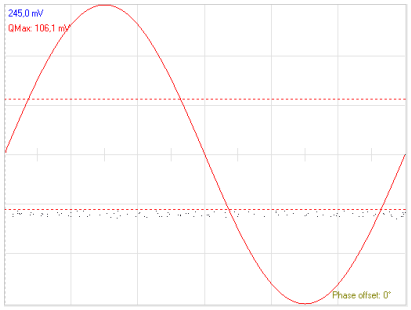	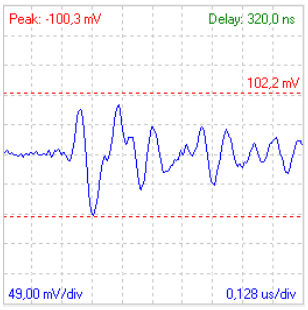

Before the beginning of the test, the measurements of the noise level have been performed in order to verify the presence of the PD pulses due to the external noise or corona effect that may come from overhead lines or other high voltage components. In particular, the analysis of the noise level for each test points showed that:

1. Outdoor terminations: during the measurements of the noise level, corona effect was registered on each phase due to the presence of the overhead line. Furthermore, it was registered an external noise of low amplitude.

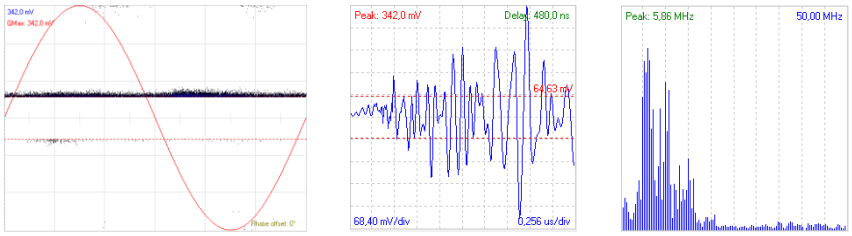

Background noise
64,63 mV

Corona effect

343 mV

2. Joint Bay 1, 2 and 3: the measurements of the noise level on the joint bays show the same corona effect that coming from the outdoor terminations. In particular, the patterns reported below show how the propagated pulses, from the outdoor termination to the joint bay F, less the amplitude and frequency content. The measurements on the joint bay A and C did not show any pulses of the corona effect but only the background noise.

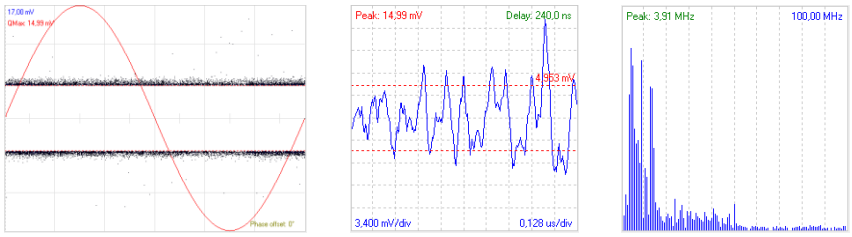

Background noise
4,95 mV

Corona effect

14,99 mV

3. GIS submarine cable terminations, shunt reactor 1 and 2: in this case the measurements show an external disturbance characterized by constant amplitude and frequency content on each phase.

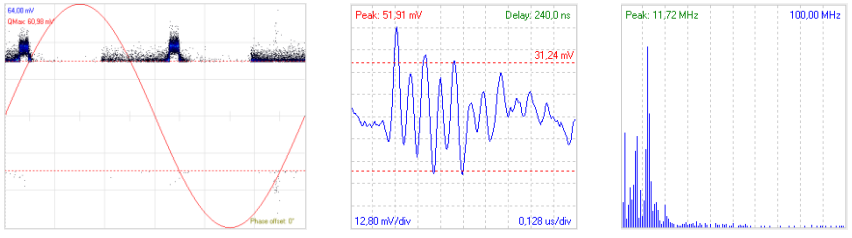

Background noise
31,24 mV

Corona effect

51,91 mV

In this section, the PD propagation phenomena have been reported (Figure 6-31). In particular, the aquired PD pulses on the outdoor termination have been registered by the wings sensors placed on each joint bay with different amplitude and waveform. The measurements showed only the corona effect on the outdoor terminations located in the substation and the same corona effect with lower amplitude on the joint bays, due to the overhead line and HV installation in air (insulator, bus bar, ODSE) close to the outdoor terminations.

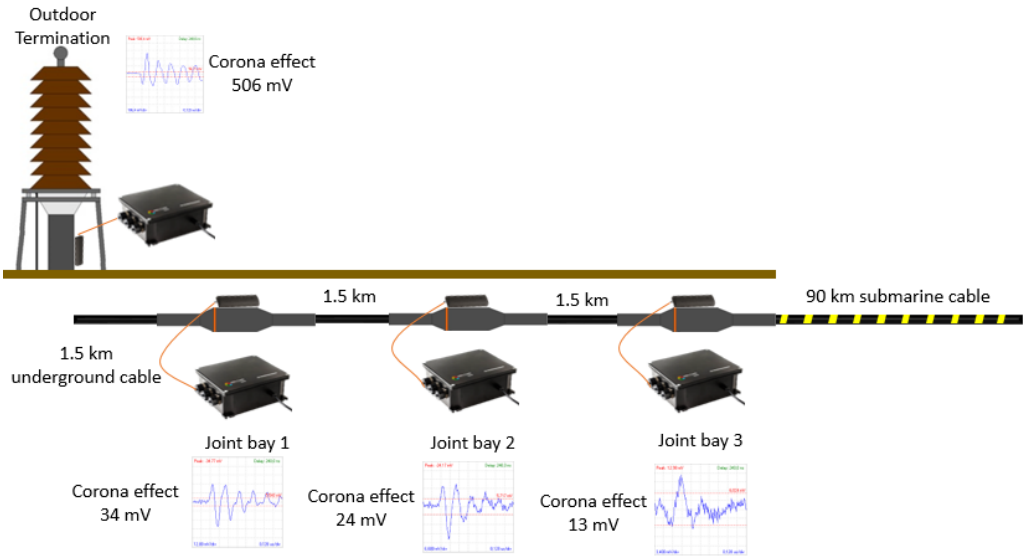

Figure 6-31. Propagation of the Corona effect

Obviously, the higher amplitude of the Pd phenomena has been registered on the outdoor termination due to the presence of several source of Corona effect generated by the presence of the overhead lines and bus bar in HV station. The max PD amplitude registered on the representative PD patter was about 506 mV (Figure 6-32).

Outdoor termination

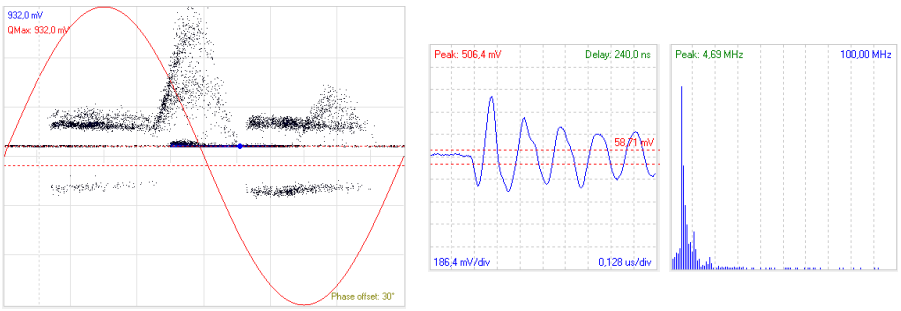

Figure 6-32. Acquired PD Pattern on the outdoor termination

The acquired PD pulse due to the propagation along the cable line show a lower amplitude of the PD phenomenon about 34 mV, but the waveform and frequency content of the pulses were unchanged.

Joint Bay 1

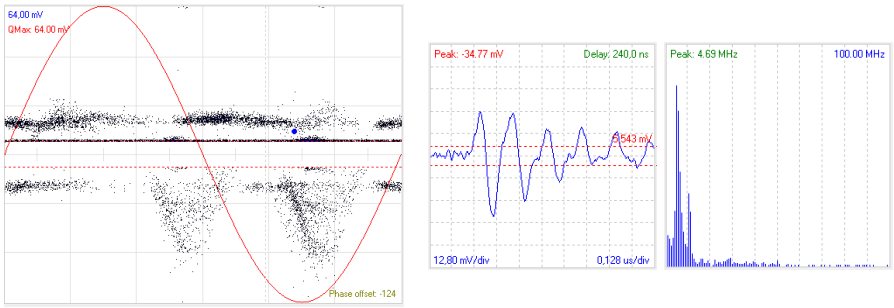

Figure 6-33. Acquired PD Pattern on Joint Bay 1

The measurements acquired on Joint bay 2 show a further reduction of the acquired PD phenomena on the outdoor termination. The PD Pattern shows a lower pulses group compared to previously cases. Moreover, the max Pd amplitude was registered around 24 mV (Figure 6-34).

Joint Bay 2

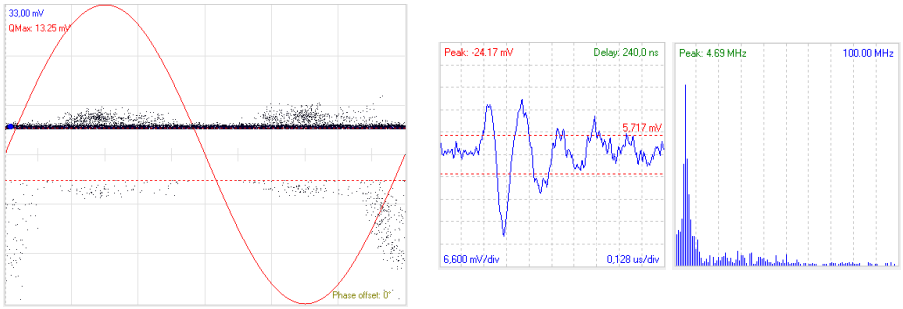

Figure 6-34. Acquired PD Pattern on Joint Bay 2

Finally, the measurements performed on the last joint present on the land side show only a part of the Corona effect that coming from the outdoor termination. In this case, the max PD amplitude was registered around of 13 mV, as reported in Figure 6-35.

Joint Bay 3

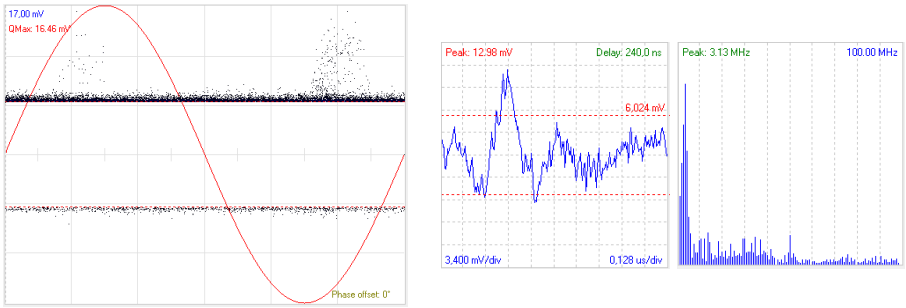

Figure 6-35. Acquired PD Pattern on Joint Bay 3

The measurements performed on platform sub-station, in detail on the GIS submarine cable termination, shunt reactor 1 and 2, show an external disturbance that could be generated by the same shunt reactors or other HV components close to the test point (Table 6-7). The acquired pulses show an external noise on each phase. In particular, it can be observed an external noise characterized by frequency of 6,25 MHz. This kind of noise could be caused by the presence of the communication devices in the Wikinger platform.

Table 6-7. Acquired Pd Pattern on platform sub-station

GIS termination	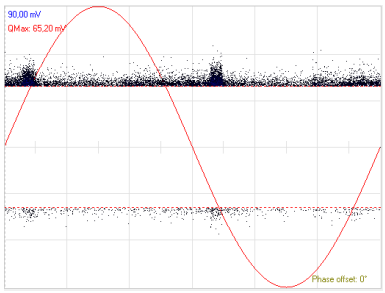	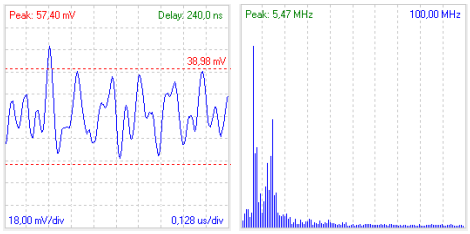
Shunt Reactor 1	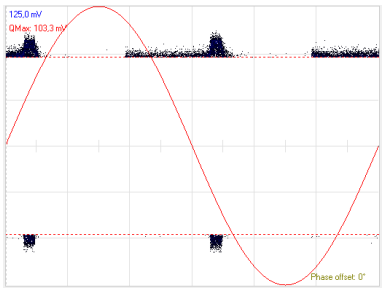	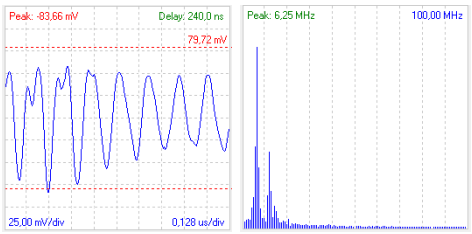
Shunt Reactor 2	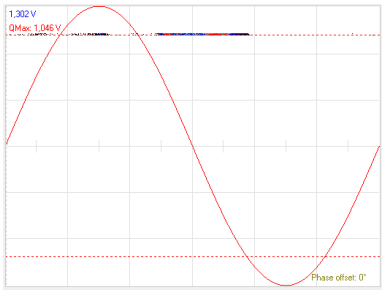	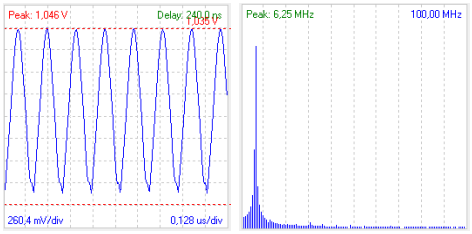

The presence of noise sources such as low frequency communication systems or electronics device close to the measurement point can have a strong impact on partial discharge acquisition systems. These types of disturbances can not be overcome easily because a filter system capable of cutting to a sufficiently high frequency band should be used. However, these kinds of disturbances are intermittent, so it is possible to evaluate the health of the component through a fixed monitoring system. Differently, a spot measure does not allow to understand the evolution of the disturbance or PDs phenomena that may be present on the system under test.

A particular phenomenon was analyzed during the test on the line in question. Specifically, the performance of partial discharges obtained during the entire test run on the red phase of the terminal is reported. The Corona phenomenon acquired on the outdoor termination in the substation, over the 24-hours period, undergoes a significant variation of the PD amplitude. It can be noted that the Corona phenomenon, depending on the environmental condition (i.e. humidity level or presence of wind) and operating conditions of the overhead-lines close to the measuring point, was present in different ways with different types of PD patterns as reported in Table 6-8.

Table 6-8. Analysis of the Corona discharge during the Soak test on Phase Red of the Outdoor Termination

Start Soak Test	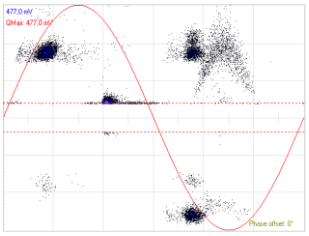	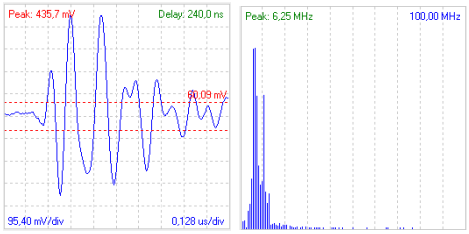	Corona PD Max PD amplitude 435 mV
After 6 hours	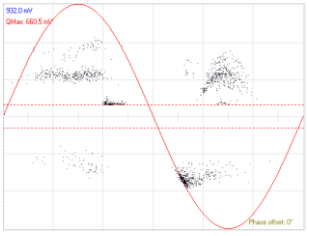	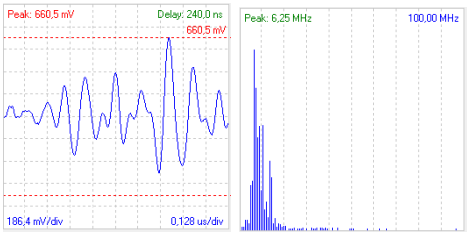	Corona PD Max PD amplitude 660mV
After 12 hours	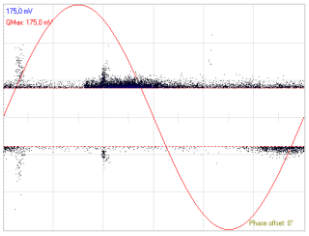	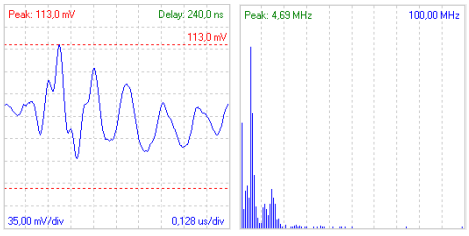	Corona PD Max PD amplitude 113 mV
After 18 hours	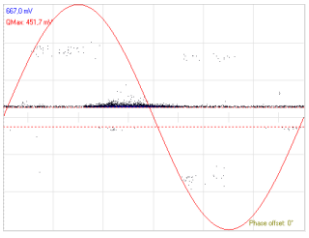	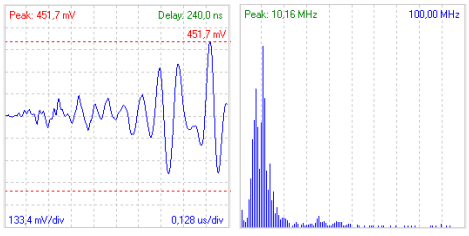	Corona PD Max PD amplitude 451 mV
End Soak Test	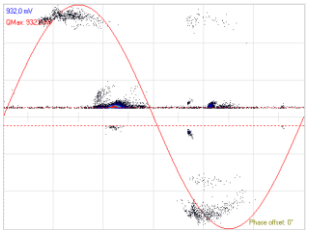	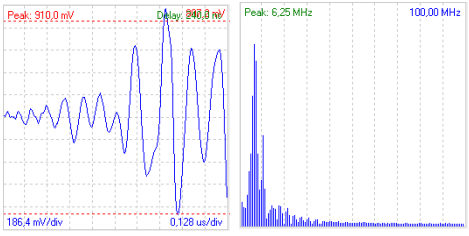	Corona PD Max PD amplitude 910 mV

The measurement analysis has allowed to identify and monitory the behaviour of the PD activity on a cable line consisting of several accessories such as outdoor termination and joints. In particular, the propagation of Corona phenomena along the cables during the HV test was evaluated. When there are strategic cable interconnections, PD monitoring system on a cable line is highly recommended, especially on accessories, which may be the most vulnerable points from the point of view of the PD.

It can to be installed a fixed monitoring system on the interest points of the cable line, also providing a dedicated alarm system that can provide a warning when the PD amplitude exceeds certain thresholds. However, as noted above, some PD phenomenon during the day undergoes an evolution that increases or decreases their amplitude. As a result, the alarm system must always be correlated with the experience of an expert in order to periodically analyze and classify the acquired PD phenomena.

6.5 PD measurements on HV system at 110 kV in Finland

PD measurement activities were performed for the Finland TSO, in Helsinki Finland, during the 24-hour commissioning of the cable line at 110 kV. Measurements have been acquired on two circuits of the line. In particular, the measurements were taken on 2x3 GIS terminations and on 2 Joints Bays with sectionalized joints. The monitoring was carried out continuously by means of the Pry-Cam Grids and Wings sensor installed on each termination and sectionalized joint. Furthermore, measurements have been performed with Pry-Cam Portable on GIS terminations in both substations and on cross bonding leads of sectionalized joints. In this case the 24-hour commissioning test was performed, in no-load condition, energizing the whole system connecting to the power grid at 110 kV.

During the commissioning, the measurements were performed on the following points, as reported in Figure 6-36 and Figure 6-37.

Figure 6-36. Pry-Cam portable placed on cables near the GIS terminations.

Figure 6-37. Pry-Cam portable placed on cross bonding leads inside pillar

In Figure 6-38 a layout of the measurement point is reported.

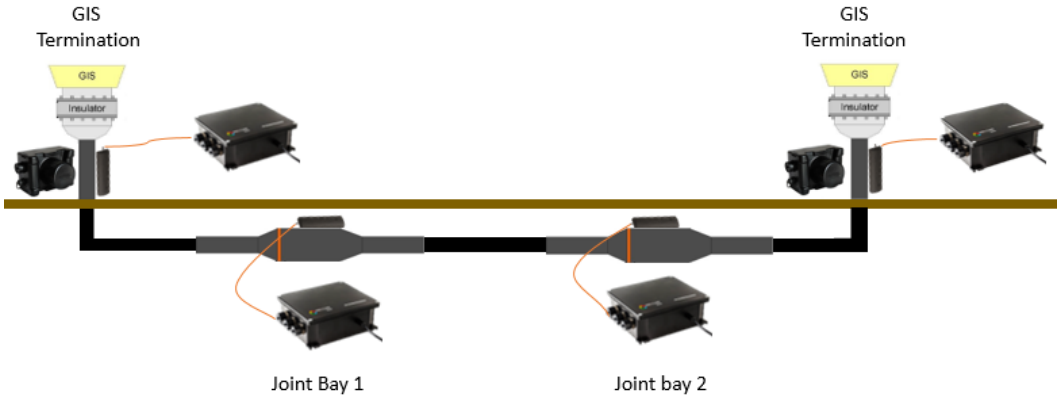

Figure 6-38. Layout of the measurement points

During the PD monitoring several PD phenomena were found on each phase as reported below in Table 6-9. The analysis of the main acquired phenomena is reported below.

Table 6-9. Acquired PD Pattern on HV line at 110 kV

Test Point	Phase R	Phase S	Phase T
GIS Terminations start line	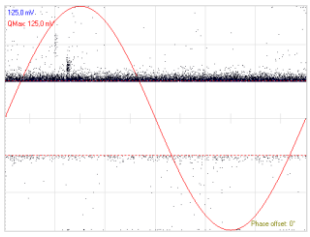	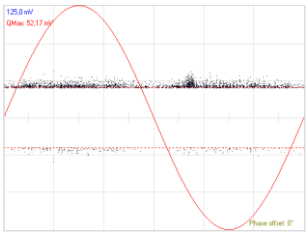	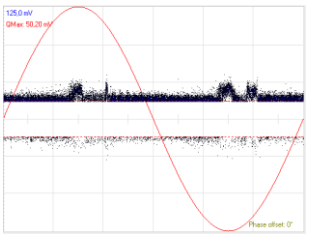
Joint Bay 1	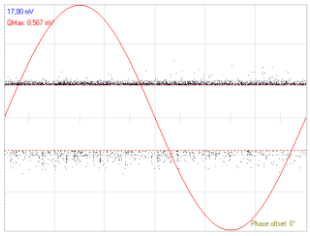	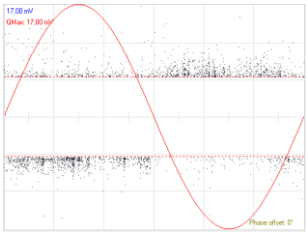	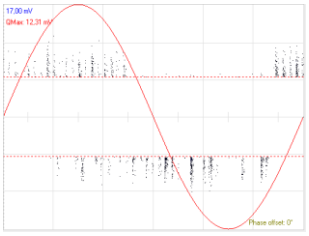
Joint Bay 2	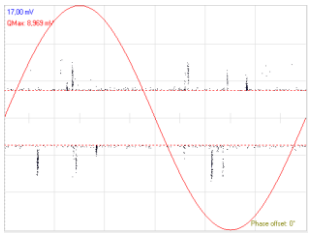	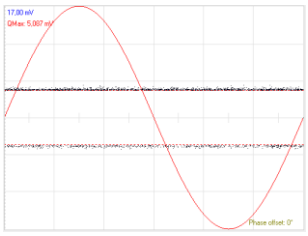	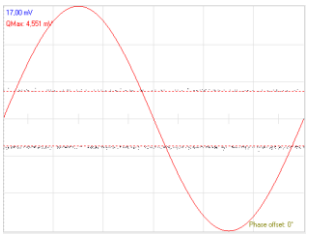
GIS Terminations End line	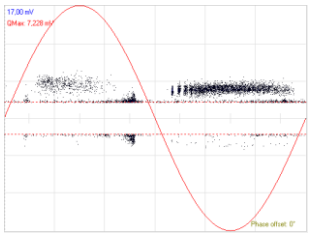	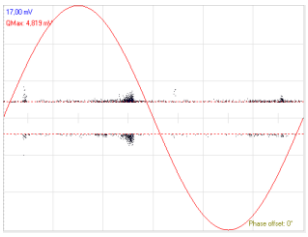	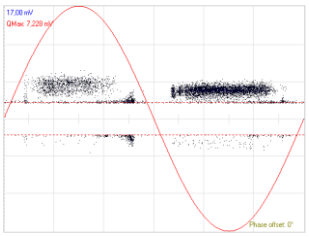

It must be emphasized that the measurements performed on Joint Bay 1 and 2 in correspondence of the cross-bonding leads inside pillar have been made without any synch. Since the measurements have been carried out on the ground connection of the sectionalized joints in no-load condition, it was not possible acquired any synchronization signal. In particular, the sectionalized joint, due to the cross-bonding and ground connection did not allow acquiring an adequate value of the electric field to engage a synch.

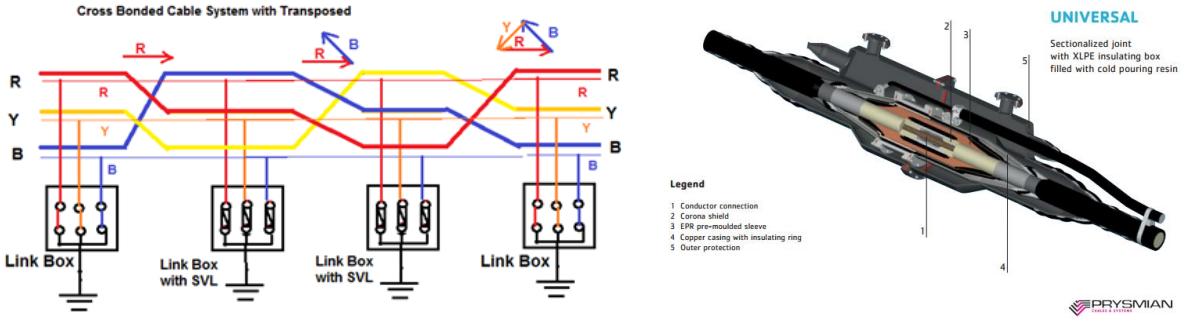

Figure 6-39. Cross-bonding and ground connection of the sectionalized joint

In this case to acquire a PD pattern with a correct synch it was necessary to perform the measurement without any synch and then resynchronize the PD pattern at 50 Hz through to the resynch function at a predetermined frequency that can be 50 or 60 Hz. An example of the resynced PD Patter is reported below.

In Figure 6-40 is reported an un-synced PD pattern, it can be noted in red square the wrong synch acquired during the measurement. Also, the acquired PD pattern does not show any group of pulse such as to form a typical shape of ones' PD phenomenon.

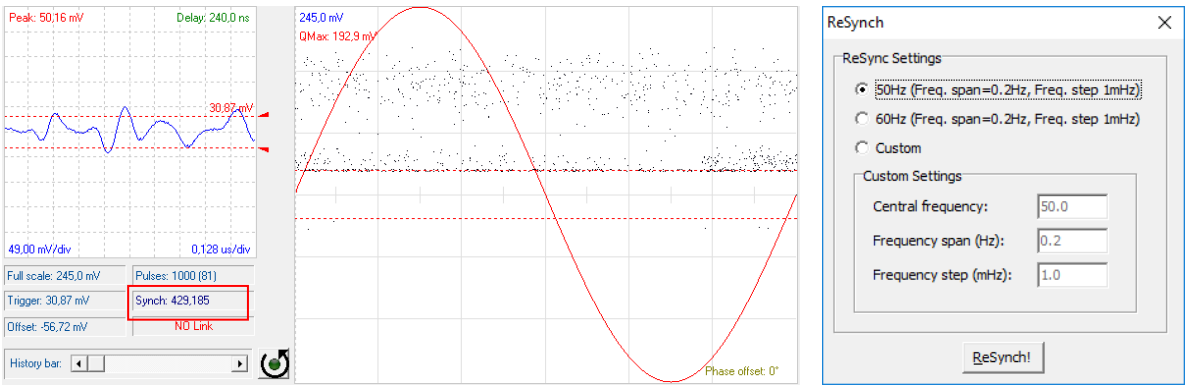

Figure 6-40. Un-synced PD Pattern and Resynch function box

The resynch function allows to resynchronize the PD pattern at 50Hz and to obtain a precise shape of the PD phenomenon. In Figure 6-41 the resynced PD pattern at 50 Hz is reported. In green square it can be noted the frequency of 50 Hz after the resynch.

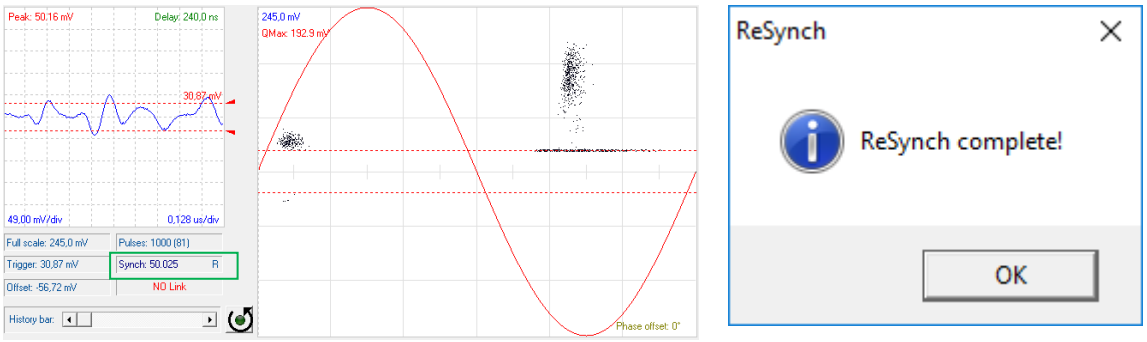

Figure 6-41. Resynced PD Pattern at 50 Hz

The first PD phenomenon was acquired on GIS termination at the end of the line and in Figure 6-42 the analysis of the acquired PD pattern on phase R is reported. The acquired PD pulses in green square was a typical external noise acquired during the measurements, indeed the PDs phenomena highlighted in blue square were characterized by slow waveform and low frequency content around 10 MHz. The pulse positions on the PD Pattern are similar to particular surface or corona discharge phenomenon. In this case, the GIS terminations were located close to outdoor terminations in the sub-station. This kind of PD phenomena were caused by the humidity on the external side of the terminations and were classified like surface in air. For this reason, it was possible to classify these PD activities as no critical.

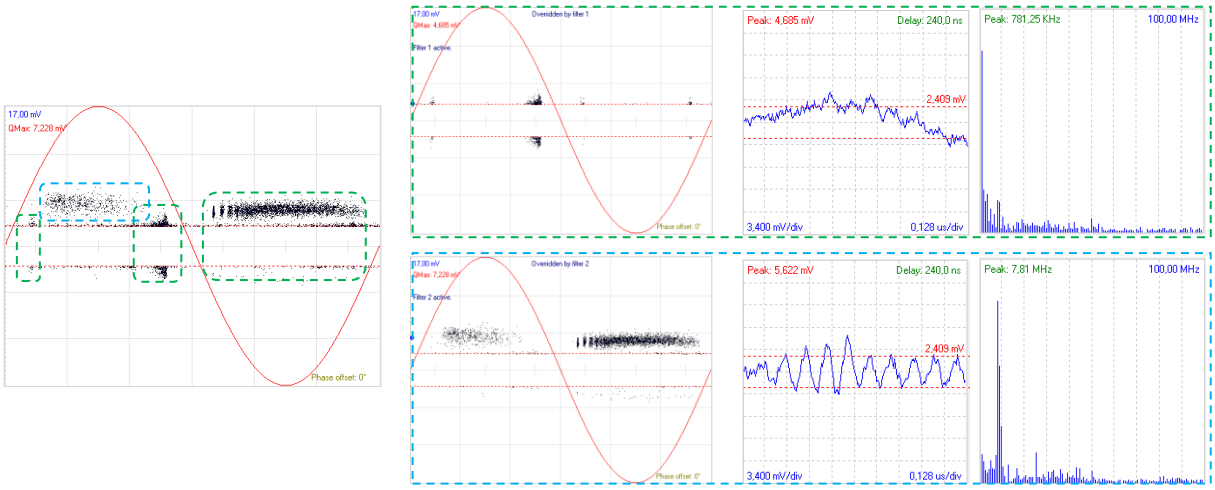

Figure 6-42. First PD phenomena: PD pattern, waveform and frequency content of the pulses

The second PD phenomenon was located and identified on the Joint Bay 1 on phases S and T. As reported in Figure 6-43 and highlighted in green and blue square, two different kinds of external noise were acquired on Joint Bay 1.

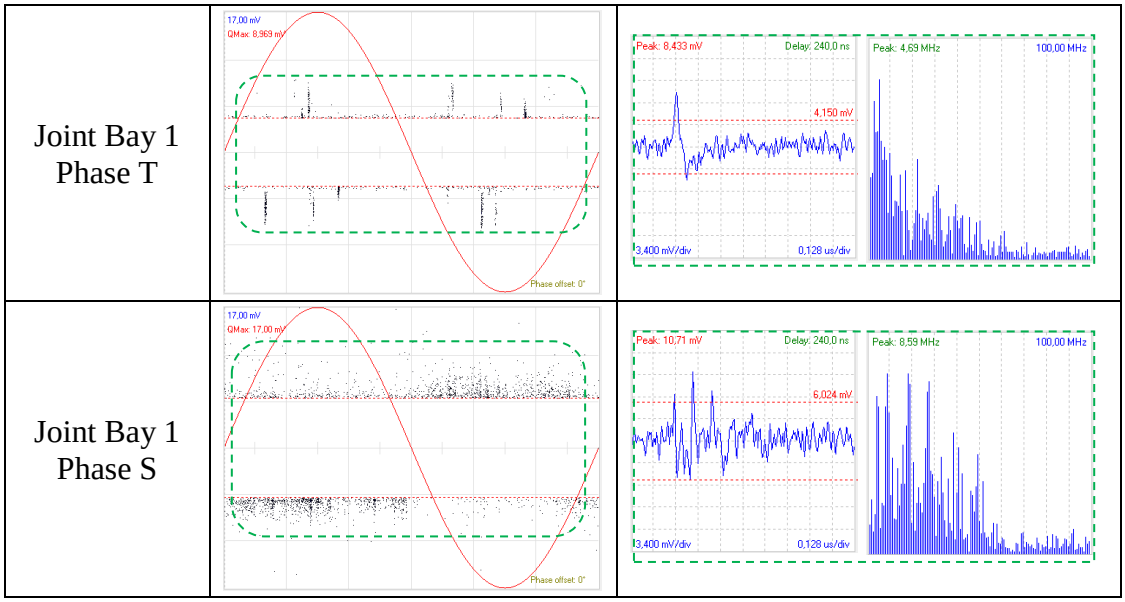

Figure 6-43. Analysis of the acquired PD Pattern on Phase S and Phase T

Both PD patterns are reported after re-synch at 50 Hz in order to analyze the acquired pulses. Clearly, both acquisitions of PD pattern show the presence of typical external noise generated by the presence of electronic devices close to the measurements point. The acquired pulses did not show a typical shape of critical PD activities even if the frequency content of the pulse was fairly high, around 50 MHz.

The above-mentioned analysis has highlighted the possibility to perform PD measurements even when it is not possible to obtain a perfect synch of the supply voltage. It is usually possible to synchronize the instrument directly with its internal sensor through the electric field. Other times, it is possible to use the external synch unit (Figure 6-44) by acquiring the magnetic field produced by the current in the line or the electric field itself. Current clamp or Rogowski sensor can be used for the recovery of the synch signal. However, when the external synch unit is not to be able to synchronize with the electric or magnetic field it is possible to use the frequency of the artificial light (100 Hz) to acquire the correct synch of 50 Hz.

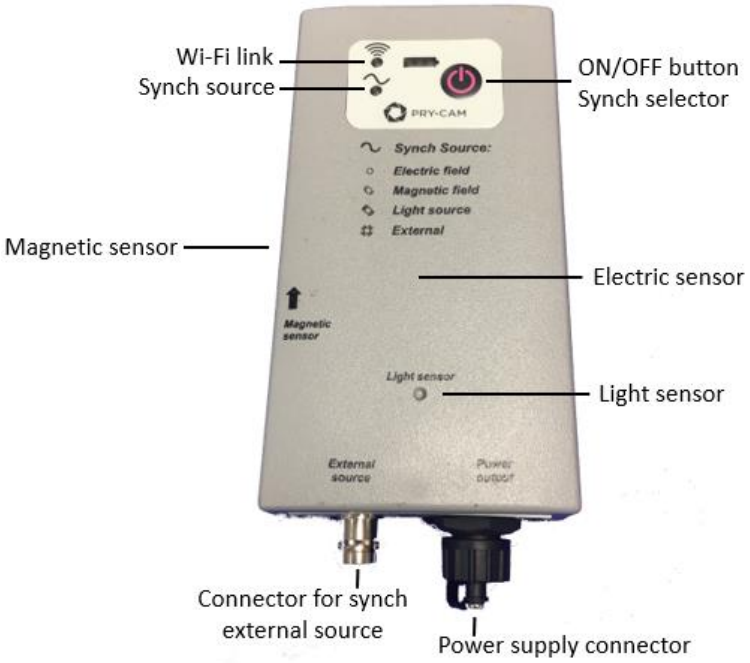

Figure 6-44. External synch Unit

6.6 PD measurements on HV system at 420 and 330 kV in Norway

Measurements have been performed for the Norway TSO in Oslo, Norway on the submarine cable at 420 kV and on cable line at 300 kV. The circuits involved during this PD survey were two for each line. The measurements were performed on the outdoor terminations, as reported in Figure 6-45, in order to check the health status of cable lines and terminations. During all the measurements, the electric systems were working and the lines were in normal activity, submitted to their rated voltage and were loaded by the current as is in continuous operation.
During this PD survey have been testing 9 outdoor terminations for the submarine cable line and 9 outdoor terminations for the land cable.

Figure 6-45. Pry-Cam portable placed on outdoor terminations

Cables were located close to the sea and the weather condition all outdoor terminations had many humidity and dirty on the external side. This condition favored the formation of several surface PD activities with high amplitude on each termination. In this case, the analysis of the measurements was very hard because critical PD activities could be covered by surface phenomena. In order to acquire all PD phenomena several measurements with different setting of gain and trigger have been performed. In this way, it was possible identify and classify all PD activities. Moreover, post processing analysis was required using the related software to remove the noise and to determine the diagnosis of the partial discharges phenomena. Below the main PD phenomena aquired on underground and submarine lines are reported.

The PD measurements performed on 420 kV and 300 kV outdoor terminations shows several surface discharges on each phase. Due to the presence of the humidity on the external side of the component and the high voltage rating system have caused the formation of high PD amplitude. In these cases, in order to evaluate the presence of critical PDs activities that may be present on the system under test, a careful post processing analysis of the acquired PD pulses using the PDiscover software must be carried out by filters. Thanks to the filters, it was possible to separate the PDs phenomena that have the same waveform and frequency content. Below the analysis of the acquired PD pattern on each phase is reported.

PD Measurements on 420 kV outdoor terminations (submarine cable)

The acquired pulses on Phase R show the presence of two different low frequency surface discharges, highlighted in green and blue squares, due to the humidity on the external side of the termination. As reported in Figure 6-46, the analysis of the acquired pulses shows slow waveform with low frequency content, around 20 MHz. No critical PDs activities were found on this outdoor termination.

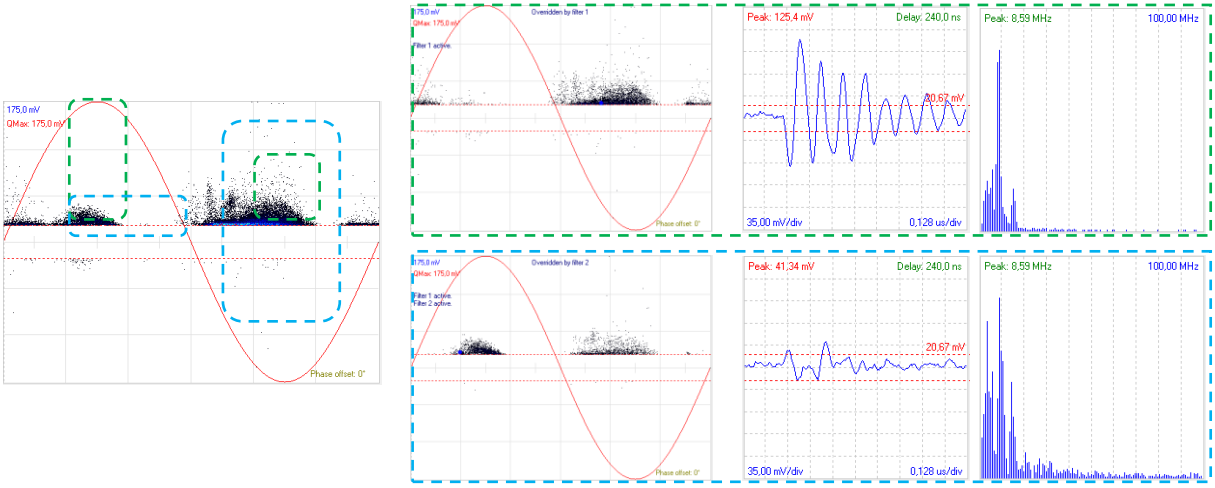

Figure 6-46. Analysis of the acquired PD Pattern on Phase R

Even in this case the acquired PD pattern on Phase S (Figure 6-47) shows the same PD phenomena highlighted in green square and in blue square. It can be noted that the acquire pulses have slow waveform and low frequency content around 10 MHz. No critical PDs activities were found on this outdoor termination.

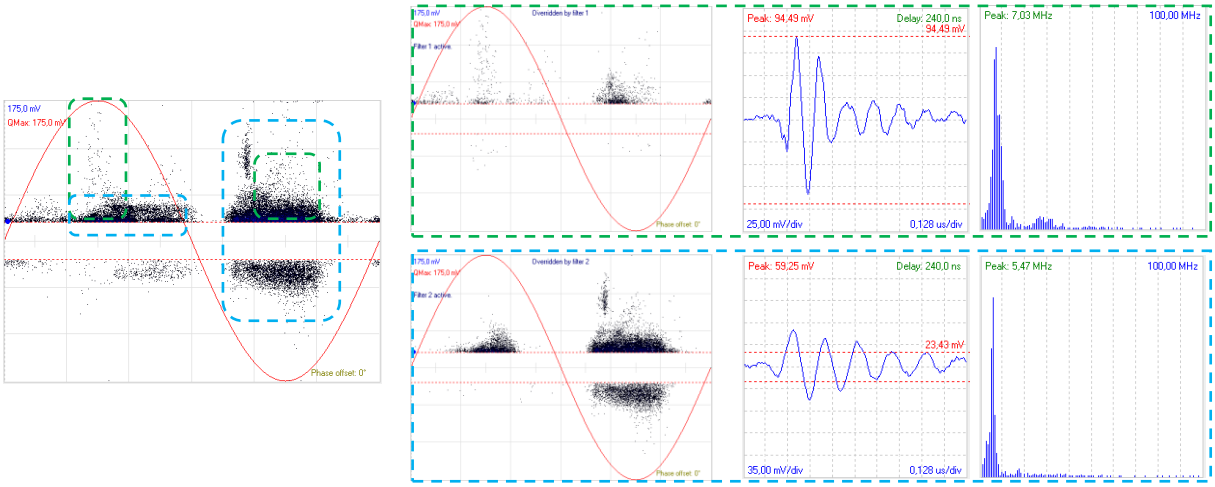

Figure 6-47. Analysis of the Acquired PD Pattern on Phase S

The acquired PD pattern on Phase T reported in Figure 6-48 shows a suspect high frequency surface discharge. In this case, in green and blue square it can be note the same surface PDs activities were detected in the previously cases, the waveform and FFT analysis of the pulses, lower than 20 MHz, do not show critical PDs. Otherwise, in red square was highlighted a suspect critical PD activities. In particular, the pulses have a high frequency content up to 60 MHz, typical of the high frequency surface PDs that could be located inside of the outdoor termination.

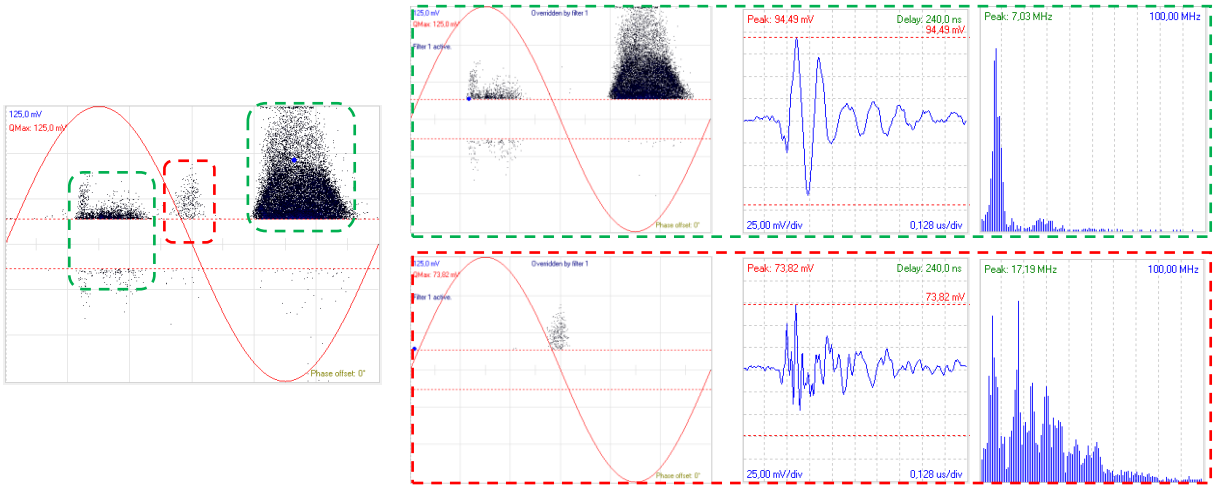

Figure 6-48. Analysis of the acquired PD Pattern on Phase T

PD Measurements on 300 kV outdoor terminations (underground cable)

The acquired PD pattern on phase R (Figure 6-49) shows several surface discharges with high pulse amplitude. The analysis of the acquired pulses shows two different surface phenomena. The first highlighted in green square characterized by slow waveform and low frequency content up to 20 MHz, the latter highlighted in yellow square characterized by average fast pulses and higher frequency content up 40 MHz. In this case, the surface PD highlighted yellow could be considered critical but due to the high concentration of humidity on the termination, the discharge activity may be transient. In these cases, it is highly recommended to install a fixed monitoring system in such a way as to continuously monitor the discharge activity.

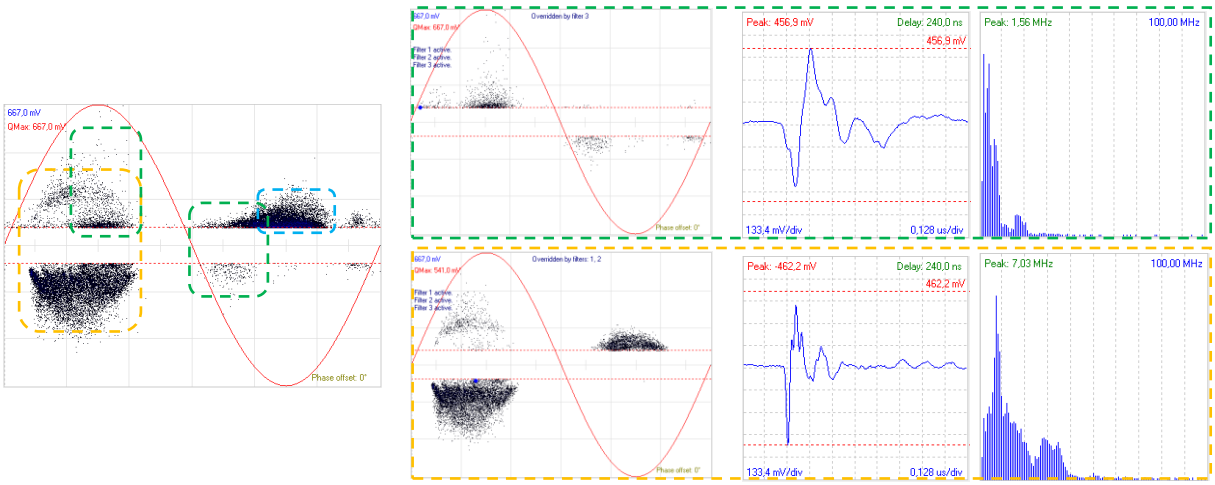

Figure 6-49. Analysis of the acquired PD Pattern on Phase R

Contrary to the previous case, the measurements performed on phase S show the presence several low frequency surface discharges highlighted in green and blue square as reported in Figure 6-50. No critical PDs activities were found on this outdoor termination.

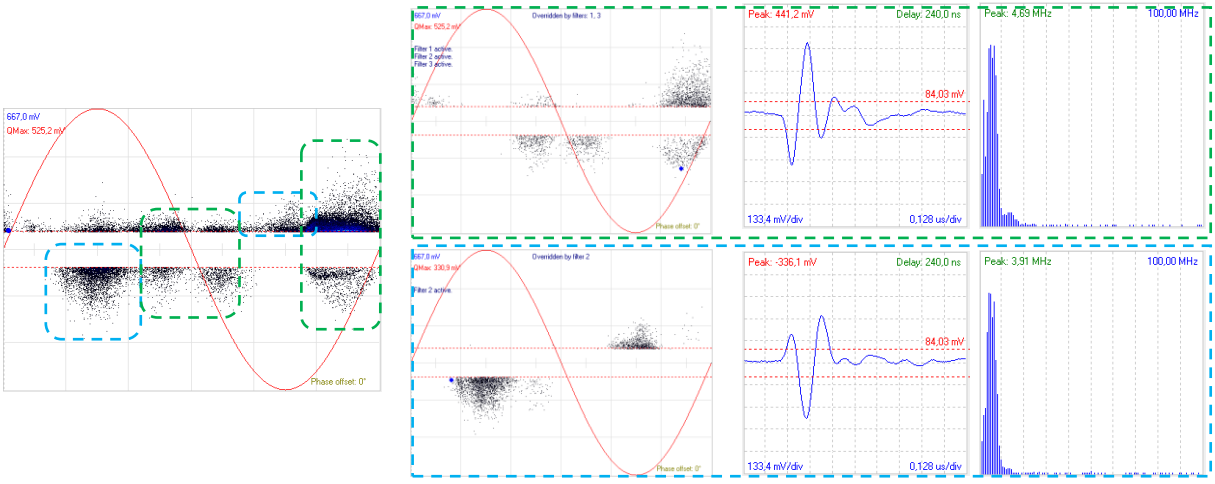

Figure 6-50. Analysis of the acquired PD Pattern on Phase S

The acquired PD pulses on Phase T show clearly a high frequency surface discharge. The analysis of the pulses allowed to identify different PD phenomena as reported in Figure 6-51.

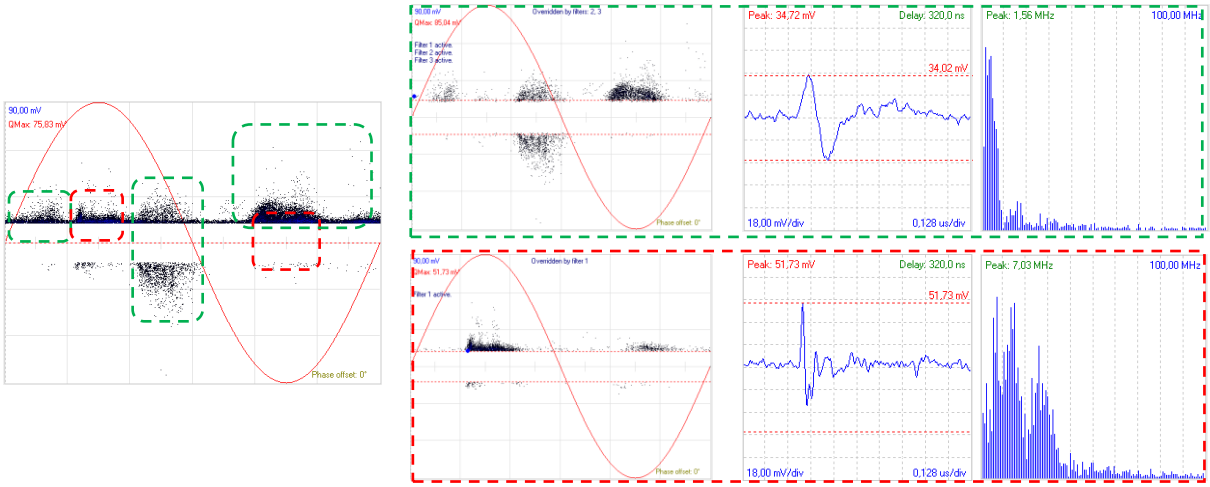

Figure 6-51. Analysis of the acquired PD Pattern on Phase T

In particular, it can be noted a low frequency surface PD activity and a crosstalk effect characterized by slower pulses and lower frequency content in a range of 20 MHz, in green square, due to the coupling from the other phases. The crosstalk effect are discharges that appear in the tested phase as a result of undesired capacitive, inductive, or conductive coupling from another phase or circuit. A crosstalk is a noise typology that affect PD patterns. However, high frequency surface PD activity, in red square, was found. The filtered pattern shows critical surface PDs activities characterized by fast pulses with high frequency content up to 40 MHz. In this case, the surface PDs activities could be located inside to the outdoor termination.

6.7 PD measurements on HV system at 154 kV in Turkey

The measurements have been acquired by Pry-Cam Portable on the outdoor terminations and GIS terminations at 154 kV (Figure 6-52). During all the measurements, the electric systems were working and the lines were in normal activity, submitted to their rated voltage at 154 kV and were loaded by the current as is in continuous operation.

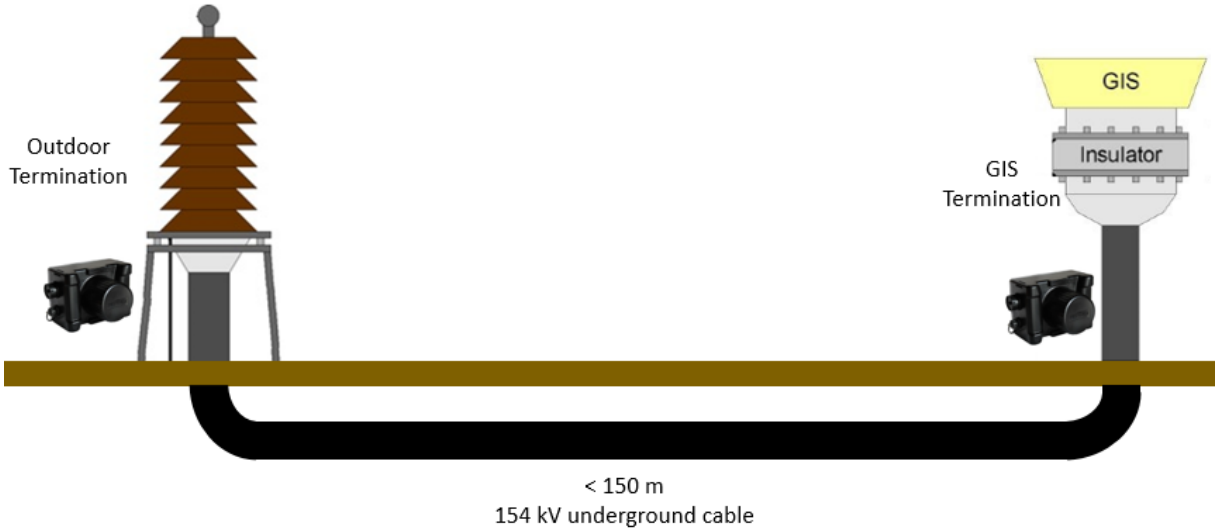

Figure 6-52. Layout of the 154 kV cable line

The Pry-Cam Portable was kept close to the test points as reported in Figure 6-53.

Figure 6-53. Pry-Cam Portable placed on cable close to the GIS and outdoor termination

Before that the measurements have been performed by Pry-Cam Portable on cables close to the GIS termination, several measurements have been performed by Omicron System by the technicians present in the substation. In according to the results of the acquired PD Pattern, critical PD activities were found on GIS termination due to the high amplitude of the acquired PD pulses. The acquired PD pattern by Omicron system on GIS terminations are reported in Figure 6-54. The measurements show the presence of several PD activities characterized by high amplitude, about 11nC, of PD pulses on Phase B and C.

GIS Termination Phase A

GIS Termination Phase B

GIS Termination Phase C

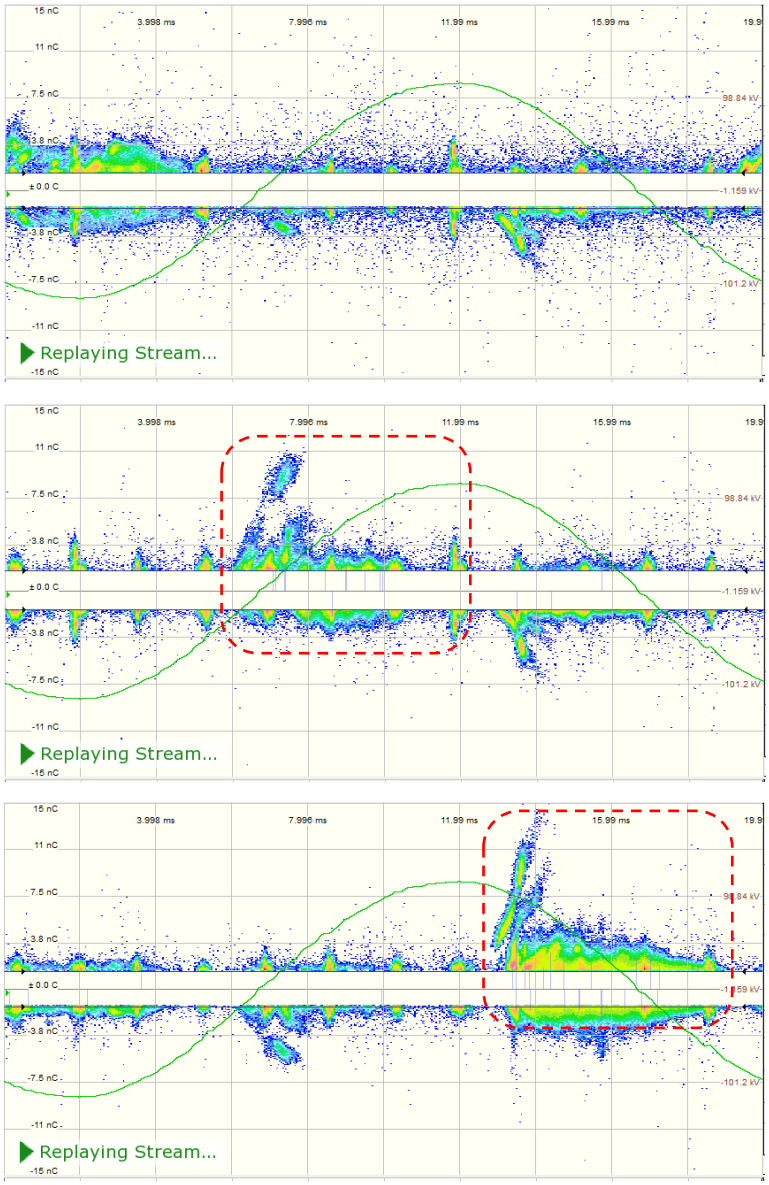

Figure 6-54. Acquired PD Pattern on GIS termination by Omicron System

Clearly, the PD amplitude and the shape of PD pattern are not enough to perform and accurate analysis of the measurements.

In order to correctly understand PD phenomena, it is crucial to analyze also the waveform and frequency content of the acquired PD pulses. Conversely by the measurements performed by Omicron System, the measurements performed by Pry-Cam Portable on GIS terminations show low frequency surface discharges on each phase, from which the 3-Phase PD pattern, highlighted in green square as reported in Figure 6-55. The analysis of the acquired PD pulses show that the PDs phenomena were not located within the GIS system but coming from to the other ends of the line where outdoor terminations were located. Indeed, the analysis show a slow pulse and a frequency content lower than 10 MHz due to the propagation phenomenon.

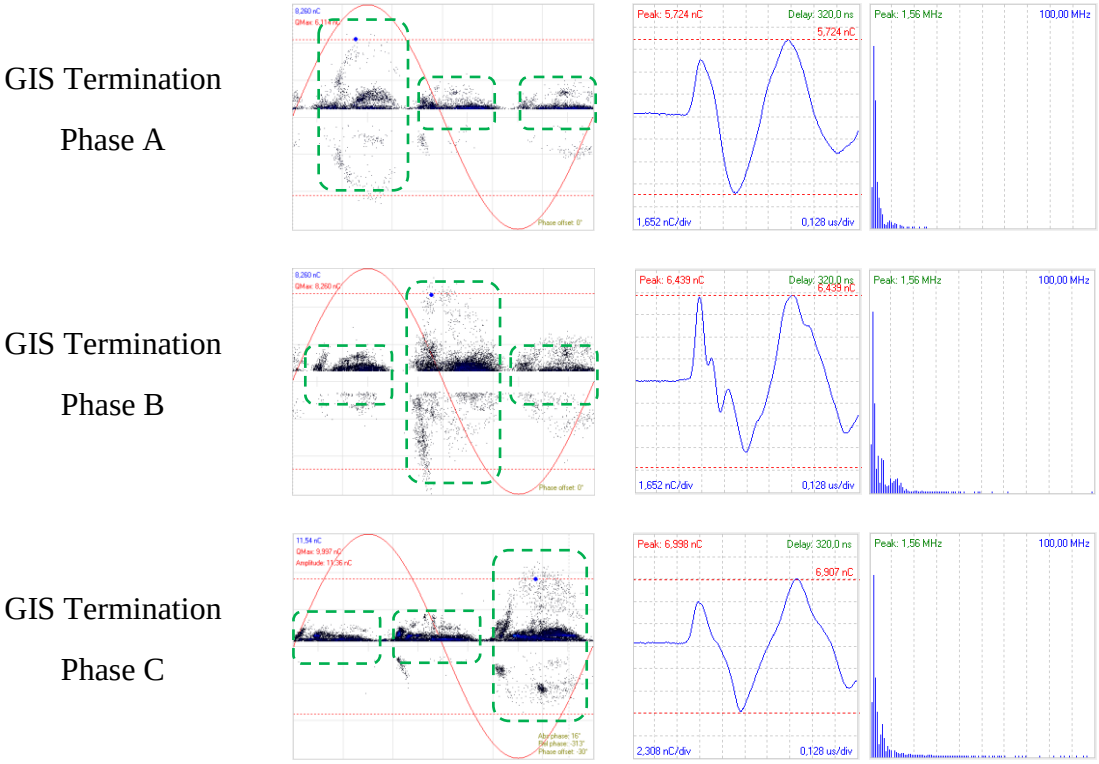

Figure 6-55. Acquired PD Pattern on GIS termination by Pry-Cam Portable

Moreover, it can be noted a particular 3-Phase PD pattern located in different position on each acquired PD Pattern. The reason behind patterns had this particular shape is because the measurements were performed on each phase of the GIS termination by acquiring the external synch on phase A (Figure 6-56), thus synchronizing through the magnetic field produced by the current in the cable. In this case, all measurements had the same synch on phase A and the PD phenomenon was acquired with a phase-shift of 120° on Phase B and of 240° on Phase C.

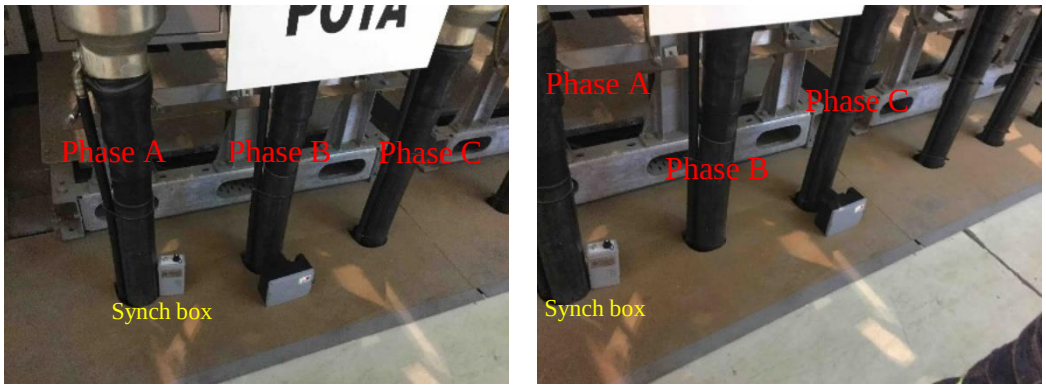

Figure 6-56. Measurements performed on GIS Termination with Synch on Phase A

Further investigation was performed on the other end of the line where outdoor terminations was located. The acquired PD measurements on each outdoor termination show the presence of the low frequency surface discharge characterized by high pulse amplitude and low frequency content. In fact, the site exhibited a high concentration of pollution that encouraged the formation of a superficial black layer on the terminations. The lack of periodic cleaning of the termination favours the accumulation of dust and pollution that can cause the formation of this type of surface discharges.

This kind of discharges are to be regarded as not critical to the health status of the line, also because discharges do not affect parts inside the termination. However, it is always advisable to minimize the presence of surface discharges on the outer surface of the termination in order to ensure greater durability and reliability of the component.

Based on the analysis of the acquired PD pattern, it can be noted that the main PD activities have been detected on the outdoor terminations. In particular, as reported Figure 6-57, the acquired pulses have faster waveform with a frequency content up to 20 MHz, compared to acquired measurements on GIS terminations. However, due to the small line length (lower than 150 meter) the pulse amplitude on both case was comparable but due to the propagation phenomenon along the line pd pulses were acquired on GIS terminations with a lower frequency content (<10 MHz).

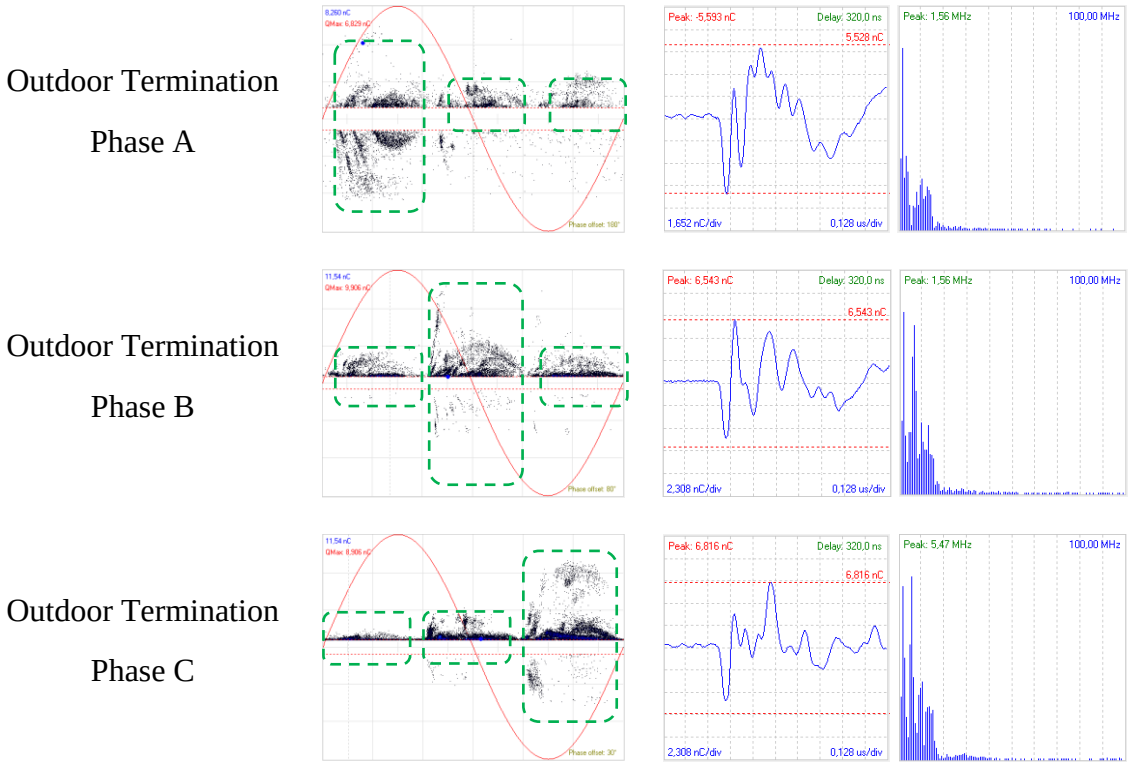

Figure 6-57. Acquired PD Pattern on Outdoor termination by Pry-Cam Portable

The case study aforementioned has been able to correctly identify the main PD source in a HV cable line consisting on GIS terminations and outdoor terminations. Of crucial importance is the possibility of analysing the waveforms of acquired impulses and their frequency content. In this case, the analysis of the PD pattern is not enough to understand whether the PD activity is critical or not, since the PD amplitude was very high could lead to erroneous analysis of the phenomenon. Therefore, in order to carry out an accurate analysis of PDs phenomena, it is necessary to analyze the patter shape to understand what type of phenomenon may be present, to analyze the different PD pulses that have a faster waveform and higher frequency content. In this way it is possible to distinguish the critical PD phenomena.

6.8 PD measurements on MV system at 20 kV in Taormina

Partial discharge measurements were performed on the 20 kV MV distribution network in Taormina. The Prysmian measuring system, Pry-Cam Portable, has been placed on MV cables close to the switchgear, transformer terminals and inspection windows of the switchgear. In particular, the PD measurements has been carried out, where possible, directly on the MV cable that connecting the various secondary substation and transformer terminations as shown in Figure 6-58

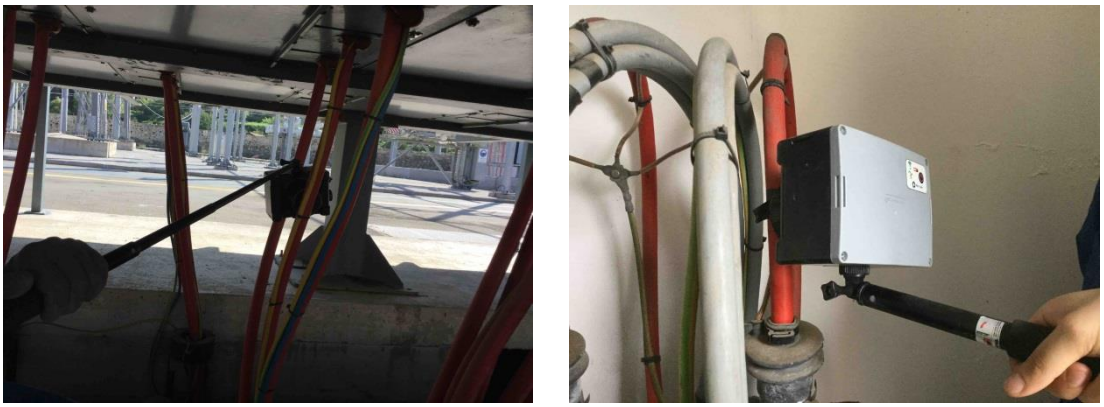

Figure 6-58. Pry-Cam Portable placed on the cables and MV transformer terminations

In some cases, where cable access was not easy, to carry out PD measurements with adequate safety margins, measurements were performed with the support of E-distribution personnel by removing the adjacent metal panels within the MV substation and positioning the Pry-Cam Portable directly on the cables that attest to the individual switchgear, as shown in Figure 6-59.

Figure 6-59. Pry-Cam Portable placed on MV close to the switchgear

In other cases, it has not been possible to have easy, secure and straightforward cable access to perform the conventional measurements due to the impossibility to removing the metal panels

(or their absence) or because the cables would directly stand on the individual compartments through inaccessible routes.

For the above reasons, in such cases, PD measurements were performed by placing the Pry-Cam Portable directly on the inspection window in correspondence of MV terminations as shown in Figure 4.

Figure 6-60. Pry-Cam Portable placed on the magazine inspection window

Since the sensor of the Pry-Cam Portable device does not appear to be in close contact with the MV accessory to be measured (cable, termination, ground connection, etc.), the measurement carried out through the inspection window determines a reduction in the sensitivity of the instrument compared to the conventional measure.

During this survey 735 MV accessories were tested including: Transformer Terminations, Joints, Switchgears and Cables.

Thanks by the high number of the measurements performed on MV accessories it was possible classified the typical PD present in a MV network during the normal operation. In particular, the measurements have shown that monitoring the partial discharge levels on the components would result in a substantial reduction in the failure rates that may occur in medium voltage networks. In many cases, after performing partial discharge measurements, it is possible to prevent faults by periodically servicing the components simply by cleaning the component, thus avoiding the occurrence of surface discharges which could cause component failure in the long term. Otherwise, measurements may show the presence of heavy discharge phenomena such as to determine the rapid replacement of the component. Moreover, following the replacement of a component, it would be desirable to carry out a partial discharge measure to verify the exact installation of the component.

The PD Measurements show, in most cases, the presence of only background noise, and corona discharges due to the presence of overhead line close to the point of measurement or low-frequency surface discharge. In such cases, only cleaning of the components eliminates the presence of low frequency surface discharge.

In other cases, several internal or high-frequency surface discharge activities have been acquired, which involves the replacement of cable terminations, transformer terminations and switchgear box.

6.8.1 Typical external noise acquired in MV secondary substations

During the PDs survey performed in MV secondary substation, several external noises have been founded. The presence of these noise could make it difficult to interpret critical discharge phenomena. In fact, some PD phenomena may exhibit a high amplitude characterized by fast waveforms and frequency content even above of 30MHz. Therefore, it is necessary to recognize and classify these external noises as best as possible in order to avoid making a wrong analysis. Most of the disturbances that may be present in MV distribution networks are sometimes conditioned by the presence of MV transformers inside the secondary substation.

In fact, because of the saturation phenomena that may be present depending on the load levels and therefore the current flowing in the transformer, it determines a particular noise that can be easily identified. This type of disturbance is characterized by a particular PD pattern that extends across the entire phase range with a cyclical PD pulses disposition.

However, this type of external noise may have different PD Patterns characterized by different shapes as well as different types of pulses (slow or fast) with a frequency content between a few MHz to 30MHz. In Table 6-10, different external noise due to the transformer saturation effect are reported.

Table 6-10. Typical external noise due to the transformer saturation effect

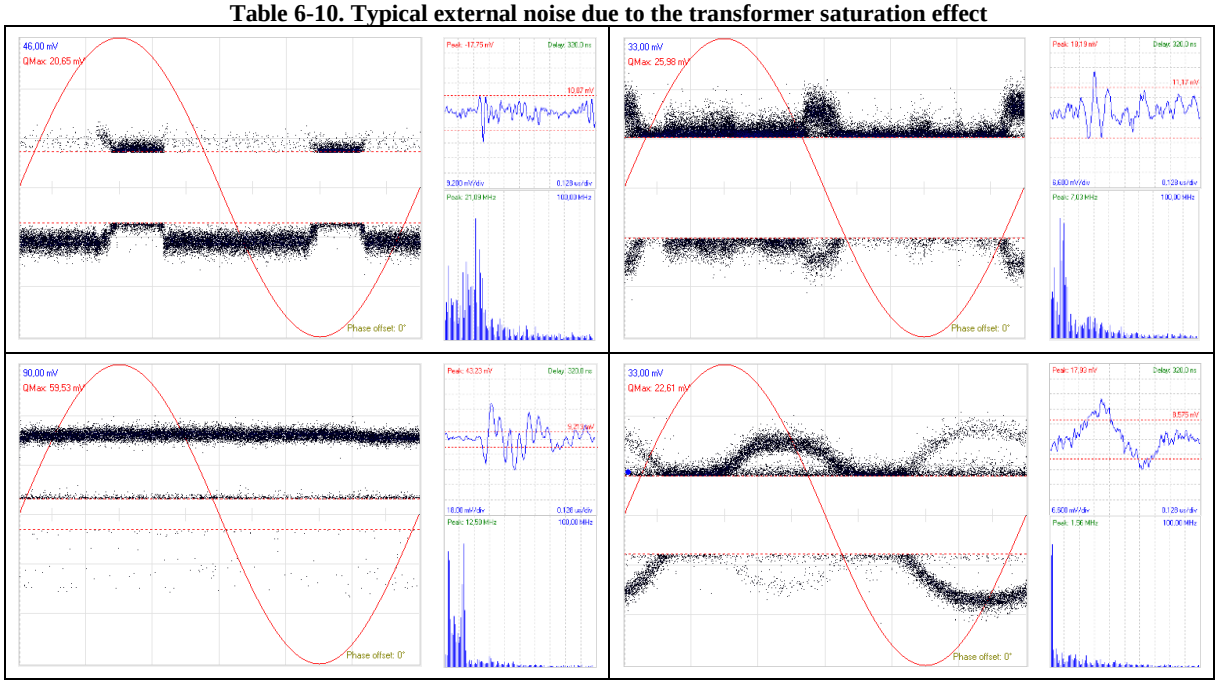

Besides the external noise of the MV transformer, several corona discharges can be acquired due to the present of HV overhead lines and their accessories close to the secondary substation.

In particular, these corona discharge can be acquired even at far points from the HV station, because the amplitude of the corona phenomena it can also be very high and PD pulses can propagate for several kilometers. Other kinds of corona discharges can be acquired due to the presence of air switchgear in old secondary station or due to the presence of an open circuit breaker in a common busbar system. In Table 6-11, typical corona discharges acquiring during the PD measurements are reported.

Table 6-11. Typical Corona discharges in MV distribution network

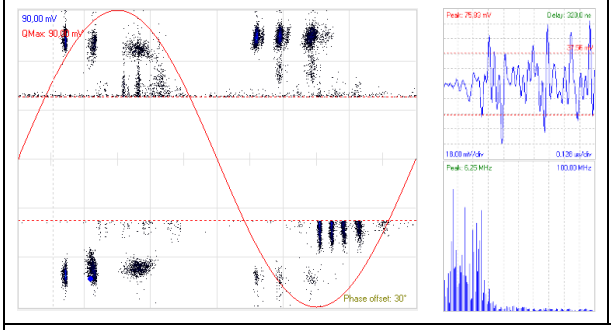	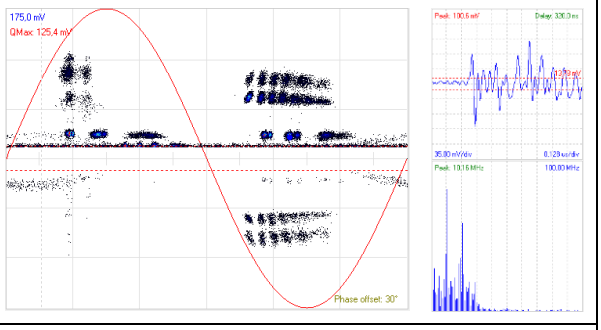
Corona effect due to the overhead lines and HV accessories	
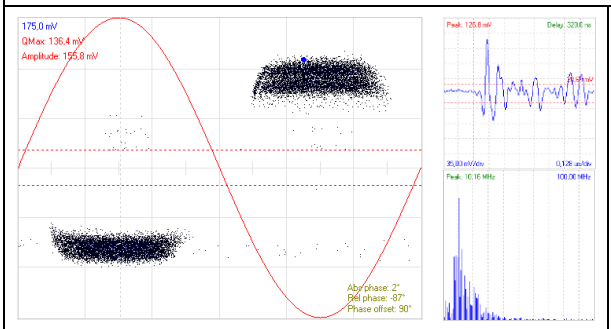	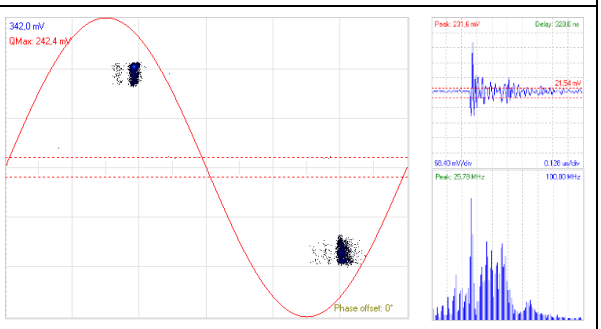
Corona effect due to the air switchgear	Corona effect due to the opened circuit breaker

In the next section, some case study of critical PD in MV components are reported. Each case represents the typical defect that can be found in a MV distribution network and the possible solution which can be taken to reduce the presence of PD activities and then faults.

For simplicity, have been reported 4 principal case studies to understand the main issue on the MV components.

6.8.2 Critical PDs activities acquired on MV components

Case study 1 – Critical PD activities on cable terminations

The measurements have been acquired on both ends on 600 meters of MV line. In particular, the measurements were performed on inspection window at Secondary Substation A, because cables could not be accessed, and on MV cables at Secondary Substation B. The acquired PD Pattern as reported Figure 6-61 show the presence of the same PD activities highlighted in red square on both side.

MV Secondary substation A
Measurement on ispection window

Line AB
About 600 mt

MV Secondary substation B
Measurement on cables

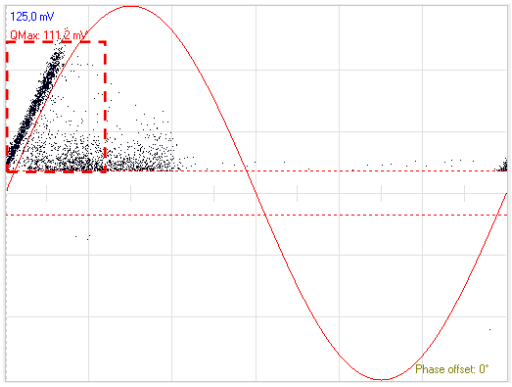

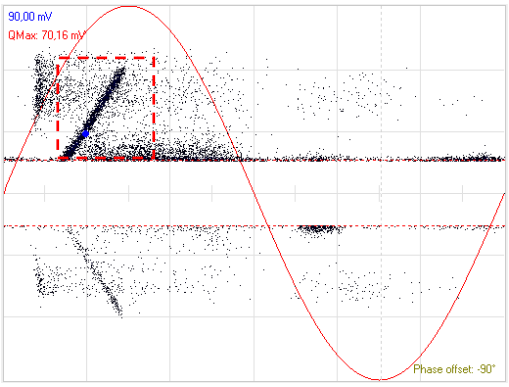

Figure 6-61. Measurement Points and acquired PD Pattern

By analysis of the acquired PD pulses, it can be noted that the main PD activity was identified on Secondary Station A. Indeed, even if the measurement was performed through the inspection window with a lower sensitivity, the acquired PD phenomenon on Substation A (Figure 6-62) present a faster waveform and higher frequency content up to 60 MHz. compared to the same acquired PD phenomenon on substation B, characterized by slow pulse and low frequency content lower than 10 MHz (Figure 6-63) due to the pulse propagation along the cable line.

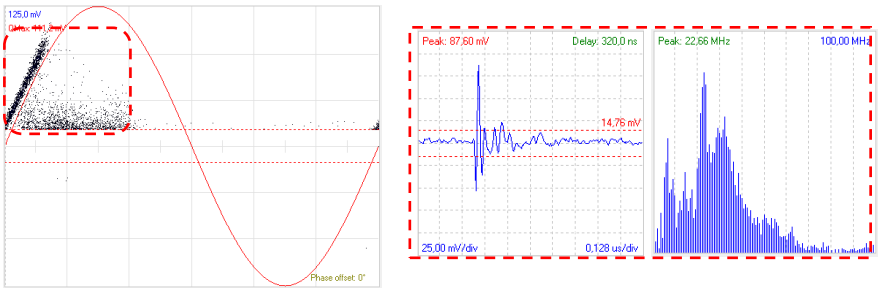

Figure 6-62. Substation A - Acquired PD Pattern through inspection window

Moreover, as reported on the filtered PD Pattern in Figure 6-63, several PD activities were found. In particular, in blue square was highlighter a heavy PD activity could be due to the badly condition of the whole switchgear box, indeed this phenomenon was found on each cable with the same amplitude. Conversely, in yellow square surface discharge was found on cable termination due to the poor maintenance.

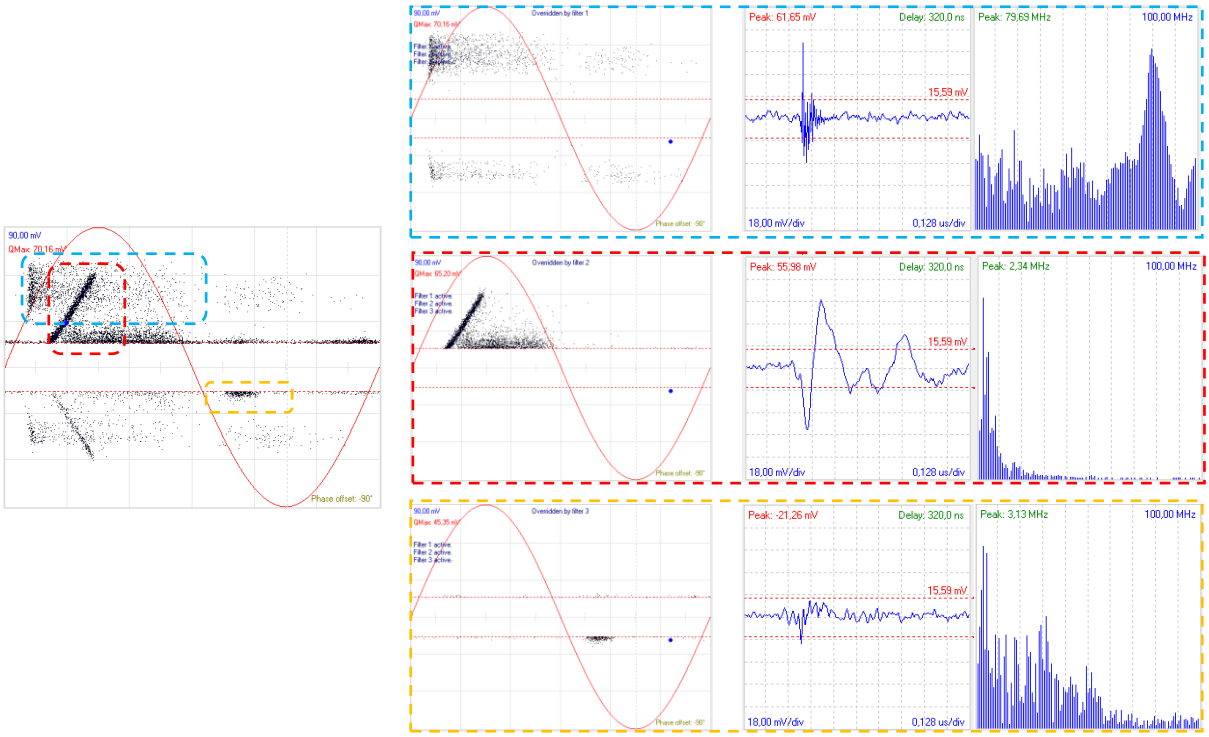

Figure 6-63. Substation B - Measurement acquired on cable

The results of this case study show how the PD measurements can be useful even when there is no direct access to the cables and components under test. Using the portable PD instrument to its antenna sensor, it can measure through the inspection window of the switchgear box to verify that there are some PD activities on cable terminations.

Of course, it is always advisable to make a measurement directly on the cables, but when it is not possible, it is possible to obtain useful information about the health status of the components with an unconventional measure. In this case, if a discharge activity is detected, as in the case just described, a further investigation could be expected to find the component with partial discharges and replace it before the failure.

Moreover, the measurements are able to capture any disturbances caused by switches caused by aging.

Case Study 2 - Critical PD activities on transformer terminations

The measurements were performed on transformer terminations as reported in Figure 6-64. The Pry-Cam Portable was placed on directly on each cable close to the transformer termination.

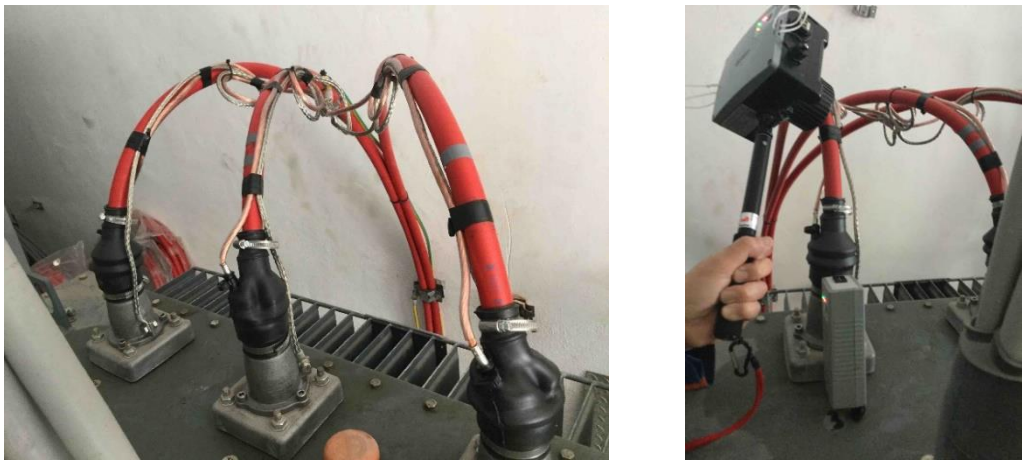

Figure 6-64. Measurements performed on Transformer Termination

The acquired PD Pattern show the presence of several critical high frequency surface discharge on each phase. By analysis of the acquired PD pulses (Figure 6-65), it can be noted that the pulse waveform was fasted with high amplitude (about 500 mV on phase U and W) and a frequency content up to 80 MHz. In this case, the wrong position and the excessive bending of the cable favored the rise of PDs activities.

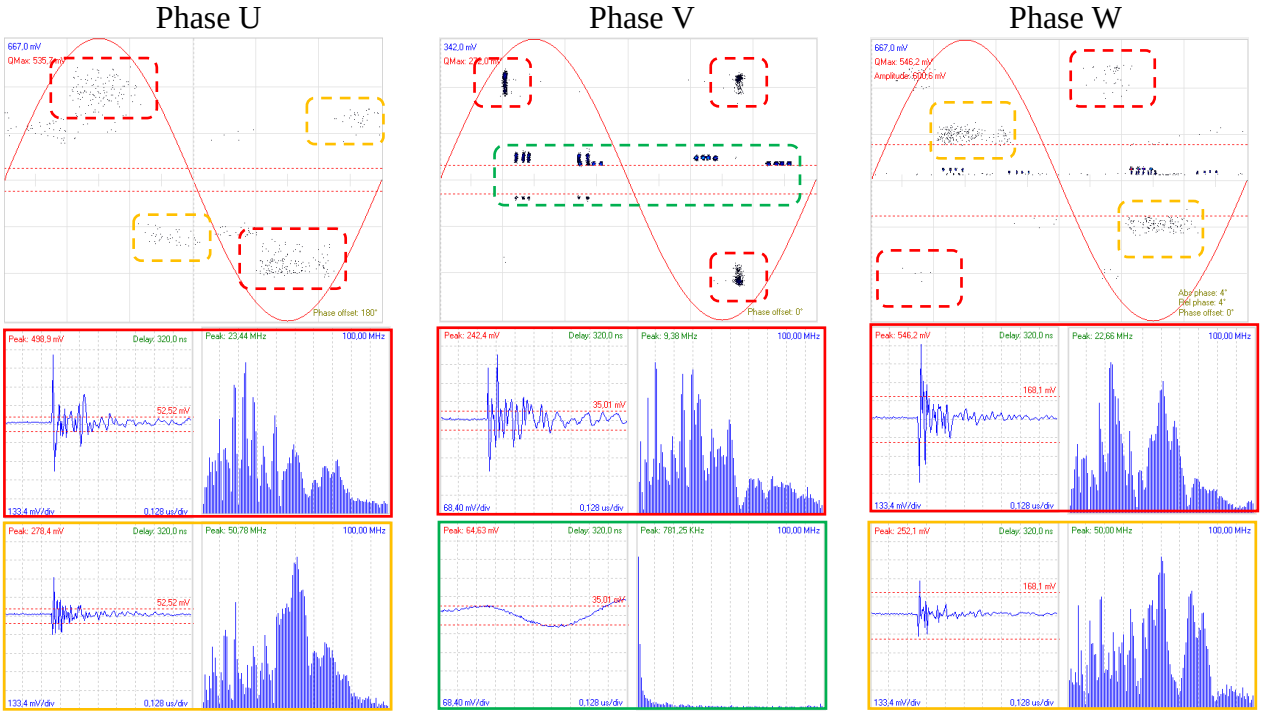

Figure 6-65. Analysis of the acquired PD pattern on transformer terminations

Since critical PDs activities were found on transformer terminations, it has been suggested the replacing on the components. Once the components have been replaced, the PD measurements have been repeated on the same transformer terminations. The acquired pulses on the replaced transformer terminations did not show any critical PDs activities, as reported on Figure 6-66.

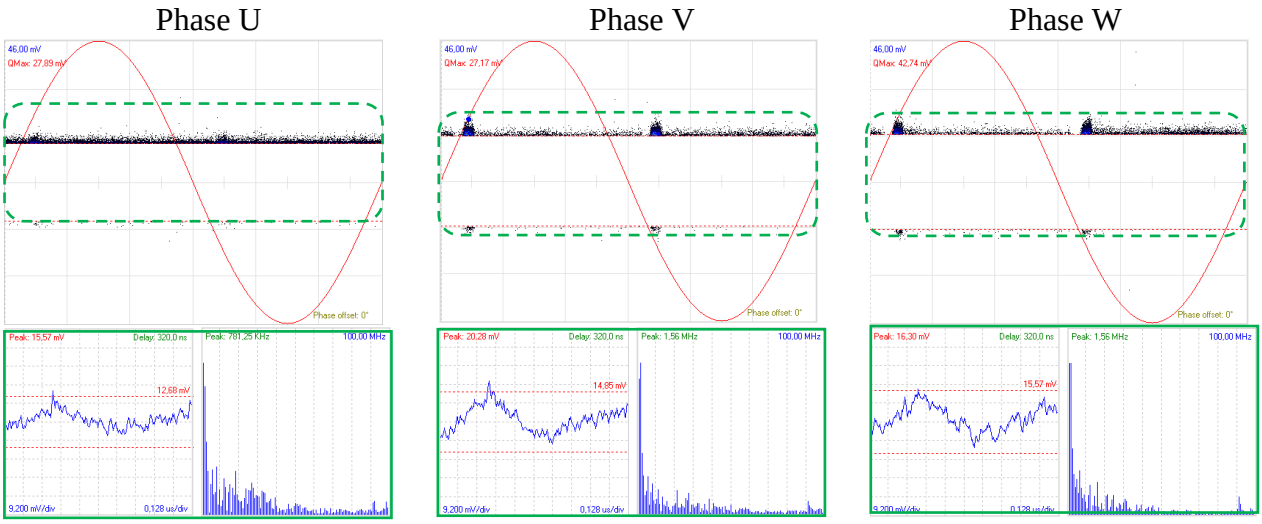

Figure 6-66. Analysis of the acquired PD pattern after replacing of the transformer terminations

The possibility to perform PD measurements after replacing components would reduce the failure due to incorrect installation and also to verify if the component was installed correctly. Since most faults are located at points where the technical staff installs a component, it would be desirable to carry out a verification of the installation not only of the visual type and through the dielectric strength test voltage but also through a PD measurement during the voltage test. In this way, it would be possible to locate the defective component easily and quickly and replace it. In these cases, the PD measurement results in a preventative and corrective action during the phases of installation and replacement of the components.

Case Study 3 - Critical PD activities on cable terminations

Another interesting case study regarding the measurements performed on cables close to the switchgear box as reported in Figure 6-67.

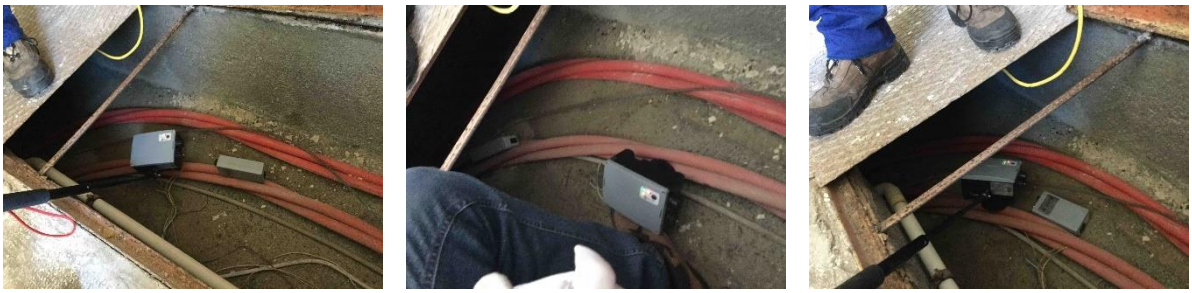

Figure 6-67. Measurement performed on cables close to the switchgear box

The acquired PD pulses show the presence of high frequency surface discharge activities on each phase. However, by comparing of the PD pattern, the amplitude and frequency content of the PD pulses, the main activity was found on cable 2, highlighted in red. In particular, as reported in Figure 6-68, the amplitude of the PD pulse on Cable 2 was registered around 50 mV compared to the amplitude of 24 mv on Cable 1 and Cable 3.

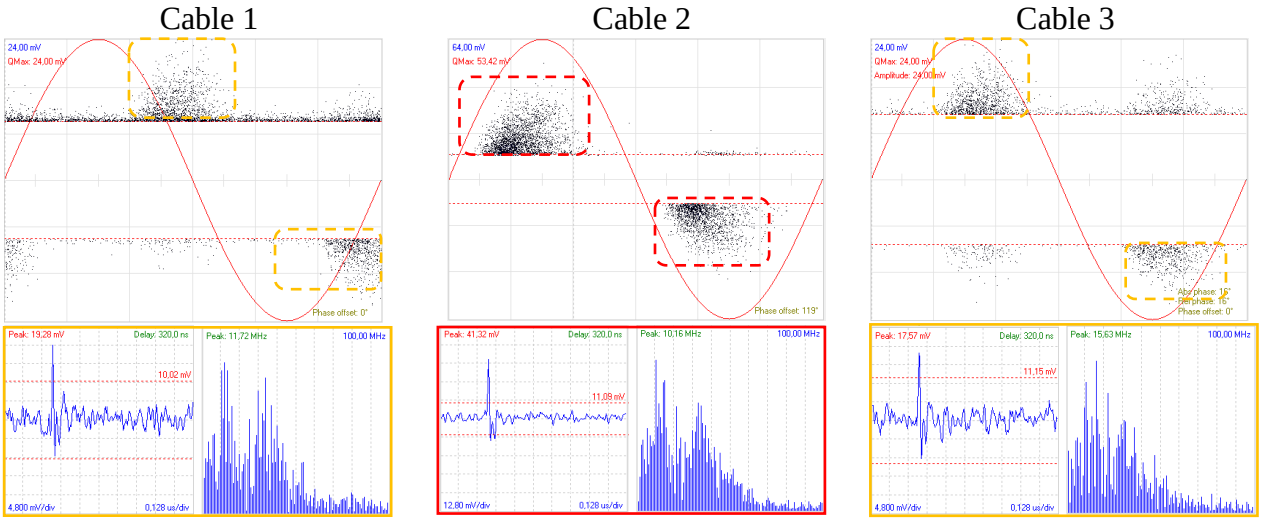

Figure 6-68. Analysis of the acquired PD pattern on cables

In this case, the acquired PD pulses on Cable 1 and Cable 2 were due to the crosstalk effect highlighted in yellow, i.e. discharges that appear in the tested phase as a result of undesired capacitive, inductive, or conductive coupling from another phase or circuit. Also, the pulse waveform acquired on Cable 2 did not show any reflection phenomenon and the frequency content was more significantly up to 60 MHz. Based on the analysis performed, it has been suggested to replace the cable termination corresponding to cable 2 and to repeat the measurements in order to verify if the PD activity still present. Nevertheless, the DSO has

replaced the entire switchgear box and not replacing the cable terminations. Therefore, once the measurements have been repeated, greater high frequency surface activities were found on the same cable termination as reported in Figure 6-69. The acquired PD Pattern on cable 2 show an increasing of the pulse amplitude of 600 mV, about ten times greater compared to the previously measurement.

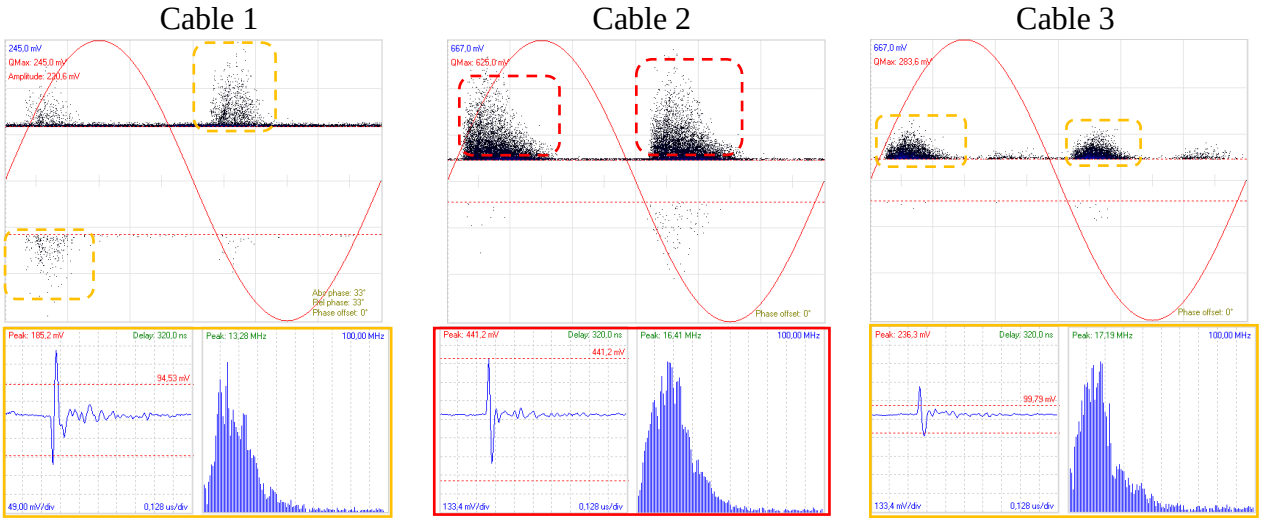

Figure 6-69. Analysis of the acquired PD pattern after replacing of the switchgears box

A comparison of the aquired PD pulses before and after replacing of the switchgear box are reported in Figure 6-70. It can be noted that the peak amplitude of the acquired pulse before was 41.32 mV and after reached the value of 441 mV.

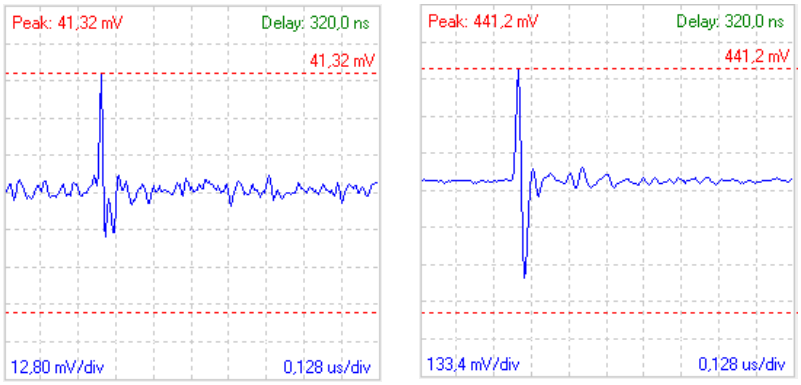

Figure 6-70. Comparison of the acquired PD pulses before and after

The possibility of performing a partial discharge measurement immediately after installing a new component would allow to see if errors were made during the installation. This way can avoid leaving PD in a component that can cause a failure over a long period of time.

Case Study 4 – Cleaning of the cable terminations

Sometimes the PDs activities were due to the poor maintenance on the MV accessories. The presence of dust or pollution could accelerate the rise of surface discharge activities on the external side of the component. The presence of these discharges for a long time could lead to a degradation of the insulation material and causes faults. In this particular case study has been reported how the simply cleaning and then a periodical maintenance can eliminate the presence of surface discharge on cable termination.

Even in this case, the measurements have been performed directly on cable close to the switchgear box as reported in Figure 6-71.

Figure 6-71. Pry-Cam Portable placed on cables

The acquired PD patterns show the presence of slight PD activities on cable 2 and cable 3. In particular, surface discharges were found characterized by low PD amplitude, about 20 mV, and high frequency content up to 50 MHz.

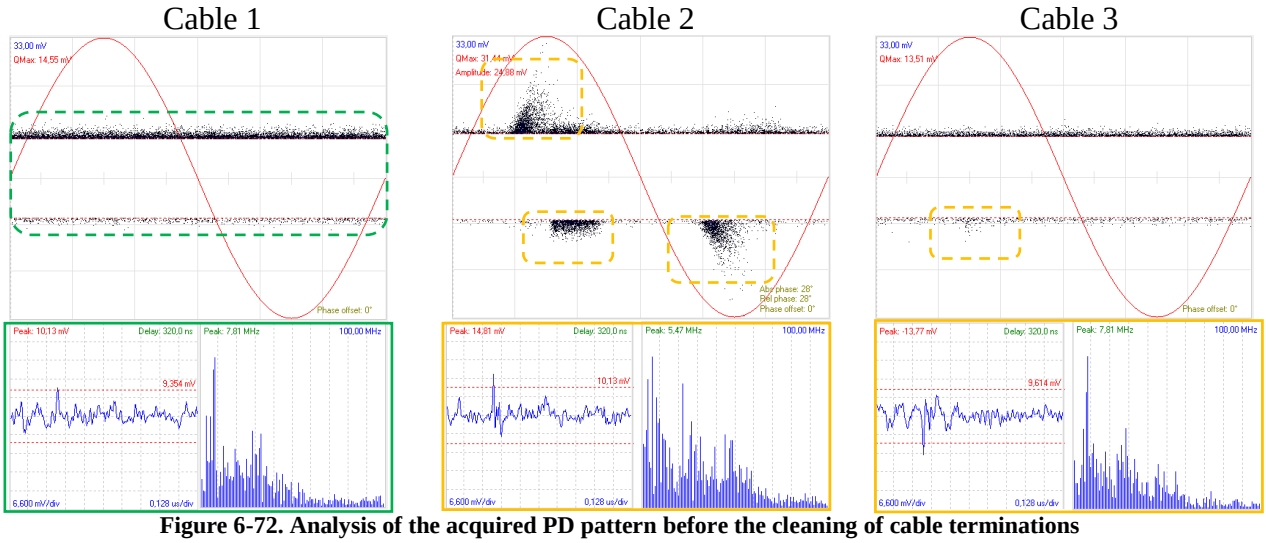

Figure 6-72. Analysis of the acquired PD pattern before the cleaning of cable terminations

In this case, before to suggest the replacement of the component, an accurate cleaning of the cable termination is the best solution. Obviously, it is necessary to repeat the measurements after the cleaning in order to check if the PD activity still present on the component under test.

If the PD activity still present, it is necessary to provide the replacement of the component, conversely the component is PD free and does not require any other action only the periodical maintenance and if possible another PD measurement after 6 months.

After cleaning of cable terminations, a new set of PD measurements have been performed. The measurements on each cable did not show any PDs activities but only the background noise as reported in Figure 6-73.

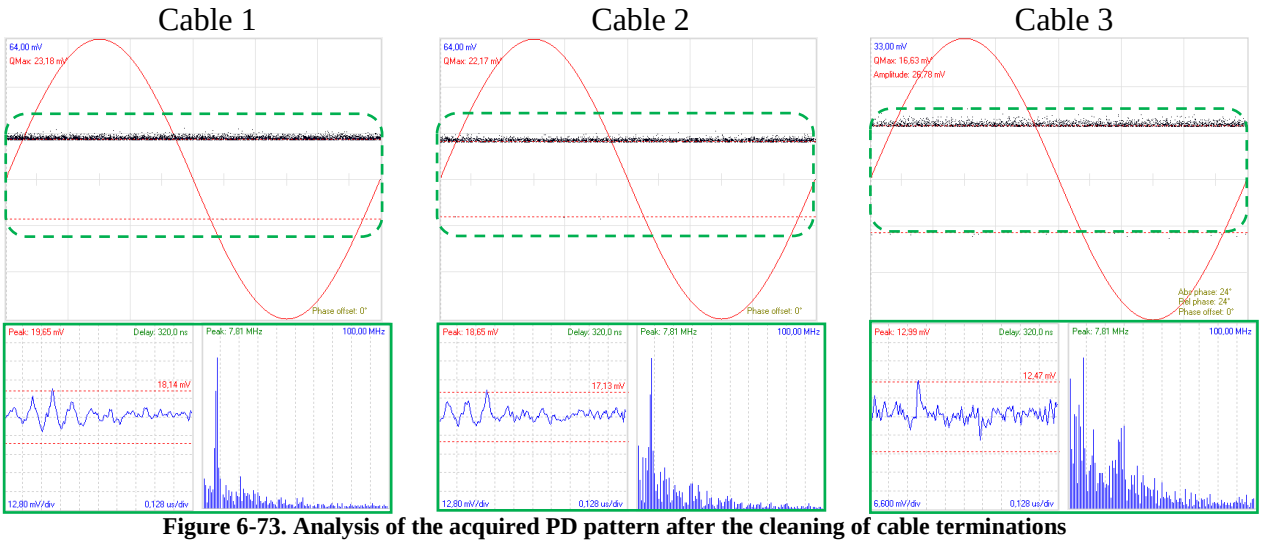

Figure 6-73. Analysis of the acquired PD pattern after the cleaning of cable terminations

As has just been reported, poor maintenance of the components can cause partial discharge due to the presence of dust and pollution. therefore, partial small discharges if neglected can inevitably lead to the degradation of the insulating material and therefore to the failure. the periodic and planned verification of partial discharge activities could drastically reduce the percentage of failures in medium voltage networks avoiding, in many cases, the complete replacement of components. Additionally, it would lead to greater reliability of the components and electrical system if a fixed monitoring system of partial discharge, such as Pry-Cam Grids, it was used in MV network in order to obtain the health status of the components in real time.

6.8.3 Investigation of ozone levels caused by Partial Discharges

Ozone (chemical formula O3) is an allotropic form of oxygen, with its characteristic garlicky odour. Its molecules are formed by three oxygen atoms (Figure 6-74). It is an unstable gas (gaseous at 20 ° C, has a three-day halving time of 20 minutes in aqueous solution), and in liquid state it is explosive. It is a very reactive gas and in particular it is an energetic oxidant, which can not be preserved by spontaneously decomposing or reacting with surrounding materials. For living beings is a highly poisonous gas and for this property it is used for purification and sterilization (eliminates a very large class of microorganisms).

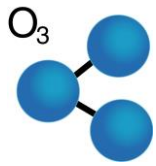

Figure 6-74. Ozone molecular (O_3)

Ozone is generated, either spontaneously or in applications where it is required, by electric shocks in the air. This generation mechanism is particularly efficient and therefore also used for industrial gas production. For applications of any kind that employ working voltages above kV ozone represents an undesirable by-product that must be kept under control given its harmfulness both on materials and human health.

Because of its high oxidising power, high-concentration gas ozone can be dangerous to human health, especially in the respiratory tract. The maximum permissible concentration for working environments with exposure 8 h/day - 5 days / week is 0.1 ppm. A concentration of 1 ppm can be tolerated for short exposures (e.g. 15 minutes). Concentrations of 100-1000 ppm can also be fatal even in a short time. In any case, ozone sensitivity depends greatly on the individual person and environmental parameters, primarily the temperature. It is advisable to use particular caution in high temperature environments. The olfactory oxygen sensitivity threshold is for humans between 0.02 and 0.05 ppm, equal to about 1/20 of the defined concentration threshold for a 15 minutes' exposure time and about 1/4 of the exposure threshold defined safe in work environments [61][63].

The partial discharge by definition is an electrical discharge that only affects a part of the dielectric existing between two conductors. The presence of partial discharge causes a slow but progressive deterioration of the dielectric material, which in the long run can lead to the collapse of the material's dielectric properties and cause destructive build-up of the components.

The main activities of PDs responsible for the spontaneous formation of ozone within an MV cabin are Corona phenomena (Figure 6-75) or external surface discharges on cables, electrodes, insulators, terminals, manoeuvrings compartments, motors and generators, etc.

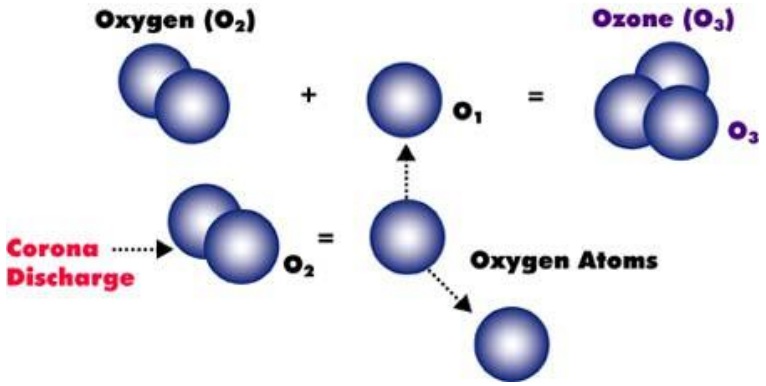

Figure 6-75. Ozone formation due to Corona discharge

The Corona discharges form in the air at exposed metal protrusions where the electric field has a high voltage gradient. This condition causes ionization of the air molecules near the projection and the start of the discharge activity resulting in ozone production. In particular, the Corona phenomenon is triggered in correspondence of metal tips or edges and at junction points between conductor, dielectric and air. Surface discharges are typically facilitated by the presence of mixed humidity with pollutants (dust, smoke, or dirt) on the outer surface of the electrical components. The presence of a high component of the electric field near the surface of a component is capable of causing a large number of discharges into the air, near the surface itself, resulting in ozone formation. The presence of superficial discharge phenomena results in the degradation of the insulating surface layer by creating a conductive and visible tracking that progresses in relation to the degree of moisture and pollution present until it reaches the complete and destructive electrical discharge. A study in [2] showed that the presence of partial discharge in the air produces significant ozone concentrations such as chemically attaching semi-conductive coatings as well as exposed metal or rubber components.

However, its high reactivity and intrinsic instability, in addition to other physical factors such as air velocity, temperature, or humidity, can favour the elimination of ozone generated by PDS.

During the aforementioned survey, the measurements of ozone levels were carried out using Prysmian Electronics instrumentation employing an electrochemical sensor and specially designed software.

In particular, the electrochemical sensor used for gas detection is an amperometric type i.e. a sensor that generating a current proportional to the volumetric fraction of detected gas. The sensor has a range of sizes from 0 to 20 ppm (parts per million). The measurements were conducted in order to verify the levels of ozone present in relation to the partial discharge phenomena that may occur within the MV cabins.

Prysmian Electronics employs both HMOS and electrochemical technologies for the production of ozone monitoring systems, selecting the most suitable according to the features of the final application.

The experiments carried out on MV devices have shown that both technologies are suitable to reliably detect and measure ozone concentrations lower than those of olfactory sensitivity of operators (thus less than about 0.02 ppm). In addition, the correlation between high levels of ozone and high levels of Corona discharge or external surface discharge on the terminals and consequent deterioration of the components has also been verified on several occasions (e.g. in MV compartments). In some cases, simple cleaning of the components was enough to drastically reduce the partial discharge level.

Ozone monitoring is therefore an excellent diagnostic indicator that can increase the operating life and functionality of the implants and thus improve the quality of the service.

The ozone measurements were carried out in parallel with the measure of partial discharge measurements on the MT distribution network at 20 kV in Taormina.
Observations of ozone levels within the MT cabs have been conditioned by several factors such as:

- **the volume of the room**: depending on the size of the cabin itself, different levels of ozone concentration can be achieved regardless of the partial discharge phenomena present. In fact, in a very large cabin where ozone depletion phenomena are present, it can not have large ozone concentrations inside it;
- **the ventilation of the room**: the presence or absence of forced and / or natural ventilation inside the room may allow the restoration of the cabin's ambient conditions by favoring the circulation of oxygen within it. In special cases where cabins have no adequate ventilation system, they do not even have a fairly large volume, ozone levels can reach very high values, causing a serious problem for electrical components but also a health risk of workers, in relation to the exposure time at very high concentrations of ozone;
- **the number of electrical components present in the room**: the presence of more electrical components inside the same room significantly increases ozone production. In fact, more electrical components such as transformers, compartments, or the presence of exposed metal parts (e.g. bars or the presence of old components at daytime) if affected by partial discharges can result in the generation of multiple ozone sources. In this case, fixed monitoring of ozone levels is highly recommended.

During the surveys carried out in the MV cabins in Taormina, it was found that some cabins had a fairly low volume, which was devoid of ventilation and with a large number of components inside. It should be noted that this type of cabins, located in the center of Taormina, are old building and some were located within private property. In these cases, the ozone levels reached high concentrations such as to allow the olfactory perception of the characteristic ozone odour. Otherwise, the newly built cabins, located in both central and peripheral areas of the city of Taormina, although a large number of compartments and transformers were present, I had a large enough room equipped with an adequate ventilation system. However, even if the presence of ozone could not be perceived at olfactory levels, it is not possible to exclude the presence of partial discharge phenomena. In addition, it is worth noting that a large amount of oxygen is injected into the cabin at the time of opening the doors, which results in a clear

reduction in ozone levels. Consequently, constant monitoring of ozone levels would allow for greater awareness of any discharge phenomena that may be present within the MV cabins.
Ozone concentration surveys were carried out during the measure of partial discharge on the MT distribution network in Taormina. The experiment was carried out on a limited number of cabins for a time period related to the main activity of partial discharge measurements. The ozone measurements carried out inside MV cabins are as follows; the measures in addition to bringing the ozone concentration in the cabin, also report the temperature and the percentage of moisture present. It should be noted that the olfactory oxygen sensitivity threshold for humans is between 0.02 and 0.05 ppm. Ozone concentrations were detected by the electrochemical sensor in ppb (parts per billion) and for greater understanding the measurements were reported in ppm (parts per million). For each measure, the description of the partial discharge activity detected inside the cabin was also reported. In most cases, the presence of partial corona discharge was detected and the nature of this discharge activity was classified as non-critical for the components. However, as confirmed by the surveys carried out, the presence of coronary phenomena, although classified non-critical, results in the formation of significant ozone concentrations within the cabin.

Case study 1
Ozone concentration (O3): 67 ppb = 0.067 ppm
Maximum discharge amplitude detected: 25.46 mV (Corona discharge)
Temperature: 21 ° C
Humidity: 52%

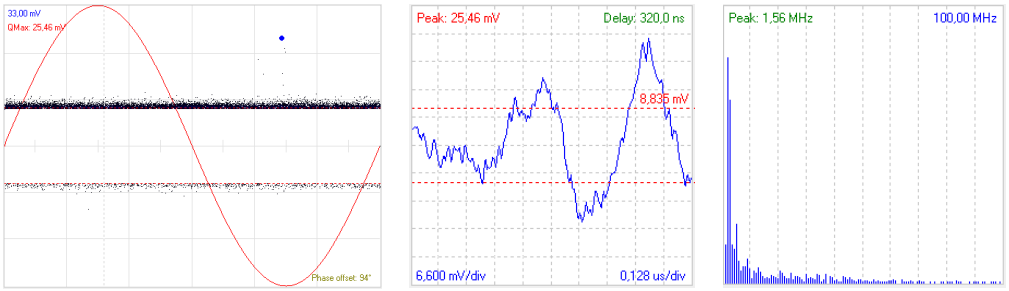

Figure 6-76. Case study 1 - Acquired PD Pattern

The cabin had a moderate activity of Corona inside it. Inside was located no. 2 transformers and due to the presence of metallic parts in the air, a concentration of ozone of 0.067 ppm was recorded so as to exceed the olfactory sensitivity level of 0.05 ppm. It should be noted that the small size of the cabin and the presence of several live components have favoured the generation of high concentrations of ozone. The effects of high ozone concentrations on the long run could favours the formation of corrosion of the live metal parts, resulting in an increase in the partial discharge phenomena, which are already present, with serious repercussions on electrical components.

Case study 2
Ozone concentration (O3): 18 ppb = 0.018 ppm
Maximum discharge amplitude detected: 32.24 mV (Background noise)
Temperature: 22 ° C
Humidity: 47%

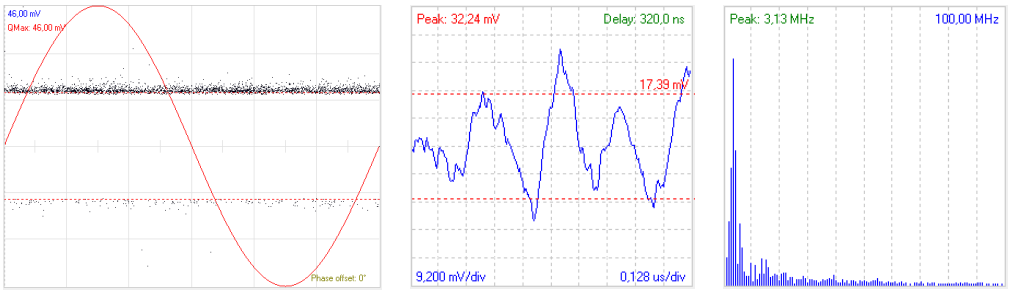

Figure 6-77. Case study 2 - Acquired PD Pattern

An ozone concentration of 0.018 ppm was detected inside the cabin. The partial discharge measurements, given the low possibility of direct access to the cables, were carried out near the inspection window. The measure did not highlight the presence of critical partial discharge activities. Therefore, the observed ozone concentration is attributed to weak discharge

phenomena within the bin that could hardly be captured by the inspection window. Ultimately, the observed ozone concentration is considered standard.

Case study 3
Ozone concentration (O3): 64 ppb = 0.064 ppm
Maximum discharge amplitude detected: 33.69 mV (external noise from TR)
Temperature: 21 ° C
Humidity: 46%

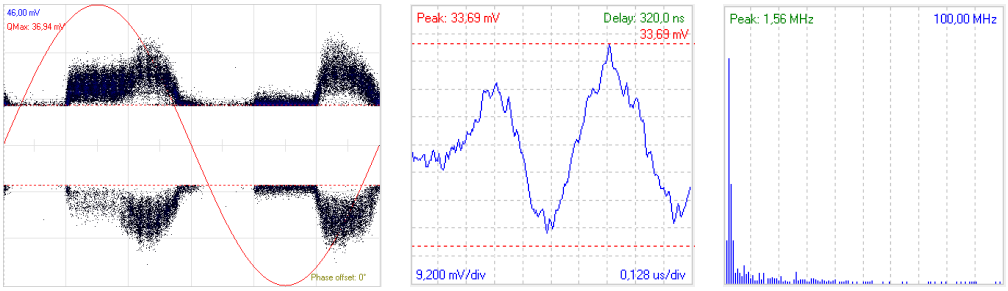

Figure 6-78. Case study 3 - Acquired PD Pattern

The measure showed a slight presence of ozone levels. Even in this case, the presence of Corona phenomena in the cabin was verified. In this case, the presence of crown phenomena, located inside the compartments, combined with the small size of the cabin, showed a moderate ozone concentration. To be taken into consideration that at the time of opening doors, the ambient conditions undergo an alteration such as to cause a reduction in the actual levels of ozone present. In order to obtain accurate ozone concentration, a fixed monitoring system and a portable partial discharge detection system should be provided.

Case study 4
Ozone concentration (O3): 1 ppb = 0.001 ppm
Maximum discharge amplitude detected: 24.19 mV (background noise)
Temperature: 24 ° C
Humidity: 44%

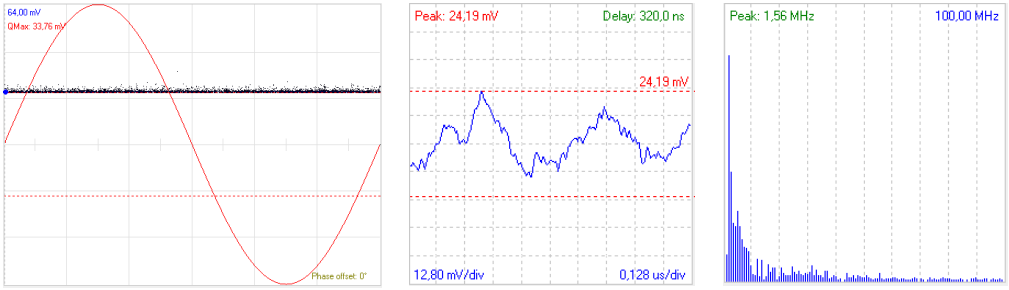

Figure 6-79. Case study 4 - Acquired PD Pattern

The measurement showed a low ozone concentration. In this case, the low value of the ozone concentration is attributable to the absence of partial discharge activity detected inside the cabin. In addition, the ozone measure was acquired in the cabin where only MT compartments

were present. The cabin, in fact, had an adjacent room where two transformers were located. Considering that no discharge activity was detected near the MT compartments and that cab access has altered the actual ozone concentration present, the measure carried out has returned a very low value.

Case study 5
Ozone concentration (O3): 53 ppb = 0.053 ppm
Maximum discharge amplitude detected: 44.19 mV (Corona discharge)
Temperature: 23 ° C
Humidity: 45%

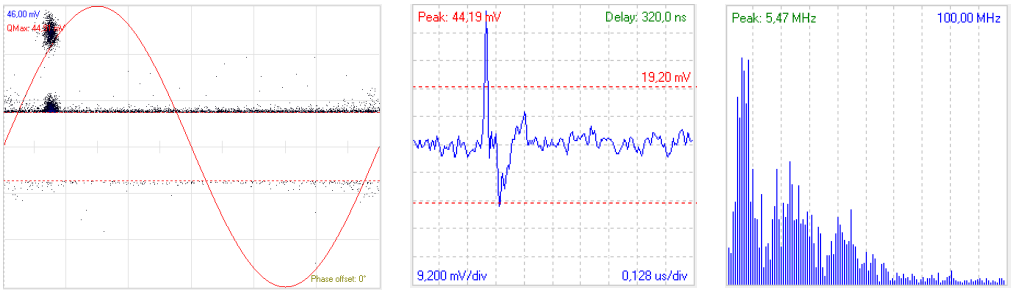

Figure 6-80. Case study 5 - Acquired PD Pattern

The measure carried out inside the cabin has shown a moderate concentration of ozone. Inside the cabin were located several sources of PDs from MV switchgear. In particular, in addition to the typical ozone odour, it was possible to hear the presence of discharge phenomena near the voltage and current transformers of measuring systems. Even in this case, the size of the room, the lack of adequate ventilation and the presence of Corona phenomena favoured the generation of a moderate ozone concentration. It is also recalled that the opening of the cabin significantly reduces the actual ozone concentration.

Case study 6
Ozone concentration (O3): 45 ppb = 0.045 ppm
Maximum discharge amplitude detected: 7.26 mV (Background noise)
Temperature: 20 ° C
Humidity: 45%

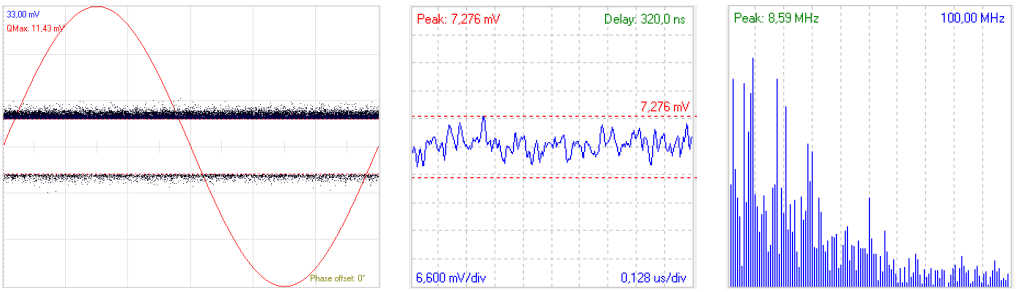

Figure 6-81. Case study 6 - Acquired PD Pattern

The measurement performed inside the cabin showed the presence of a medium to low ozone concentration. The PD measurements on the cables near the compartments did not indicate the presence of partial discharges. However, there was a transformer with metal terminals exposed in the air inside the cabin. Therefore, the observed ozone concentration was due to the presence of Corona phenomena located on the metal parts of the transformer terminals.

Case study 7
Ozone concentration (O3): 43 ppb = 0.043 ppm
Maximum discharge amplitude detected: 42.74 mV (Surface discharge)
Temperature: 23 ° C
Humidity: 44%

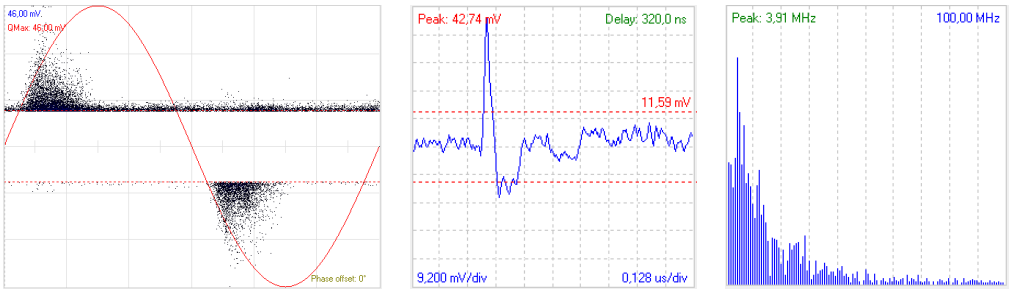

Figure 6-82. Case study 7 - Acquired PD Pattern

The measurement carried out inside the cabin showed the presence of an average ozone concentration. Unlike the previous cases, PD measurements have shown the presence of surface discharges on cable terminations. Inside the room it was located only the MV switchgear box and there were not transformers. In this case, ozone produced and detected inside the cabin is due to the presence of the above-mentioned surface discharge due to the accumulation of dust or dirt on MV terminations. In order to remove the surface discharge, and then reduce the ozone

concentration inside the cabin, it is recommended an accurate cleaning of the terminations and compartments. Considering that the dimensions of the cabin are large enough and that after the opening of the cabin was favoured the replacement of oxygen inside it, a moderate concentration of ozone was detected.

The ozone generation process due to the partial discharge is very efficient and, if not well-controlled, leads to increased concentration of gas in environments with negative effects both on the durability of the materials and on the health of workers.

On the other hand, just monitoring the levels of ozone provides a good indication of the operating conditions of MV or HV systems, since components in good condition do not exhibit significant external partial discharge. Monitoring ozone levels, therefore, has a twofold value: keeping track of equipment's health status and preventing early degradation of the equipment, as well as providing safe working conditions for personnel [64]

The ozone measurements carried out at Taormina confirmed the close correlation between the partial discharge of air and the ozone concentration within MV cabins.

However, in order to establish an absolute reference (and alarm) threshold for ozone levels, it is necessary to carry out on-site monitoring in a specific site, to compensate for specific factors such as room volumes, type of ozone ventilation and quantity and type of equipment in operation. Typical ozone levels reported in literature such as normal, pre-alarm and alarm (up to 20 ppb, from 20 to 60 ppb and above 60 ppb respectively) are therefore indicative in the absence of such corrections or prolonged observation period.

In addition, although monitoring may be performed occasionally by using laptops, it should be noted that easy access to premises by door opening or in most cases significantly alters ozone levels. Occasionally, readings do not reflect the actual state of the environment under stationary conditions. To this we must add that it is not possible to have an early warning before accessing the premises in case of dangerous gas concentrations. For this reason, it is recommended to use fixed monitoring and alarm systems.

6.9 Conclusion

This chapter has reported several cases of PD measurements carried out on MV and HV systems, both during HV test to commissioning new interconnections or during normal operating condition. The experience gained in the field has enabled to understand that the acquired PD phenomena although can be classified into a very precise phenomenon have different evolutions and behaviours depending on the rating voltage of the system under test, environmental conditions, the type of components, the presence or not of disturbances that may compromise the outcome of a measurement. It is important to emphasize the importance of the PD measurements carried out during the HV tests, because a poor interpretation of the acquired signals could seriously undermine the result of the analysis, resulting in a failure hazard for the measured component, but also to determine a situation danger in a HV and MV network in case of component failure. Therefore, the classification of PD phenomena as well as noise sources can not be based on a given number of measurements and analyses, because each PD phenomenon has its evolution characterized by PD pulse that may have different trends, amplitudes and frequency content case by case. Even if fixed monitoring systems are set up with relative alarms triggered when the amplitude of the acquired pulses exceeds a critical threshold, a rigorous analysis of the phenomenon must be carried out through the experience of an expert. One can expect to train an electronic brain that is able to identify the possible criticalities, but must always be accompanied and guided by human experience.

Bibliography

[1] IEC international standard 60270. high voltage test techniques - partial discharge measurements, 2000. 2.1, 2.2.5.

[2] IEEE Guide for Partial Discharge Testing of Shielded Power Cable Systems in a Field Environment, 5 Feb. 2007, 10.1109/IEEESTD.2007.305045.

[3] MORSHUIS, Peter HF. Partial discharge mechanisms. Delft University of Technology, 1993.

[4] R. Candela, A. Di Stefano, G. Fiscelli, S.F. Bononi, L. De Rai," A novel partial discharge detection system based on wireless technology", AEIT Annual Conference, 3-5 October 2013 – Mondello, pp.1 - 6, DOI: 10.1109/AEIT.2013.6666803.

[5] F. Viola, P. Romano, R. Miceli, A. Contin, "Performance of the shape of Partial Discharge signal wireless probes", In Power Engineering, Energy and Electrical Drives (POWERENG), 2013 Fourth International Conference on, Istanbul, Turkey, 13-17 May 2013 pp. 1801-1806. IEEE

[6] IEC, White paper on Strategic asset management of power networks, http://www.iec.ch/whitepaper/pdf/iecWP-assetmanagement-LR-en.pdf.

[7] R. Bartnikas, "Partial discharges. Their mechanism, detection and measurement." Dielectrics and Electrical Insulation, IEEE Transactions on 9.5 (2002): 763-808.

[8] Y. Jiang, et al, "Partial discharge pattern characteristic of HV cable joints with typical artificial defect", In Power and Energy Engineering Conference (APPEEC), 2010 March (pp. 1-4).

[9] R. Candela, E.R. Sanseverino, P. Romano, "Partial discharge on-line measures in cable's EPR insulation", Electrical Insulation and Dielectric Phenomena, Annual Report Conference 2004 pp. 470 - 473,

[10] C. Hudon, M. Belec. "Partial discharge signal interpretation for generator diagnostics." Dielectrics and Electrical Insulation, IEEE Transactions on 12.2 (2005): 297-319.

[11] J. De La Ree, et al. "Synchronized phasor measurement applications in power systems." Smart Grid, IEEE Transactions on 1.1 (2010): 20-27.

[12] P. C. J. M Van der Wielen, P. A. A. F. Wouters, J. Veen, D. M. Van Aartrijk, "Synchronization of on-line PD detection and localization setups using pulse

injection". In Properties and Applications of Dielectric Materials, 2003. Proceedings of the 7th International Conference on (Vol. 1, pp. 327-330). IEEE. June 2003.

[13] Candela R., Di Stefano A., Fiscelli G., Giaconia G.C., "Portable Partial Discharge Detection Device", Patent EP2297589 / WO2009150627, 11 June 2009.

[14] V. Terzija, G. Valverde, D. Cai, P. Regulski, V. Madani, J. Fitch, A. Phadke, "Wide-area monitoring, protection, and control of future electric power networks". Proceedings of the IEEE, 2011, Vol. 99, No. 1, January 2011.

[15] Bose, A. (2010). Smart transmission grid applications and their supporting infrastructure. *Smart Grid, IEEE Transactions on* smart grid, vol. 1, no. 1, june 2010.

[16] Terna Technical Specification Annex A.3 - "Requisiti e caratteristiche di riferimento di stazioni e linee elettriche della RTN".

[17] Li Vigni V, "Design of a fault and partial discharges location device for cable power network", PhD Thesis, http://hdl.handle.net/10447/220894.

[18] INTERNATIONAL STANDARD IEC 60044-2 - Instrument transformers – Part 2: Inductive voltage transformers.

[19] Riva Sanseverino, E., Madonia, A., Romano, P., Candela, R., Li Vigni, R., Filippone, G., et al. (2017). "Sulla sincronizzazione delle misure wireless di scariche parziali con il segnale di tensione a 50 Hz". L'ENERGIA ELETTRICA, 94(2), 53-62.

[20] Li Vigni, V., Madonia, A., Sanseverino, E. R., Romano, P., & Candela, R. (2016, June). "Overcoming synchronization issues in wireless technology partial discharge measurement". In Environment and Electrical Engineering (EEEIC), 2016 IEEE 16th International Conference on (pp. 1-4). IEEE.

[21] Madonia, A., Vigni, V. L., Sanseverino, E. R., Romano, P., Viola, F., & Candela, R. (2016, July). "Remote voltage synchronization for wireless partial discharge diagnostics". In Dielectrics (ICD), 2016 IEEE International Conference on (Vol. 2, pp. 947-950). IEEE.

[22] Koltunowicz, T. L., Kochetov, R., Bajracharya, G., Djairam, D., & Smit, J. J. (2011, June). Repetitive transient aging, the influence of repetition frequency. In Electrical Insulation Conference (EIC), 2011 (pp. 444-448). IEEE.

[23] D. Fabiani e G. Montanari, "The effect of voltage distortion on ageing acceleration of insulation systems under partial discharge activity" Electrical Insulation Magazine, IEEE, vol. 17, n. 3, pp. 24-33, May-June 2001.

[24] B. Florkowska, M. Florkowski, J. Roehrich, P. Zydron, “Measurement and analysis of surface partial discharges at semi-square voltage waveforms”, Dielectrics and Electrical Insulation, IEEE Transactions on, vol. 18 n°4, pp. 990-996, August 2011

[25] F. P. Espino-Cortes, E. A. Cherney, S. H. Jayaram, “Impact of inverter drives employing fast-switching devices on form-wound AC machine stator coil stress grading”. Electrical Insulation Magazine, IEEE, 23(1), 2010, pp.16-28.

[26] P. Wang, A. Cavallini, G.C. Montanari “The effects of square wave voltage rise time on PD statistics in time and frequency domain”. In Electrical Insulation Conference (EIC), 2015 IEEE (pp. 262-265). IEEE.

[27] Cavallini A., Fabiani D., Montanari G. C., “Power electronics and electrical insulation systems Part 2: Diagnostic Properties”. Electrical Insulation Magazine, IEEE, vol. 26 n°5, 2010, pp. 30-40

[28] X. Xu, “Partial Discharges Studied by Dielectric Response Method”, Doctoral thesis, Chalmers University of Technology, Göteborg, Sweden, June 2015.

[29] Madonia A., Romano P., Hammarström T., Gubanski S. M., Viola F., Imburgia A. “PD characteristics at Square Shaped Voltages Applying Two Different Detecting Techniques” In Electrical Insulation and Dielectric Phenomena (CEIDP), 2016 Annual Report Conference on, 16-19 October 2016, pp. 1-4.

[30] T. Hammarström, “Partial Discharges at Fast Rising Voltages”, PhD thesis, ISBN 978-91-7597-054-7, Chalmers University of Technology, Gothenburg Sweden, 2014.

[31] A. Cavallini, M. Conti, A. Contin, G. C. Montanari, “Advanced PD Inference in On-Field Measurements. Part 2: Identification of Defects in Solid Insulation Systems”, Dielectrics and Electrical Insulation, IEEE Transactions on, vol. 10, n°3, pp 528-538.2003.

[32] Robles, G.; Martínez-Tarifa, J.M.; Rojas-Moreno, M.V.; Albarracín, R.; Ardila-Rey, J. “Antenna selection and frequency response study for UHF detection of partial discharges”, In Instrumentation and Measurement Technology Conference (I2MTC), 2012 IEEE International (pp. 1496-1499). May 2012.

[33] A. Haddad and D. Warne, editors. “Advances in High Voltage Engineering”, 1st ed., IEE Press: London, ISBN 0852961588, p. 56, 2004.

[34] A. Cavallini, G. C. Montanari, F. Puletti and A. Contin, "A new methodology for the identification of PD in electrical apparatus: properties and applications," in IEEE

Transactions on Dielectrics and Electrical Insulation, vol. 12, no. 2, pp. 203-215, April 2005.

[35] S. Bahadoorsingh, S.M. Rowland, “Investigating the impact of harmonics on the breakdown of epoxy resin through electrical tree growth”, IEEE Trans. Dielectr. Electr. Insul. vol. 17, pp. 1576-1584, 2010

[36] R. Sarathi, M. Archana, “Investigation of partial discharge activity by a conducting particle in transformer oil under harmonic AC voltages adopting UHF technique”, IEEE Trans. Dielectr. Electr. Insul., vol. 19, pp.1514-1520, 2012

[37] B. Florkowska, M. Florkowski, J. Furgał, J. Roehrich, P. Zydron, “Impact of fast transient phenomena on electrical insulation systems”, Publishing House AGH, Kraków, 2012

[38] Bahadoorsingh, S., & Rowland, S. M. (2009, October). “Modeling of partial discharges in the presence of harmonics”. In Electrical Insulation and Dielectric Phenomena, 2009. CEIDP'09. IEEE Conference on (pp. 384-387). IEEE.

[39] Bahadoorsingh, S., Rowland, S. M., Catterson, V. M., Rudd, S. E., & McArthur, S. D. J. (2010, July). “Interpretation of partial discharge activity in the presence of harmonics”. In Solid Dielectrics (ICSD), 2010 10th IEEE International Conference on (pp. 1-4). IEEE.

[40] Bahadoorsingh, S., & Rowland, S. M. (2010). “Investigating the impact of harmonics on the breakdown of epoxy resin through electrical tree growth”. IEEE Transactions on Dielectrics and Electrical Insulation, 17(5).

[41] Florkowski M., B Florkowska B., “Distortion of partial-discharge images caused by high-voltage harmonics”. IEE Proceedings-Generation, Transmission and Distribution, 2006, 153.2: 171-180.

[42] Florkowski, M., Florkowska, B., Furgal, J., & Zydron, P. (2013). “Impact of high voltage harmonics on interpretation of partial discharge patterns”. IEEE Transactions on Dielectrics and Electrical Insulation, 20(6), 2009-2016.

[43] Florkowski, M., Florkowska, B., & Zydroń, P. (2014, September). “Influence of high voltage harmonics on partial discharge patterns modulation”. In High Voltage Engineering and Application (ICHVE), 2014 International Conference on (pp. 1-4). IEEE.

[44] Florkowska, B., Florkowski, M., & Zydron, P. (2007, July). “The role of harmonic components on partial discharge mechanism and degradation processes in epoxy resin insulation”. In Solid Dielectrics, 2007. ICSD'07. IEEE International Conference on (pp. 560-563). IEEE.

[45] Florkowski, M. (1997, May) “Influence of high voltage harmonics on partial discharge patterns”. In Properties and Applications of Dielectric Materials, 1997., Proceedings of the 5th International Conference on (Vol. 1, pp. 303-306). IEEE.

[46] Montanari, G. C., & Fabiani, D. (1999). “The effect of nonsinusoidal voltage on intrinsic aging of cable and capacitor insulating materials”. IEEE Transactions on Dielectrics and Electrical Insulation, 6(6), 798-802.

[47] R. Candela, G. Mirelli, R. Schifani “PD Recognition by Means of, Statistical and Fractal Parameters and Neural Network”. IEEE Transactions on Dielectric and Electrical Insulation 2000; Vol. 7 No.1, pp. 87-94.

[48] M. Bawart, M. Marzinotto, G. Mazzanti, “Diagnosis and location of faults in submarine power cables”, IEEE Electrical Insulation Magazine, Vol. 32, No. 4, pp. 24-37, luglio/agosto 2016

[49] J.P. Steiner, P.H. Reynolds, and W.L. Weeks. “Estimating the Location of Partial Discharges in Cables”, IEEE Trans. EI-27, pp. 44-59, No. 1, February 1992.

[50] S. Boggs, A. Pathak and P. Walker, “Partial Discharge XXIII: High Frequency Attenuation in Shielded Solid Dielectric Power Cable and Implications Thereof for PD Location”, IEEE Electr. Insul. Mag., Vol. 12, No. 1, pp. 9-16, Jan./Feb. 1996.

[51] S.A. Boggs, “Partial Discharge - Part II: Detection Sensitivity,” IEEE Electr. Insul. Mag., Vol. 6, No. 5, pp. 35-42, Sept./Oct. 1990.

[52] F. Petzold, H. Schlapp, E. Gulski, P. P. Seitz, and B. Quak, "Advanced solution for on-site diagnosis of distribution power cables", IEEE Trans. Dielectr. Electr. Insul., vol. 15, no. 6, pp. 1584-1589, Dec. 2008.

[53] B. Clegg and N. G. Lord, "Modern cable-fault-location methods," in Proceedings of the Institution of Electrical Engineers, vol. 122, no. 4, pp. 395-402, Apr. 1975.

[54] F. Petzold and M. Zakharov, "PD diagnosis on medium voltage cables with Oscillating Voltage (OWTS)", in 2005 IEEE Power Tech, St. Petersburg, Russia, 2005, pp. 1-7.

[55] Working Group B1.10, “Update to Service Experience of HV Underground and Submarine Cable System”, Cigrè Brochure 379, April 2009.

[56] Working group B1.21 “Third-Party Damage to Underground and Submarine Cable”, Cigrè Brochure 398, December 2009.

[57] “AC resonant test system for on-site testing of extruded HV cables”, https://www.highvolt.de/portaldata/1/Resources/HV/Downloads/8-02-4.pdf.

[58] Schikarski, P., Gamlin, M., Rickmann, J., Peeters, P., Nienwendijk, P. V. D., & Koning, R. (1999). Two years of experience with a mobile resonant test system for testing of installed medium-and high voltage power cables. In High Voltage Engineering, 1999. Eleventh International Symposium on (Conf. Publ. No. 467) (Vol. 5, pp. 236-239). IET.

[59] Wild, M., Tenbohlen, S., Gulski, E., & Jongen, R. (2017). “Basic aspects of partial discharge on-site testing of long length transmission power cables”. IEEE Transactions on Dielectrics and Electrical Insulation, 24(2), 1077-1087.

[60] Albert Jenni, Michel Pasquier, Roger Gleyvod, Peter Thommen, “Testing of High Voltage Power. Cables with Series Resonant Systems and Water Terminations”. E 1-77 Haefely High voltage techonology.

[61] Lemesch, G., “Ozone measurement – A diagnosis tool for Pd-detection in large generators”, Iris Rotating Machine Conference, 2004.

[62] Rux, L.M. and Becker L., “Ozone monitoring and corrective actions for an aircooled hydroelectric generator stator winding”, Iris Rotating Machine Conference, New Orleans, June 19-22, 2000.

[63] Cartlidge, D.M., Glass fragment, D.W., Franklin D.E., Macdonald J.A., Pollock, B.C., “Machine condition monitoring: Ozone monitor for air cooled generators”, CEA report No 9134 G 864, 1994.

[64] Louis Lépine, Denise Lessard-Déziel, Mario Bélec, Calogero Guddemi, Duc Ngoc Nguyen. “Understanding ozone distribution inside stator core and measurements inside air-cooled generators to assess partial discharges problems”. Institut de Recherche d’Hydro-Québec (IREQ), 1800 Boul Lionel-Boulet, Varennes, Qc, Canada, J3X 1S1.